# Cyclin E-Induced Replication Stress Drives p53dependent Mitotic Bypass and Whole Genome Duplication

Jingkun Zeng

University College London and

The Francis Crick Institute

PhD Supervisor: Dr. John Diffley

A thesis submitted for the degree of Doctor of Philosophy
University College London
2023

## **Declaration**

I, Jingkun Zeng, confirm that the work presented in this thesis is my own. Where information has been derived from other sources, I confirm that this has been indicated in the thesis. Certain names of reagents, technical terms and part of the methods section may be derived from a publication that this work has resulted in (Zeng et al., 2023), to maintain consistency for readers.

## **Acknowledgements**

Foremost, I would like to express my deepest gratitude to my PhD supervisor, Dr. John Diffley, for not only providing me with continued guidance and support throughout my PhD but also for giving me the freedom and encouragement to explore a cell biology project in his world-leading biochemistry lab. I also extend my gratitude to past and present members of the lab, for their stimulating discussions, insightful feedback, and for making the lab an enjoyable place to work. A special thanks to Steph and Eiko for training me in my first year and co-work on this project, and my other mammalian buddy Agos.

I would like to thank the Boehringer Ingelheim Fonds and the Crick
Studentship programme for funding my PhD. I feel lucky to have worked
within such a supportive environment at the Francis Crick Institute. Thanks to
the Crick Science and Technology Platforms, especially Cell Services, Flow
Cytometry and Advanced Light Microscopy, whose work is essential for the
progress of this project.

I am also very grateful to Professor Rob de Bruin and Dr. Simon Boulton for their helpful discussion and guidance.

I would like to thank all my friends who have made my time during PhD fun and less stressful. Thanks to Jiang, who has been there for my highs and lows. Finally, I would like to express my deepest appreciation to my family, 爸妈,爷爷奶奶,姑姑一家,妹妹,for their unwavering love and support throughout my journey in the UK.

#### **Abstract**

Whole genome duplication (WGD) is seen in 30-40% tumours and can lead to extensive aneuploidies. The p53 tumour suppressor prevents the progression of the G1 phase of tetraploid cells; however, around 50% of WGD events in cancer occur in p53-proficient cells. In p53-proficient tumours, abnormal activation of the E2F pathway, especially amplification of the cyclin E gene, correlates with WGD. In this work we show that cyclin E induces replication stress, which causes a prolonged checkpoint-dependent arrest in G2 phase followed by mitotic bypass and endoreduplication. Another inducer of replication stress, aphidicolin, also causes mitotic bypass with similar kinetics in the absence of cyclin E expression. Surprisingly, mitotic bypass induced by either cyclin E expression or aphidicolin requires the presence of the p53 tumour suppressor and its downstream target, the p21 cyclin dependent kinase inhibitor. Together with WEE1, p21 inhibits mitotic CDK to activate APC/CCDH1 to degrade G2 markers, leading to mitotic bypass. After mitotic bypass, cells enter a senescence-like state, but loss of p53 or expression of cyclin E can drive these cells to complete the endoreduplication cycle. Our results provide evidence that p53 can play an essential role in WGD and help explain how WGD can occur in p53-proficient cancers.

### **Impact Statement**

Cancer is a leading cause of death that contributes to about one in six deaths globally. Around 19.3 million people developed cancer and 10.0 million people died from cancer in 2020 (Sung et al., 2021). Understanding tumorigenesis is therefore important for improving global health. One hallmark of cancer is aneuploidy. About 90% of tumours are aneuploid and one major genomic event that leads to massive aneuploidy is whole genome duplication (WGD). WGD occurs in 30-40% of tumours and indicates worse prognosis in patients (Bielski et al., 2018, Zack et al., 2013). Some genetic alterations are associated with WGD, but the underlying mechanisms of how they lead to WGD are unclear.

Cyclin E is a protein that regulates cell cycle transition. Amplification of the cyclin E gene is seen in many tumours and correlates with WGD in patients. In this work cell models that can overexpress cyclin E were established, and I used them to uncover a mechanism that links replication stress and WGD. Elevated cyclin E expression has been shown to cause replication stress by de-regulating replication origin usage (Ekholm-Reed et al., 2004, Tanaka and Diffley, 2002, Matson et al., 2017, Halazonetis et al., 2008). Using fluorescent live-cell imaging techniques I found that cyclin E-overexpressing cells underwent WGD by bypassing mitosis. This mitotic bypass seemed to be caused by replication stress because I showed that cells in other forms of replication stress such as inhibiting DNA polymerases or reactive oxygen species also bypassed mitosis.

One major finding of this study is about the role of p53 in replication stress-induced WGD. p53, the most frequently mutated gene in cancer, is a tumour suppressor known to maintain genome integrity. However, I discovered that p53 can play a positive role in WGD, an event that undermines genome integrity. Using CRISPR knockout, I found cells without p53 did not bypass mitosis in replication stress but instead underwent catastrophic mitosis. I further showed that p53 promotes mitotic bypass by upregulating a CDK inhibitor p21, which leads to activation of APC/C<sup>CDH1</sup> that degrade G2 markers. The somewhat surprising discovery in this work provides new insights about how the most studied tumour suppressor p53 can contribute to cancer genome evolution.

As a basic research project, the findings I present here lead to new knowledge about WGD, and are particularly beneficial to the scientific community focused on cancer evolution.

## **Publications**

This work has resulted in a publication (Zeng et al., 2023). A PDF version of the paper is attached at the end of this thesis.

## **Table of Contents**

| ACKNOWLEDGEMENTS |   |      |  |  |  |
|------------------|---|------|--|--|--|
| ABSTRACT         |   |      |  |  |  |
|                  |   |      |  |  |  |
| LIST OF FIG      | GURES   | 11   |  |  |  |
| LIST OF TA       | \BLES   | 13   |  |  |  |
| ABBREVIA         | TIONS   | 14   |  |  |  |
| 1                | CHAPTER 1. INTRODUCT  | ΓΙΟΝ |  |  |  |
|                  |   | 16   |  |  |  |
| 1.1              | CELL CYCLE CONTROL  | 16   |  |  |  |
| 1.1.1            | G1 phase and G1-S transition  | 16   |  |  |  |
| 1.1.2            | G1 phase-related oncogenes and tumour suppressors                   | 18   |  |  |  |
| 1.1.3            | Mitotic entry and exit  | 19   |  |  |  |
| 1.2              | CYCLIN E  | 21   |  |  |  |
| 1.2.1            | Cyclin E in normal physiology                                       | 21   |  |  |  |
| 1.2.2            | Elevated cyclin E levels in cancer                                  | 23   |  |  |  |
| 1.2.3            | Cyclin E-induced replication stress and genome instability          | 24   |  |  |  |
| 1.3 C            | CELL CYCLE CHECKPOINTS  | 26   |  |  |  |
| 1.3.1            | Sources of genotoxic stress   | 27   |  |  |  |
| 1.3.2            | DNA damage checkpoint   | 28   |  |  |  |
| 1.3.3            | The replication checkpoint  | 29   |  |  |  |
| 1.4 T            | UMOUR SUPPRESSOR P53  | 30   |  |  |  |
| 1.4.1            | Overview  | 31   |  |  |  |
| 1.4.2            | p53-mediated cell cycle arrest                                      | 33   |  |  |  |
| 1.4.3            | Perturbation of the p53 pathway in cancer                           | 35   |  |  |  |
| 1.5 T            | WO TYPES OF ANEUPLOIDY IN CANCER: CHROMOSOMAL INSTABILITY AND WHOLE |      |  |  |  |
| CENOME           |   | 40   |  |  |  |

|   | 1.6 V  | WHOLE GENOME DUPLICATION  | 42   |
|---|--------|---|------|
|   | 1.6.1  | Routes to WGD: cell fusion, mitotic defects, and mitotic bypass | 42   |
|   | 1.6.2  | Role of p53 in regulating ploidy                                | 45   |
|   | 1.6.3  | Genetic correlation with WGD in cancer                          | 46   |
|   | 1.7    | SENESCENCE  | 47   |
|   | 1.7.1  | Induction of senescence   | 47   |
|   | 1.7.2  | Biomarkers for senescent cells                                  | 48   |
|   | 1.7.3  | p53-dependent cell cycle exit from G2                           | 49   |
|   | 1.8 F  | RESEARCH AIMS   | 51   |
| 2 |        | CHAPTER 2. MATERIALS & MET                                      | HODS |
|   |        |   | 52   |
|   | 2.1    | CELL CULTURE AND CELL LINES                                     | 52   |
|   | 2.2 F  | PLASMIDS AND CELL LINES   | 53   |
|   | 2.2.1  | Plasmids and cloning  | 53   |
|   | 2.2.2  | Cell line establishment   | 54   |
|   | 2.3 F  | PREPARATION OF FROZEN CELL STOCK                                | 57   |
|   | 2.4 F  | RNA INTERFERENCE  | 58   |
|   | 2.5    | SMALL MOLECULE COMPOUNDS  | 58   |
|   | 2.6 N  | METAPHASE SPREADING   | 59   |
|   | 2.7 L  | LIVE-CELL IMAGING   | 60   |
|   | 2.8    | CELL TRACKING   | 62   |
|   | 2.9    | NUMERICAL ANALYSIS  | 63   |
|   | 2.10 F | FLOW CYTOMETRY  | 63   |
|   | 2.10.1 | Barcoding   | 63   |
|   | 2.10.2 | EdU incorporation assay and DNA content analysis                | 65   |
|   | 2.10.3 | Whole cell and chromatin-bound protein analysis                 | 65   |
|   | 2.10.4 | Multichannel FACS assay and analysis                            | 66   |
|   | 2.10.5 | 5 Cell sorting  | 66   |
|   | 2.11 V | Western blot  | 66   |
|   | 2 12 / | ANTIDODIES  | 67   |

| 3CHAPTER 3. RESULT 1. CYCLIN E EXP       | RESSION INDUCES ENDOREDUPLICATION          |
|--|--|
| THROUGH MITOTIC BYPASS                   | 70   |
| 3.1 Introduction                         | 70   |
| 3.2 RESULTS                              | 71   |
| 3.2.1 Cyclin E1 expression induces w     | hole genome duplication in U2OS cells71    |
| 3.2.2 Cyclin E1-induced whole genom      | ne duplication occurs by mitotic bypass77  |
| 3.2.3 Role of the DNA damage check       | point83                                    |
| 3.3 CONCLUSIONS                          | 91   |
| 4. CHAPTER 4. RESULT 2. REPLICATION S    | STRESS DRIVES MITOTIC BYPASS IN U2OS       |
| AND RPE1 CELLS                           | 93   |
| 4.1 Introduction                         | 93   |
| 4.2 RESULTS                              | 93   |
| 4.2.1 Replication stress in general ind  | luces endoreduplication in U2OS cells93    |
| 4.2.2 Replication Stress-Induced Mito    | tic Bypass in RPE1 Cells100                |
| 4.3 CONCLUSIONS                          |  |
| 5 CHAPTER 5. RESULT 3. ROLE O            | F THE P53-P21 PATHWAY IN REPLICATION       |
| STRESS-INDUCED MITOTIC BYPASS            | 109  |
| 5.1 Introduction                         | 109  |
| 5.2 RESULTS                              | 109  |
| 5.2.1 p53 is required for replication st | ress-induced mitotic bypass109             |
| 5.2.2 p21 is essential for mitotic bypas | ss by inhibiting CDK116                    |
| 5.2.3 Cyclin E overexpression preven     | ts EC-G1 arrest and reverses senescence126 |
| 5.3 CONCLUSIONS                          | 131  |
| 6  | CHAPTER 6. DISCUSSION                      |
|  | 133  |
| 6.1 STATEMENT OF LIMITATIONS             | 141  |
| DEFEDENCE LIST                           | 440  |

## **List of Figures**

| FIGURE 1.1 ONCOGENES AND TUMOUR SUPPRESSOR GENES IN THE G1-S TRANSITION PATHWAY. 1     |
|--|
| FIGURE 1.2 FREQUENCIES OF DIFFERENT ALTERATIONS OF SELECTED TUMOUR SUPPRESSORS IN      |
| CANCER3  |
| FIGURE 1.3 THREE EXPERIMENTALLY DESCRIBED PATHWAYS TO WGD                              |
| FIGURE 3.1 CYCLIN E OVEREXPRESSION LEADS TO WHOLE GENOME DUPLICATION IN U2OS CELLS.    |
| 7  |
| FIGURE 3.2 KARYOTYPES OF CYCLIN E-INDUCED U2OS WGD CLONES                              |
| FIGURE 3.3 DEPLETION OF FBXW7 INDUCES WGD  |
| FIGURE 3.4 ESTABLISHMENT OF FUCCI CELLS  |
| FIGURE 3.5 FUCCI IMAGING OF U2OS CELLS OVEREXPRESSING CYCLIN E                         |
| FIGURE 3.6 ABNORMAL CELL CYCLE TRANSITIONS IN CYCLIN E-OVEREXPRESSING CELLS            |
| FIGURE 3.7 G2 ARREST OF CYCLIN E-OVEREXPRESSING U2OS CELLS                             |
| FIGURE 3.8 REPLICATION STRESS IN CYCLIN E-OVEREXPRESSING U2OS CELLS                    |
| FIGURE 3.9 ENDOREDUPLICATING CELLS START WITH UNDER-REPLICATED DNA                     |
| FIGURE 3.10 WHOLE GENOME DUPLICATED CELLS UNDERGO ABNORMAL MITOSIS9                    |
| FIGURE 4.1 APHIDICOLIN INDUCES MITOTIC BYPASS IN U2OS CELLS                            |
| FIGURE 4.2 APHIDICOLIN INDUCES WHOLE GENOME DUPLICATIIN IN U2OS CELLS                  |
| FIGURE 4.3 OTHER ONCOGENES CAN INDUCE MITOTIC BYPASS IN U2OS CELLS                     |
| FIGURE 4.4 CYCLIN E OVEREXPRESSION INDUCES REPLICATION STRESS AND WGD IN RPE1 CELLS    |
|  |
| FIGURE 4.5 MITOTIC BYPASS OF CYCLIN E-OVEREXPRESSING RPE1 CELLS IS DEPENDENT ON ATR    |
|  |
| FIGURE 4.6 APH-INDUCED RPE1 EC-G1 CELLS ENTER A SENESCENCE-LIKE STATE                  |
| FIGURE 5.1 ESTABLISHMENT OF P53-KNOCKOUT CELLS   |
| FIGURE 5.2 P53 KNOCKOUT IN RPE1 CELLS ABOLISHES APHIDICOLIN-INDUCED MITOTIC BYPASS.11. |
| FIGURE 5.3 P53 KNOCKOUT IN RPE1 CELLS ABOLISHES CYCLIN E-INDUCED MITOTIC BYPASS 114    |
| FIGURE 5.4 P53-KNOCKOUT CELLS CAN HAVE EXTENDED G2 ARREST IN REPLICATION STRESS 115    |
| FIGURE 5.5 P21 IS REQUIRED FOR REPLICATION STRESS-INDUCED MITOTIC BYPASS IN RPE1 CELLS |
| 11'  |

| FIGURE 5.6 REPLICATION STRESS-INDUCED MITOTIC BYPASS IS DEPENDENT ON P53 AND P21 IN A |
|---|
| PANEL OF CELL LINES   |
| FIGURE 5.7 P21 PROMOTES REPLICATION STRESS-INDUCED MITOTIC BYPASS BY INHIBITING CDK   |
| LEVELS  |
| FIGURE 5.8 DIFFERENCE BETWEEN DNA DAMAGE- AND REPLICATION STRESS-INDUCED WHOLE        |
| GENOME DUPLICATION  |
| FIGURE 5.9 CYCLIN E OVEREXPRESSION RESTORES ENDOREDUPLICATION OF EC-G1 CELLS IN       |
| SENESCENCE  |
| FIGURE 5.10 REVERSAL OF SENESCENT EC-G1   |
| FIGURE 5.11 CYCLIN E OVEREXPRESSION RE-ESTABLISHES REPLICATION OF SENESCENT CELLS     |
| INDUCED BY CHEMOTHERAPEUTIC AGENTS  |
| FIGURE 6.1 MODEL OF WGD DRIVEN BY CYCLIN E-INDUCED REPLICATION STRESS                 |
| FIGURE 6.2 MODELS OF WGD DRIVEN BY REPLICATION STRESS AND DSB/TELOMERE ATTRITION.     |
| 138   |

## **List of Tables**

| TABLE 1. EXPERIMENTAL MODELS USED IN THE STUDY                                    | .52 |
|---|-----|
|   |     |
| TABLE 2. COMMERCIAL PROVIDER AND CATALOGUE NUMBER OF CHEMICALS USED IN THE STUDY. | .59 |
|   |     |
| TABLE 3. LIST OF ANTIBODIES USED IN THE STUDY                                     | .67 |

#### **Abbreviations**

APC/C anaphase-promoting complex/cyclosome

Aph aphidicolin

ATM ataxia-telangiectasia mutated

ATR ataxia-telangiectasia and Rad3-related

a.u. arbitrary unit

BJ-LT BJ cells transformed with SV40LT

CAK CDK-activating kinase

CDK cyclin-dependent kinase activating kinase

CIN chromosome instability

CPT camptothecin
cyclin D cyclin D1
cyclin E cyclin E1
cyclin B cyclin B1

DDR DNA damage response DNE dominant negative effect

Dox doxycycline

DSB double-stranded break EC-G1 endoreduplication cycle G1

ESC embryonic stem cell

FBXW7 F-box and WD repeat domain containing 7

FUCCI fluorescent, ubiquitination-based cell cycle indicator

FI fluorescence intensity

G1 gap 1 G2 gap 2

GOF gain-of-function HA hemagglutinin

HPV human papilloma virus

KO knockout M mitosis

MCM minichromosome maintenance complex MDM2 mouse double minute 2 homologue

MEF mouse embryonic fibroblast MFI mean fluorescence intensity

mVenus-Gem mVenus-geminin NAC N-acetyl cysteine

NHEJ nonhomologous end joining

N.T. non-treated

PIKK phosphoinositide 3-kinase-related kinase

POT1 protection of telomeres 1
pre-RC pre-replication complex

PTM posttranslational modification

reactive oxygen species ROS replication protein A RPA

retinal pigment epithelial 1 RPE1

S synthesis

spindle assembly checkpoint SAC

SD standard deviation single-stranded break SSB

simian virus 40 large T-antigen SV40LT

half time *t*1/2

transcriptional activation domain TAD

UV ultraviolet

whole genome duplication WGD

## **Chapter 1. Introduction**

#### 1.1 Cell cycle control

The mitotic cell cycle can be divided into four stages, G1 (gap one) phase, S (synthesis) phase, G2 (gap two) phase and M (mitosis) phase, with G1, S and G2 together being called the interphase. Different cyclins, which are expressed in different phases in a cyclic manner, couple with cyclin-dependent kinases (CDKs) to drive the progression of the cell cycle. A complex network of regulatory elements, including mitogenic signalling, ubiquitin-mediated proteolysis and DNA damage and replication checkpoints, orchestrate with cyclin-CDK to tightly control the cell cycle. This strict control has a central goal: faithful duplication and separation of the genetic material. Alterations in the cell cycle control pathways can comprise genome stability and lead to uncontrolled cell division, a common precursor to tumorigenesis.

#### 1.1.1 G1 phase and G1-S transition

When mitosis is finished, cells need to decide whether to exit the cell cycle and enter quiescence (G<sub>0</sub>), a non-proliferative state that most human adult cells are in, or enter G1 to continue the cell cycle. In mammals, the mitogenic D-type cyclin, cyclin D1 (gene product of *CCND1*, hereafter referred to as cyclin D), coupled with CDK4/6, plays a central role in this decision. Inhibition of CDK4/6 activity makes cells exit the cell cycle and enter quiescence (Yoshida and Diehl, 2015, Finn et al., 2009, Anders et al., 2011). Expression of cyclin D is triggered by mitogenic signalling pathways such as the RAS/RAF/MEK/ERK pathway (Wee and Wang, 2017, Albanese et al., 1995).

The key event that determines the G1-S transition is activation of the E2F transcription factor. The E2F transcription network includes hundreds of genes that encode proteins involved in cell cycle progression and DNA replication machinery assembly (DeGregori et al., 1995). The unphosphorylated form of pocket RB1 and its family members inhibit E2F before cells commit to DNA replication (Dyson, 1998, Chellappan et al., 1991). The classical view is that cyclin D-CDK4/6 activity first hyperphosphorylates RB1, leading to inactivation of RB1 and thus activation of E2F. E2F then leads to the expression of the E-type cyclin, cyclin E1 (gene product of CCNE1, hereafter referred to as cyclin E) (see also Chapter 1.2), that couples with CDK2 to further phosphorylate RB1, forming a positive feedback loop for E2F activation and making cells pass the irreversible 'restriction point' (Johnson and Skotheim, 2013, Skotheim et al., 2008, Bartek et al., 1996). However, this view has been challenged by recent studies showing that cyclin D-CDK4/6 only mono-phosphorylates RB1 and does not lead to activation of E2F, but rather RB1 hyper-phosphorylation is achieved by cyclin E-CDK2 only (Narasimha et al., 2014). One of the existing models hypothesises that cyclin D-CDK4/6 mono-phosphorylation of RB1 'primes' phosphorylation by cyclin E-CDK2 (Matthews et al., 2022, Sanidas et al., 2019, Narasimha et al., 2014). Moreover, recent data suggest that the mammalian 'restriction point' is not marked by RB1 hyper-phosphorylation. but rather a later point when the E3 ubiquitin ligase APC/C (anaphasepromoting complex/cyclosome) is inactivated (Cappell et al., 2016, Cappell et al., 2018). These studies show that the mammalian G1-S phase transition

remains an active field of research, and more studies are needed to elucidate the roles of specific events in its regulation.

E2F targets include genes that encode proteins in the pre-replication complex (pre-RC) such as MCM (minichromosome maintenance complex), CDT1 and CDC6 (Bracken et al., 2004). The pre-RC is assembled onto replication origins in G1 in a process called origin licensing. In mammalian cells, CDT1 is regulated by an additional inhibitor, geminin (Tada et al., 2001, Wohlschlegel et al., 2000). In G1, geminin is degraded by the CDH1 (gene product of *FZR1*, hereafter referred to as CDH1) form of APC/C (APC/CCDH1) to allow CDT1 to access the pre-RC, while it accumulates in S and G2 to prevent origin licensing and re-replication (Diffley, 2004). The APC/C associates with different co-activators in different cell cycle phases, in particular, CDH1 in G1 and CDC20 in mitosis (Kramer et al., 2000).

#### 1.1.2 G1 phase-related oncogenes and tumour suppressors

Genes involved in the cell cycle control are frequently mutated in cancer.

Genes in the G1 to S phase transition pathway are particularly prone to alterations during tumorigenesis because of their ability to modulate cell proliferation speed (Figure 1.1). The pathway includes proto-oncogenes such as genes encoding cyclin E (see also Chapter 1.2), MYC, CDC25A and RAS, which are often mutated to become hyperactivated or amplified to be overexpressed in cancer (Matthews et al., 2022). These activated oncogenes can lead to increased G1 CDK activities that accelerate E2F activation.

Tumour suppressors regulating G1-S phase transition, such as RB1 and p53

(gene product of *TP53*, hereafter referred to as p53), are frequently mutated or deleted to lose activity in cancer. Certain tumorigenic viruses secrete oncoproteins to disrupt the G1-S regulation (See also Chapter 1.4.3). For example, HPV E7 protein can associate with and inactivate RB1 and E6 protein can inactivate p53 (Jones and Munger, 1996, Crook et al., 1991).

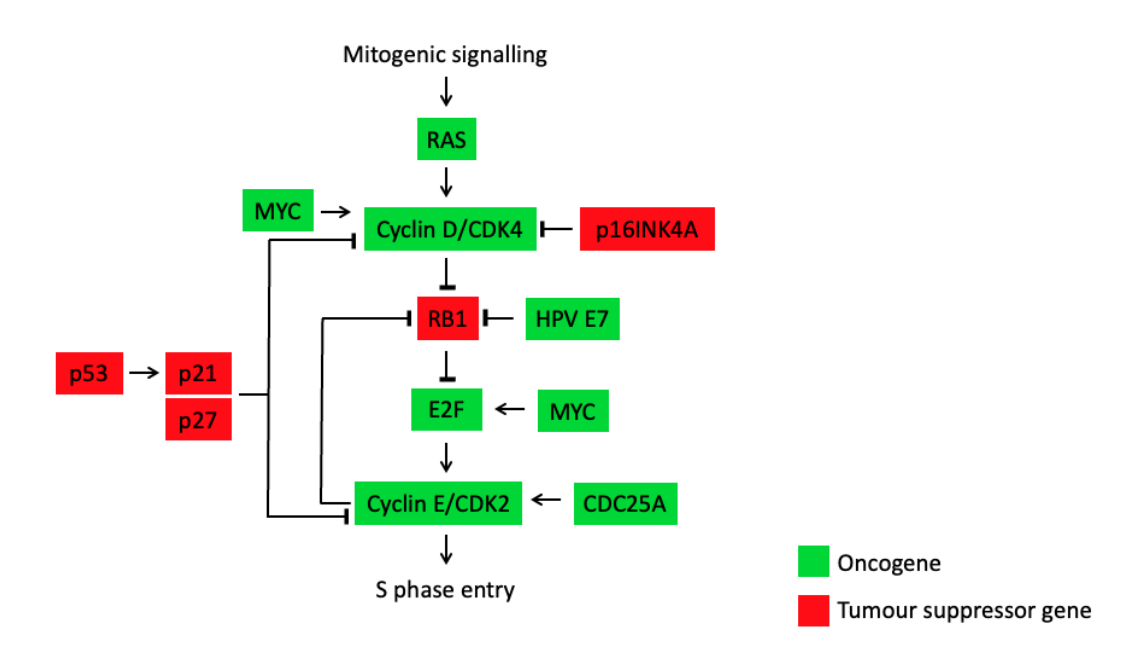


Figure 1.1 Oncogenes and tumour suppressor genes in the G1-S transition pathway.

A simplified model of the E2F G1-S transition pathway. Oncogenes are labelled in green. Tumour suppressor genes are labelled in red. The figure is created by Stephanie Hills.

#### 1.1.3 Mitotic entry and exit

Activation of CDK1 plays a central role in driving mitotic entry. Inhibition of CDK1 using chemical inhibitors arrests cells at the G2/M border (Vassilev, 2006). The activity of CDK1 is controlled at multiple layers (reviewed in (Crncec and Hochegger, 2019)). CDK1 requires association with cyclin A2 (gene product of *CCNA2*, hereafter referred to as cyclin A) or cyclin B1 (gene

product of *CCNB1*, hereafter referred to as cyclin B) (Pines and Hunt, 1987, Kobayashi et al., 1992). Cyclin A level remains high in S phase, while cyclin B accumulates in S phase and peaks around the end of S phase. CDK1 is also controlled by activating and inhibitory phosphorylations by different kinases. Cyclin H (gene product of *CCHN*)-CDK7, components of the CDK-activating kinase (CAK) complex, activates CDK by phosphorylating at T160 in the T-loop (Makela et al., 1994, Fisher and Morgan, 1994). Inhibitory phosphorylations at T14 and T15 are maintained by WEE1 and PKMYT1 kinases, with WEE1 being primarily responsible in somatic mammalian cells (Mueller et al., 1995, Gould and Nurse, 1989, Heald et al., 1993, McGowan and Russell, 1993, Parker and Piwnica-Worms, 1992). The removal of T14 and T15 inhibitory phosphorylations on CDK1, mediated by CDC25 phosphatases (CDC25A, B and C) (Kumagai and Dunphy, 1991), is the key event that triggers the mitotic switch.

Proteolytic turnover of cell cycle-related proteins is essential for successful and timely cell cycle transitions. The APC/C is responsible for cyclin destruction in mitosis (reviewed in (Peters, 2006)). Its activator CDC20 is expressed in G2 but can only associate efficiently with APC/C after subunits of APC/C become phosphorylated by CDK1 and to a lesser extent by PLK1 (Qiao et al., 2016, Kraft et al., 2003, Golan et al., 2002). In contrast, another activator of the APC/C, CDH1, is prevented from associating with APC/C by CDK (Jaspersen et al., 1999, Zachariae et al., 1998). Therefore, APC/C<sup>CDC20</sup> is assembled early in mitosis when CDK activity is high and initialises proteolysis of mitotic cyclins. This results in a drop in CDK activity and

creates a window for CDH1 to associate with APC/C at mitotic exit. CDC20 itself is then targeted for degradation by APC/C<sup>CDH1</sup> (Huang et al., 2001). The opposing effects of CDK activity on CDC20 and CDH1 ensures that the former is only active in mitosis while the latter is only active in G1.

#### 1.2 Cyclin E

#### 1.2.1 Cyclin E in normal physiology

Two E-type cyclins (cyclin E), cyclin E1 and cyclin E2, encoded by CCNE1 and CCNE2 genes respectively, exist in mammalian cells. The two E-type cyclins are thought to be largely functionally redundant, though cyclin E2 has been shown to play a major role in spermatogenesis (Martinerie et al., 2014). Coupled with CDK2, cyclin E drives G1 progression by hyperphosphorylating RB1 to release inhibition on the E2F transcription factor. Cyclin E itself is a direct target of E2F (Bracken et al., 2004), and therefore E2F activation by cyclin E-CDK2 leads to a positive feedback loop to reinforce its own expression (Bartek et al., 1996, Skotheim et al., 2008). In addition to RB1, cyclin E-CDK2 phosphorylates several other substrates and has important functions. Cyclin E-CDK2 can phosphorylate p27KIP1 (gene product of CDKN1B), an CDK inhibitor of its own, for proteasomal degradation (Sheaff et al., 1997), thereby amplifying its activity. This kinase activity may also be required to inactivate CDH1 in G1 (Cappell et al., 2016) to allow accumulation of the S-phase cyclin A which is targeted for degradation by APC/CCDH1 (Peters, 2006, den Elzen and Pines, 2001). However, in vitro work using purified proteins show that cyclin E-CDK2 does

not directly phosphorylate CDH1 or inhibit binding of CDH1 to APC/C (Lukas et al., 1999). Cyclin E-CDK2 plays a role in assembly of the pre-RC; the licensing factor CDC6 can be phosphorylated by cyclin E-CDK2 to be protected from proteolysis when cells exit G<sub>0</sub> (Mailand and Diffley, 2005). Other important functions of cyclin E-CDK2 activity include promoting duplication of centrosomes, histone biosynthesis, and regulating splicing programmes (Chu et al., 2021).

During S phase, cyclin E levels are regulated by two main pathways involving the ubiquitin-proteasome system. The first pathway involves the SCFFBXW7 ubiquitin ligase. FBXW7, a F-box protein that binds multiple factors involved in cell growth, is a substrate recognition component of SCF. Apart from cyclin E, substrates of SCFFBXW7 include MYC, JUN, NOTCH, and a few other oncoproteins (Yeh et al., 2018, Gupta-Rossi et al., 2001, Nateri et al., 2004, Yada et al., 2004, Strohmaier et al., 2001). Ubiquitination of cyclin E by SCFFBXW7 is triggered by multisite phosphorylation on cyclin E (Siu et al., 2012, Koepp et al., 2001, Welcker et al., 2003). Two kinase activities can phosphorylate cyclin E. Cyclin E-CDK2 auto-phosphorylates at T62, T380 and S384, and glycogen synthase kinase 3 (GSK3) phosphorylates at T380 (Welcker et al., 2003, Clurman et al., 1996). CDK2-bound, phosphorylated cyclin E can then be bound by FBXW7. The second degradation pathway involves the BCR (BTB-CUL3-RBX1) ubiquitin ligase that targets monomeric, unphosphorylated cyclin E (Siu et al., 2012, Singer et al., 1999).

Double deletion of *CCNE1* and *CCNE2* in mice leads to early embryonic lethality due to placental defects (Geng et al., 2003, Parisi et al., 2003). Absence of cyclin E causes defective endoreduplication of trophoblast giant cells, leading to placental failure, and reduces endoreduplication of megakaryocytes (Geng et al., 2003, Parisi et al., 2003). However, in postnatal mice, acute ablation of cyclin E does not lead to developmental defects or lethality, suggesting that cyclin E is not essential in adults (Geng et al., 2018). This is likely because other cyclins can compensate the loss of cyclin E in adults. Deletion of cyclin E homologues in *Drosophila* and *Caenorhabditis elegans* also reduces endoreduplication in certain organs and causes developmental defects (Chu et al., 2021, Knoblich et al., 1994, Fox et al., 2011). These suggest that cyclin E plays an evolutionarily conserved role in endoreduplication during development.

#### 1.2.2 Elevated cyclin E levels in cancer

Elevated levels of cyclin E have been reported in many cancers. Studies show high levels of cyclin E correlate with poor clinical outcome (Hwang and Clurman, 2005) and increased therapeutic resistance (Etemadmoghadam et al., 2009, Gorski et al., 2020). Three main mechanisms deregulate cyclin E expression in cancer. The first one is via increased E2F activity. Many oncogenes within the mitogenic signalling pathway or genes that regulate RB1 can lead to increased E2F-dependent cyclin E expression if mutated. The second mechanism is via gene amplification. Amplification of *CCNE1* and *CCNE2* is seen in ~8% of all cancers and can happen at a frequency of up to 25% in ovarian cancers and 12% in breast cancers (Chu et al., 2021).

Disrupted cyclin E proteolysis is another mechanism that leads to elevated cyclin E levels in cancer. *FBXW7* loss-of function mutations can disrupt interaction with cyclin E, thereby compromising ubiquitin-mediated proteolysis (Yeh et al., 2018, Koepp et al., 2001, Strohmaier et al., 2001, Welcker and Clurman, 2008). Loss of *FBXW7* alleles, which lie in 4q32, has also been reported (Spruck et al., 2002). In total, alterations in *FBXW7* occur in ~5% of all cancers (cBioPortal database) (Gao et al., 2013). Reduced CUL3 levels have also been observed in liver cancers (Kossatz et al., 2010). Additional mechanisms exist to deregulate cyclin E expression, including mutations in phospho-regulatory residues and overexpression of tissue-specific oncogenes such as *ELAVL1* in breast cancer and *GCN5* in lung cancer (Chu et al., 2021, Chen et al., 2013, Guo and Hartley, 2006).

#### 1.2.3 Cyclin E-induced replication stress and genome instability

Activated oncogenes cause replication stress, characterised by increased replication fork stalling and collapse (Hills and Diffley, 2014). Cyclin E overexpression is reported to cause replication stress (reviewed in (Fagundes and Teixeira, 2021)). This replication stress could result from a few mechanisms. One of the main mechanisms is via interfering with origin licensing. In normal cells, MCM becomes loaded onto replication origins mostly in G1. Elevated levels of cyclin E shorten the length of G1, lead to premature S phase entry, and therefore reduce the level of MCM loaded onto chromatin (Ekholm-Reed et al., 2004, Tanaka and Diffley, 2002, Matson et al., 2017). This impairs licensing mainly on origins in heterochromatic

regions, as licensing in heterochromatin takes longer than in euchromatin (Mei et al., 2022). Consequently, cyclin E-induced DNA damage signals are seen preferentially in heterochromatin. Interestingly, embryonic stem cells (ESC) have high levels of cyclin E and short G1 phase to keep them undifferentiated, as differentiation occurs when G1 phase becomes extended (Matson et al., 2017). It is unclear how ESCs maintain normal replication dynamics with such short G1 phase. On top of interfering with origin licensing, cyclin E overexpression may also induce replication stress by causing aberrant origin firing. Elevated levels of cyclin E have been shown to disrupt the location of origin firing, leading to firing at novel origins that map within active coding regions (Macheret and Halazonetis, 2018). This may lead to increased transcription-replication collisions and formation of R-loops. Consistently, inhibition of transcription or replication has been shown to reduce DNA damage markers in cyclin E-overexpressing cells (Jones et al., 2013). Another possible reason why replication stress is seen in cyclin Eoverexpressing cells is nucleotide deficiency (Bester et al., 2011). Nucleotide biosynthesis is a tightly regulated process and is essential for normal DNA replication. Since high levels of cyclin E lead to premature S phase entry, this does not allow sufficient nucleotide synthesis in the shortened G1 phase. As a consequence, cells replicate with comprised levels of nucleotides. DNA damage checkpoints (see also Chapter 1.3) are activated in response to oncogene-induced replication stress and are proposed as a first-in-line barrier to tumorigenesis (Bartkova et al., 2005). It is not entirely clear how cyclin E-driven cancers continue to develop in the presence of sustained replication stress and checkpoint activation.

Interference with DNA replication can cause genome instability, a hallmark of cancer that is observed in various forms such as chromosomal rearrangements, chromosome gains/losses, focal copy number alterations, and whole genome duplication (see also chapter 1.4). In experimental models overexpressing cyclin E, different forms of genome instability are observed (Fagundes and Teixeira, 2021), including chromosomal rearrangements, chromosome gains and losses, tandem duplications, and micronucleus formation (Mussman et al., 2000, Spruck et al., 1999, Menghi et al., 2018, Miron et al., 2015, Costantino et al., 2014, Teixeira et al., 2015). One study found that cyclin E-overexpressing cells accumulate large amount of extra DNA, to form a population of cells with >4N DNA content (Bartkova et al., 2005). This was attributed to partial re-replication but largely unexplored. Additionally, genomics studies looking at whole genome duplication in cancer patients show that tumours with CCNE1 amplifications are correlated with WGD (Bielski et al., 2018, Zack et al., 2013)(see also Chapter 1.6).

## 1.3 Cell cycle checkpoints

Cell cycle checkpoints are in place to prevent cells from accumulating and propagating genetic errors. Major cell cycle checkpoints include RB1-mediated G1-S checkpoint, intra-S DNA replication checkpoint, DNA damage checkpoint, and spindle assembly checkpoint (SAC) in mitosis. These checkpoints are mediated by distinct but in some cases overlapping signalling pathways in response to different forms of genotoxic stress, and

coordinate with DNA repair pathways to restore the integrity of genetic information.

#### 1.3.1 Sources of genotoxic stress

Each cell in our body experiences on average tens of thousands of DNA lesions daily (Lindahl and Barnes, 2000). These DNA lesions can come from either intrinsic or external sources. The most common form of intrinsic DNA lesion is perhaps hydrolytic depurination where the purines are lost from adenine or guanine, leaving an abasic site on the DNA (Lindahl, 1993). This can happen spontaneously under physiological conditions due to the intrinsic fragility of the N-glycosidic bond. It is estimated that in each cell spontaneous depurination occurs around 2,000-10,000 times per day (Lindahl and Nyberg, 1972). DNA replication itself is not error-free and can generate base mismatches. Normal cellular metabolism can produce toxic by-products such as reactive oxygen species (ROS) that can lead to DNA modifications. External environmental sources, such as ultraviolet (UV) radiation from sunlight, chemicals from cigarette smoke and alcohol metabolites from wines and beers, can also lead to DNA damage and cause mutations that enhance cancer risk (Hoeijmakers, 2001). Most of these sources can attack DNA, leading to abasic sites, adducts, or single-stranded breaks (SSBs). SSBs also accumulate if the DNA replication polymerase activity is inhibited and uncouples from the unwinding activity of the DNA replication helicase (Byun et al., 2005). When two SSBs arise in close proximity, or the DNA replication machinery encounters SSBs, double-stranded breaks (DSBs) can form (Jackson and Bartek, 2009). DSBs can also be directly induced by ionising

radiation and some chemicals. Although DSBs occur less frequently than SSBs, they are considered extremely toxic and difficult to repair (Khanna and Jackson, 2001). Mutations may arise in cells exposed to these DNA damaging sources and eventually activate oncogenes, causing persistence replication stress that further compromises the DNA.

#### 1.3.2 DNA damage checkpoint

The ataxia-telangiectasia (A-T) mutated (ATM) kinase, a member of the phosphoinositide 3-kinase-related kinases (PIKKs) family, is the centre for mediating global cellular responses to DSBs, which include cell cycle arrest, DNA repair, senescence, and apoptosis (reviewed in (Marechal and Zou, 2013, Blackford and Jackson, 2017)). Cells deficient in ATM derived from A-T patients are defective in DSB repair (Savitsky et al., 1995, Taylor et al., 1976). ATM is recruited by the MRN complex (MRE11-RAD50-NBS1) to sites of DSBs and evidence shows that the MRN complex also activates ATM (Lee and Paull, 2005, Uziel et al., 2003). Activated ATM phosphorylates a cascade of substrates including H2AX, CHK2, BRCA1, and p53. Phosphorylation of the histone variant H2AX by ATM, to form  $\gamma$ H2AX, is reported to occur within minutes after induction of DSBs, and spread over 500 kb chromatin areas flaking the DSB sites (Savic et al., 2009, Meier et al., 2007). These long tracks of γH2AX are shown to promote accumulation of DNA repair proteins and chromatin-remodelling proteins (Marechal and Zou, 2013). Key targets of ATM for cell cycle control include p53 and CHK2 (Banin et al., 1998, Matsuoka et al., 1998, Ahn et al., 2000). In G2, the CHK2 effector kinase phosphorylates CDC25, a phosphatase that removes

inhibitory phosphorylations from CDK1, for degradation (Falck et al., 2001). This allows WEE1 kinase to introduce inhibitory phosphorylations on CDK1, thereby preventing mitotic entry (Gould and Nurse, 1989, Heald et al., 1993, McGowan and Russell, 1993, Parker and Piwnica-Worms, 1992). In addition, checkpoint-dependent p53 activation induces expression of the CDK inhibitor p21CIP1 (gene product of *CDKN1A*, hereafter referred to as p21) (el-Deiry et al., 1993), which is reported to inhibit several CDK activities during interphase (see also chapter 1.4).

Another kinase involved in DSB repair is DNA-PKcs (gene product of *PRKDC*, hereafter referred to as DNA-PKcs), though DNA-PKcs appears to regulate primarily nonhomologous end joining (NHEJ) (reviewed in (Marechal and Zou, 2013, Blackford and Jackson, 2017)). DNA-PKcs is recruited and activated by the KU complex which has a basket structure that accommodates DSB ends (Walker et al., 2001).

#### 1.3.3 The replication checkpoint

The replication checkpoint (also referred to as the intra-S phase checkpoint) functions in S phase when replication forks encounter impediments and SSBs are exposed (reviewed in (Marechal and Zou, 2013, Blackford and Jackson, 2017, Saldivar et al., 2017)). Replication protein A (RPA)-coated ssDNA is an activation signal for the checkpoint kinase ATR (ataxiatelangiectasia and Rad3-related), another member of PIKK family (Zou and Elledge, 2003). ATR is supposed to be activated in response to a wider range of genotoxic stresses than ATM, because ssDNA is generated in the

process of repairing various forms of damage including DSBs (Blackford and Jackson, 2017, Raderschall et al., 1999). Unlike ATM, ATR is essential in dividing cells (Brown and Baltimore, 2000, de Klein et al., 2000), potentially because of its role in maintaining replication fork stability (Lopes et al., 2001). ATR is recruited to RPA-coated ssDNA by a partner protein ATRIP, and activated by activator proteins such as TOPBP1 (Kumagai et al., 2006). A key downstream target of ATR is the effector checkpoint kinase CHK1 (Hekmat-Nejad et al., 2000, Guo et al., 2000). Phosphorylation on serines 317 and 345 of CHK1 by ATR is required for CHK1 activation and typically used as markers for ATR activation (Zhao and Piwnica-Worms, 2001). Like the CHK2 kinase, CHK1 can also phosphorylate CDC25, leading to inhibition of CDK1 and G2 arrest (Sorensen et al., 2003, Zhao et al., 2002). As mentioned earlier, DSBs can also lead to ATR activation. This is because DNA end resection during DSB repair generates RPA-coated ssDNA intermediates, which act as activation signals for ATR (Marechal and Zou, 2013, Jazayeri et al., 2006, Myers and Cortez, 2006). It is thought that both ATM and ATR contribute to the maintenance of intra-S and G2/M checkpoints. However, the G1/S checkpoint is maintained primarily by ATM because in G1, DSBs are not resected significantly to activate ATR (Blackford and Jackson, 2017, Jazayeri et al., 2006). p53 appears to be at the centre of both ATM and ATR-mediated DNA damage response pathways, as ATM/ATR and CHK1/CHK2 can all phosphorylate and stabilise p53 (Ou et al., 2005).

## 1.4 Tumour suppressor p53

#### 1.4.1 Overview

The p53 transcription factor, a 53 kDa polypeptide encoded by the *TP53* gene in human, is a tumour suppressor and the most studied gene of all time with 110,000+ entries on PubMed as of October 2022. *TP53* is also the most frequently mutated gene in human cancer, with 36% of tumours harbouring *TP53* mutations (TCGA PanCancer Atlas Studies). p53 is involved in regulation of a variety of stress-induced cellular responses, including cell cycle arrest, apoptosis, DNA repair, senescence, and differentiation (Vousden and Lu, 2002). Despite its importance and high popularity in research, there are many unsolved mysteries about p53. This section will provide a general overview on the current understanding of the function and regulation of p53.

The p53 gene is evolutionarily conserved and there are five highly conserved regions, termed domains I-V (Soussi and May, 1996). These conserved regions are expected to be functionally important for p53 and are mutation hotspots in cancer. The human p53 protein has 393 amino acids and is divided into 4 major functional domains: a transcriptional activation domain (TAD) at the N-terminus, a central DNA binding domain, a tetramerisation domain and a regulatory domain at the C-terminus. p53 monomers interact via the tetramerisation domain to form oligomers (Soussi and May, 1996). Under unstressed conditions, p53 exists primarily as dimers (Gaglia et al., 2013). Genotoxic stress increases p53 concentration in cells and this induces dimers to form tetramers. p53 tetramers recognise specific p53 response elements with a symmetrical consensus sequence containing two

copies of the 10 bp motif RRRC(A/T)(T/A)GYYY (in which R=purine and Y= pyrimidine), separated by a spacer of 0-13 bp (Bieging et al., 2014, el-Deiry et al., 1992). It is shown that one copy of the consensus motif is not sufficient for p53 binding and p53 monomers do not bind to DNA efficiently, suggesting tetramerisation is crucial for p53 function (May and May, 1999, Pietenpol et al., 1994, Kraiss et al., 1988). There are ~14,000-21,000 predicted p53 binding sites in the human genome depending on the prediction model used, but only a small fraction of these sites is situated in gene promoters (Hafner et al., 2019, Hafner et al., 2020, Verfaillie et al., 2016, Wei et al., 2006). Transcriptional profiling studies show that ~100-1500 genes are affected by p53, depending on activation signals, though these studies do not differentiate between direct and indirect p53 targets (Hafner et al., 2019, Madden et al., 1997, Mirza et al., 2003).

p53 is regulated by posttranslational modifications (PTMs). There are over 300 p53 PTMs detected by mass spectrometry including phosphorylation, methylation, acetylation, and ubiquitination (Hafner et al., 2019, DeHart et al., 2014). In unstressed conditions, p53 is degraded by the E3 ubiquitin ligase MDM2 (Honda et al., 1997, Kubbutat et al., 1997, Haupt et al., 1997). MDM2 ubiquitin ligase activity recognises the N-terminal TAD domain of p53 and on top of that MDM2 can act as a direct inhibitor of p53 activity. MDM2 is a direct target of p53 transcriptional activity, thereby forming a negative feedback loop to keep p53 level low under unstressed conditions (Barak et al., 1993). In the presence of DNA damage signals, phosphorylation by checkpoint kinases within the MDM2-binding site in p53 stabilises p53 by

interfering with MDM2 binding (Shieh et al., 1997). ATR, CHK1, ATM, CHK2 and DNA-PKcs can all phosphorylate the N-terminus of p53 (Ou et al., 2005). p53 PTMs can be specific to types of DNA damage and lead to different cell fate decisions (Hafner et al., 2019, Maki and Howley, 1997, Kapoor and Lozano, 1998, Appella and Anderson, 2001). For example, phosphorylation on serine 15 by checkpoint kinases has been shown to be required for cell cycle arrest (Tibbetts et al., 1999, Siliciano et al., 1997). In addition, activities of p53 and RB, are modulated by two products of the *CDKN2A* locus, p16INK4a and p14ARF (p19<sup>ARF</sup> homologue in mouse), both of which are tumour suppressors (Sherr and Weber, 2000, Quelle et al., 1995). p16INK4a functions by inhibiting the G1 kinase CDK4/6, thereby preventing RB1 phosphorylation, whereas p14ARF sequesters MDM2 and antagonises MDM2 ubiquitin ligase activity to enhance p53 level (Pomerantz et al., 1998, Stott et al., 1998).

#### 1.4.2 p53-mediated cell cycle arrest

p53 can provoke a range of cellular responses to stress such as cell cycle arrest, apoptosis, and senescence. How p53 balances these cell fate decisions is an ongoing puzzle in the field (reviewed in (Hafner et al., 2019)). One model for p53-mediated cell fate decision is the 'affinity model', which postulates that p53 induces expression of genes for apoptosis and cell cycle arrest at different concentrations. Studies have shown that genes implicated in cell cycle arrest have promoters with strong p53 binding sites, whereas those implicated in apoptosis are predicted to have low-affinity promoters (Chen et al., 1996b, Schlereth et al., 2010). Another model suggests

chromatin structure determines p53 binding, based on findings showing that p53 has higher affinity for chromatin than DNA oligonucleotides (Espinosa and Emerson, 2001). Also as previously mentioned, different p53 PTMs may lead to expression of different genes. This section will focus on discussing targets of p53 involved in mediating cell cycle arrest.

The p21CIP1 CDK inhibitor (gene product of *CDKN1A*, hereafter referred to as p21), encoded by CDKN1A, is a major target of p53 involved in cell cycle regulation (reviewed in (Abbas and Dutta, 2009)). p21 is a member of the CIP/KIP family of CDK inhibitors that include also p27 and p57. p21 binds to and inhibits cyclins via a N-terminal Cy1 motif and a weaker C-terminal Cy2 motif. It can also bind to CDKs through a N-terminal CDK binding motif (Chen et al., 1996a). Via these motifs, p21 inhibits CDK activities by disrupting cyclin-CDK interactions. p21 can also block activating phosphorylations on CDKs from CAK in an unknown mechanism (Smits et al., 2000). p53-dependent p21 expression is mostly seen in G1, G2 and M phases because in S phase, p21 is downregulated by PCNA-dependent degradation through the ubiquitin ligase CRL<sup>CDT2</sup> (Abbas et al., 2008). *In vitro* kinase assays and binding assays show that p21 is a potent inhibitor of G1 CDKs, CDK2 and CDK4/6 (K<sub>i</sub> ~0.5-15 nM), but is less effective towards the G2 CDK cyclin B-CDK1 (K<sub>i</sub> ~400 nM) (Harper et al., 1995). It is therefore assumed that p21 is mostly involved in G1 arrest in response to DNA damage. Nonetheless, it is shown that in CDK2<sup>-/-</sup> cells, CDK1 can compensate CDK2 activity and p21 inhibition of CDK1 is important for G1 arrest in response to DNA damage (Satyanarayana et al., 2008), suggesting

p21 can inhibit CDK1 activity in cells. However, the role of p21 in G2/M checkpoint is unclear; deletion of p53 or p21 leads to aberrant mitosis after DNA damage (Bunz et al., 1998) but overexpression of p21 in G2 leads to endoreduplication (Bates et al., 1998).

Other transcriptional targets of p53 involved in cell cycle arrest include 14-3-3σ (gene product of *SFN*, hereafter referred to as 14-3-3σ) and GADD45A (reviewed in (Taylor and Stark, 2001)). Both proteins are reported to be involved in regulating G2/M transition. Expression of both proteins in response to DNA damage is in a p53-dependent manner. Dephosphorylation by CDC25 and nuclear translocation of cyclin B-CDK1 is a key step to initiate mitosis (Moore et al., 1999). 14-3-3σ arrests cells in G2 by binding to phosphorylated cyclin B-CDK1 and sequestering them in the cytoplasm (Hermeking et al., 1997). GADD45A has been shown to bind to CDK1 and block its interaction with cyclin B (Zhan et al., 1999). Microinjection of GADD45A protein into human cells arrests them in early prophase before nuclear envelope breakdown (Wang et al., 1999).

#### 1.4.3 Perturbation of the p53 pathway in cancer

The p53 tumour suppressor, encoded by the *TP53* gene in human, is mutated in around 30-40% of all human tumours, making p53 mutation the most frequent event during tumorigenesis (Olivier et al., 2010). Unlike most tumour suppressors which are usually inactivated by deletions or nonsense mutations, p53 mutations are mostly missense mutations that leaves a single amino acid change (a point mutation) in the protein sequence (Figure 1.2). In

fact, p53 was originally considered an oncogene in the first decade of its discovery, because overexpression of p53 mutants could transform cells and was tumorigenic in mice (Hinds et al., 1990, Hinds et al., 1989, Levine and Oren, 2009, Linzer and Levine, 1979, Lane and Crawford, 1979, Oren and Levine, 1983). Later this was attributed to the dominant negative effect (DNE) of p53 mutants; mutant forms of p53 can inhibit the remaining wild-type allele by formation of mutant/wild-type co-tetramers (Friedman et al., 1993, Gaglia et al., 2013). In a cell with equal copies of p53 wild-type protein and p53 mutant protein, wild-type tetramers should only consist of 1/16 of all tetramer combinations, though studies have shown that 3 copies of mutant p53 protein are needed in a tetramer to fully abolish p53 activity (Chan et al., 2004).

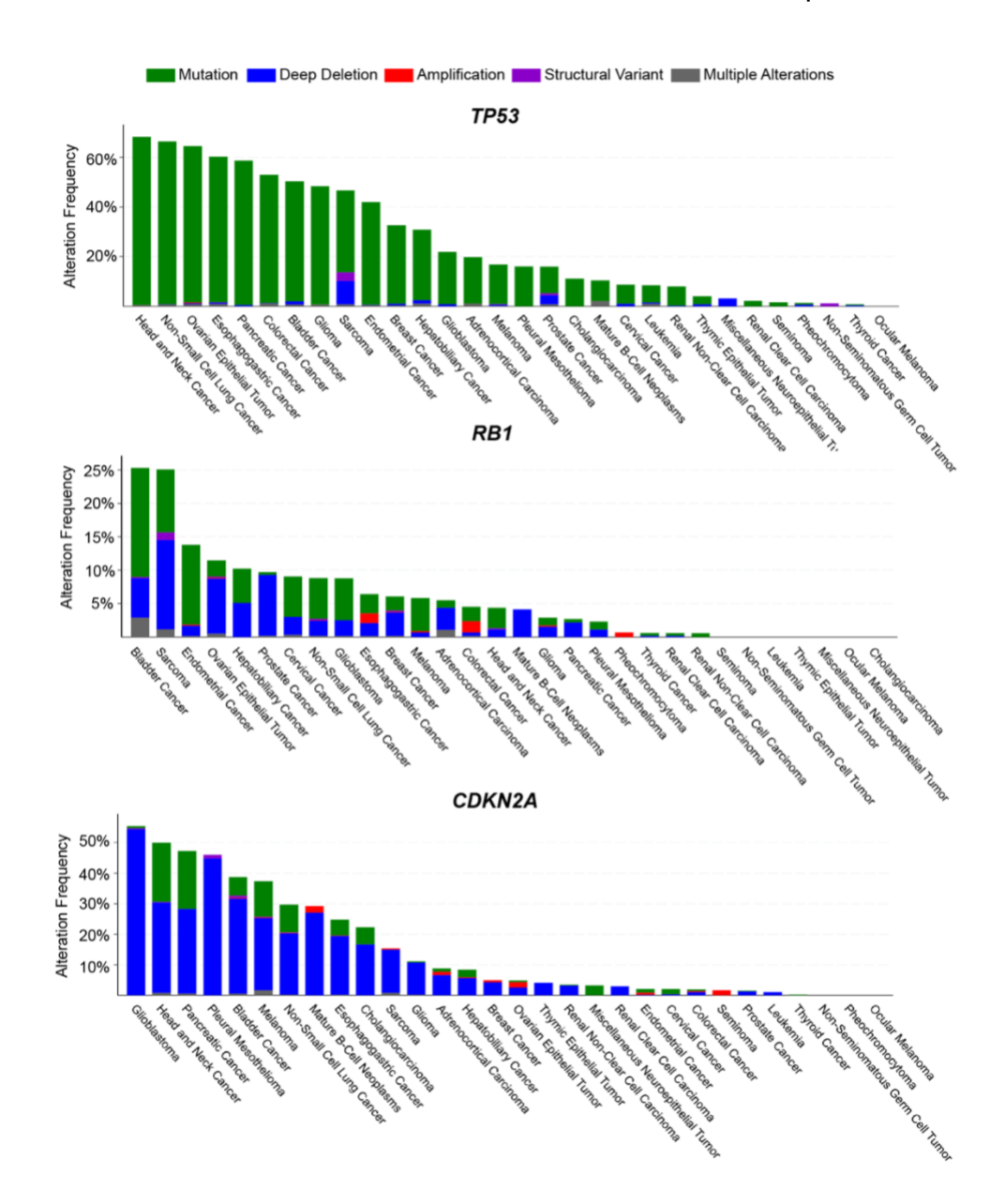


Figure 1.2 Frequencies of different alterations of selected tumour suppressors in cancer.

Visualisation is generated using cBioPortal analysis tool. The x-axis shows different tumour types and the y-axis shows alteration frequency. Deep Deletion indicates a possible homozygous deletion as defined by cBioPortal.

Moreover, mutant p53 is shown to accumulate to high levels in cancer (Sigal and Rotter, 2000, Benchimol et al., 1982, Bartek et al., 1991), although why mutant p53 is not degraded is not fully clear. Some studies suggest MDM2 ubiquitination of mutant p53 is less efficient than wild type (Lukashchuk and Vousden, 2007) and heat shock proteins can protect mutant p53 form

degradation (Vijayakumaran et al., 2015, Li et al., 2011). The majority of p53 mutations occur in the DNA-binding domain that disrupt the ability to bind promoters and transactivate targets. Mutations in 6 of the 'hotspots' (R248, R273, R175, G245, R249, R282) in the DNA-binding domain constitute around 30% of all p53 mutations (Freed-Pastor and Prives, 2012). It is shown that the hotspot sites are prone to being mutated because of the inherent mutability of their encoding DNA sequences (Giacomelli et al., 2018) rather than providing greater survival advantage for tumours.

It is proposed that mutant p53 can have gain-of-function (GOF) activity in addition to acting as dominant negative inhibitors of wild-type p53. This is evidenced by studies showing that expression of p53 mutants in p53-null cells significantly increases their ability to form tumours in mice (Wolf et al., 1984, Dittmer et al., 1993). Studies also suggest mutant p53 can rewire cancer cells' metabolism (Mantovani et al., 2019). However, these studies do not necessarily show that the neomorphic activities of p53 mutant proteins are required for tumorigenesis. It is possible that p53 mutants may lose the ability to transactivate downstream tumour suppressors while retaining other aspects of wild-type function (Freed-Pastor and Prives, 2012, Jordan et al., 2008, Resnick and Inga, 2003, Kato et al., 2003, Di Como and Prives, 1998). It is also possible that residual transactivation activities of p53 mutant proteins (Kakudo et al., 2005, Kawaguchi et al., 2005) may offer tumour cells advantages and protection against adverse events considering that p53 is involved in DNA repair and genome maintenance.

In tumours that retain wild type copies of p53, p53 activity can be directly or indirectly inhibited by several other mechanisms, it can be dampened by viral effectors. About 15% of human cancers are induced by viruses (Plummer et al., 2016) and many of these tumorigenic viruses produce oncoproteins that inactivate p53. In fact, p53 was first discovered in a complex with a viral oncoprotein, the simian virus 40 large T-antigen (SV40LT) (Lane and Crawford, 1979, Linzer and Levine, 1979), which directly binds to and inhibits p53 transactivation activity. Several DNA tumour viruses encode proteins that directly binds to p53, such as human papilloma virus (HPV) E6 protein, adenovirus E1B protein, Epstein-Barr virus (EBV) BZLF1 protein and hepatitis C virus (HCV) NS5 protein (Levine, 2009, Tornesello et al., 2018, Lan et al., 2002, Sato et al., 2009, Sarnow et al., 1982, Martinez-Zapien et al., 2016). Other viral oncoproteins can indirectly inhibit p53-dependent transcription. For example, the Tax oncoprotein produced by the human T cell lymphotropic virus-1 (HTLV-1) can reduce p53 activity by modulating its cofactor p300/CBP (Zane et al., 2012).

Other alternative mechanisms of p53 deregulation include MDM2 gene amplification and ARF gene silencing/deletion. The gene that encodes MDM2, an E3 ubiquitin ligase that degrades p53, is amplified in ~7% human tumours overall (Momand et al., 1998). The p14ARF tumour suppressor, encoded by the *CDKN2A* locus, prevents binding of MDM2 to p53 (Pomerantz et al., 1998, Stott et al., 1998). The promoter region of the p14ARF gene has CpG islands and can be methylated to silence p14ARF expression. Hyper-methylation in the p14ARF promoter region is very

common in cancer and the frequency reaches up to 50% in certain types of cancer (Ozenne et al., 2010). Homozygous deletions of *CDKN2A* are also seen in a range of tumours (Sharpless, 2005).

## 1.5 Two types of aneuploidy in cancer: chromosomal instability and whole genome duplication

Tumours often develop chromosome abnormalities during evolution. Such abnormalities are extremely complex and diverse, contributing to tumour heterogeneity (Burrell et al., 2013). Indeed, on top of numerical changes in whole chromosomes, structural changes such as chromosome arm deletions, amplifications and translocations can occur. In this section, I will focus on describing whole chromosome number changes and refer to such changes as aneuploidy.

Aneuploidy is seen in almost 90% of human cancers (Taylor et al., 2018). In many tumours, only a few chromosomes are gained or lost, having near-diploid karyotypes. Such changes are often attributed to chromosome instability (CIN), characterised by an elevated rate in chromosome gain or loss (Holland and Cleveland, 2009, Lengauer et al., 1997). CIN can be explained by errors in sister chromatid separation in mitosis, although the primary mechanism for CIN in cancer is unclear (Davoli and de Lange, 2011). Several mechanisms for CIN in cultured cells have been described. Defects in mitotic checkpoint signalling pathway can lead to CIN (Cahill et al., 1998). Under normal conditions, the spindle assembly checkpoint (SAC) delays mitotic progression upon detection of a single unattached kinetochore

(Rieder et al., 1995, Lara-Gonzalez et al., 2012). Inhibition of SAC can initiate premature anaphase before proper spindle attachments, leading to chromosome missegregation (Kops et al., 2004). However, mutations in the SAC components are only seen in a relatively minor proportion of aneuploid human cancers (Holland and Cleveland, 2009, Thompson et al., 2010). Defects in chromosome cohesion underlie another mechanism for CIN. Sister chromatids are held together during cohesion establishment in S phase and are separated in mitosis (Uhlmann et al., 1999). Depletion of cohesion subunits or overexpression of separase (gene product of ESPL1) causes cohesion defects and cytokinesis failure, although alterations in genes for cohesion pathways are also relatively rare in cancer (Thompson et al., 2010, Zhang et al., 2008, Barber et al., 2008, Greenman et al., 2007). Formation of supernumerary centrosomes can lead to lagging chromosomes, possibly the most common mitotic defects observed in human can cell lines with CIN (Thompson and Compton, 2008, Ganem et al., 2009). Supernumerary centrosomes can be generated either by deregulated centrosome duplication cycle or as a by-product of polyploidisation (Thompson et al., 2010, Lentini et al., 2007, Ganem et al., 2009). Cells undergoing tetraploidisation duplicate both their DNA and centrosomes twice before mitosis, potentially leading to a very unstable anaphase. Indeed, tetraploid cells frequently have multipolar spindles and lagging chromosomes (Ganem et al., 2009).

In many tumours, chromosome numbers are much higher, with ploidies often seen as hyper-triploid or sub-tetraploid, which cannot be explained by CIN. Such extensive aneuploidies likely transitioned from a tetraploid intermediate (Davoli and de Lange, 2011), generated in a process called whole genome duplication/doubling (WGD), with concomitant or subsequent chromosome loss. In certain tumours there is direct evidence of a transient tetraploid state (Davoli and de Lange, 2011, Galipeau et al., 1996, Reid et al., 1996).

Genomics studies show WGD occur in approximately 30-40% of human cancers (Zack et al., 2013, Bielski et al., 2018, Quinton et al., 2021), making it one of the most frequent macro-genomic events during tumorigenesis.

Patients with tumours that have undergone WGD have worse prognosis than patients with diploid tumours across almost all cancer types. Thus, it is important to understand the causes and consequences of WGD in cancer biology. In section 1.6, I will discuss in more detail about the current understanding of WGD.

## 1.6 Whole genome duplication

#### 1.6.1 Routes to WGD: cell fusion, mitotic defects, and mitotic bypass

Three distinct mechanisms for generating WGD have been described experimentally: cell-cell fusion, detects in mitosis and mitotic bypass/endoreduplication following telomere damage or DSBs (Duelli et al., 2007a, Davoli et al., 2010, Ganem et al., 2007) (Figure 1.3). Whether these are the only mechanisms for generating WGD in cancer and how prevalent each mechanism is in oncogenesis is largely unknown.

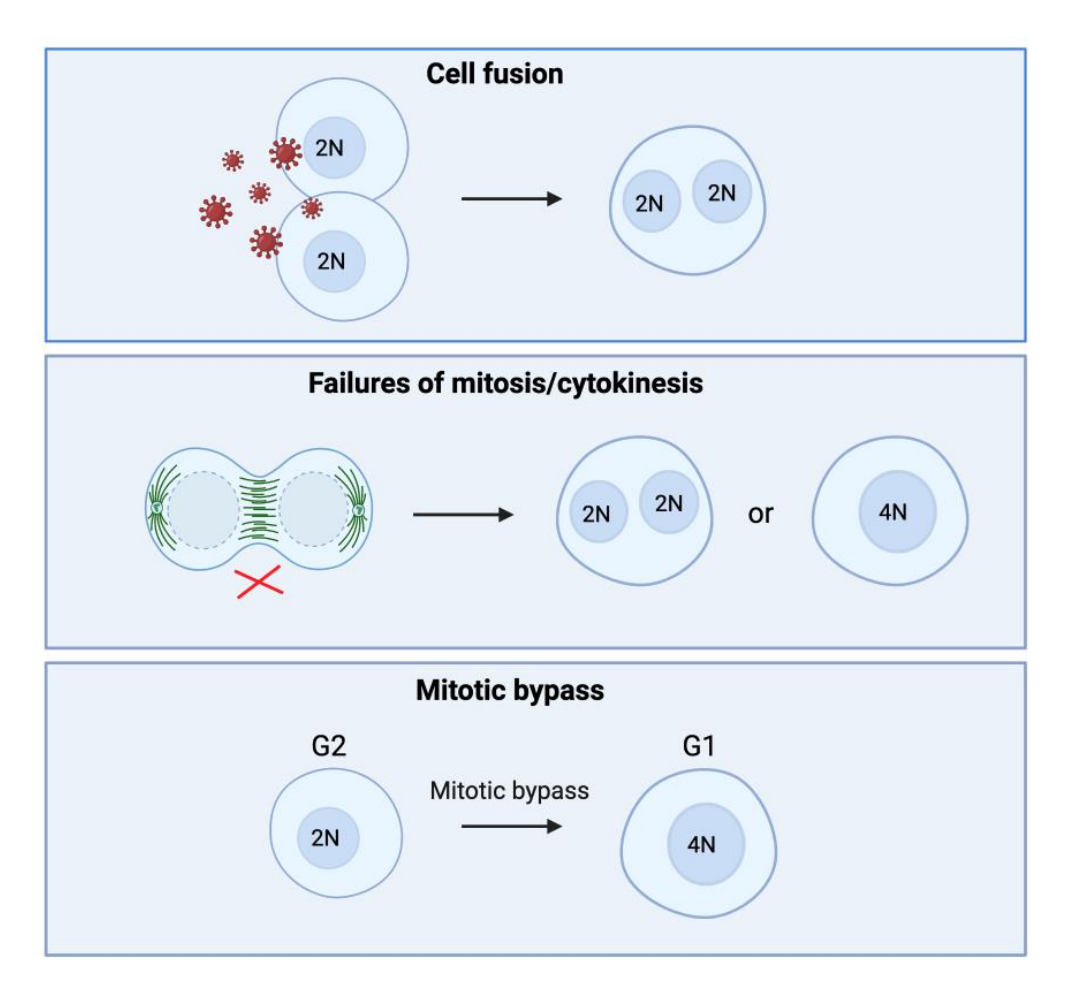


Figure 1.3 Three experimentally described pathways to WGD.

Infection by many human viruses such as HPV, which causes nearly all cervical cancers, can induce cell-cell fusion *in vivo* and *in vitro* (Duelli et al., 2007b). Enveloped viruses enter the cell by fusion of membranes with the help of viral proteins. A common side consequence of this is that it can cause fusion of a surrounding cell with the infected cell. This generates a binucleate cell, but the two nuclei can merge after nuclear envelope breakdown in the subsequent mitosis to generate a tetraploid nucleus. Many oncogenic viruses not only cause cell fusion, but also produce viral factors that deregulate the cell cycle or inhibit tumour suppressors (Duelli et al., 2007b). Take HPV for

example, it produces E5 protein that causes cell fusion and E6 protein that inhibits p53 (Hu et al., 2009).

Failing to complete or exit mitosis can lead to WGD, via two main events, cytokinesis failure or mitotic slippage (reviewed in (Davoli and de Lange, 2011)). Overexpression of a number of proteins including MAD2, EMI1 and aurora kinase A (gene product of AURKA) has been shown to cause cytokinesis failure in cultured cells (Sotillo et al., 2007, Lehman et al., 2006). Inhibition of LATS1, a kinase involved in actin polymerisation in mitosis, also leads to cytokinesis failure (Yang et al., 2004). Cells experiencing persistent lagging chromosomes can also fail cytokinesis because the cleavage furrow can regress (Mullins and Biesele, 1977). Considering that many genetic defects result in lagging chromosomes, cytokinesis failure is likely a common mechanism for WGD (Davoli and de Lange, 2011). Another possible mechanism for WGD via a failed mitosis is mitotic slippage. Mitotic slippage occurs when cells are stuck earlier in mitosis. This can be induced by nocodazole, a chemical that interferes with the dynamics of microtubule polymerisation (Jordan et al., 1992). Nocodazole-treated cells cannot form mitotic spindles and unattached kinetochores activate the spindle assembly checkpoint (SAC), causing cells to arrest in prometaphase (Brito and Rieder, 2006). During prolonged SAC activation, the G2/M cyclin B is gradually degraded via a proteasome-mediated pathway independent of the mitotic and G1 E3 ubiquitin ligases APC/CCDC20 and APC/CCDH1 (Brito and Rieder, 2006). Instead, cyclin B degradation during mitotic slippage is likely mediated by CRL2<sup>ZYG11</sup>, a E3 ubiquitin ligase redundant for normal mitosis (Balachandran et al., 2016).

Mitotic bypass and endoreduplication have been observed in vitro in cells experiencing persistent telomere damage or double strand DNA breaks (Davoli et al., 2010, Davoli and de Lange, 2012). Short telomeres are recognised as sites of DNA damage, activating both ATM/CHK2 and ATR/CHK1 signalling (Davoli and de Lange, 2011). If the damage signal lasts for an extended period of time, after prolonged G2 arrest imposed by checkpoint activation, the cells ultimately degrade cyclin B, bypass mitosis, and enter a G1-like state (Davoli et al., 2010). The difference between mitotic bypass and mitotic slippage is that mitotic bypass occurs without nuclear envelope breakdown or any other signs of mitosis. Because of checkpoint inhibition of cyclin B/CDK1 activity, cells cannot enter mitosis. Since cyclin B/CDK1 represses the CDH1 form of APC/C (Jaspersen et al., 1999. Zachariae et al., 1998), CDK inhibition by the checkpoint creates a permissive setting for APC/CCDH1 activation, which ultimately degrades cyclin B and allows cells to enter a G1-like state (Davoli et al., 2010). APC/CCDC20 is not activated, and therefore the duplicated sister chromatids remain linked, resulting in diplochromosomes in the following mitosis (Davoli et al., 2010). However, DSB- and telomere attrition-induced endoreduplication only happens in p53 deficient cells, as p53 activates a G1 arrest following DNA damage.

#### 1.6.2 Role of p53 in regulating ploidy

p53 is known as the guardian of ploidy. p53 deficient tumours frequently have abnormal karyotypes, and tetraploid cells experimentally induced by mitotic failure undergo a p53-dependent tetraploid G1 arrest (Andreassen et al., 2001). However, it is not understood how p53 is activated in response to aneuploidy and it remains controversial whether a p53-dependent tetraploid checkpoint exists. It is unlikely that p53 can sense the number of chromosomes per se, as many aneuploid tumours have wild type p53. Instead, Soto et al shows that p53 prohibits growth of cells with structural aneuploidies but not numerical aneuploidies after mitotic failure (Soto et al., 2017), suggesting that chromosome number change does not act as a signal for p53 activation. It also suggests p53 activation in aneuploid cells is potentially due to stress signals caused by chromosome structural aberrations such as arm breakages. Other signalling pathways may also be triggered during WGD to activate p53. Ganem et al shows that the Hippo pathway is triggered by abnormal centrosomes after cytokinesis failure to activate LATS2 kinase that in turn stabilises p53 (Ganem et al., 2014). These studies suggest that p53 does not respond to tetraploidy per se, but rather becomes activated by DNA damage and other errors generated in the process of WGD.

#### 1.6.3 Genetic correlation with WGD in cancer

WGD is one of the most common events in cancer and is observed in 30-40% of human cancers (Bielski et al., 2018). It also predicts worse overall survival rate across all cancer types; patients with WGD tumours die on average 20% faster than patients with diploid tumours. The median ploidy of

tumours, in a cohort of 9,000+ patients, that have undergone WGD is 3.3 (Bielski et al., 2018), suggesting tumours tend to lose chromosomes after WGD.

WGD is proposed to occur after a driver mutation (Bielski et al., 2018, Zack et al., 2013). ~40% of WGD tumours harbour TP53 mutations. But more than half WGD tumours have wild-type p53, suggesting p53 deficiency is not necessary for WGD to occur. In WGD tumours with wild-type p53, defects in the regulation of the E2F pathway are frequently seen (31.8% of all p53 wildtype WGD tumours), among which amplifications of CCNE1 and loss of RB1 are strongly associated (Bielski et al., 2018). Amplifications of CCND1 are also modestly associated. Despite a genetic link, the molecular or cellular mechanisms by which these alterations lead to WGD are not clear. Alterations in several genes previously shown to cause WGD by mitotic failure in experimental models are not associated with WGD in genomics studies, including mutations in *LATS1* and *AURKA* (Bielski et al., 2018). Telomere attrition has been shown to induce endoreduplication in p53negative cells, but there is no association between telomere length or mutations in telomerase promoter with WGD in patients (Bielski et al., 2018). Therefore, further studies are needed to provide mechanistic insights into how WGD arises under different genetic alterations.

## 1.7 Senescence

#### 1.7.1 Induction of senescence

Senescence is a cellular state characterised by permanent cell cycle arrest and dramatic changes in metabolic activity and cell morphology (reviewed in (Kuilman et al., 2010)). Two types of senescence, replication senescence and premature senescence, are observed in vitro. Telomeres get shortened as cells propagate in cell culture, eventually causing cells to reach their 'Hayflick limit' and enter replication senescence (Hayflick, 1965). Oncogene activation or genotoxic agents can cause cells to enter premature senescence (Land et al., 1983, Johnura et al., 2014, Chen and Ames, 1994). Both replication senescence and premature senescence are initiated by persistent DNA damage response (DDR); overly short telomeres are recognised as DNA breaks and oncogene activation causes replication stress (Davoli and de Lange, 2011, d'Adda di Fagagna et al., 2003). These activate p53-p21 via ATM/ATR-mediated checkpoint signalling, leading to cell cycle arrest (Ou et al., 2005). The CDK inhibitor p21 inhibits G1 and S cyclin-CDKs to prevent progression through G1 phase and initiation of DNA replication (Harper et al., 1995, Di Leonardo et al., 1994). Another CDK inhibitor p16INK4a, that specifically inhibits cyclin D-CDK4/6, is induced later compared to p21, and hence is believed to be implicated in the long-term maintenance of senescence (Stein et al., 1999, Serrano et al., 1997, Gire and Dulic, 2015).

#### 1.7.2 Biomarkers for senescent cells

Senescent cells display a number of changes in cellular characteristics that allow their identification (reviewed in (Kuilman et al., 2010)). Morphologically, senescent cells are generally large, flat with large or multinucleated nuclei

and sometimes display extensive vacuolisation (Serrano et al., 1997, Chen and Ames, 1994, Denoyelle et al., 2006). Also as mentioned above, senescent cells have high levels of p21 and p16INK4a expression (Stein et al., 1999). A commonly used biomarker to identify senescent cells in vitro is SA-β-GAL (senescence-associated beta-galactosidase) (Dimri et al., 1995). Beta-galactosidase activity is increased in senescent cells that allows its detection at a suboptimal pH 6, partly due to overexpression of betagalactosidase and expansion of the lysosome (where beta-galactosidase is stored) (Kurz et al., 2000), though it is not required for senescence (Lee et al., 2006). An altered chromatin structure is observed in senescent cells in vitro, leading to formation of senescence-associated heterochromatic foci (SAHF) that produce punctate staining patterns (Narita et al., 2006). Senescent cells also undergo significant changes in the transcriptome and secretome, leading to abnormal secretion of immune factors, a phenotype termed the senescence-associated secretory phenotype (SASP) (Shelton et al., 1999).

## 1.7.3 p53-dependent cell cycle exit from G2

It is generally thought that senescent cells irreversibly arrest in G1. However, a number of studies observed that cells undergoing senescence frequently exit the cell cycle from G2 in a p53-dependent manner. It seems that almost all the known stimuli that induce senescence can trigger such a 'G2 exit' (Gire and Dulic, 2015). Baus *et al* shows treatment with a topoisomerase II inhibitor causes normal human fibroblasts (NHF) to degrade cyclin A and cyclin B1, and withdraw from the cell cycle in G2 (Baus et al., 2003). Since

G2 markers are degraded, these cells can be characterised as in G<sub>0</sub> or G1 but with 4N DNA content. Johnura et al shows that a number of stimuli, including replication senescence, oncogenic Ras, DNA damage-inducing agents and reactive oxygen species (ROS), can all induce HCA2 cells (a normal human fibroblast cell line) to degrade cyclin B, bypass mitosis and enter 4N G1 (Johmura et al., 2014). This mitotic bypass requires p53 and p21, as p53/p21-depleted cells still attempt mitosis that is often aberrant and frequently leads to cell death. This work also found cyclin B-negative senescent 4N cells in human nevi, a type of benign tumours, providing physiological relevance for mitotic bypass in tumorigenesis. These findings corroborate with findings in human retinal pigment epithelial 1 cells (RPE1) by Krenning et al, which found that transient induction of p53 by the p53stabilising drug Nutlin is sufficient to induce mitotic bypass and senescence (Krenning et al., 2014). In these studies, p53 and p21 are clearly required for mitotic bypass. A possible mechanism is that p21 inhibits CDK1 to allow activation of APC/CCDH1, which degrades cyclin B. In a clear contrast, Davoli et al shows p53-deficient mouse embryonic fibroblast cells (MEF) and human BJ cells can bypass mitosis and endoreduplicate in response to telomere dysfunction (POT1 depletion) and DSBs (Davoli et al., 2010, Davoli and de Lange, 2012). One possible explanation is that strong ATM/ATR checkpoint activation induced by DSBs and POT1 depletion can inhibit CDK1 enough without the need for p21. The way to inactivate p53 may also contribute to the differences; human cells were transformed with p53-repressing viral oncoproteins in Davoli et al but it is not known whether there was residual

p53 activity in those cells. Further studies are needed to elucidate the mechanism of mitotic bypass and its role in senescence establishment.

## 1.8 Research aims

It is important to understand the causes and consequences of WGD. Genomics studies associate several gene alterations with WGD, but the underlying mechanism of these associations is not clear. In particular, it is not understood how alterations in the E2F transcription pathway, such as *CCNE1* amplifications, can lead to WGD in p53 wild type tumours. One study observed that cyclin E-overexpression leads to accumulation of cells with >4N DNA content in cell culture (Bartkova et al., 2005). This was attributed to partial re-replication but poorly characterised. Instead, preliminary data by Stephanie Hills in our lab suggested that cyclin E-overexpressing cells may actually undergo WGD (Figure 5.3D). Thus, using the cyclin E overexpression system, this work aims to investigate: (1) the route to WGD in cyclin E-overexpressing cells, by cell fusion, mitotic detects or mitotic bypass? (2) the link between cyclin E-induced replication stress and WGD. (3) the role of p53 in cyclin E-induced WGD.

## **Chapter 2. Materials & Methods**

## 2.1 Cell culture and cell lines

All cells in the study were cultured using Dulbecco's Modified Eagle Medium (Gibco, 41966052 or Merck, D6429) added with 10% heat inactivated FBS (fetal bovine serum) at 37 °C and 5% CO<sub>2</sub>, without antibiotics. Cell lines used in this study are listed in the following table. Cell lines are authenticated by the Crick Cell Services using STR (short tandem repeats) profiling.

Table 1. Experimental models used in the study.

| Name                                  | Source     | Generator       |
|---------------------------------------|------------|-----------------|
| Human: U2OS                           | ATCC       |                 |
| Human: hTERT RPE1                     | ATCC       |                 |
| Human: HCT116                         | ATCC       |                 |
| Human: IMR90                          | ATCC       |                 |
| Human: U2OS TetON cyclin E            | This study | Stephanie Hills |
| Human: U2OS TetON HRAS <sup>12V</sup> | This study | Stephanie Hills |
| Human: U2OS TetON MYC                 | This study | Stephanie Hills |
| Human: U2OS TetON CDC25A              | This study | Stephanie Hills |
| Human: U2OS TetON cyclin D            | This study | Jingkun Zeng    |
| Human: U2OS TetON cyclin E            | This study | Jingkun Zeng    |
| p53KO                                 |            |                 |
| Human: U2OS TetON cyclin E            | This study | Jingkun Zeng    |
| p21KO                                 |            |                 |

| Human: U2OS TetON cyclin E   | This study    | Jingkun Zeng |
|------------------------------|---------------|--------------|
| FUCCI H2B                    |               |              |
| Human: RPE1-T-Rex            | This study    | Eiko Ozono   |
| Human: RPE1 TetON cyclin E   | This study    | Eiko Ozono   |
| Human: RPE1 TetON cyclin E   | This study    | Jingkun Zeng |
| p53KO C1 & C2                |               |              |
| Human: RPE1 TetON cyclin E   | This study    | Jingkun Zeng |
| p21KO                        |               |              |
| Human: RPE1 TetON cyclin E   | This study    | Jingkun Zeng |
| FUCCI                        |               |              |
| Human: RPE1 TetON cyclin E   | This study    | Jingkun Zeng |
| FUCCI H2B                    |               |              |
| Human: RPE1 TetON cyclin E   | This study    | Jingkun Zeng |
| p53KO FUCCI                  |               |              |
| Human: U2OS TetOFF cyclin E  | Laboratory of |              |
|                              | Jiri Bartek   |              |
| Human: BT-LT                 | Laboratory of |              |
|                              | Mariia Yuneva |              |
| Human: RPE1 p53KO (no zeocin | Laboratory of |              |
| resistance)                  | Karen Vousden |              |

## 2.2 Plasmids and cell lines

## 2.2.1 Plasmids and cloning

For constructing plasmids for inducible expression of oncogenes, cDNA sequences of human cyclin E1, MYC, CDC25A, HRAS<sup>V12</sup> were inserted into

the pcDNA4/TO vector (Invitrogen) respectively by Stephanie Hills, tagged with a hemagglutinin (HA) fragment (DNA sequence:

GAGTACCCATACGATGTTCCAGATTACGCTCTCCTCCTC) at the N-terminus of the cDNA sequences. cDNA of cyclin D1 was cloned into pcDNA4/TO by Jingkun Zeng, also with a HA tag at the N-terminus.

For constructing plasmids for gene knockout, gRNA sequences were cloned into the pSpCas9(BB)-2A-Puro (PX459) V2.0 vector (Addgene, 62988) following ZhangLab's protocol on Addgene. gRNAs were chosen to target an early coding exon and an exon that is present in all splice variants. Exon information was checked on Ensembl. Ensembl gene ID for *TP53* is ENSG00000141510, and the isoform ENST00000617185.4 were selected for gRNA design. gRNA sequences were chosen by using gRNA selection software on Benchling (tutorial: https://blog.benchling.com/how-to-design-grnas-to-target-your-favorite-gene/). gRNAs that have high ON and OFF target scores were selected. gRNAs designed in this way are: 5' CCATTGTTCAATATCGTCCG 3' targeting exon 4 and 5' TCCTCAGCATCTTATCCGAG 3' targeting exon 6 for p53-knockout; 5' CCATTAGCGCATCACAGTCG 3 for p21-knockout.

#### 2.2.2 Cell line establishment

## 2.2.2.1 Establishment of doxycycline-inducible oncogeneoverexpressing cell lines

U2OS-T-Rex cells stably expressing the Tet repressor were purchased from Invitrogen. RPE1-T-Rex cells constitutively expressing TetR were generated

by Eiko Ozono by transfecting RPE1 cells with the pcDNA6/TR plasmid (Invitrogen) and selecting single cell clones in 5 μg/ml Blasticidin. Single cell clones were isolated by clone cylinders. For creation of U2OS and RPE1 TetON cells expressing oncogenes, the pcDNA4/TO plasmid with an oncogene cDNA insert described above in the plasmids section was transfected into U2OS-T-Rex or RPE1-T-Rex cells using Lipofectamine 3000 (Invitrogen) or JetPRIME (Polypus). Single cell clones were selected in 200-500 μg/ml Zeocin. Single cell clones were isolated by clone cylinders. Experimental procedure is described in more detail below.

On the first day, RPE1-T-Rex or U2OS-T-Rex cells were seeded at a density of 3 x 10^5 cells per 6-well. Also a control well without transfection was seeded. On the second day 1  $\mu$ g plasmid DNA (pcDNA4/TO-oncogene) was transfected using Lipofectamine 3000 (Invitrogen) into each 6-well. On the third day cells in each well were split into 10-cm dishes at fractions of 1:2, 1:10, 1:100 or 1:1000. Selection media containing antibiotics were added the next day. For RPE1 cells, 500  $\mu$ g/ml zeocin is supplemented. For U2OS cells, 200  $\mu$ g/ml zeocin is supplemented. Selection media were changed every 3-4 days until untransfected cells in the control plate die out. Clones of appropriate size without close proximity to surrounding clones were selected using cloning cylinders (Merck).

#### 2.2.2.2 Establishment of p53-knockout and p21-knockout cell lines

For creation of p53-knockout cells, the PX459 plasmids with guide sequences targeting exon 4 and exon 5 described in the plasmids section

were co-transfected into cells using Lipofectamine 3000. For creation of p21knockout cells, the single PX459 plasmid containing the guide described in the plasmids section was transfected into cells using Lipofectamine 3000. The PX459 plasmid contains puromycin resistance gene so U2OS cells can be selected using puromycin. Wild type RPE1 cells already have puromycin resistance so they cannot be selected using puromycin. Knockout of *TP53* (encoding p53) and CDKN1A (encoding p21) was very efficient so puromycin selection was not necessary. Instead, cells were selected by single-cell sorting into 96-well plates 5 days post transfection. DNA staining was not needed for this sorting. Any viable cell can be sorted into the plate. After expansion into 24-wells, successful clones were validated using western blot first. PCR and sanger sequencing were then further used for validation. To do these, genomic DNA were extracted from cells using Qiagen DNeasy Blood and Tissue kit. Then a forward primer P1 (TCCTCTGACTGCTCTTTTCAC for TP53, GCAAAGCCCGGCCAGGTAACAT for *CDKN1A*) and a reverse primer P2

GCAAAGCCCGGCCAGGTAACAT for *CDKN1A*) and a reverse primer P2 (CCACTGACAACCACCCTTAAC for *TP53*,

TCACTGCACTCCAGTCTGGCCA for *CDKN1A*) were used to amplify gene regions by PCR. An agarose gel was then run to compare gene sizes in control cell line and KO cell lines, or sanger sequencing using primers P1 and P2 was used to sequence PCR products. Details of validation of RPE1 TetON cyclin E p53KO C1 & C2 cells, and RPE1 TetON cyclin E p21KO are described in the results chapter.

#### 2.2.2.3 Establishment of FUCCI cell lines

For creation of cells containing FUCCI reporters, the FUCCI(CA)2 plasmid (Sakaue-Sawano et al., 2017) carrying a mCherry-tagged CDT1 fragment and a mVenus-tagged geminin fragment, was introduced into cells using lentiviral transduction. Virus packaged with the plasmid was produced by Joe Padget from Silvia Santos' lab using a 2<sup>nd</sup> generation lentiviral production system. To transduce cells, 1 ml media containing the virus was added to a 6-well seeded with 4x10^5 cells, supplemented with 1 µl polybrene (10 mg/ml stock). In the next day the well was changed with 4 ml fresh media. After 3 media changes and allowing cells to recover for one week, cells positive for fluorescent signals were single-cell sorted into 96-well plates to obtain stable clones. The pCSII EF1a hH2B-Turg plasmid was introduced into cells by lentiviral transduction to generate cells with mTurquoise-tagged H2B. Cells positive for mTurquoise signals were single-cell sorted into 96well plates to obtain stable clones. See methods section below for cell sorting. Emission channels on the sorter for the fluorescent proteins were chosen around 530 nm for mVenus, 610 nm for mCherry and 475 nm for mTurquoise. Details of generation of U2OS TetON cyclin E FUCCI H2B cells are described in the results chapter.

## 2.3 Preparation of frozen cell stock

For mammalian cell stock preparation, culture was grown to 90-100% confluence before preparation. Cells were pelleted and resuspended in cryoprotectant medium (90% FBS + 10% DMSO) at a concentration of ~2 x 10^6 cells per ml. Cell suspension was then aliquoted into cryogenic tubes at

0.5-1 ml per tube. Cells stocks were first put in a Mr. Frosty at -80°C overnight then transferred to storage at -80°C.

#### 2.4 RNA interference

For gene knockdown, siRNAs were reverse transfected into cells using RNAiMAX (Invitrogen) and OptiMEM (Invitrogen) at a final concentration of 40 nM. The following siRNAs were used: SMARTpool On-TARGETplus FZR1(CDH1) siRNA (Dharmacon, L-015377-00), siGENOME TP53 siRNA (Dharmacon, D-003329-26), SMARTpool siGENOME CDKN1A siRNA (Dharmacon, M-003471-00), SMARTpool siGENOME GADD45A siRNA (Dharmacon, M-003893-02), SMARTpool siGENOME SFN (14-3-3σ) siRNA (Dharmacon, M-005180-00), SMARTpool siGENOME FBXW7 siRNA (Dharmacon, M-004264-02), SMARTpool siGENOME POT1 siRNA (Dharmacon, M-004205-01), SMARTpool siGENOME RB1 siRNA (Dharmacon, M-003296-03) and a control siRNA siGL2 against Firefly luciferase (Ohrt et al., 2006) with sequence CGU ACG CGG AAU ACU UCG AUU.

## 2.5 Small molecule compounds

The following small molecule compounds were used: aphidicolin (Sigma Aldrich), AZD 7762 (CHK1i, Axon MedChem), MK 1775 (WEE1i, Axon MedChem), KU-55933 (ATMi, Selleckchem), VE-822 (ATRi, Selleckchem), RO-3306 (CDK1i, Merck), CVT-313 (CDK2i, Cambridge Bioscience), Abemaciclib (CDK4/6i, Selleckchem), nocodazole (Sigma Aldrich), colcemid

(Thermo), Doxycycline (Sigma Aldrich). See table below for catalogue numbers of chemicals used.

Table 2. Commercial provider and catalogue number of chemicals used in the study.

| Aphidicolin                   | Sigma Aldrich        | Cat# A0781       |
|-------------------------------|----------------------|------------------|
| AZD 7762                      | Axon MEDCHEM         | Cat# 1399        |
| MK 1775                       | Axon MEDCHEM         | Cat# 1494        |
| KU-55933                      | Selleckchem          | Cat# S1092       |
| VE-822                        | Selleckchem          | Cat# S7102       |
| Abemaciclib                   | Selleckchem          | Cat# S7158       |
| RO-3306                       | Merck                | Cat# SML0569     |
| CVT-313                       | Cambridge Bioscience | Cat# B1137       |
| Nocodazole                    | Sigma Aldrich        | Cat# M1404       |
| Colcemid                      | ThermoFisher         | Cat# 15212012    |
| Doxycycline                   | Sigma Aldrich        | Cat# D9891       |
| DyeCycle Ruby                 | ThermoFisher         | Cat# V10309      |
| Hoechst 33342                 | ThermoFisher         | Cat# 62249       |
| DAPI                          | Sigma Aldrich        | Cat# D9542       |
| Alexa Fluor 488 NHS Ester     | ThermoFisher         | Cat# A20000      |
| Vectashield Antifade Mounting | Vector Laboratories  | Cat# H-1200      |
| Medium with DAPI              |                      |                  |
| Protease Inhibitor Cocktail   | Sigma Aldrich        | Cat# 11873580001 |
| Zeocin                        | Invivogen            | Cat# ant-zn-1    |
| Blasticidin                   | Invivogen            | Cat# ant-bl-05   |

## 2.6 Metaphase spreading

Cells were grown at exponential phase in 10-cm dishes. To arrest cells in metaphase, U2OS endoreduplicated clones were incubated with 167 ng/ml colcemid for 3 h and RPE1 endoreduplicated clones were incubated with 200 ng/ml colcemid for 1 h. Cells were then washed with PBS once. Both the culture media and the wash were collected in a falcon tube. Cells were then treated with trypsin for less than 2 min and collected. Cells were then pelleted by centrifugation at 200 g for 10 min, and resuspended gently. A hypotonic buffer of 75 mM potassium chloride solution was added dropwise to resuspended cells. Cells were then incubated at 37°C for 10 min before being pelleted by centrifugation at 200 g for 5 min. Cells were then fixed with fresh Carnoy's Fixative (3:1 methanol: pure acetic acid). Samples can be stored in Carnoy's Fixative for up to a year. For spreading, samples were dropped from 10-30 cm above onto glass slides tilted at an angle of 45 degrees. After airdrying, slides were mounted with DPX moutant with DAPI (Vector Laboratories), covered with coverslips and sealed with manicure. Slides were imaged on a Zeiss AXIO Observer Z1 microscope.

## 2.7 Live-cell imaging

Cells were plated onto 4-well polymer bottom slides (Ibidi, 80446) in DMEM containing 10% FBS, and allowed to attach to the bottom for at least 5 h before imaging. A Nikon Eclipse Ti inverted microscope fitted with a custom humidified enclosure (Okolabs) maintained at 37°C and a CO<sub>2</sub> level at 5% was used for time-lapse live-cell imaging. Cover lid for the imaging chamber should remain closed to ensure proper CO<sub>2</sub> level. Water should be replenished in the water container to ensure humidity. Images of phase-

contrast or fluorescent channels were taken at 20 min intervals under a 20x objective (Numerical Aperture: 0.75), with the Nikon Perfect Focus System (PFS) used for autofocus. Laser intensities and exposure times were optimised to obtain clear signals without obvious phototoxicity. Slides were replenished with fresh media every 2 or 3 days. More detailed sample preparation procedures for different FUCCI experiments are described below.

For cyclin E overexpression FUCCI experiments, cells were seeded at approximately 20% confluency of each well in the 4-well polymer bottom slides (Ibidi, 80446). If Doxycycline needs to be supplemented, Doxycycline was added to cell suspension prior to seeding. The slide should not be shaken after seeding. Imaging is usually started at 24 h or 48 h after cells have attached to the bottom of the wells, and finished at 96 h timepoint.

For aphidicolin treatment FUCCI experiments, cells were seeded at approximately 60% confluency of each well in the 4-well polymer bottom slides (Ibidi, 80446). If aphidicolin needs to be supplemented, aphidicolin was added to cell suspension prior to seeding. The slide should not be shaken after seeding. Imaging is usually started at 24 h or 48 h after cells have attached to the bottom of the wells, and finished at 72 h or 96 h timepoint.

For experiments to test dependence of cyclin E-induced or aphidicolininduced mitotic bypass on ATM, ATR, CHK1 or WEE1, cells are seeded as above with either Doxycycline or aphidicolin. Inhibitors of ATM, ATR, CHK1 or WEE1 are usually added at 48 h. To do this, a fresh tube of media was prepared containing appropriate concentrations of inhibitors, supplemented with Doxycycline or aphidicolin. Then the inhibitor mix was used to replace the media in the wells. Concentrations for the inhibitors used were: 500 nM for ATMi (KU-55933), 200 nM for ATRi (VE-822), 50 nM for CHK1i (AZD7762), and 1 µM for WEE1i (MK1775). Imaging should be started within 30 min after the inhibitors are added.

## 2.8 Cell tracking

Image processing and analysis were performed in FIJI (1.53c). An in-house macro developed based on a plugin, Trackmate (Tinevez et al., 2017), was co-developed with Matt Renshaw from Crick Advanced Light Microscopy STP for automated cell tracking (The macro is deposited at https://github.com/zeng-j-k/Cell-FUCCI-analysis, with the file named as fucci\_imageProcessing\_analysis\_includePC.ijm). In the macro, filtering and background subtraction were applied before using Trackmate. The H2B-mTurquoise signal was used for tracking cell nuclei. Parameters were optimised as following: for U2OS cells a radius of 11 µm was used and for RPE1 cells a radius of 9 µm was used in the LoG detector; The Simple LAP Tracker was used using a max linking distance of 15, a max gap closing distance of 15 and a max frame gap of 2. H2B-mTurquiose, cdt1-mCherry and geminin-mVenus channels were measured for intensities on identified nuclear regions. The macro will output a spreadsheet of recorded fluorescent intensities. The spreadsheet was imported into MATLAB for curve plotting

(the MATLAB script can be found at https://github.com/zeng-j-k/Cell-FUCCI-analysis). Fluorescence intensities over time were plotted for single cells with tracks longer than 36 h. A spike in the H2B-mTurquiose signal was used to indicate mitosis due to chromosome condensation, accompanied by an abrupt disappearance of the mVenus-Geminin signal due to geminin degradation.

For samples treated with aphidicolin, CHK1i, WEE1i, ATMi and ATRi, cells were tracked manually. Mitosis was observed when cells rounded up in the phase contrast channel.

## 2.9 Numerical analysis

To calculate the degradation rate of mVenus-Gem, fluorescence intensities over time were excised around local maxima and minima. Excised intensities were normalised and scaled to 0-100, and fitted to a logistic growth equation below (Sakaue-Sawano et al., 2017):

Normalised Intensity = 
$$\frac{100}{1 + e^{(-k(t - t_{1/2}))}}$$

Fitting was performed using the Isqcurvefit function in MATLAB, where k is the degradation rate of mVenus-Gem with a unit of 1/minute,  $t_{1/2}$  (half-life, minute) is time at which mVenus-Gem degrades to half of the maximum.

## 2.10 Flow cytometry

## 2.10.1 Barcoding

Multiplexed flow cytometry analysis was enabled by fluorescent barcoding (Rodriguez-Martinez et al., 2020). Cell samples were fixed in 4% formaldehyde for 10 min and 70% ethanol respectively with one PBS wash in between. A barcoding dye Alexa Fluor 488 NHS Ester (Thermo, A20000) diluted at 15, 5, 1.3. 0.3, 0.075, 0 µg/ml concentrations in 70% ethanol were then added to up to 6 cell samples for multiplexing to allow unbiased staining of the combined samples in subsequent steps. 2 washes in 1% BSA/PBS were required to remove excessive barcoding dye before combining samples. An aliquot of combined barcoded samples was taken each time before staining with other dyes for compensation for data analysis. A more detailed procedure for barcoding is described below.

Barcoding dye stock was prepared by diluting ThermoFisher Alexa Fluor 488 NHS Ester A20000 powder in DMSO at a concentration of 1 mg/ml, stored at -80°C. Each sample will be incubated with one concentration of barcoding dye at 15, 5, 1.3. 0.3, 0.075 or 0 µg/ml final concentrations in 70% ethanol at room temperature for 10 min. Non-stick 1.5 ml tubes were used to store cell pellet samples to minimise cell loss during staining. Samples were then washed with 1% BSA/PBS twice before being combined in a single tube. A small aliquot of pooled samples was taken at this stage before subsequent staining as a compensation control for FACS analysis.

6 samples can be barcoded and pooled together at max. Barcoding enables simultaneous staining with fluorescent dyes in one tube in subsequent steps.

Samples with different fluorescent intensities of the barcoding dye can be easily distinguished from flow cytometry.

### 2.10.2 EdU incorporation assay and DNA content analysis

Cells in culture were pulsed with 10 µM EdU for 30 min before they were harvested and fixed. After barcoding, to stain EdU, a Click-iT chemistry-based kit Click-iT EdU Alexa Fluor 647 Flow Cytometry Assay Kit (Thermo, C10424) was used following manufacturer's instructions.

For DNA content analysis, samples were incubated with 100  $\mu$ g/L RNase A and 1  $\mu$ g/ml DAPI diluted in 1% BSA/PBS at room temperature for 10 min. No wash is needed.

## 2.10.3 Whole cell and chromatin-bound protein analysis

To analyse whole cell protein level such as cyclin B1 level, whole cells were fixed in 4% formaldehyde after collection. To analyse chromatin-bound protein level such as MCM7 level, at least 4 x 10^6 cells should be collected (normally a 10-cm dish of cells are used) and cells were extracted with 1 ml CSK buffer (10 mM HEPES-KOH pH 7.9, 100 mM NaCl, 3 mM MgCl<sub>2</sub>, 1 mM EGTA, 300 mM sucrose, 1% BSA, 0.2% Triton X-100, 1 mM DTT, 1X Roche Complete protease inhibitor cocktail) before formaldehyde fixation. Barcoded samples were then stained with primary antibodies at 1:100-1:200 concentration in 300-500 µl volumes for one hour before one wash in 500 µl 1% BSA/PBS. Samples were then stained with secondary antibodies (Alexa

Fluor 555, Thermo) at 1:500 concentration in 500 µl volume for 30 min.

Details of antibodies can be found in the Antibodies section.

### 2.10.4 Multichannel FACS assay and analysis

Samples were stained with 4 dyes at maximum. Staining order was barcoding (Alexa Fluor 488), whole-cell or chromatin-bound protein (Alexa Fluor 555), EdU (Alexa Fluor 647) and DAPI. Samples were measured on a DB Fortessa flow cytometer using FACS DIVA software. Compensation was performed on the FACS DIVA software.

Sample analysis was performed by FlowJo. Cells were gated to exclude doublets and cell clumps using a violet-450 nm area (violet-A, DAPI staining) vs violet-450 nm height (violet-H, DAPI staining) plot.

#### 2.10.5 Cell sorting

To isolate cells based on DNA content, cells were trypsinised, collected, and resuspended in 2% FBS/DMEM supplemented with either Hoechst 33342 (5 µg/ml, Thermo) (then incubation at 37 °C for 30 min), or DyeCycle Ruby (1:10,000, Thermo, V10309) (then incubation at 37 °C for 15 min). FCASAria Fusion flow cytometer (BD) was used for sorting. For sorting U2OS cells, U2OS WGD cells and RPE1 cells, a nozzle size of 100 µm was used. For sorting RPE1 WGD cells, a nozzle size of 130 µm was used. Sorting chamber temperature was set at room temperature. Collection plates were Falcon 96-well flat-bottom plates.

#### 2.11 Western blot

Whole cell extracts were prepared by adding 1x Laemmli sample buffer (Biorad, 1610747) supplemented with 10% beta-mercaptoethanol to cooled plated cells, before being boiled at 95 °C for 5 min. Cell extracts were loaded into Biorad TGX 10% or 10-15% gels and electrophoresis was run in 1x TGX buffer. Protein was semi-dry transferred to nitrocellulose membranes (Trans-Blot Turbo Transfer Packs, Biorad) using a Biorad Turbo blotter. Membranes were blocked in 5% milk/TBST or 3% BSA/TBST for one hour before incubating with primary antibodies at 4 °C overnight. After washes in TBST, membranes were incubated with secondary HRP antibodies for 2 hours at room temperature. Pierce ECL Western blotting substrate (Thermo) was used to visualise HRP and Amersham Imager 600 was used to detect chemiluminescence. Details of antibodies can be found in the Antibodies section.

#### 2.12 Antibodies

Table 3. List of antibodies used in the study.

| Name              | Supplier       | Cat#          | Dilution | Dilution |
|-------------------|----------------|---------------|----------|----------|
|                   |                |               | for WB   | for FACS |
| Mouse monoclonal  | Santa Cruz     | Cat# sc-247   | 1:1000   |          |
| anti-Cyclin E1    | Biotechnology  |               |          |          |
| Mouse monoclonal  | Santa Cruz     | Cat# sc-81178 | 1:1000   |          |
| anti-beta Actin   | Biotechnology  |               |          |          |
| Rabbit polyclonal | Cell Signaling | Cat# 9284     | 1:1000   |          |
| anti-Phospho-p53  | Technology     |               |          |          |
| (Ser15)           |                |               |          |          |

| Rabbit monoclonal   | Cell Signaling | Cat# 2348     | 1:1000 |       |
|---------------------|----------------|---------------|--------|-------|
| anti-Phospho-CHK1   | Technology     |               |        |       |
| (Ser345)            |                |               |        |       |
| Rabbit polyclonal   | Bethyl         | Cat# A300-    | 1:5000 |       |
| anti-Phospho-       |                | 245A          |        |       |
| RPA32 (S4/S8)       |                |               |        |       |
| Mouse monoclonal    | BioLegend      | Cat# 901533   | 1:1000 |       |
| anti-HA.11 Epitope  |                |               |        |       |
| Tag                 |                |               |        |       |
| Rabbit polyclonal   | Santa Cruz     | Cat# sc-805   | 1:1000 |       |
| anti-HA Epitope Tag | Biotechnology  |               |        |       |
| Mouse monoclonal    | Santa Cruz     | Cat# sc-126   | 1:1000 |       |
| anti-p53            | Biotechnology  |               |        |       |
| Rabbit monoclonal   | Cell Signaling | Cat# 2947     | 1:1000 |       |
| anti-p21            | Technology     |               |        |       |
| Mouse monoclonal    | Sigma-Aldrich  | Cat# T5168    | 1:4000 |       |
| anti-alpha-Tubulin  |                |               |        |       |
| Mouse monoclonal    | Santa Cruz     | Cat# sc-56324 | 1:1000 | 1:200 |
| anti-MCM7           | Biotechnology  |               |        |       |
| Rabbit monoclonal   | Abcam          | Cat# ab32053  | 1:1000 | 1:200 |
| anti-Cyclin B1      |                |               |        |       |
| Mouse monoclonal    | Millipore      | Cat# 05-636   |        | 1:200 |
| anti-phospho-       |                |               |        |       |
| Histone H2A.X       |                |               |        |       |
| (Ser139)            |                |               |        |       |
| Rabbit polyclonal   | Novus          | Cat# NB500-   | 1:1000 |       |
| anti-POT1           | Biologicals    | 176           |        |       |
|                     |                |               |        |       |

## Chapter 2. Materials & Methods

| Rabbit polyclonal     | Proteintech   | Cat# 55290-1- | 1:1000 |       |
|-----------------------|---------------|---------------|--------|-------|
| anti-FBXW7            |               | AP            |        |       |
| Anti-p-CDK1           | In-house by   | N/A           | 1:1000 |       |
| T14/Y15               | Julian Gannon |               |        |       |
| Anti-CDH1             | In-house by   | N/A           | 1:1000 |       |
|                       | Julian Gannon |               |        |       |
| Goat polyclonal Anti- | Agilent       | Cat# P0447    | 1:5000 |       |
| Mouse                 |               |               |        |       |
| Immunoglobulins       |               |               |        |       |
| Donkey polyclonal     | Jackson       | Cat# 711-035- | 1:5000 |       |
| Anti-Rabbit IgG       | ImmunoResea   | 152           |        |       |
| (H+L)                 | rch Labs      |               |        |       |
| Goat polyclonal anti- | Thermo Fisher | Cat# A-21428  |        | 1:500 |
| Rabbit IgG (H+L)      | Scientific    |               |        |       |
| Cross-Adsorbed        |               |               |        |       |
| Secondary Antibody,   |               |               |        |       |
| Alexa Fluor 555       |               |               |        |       |
| Goat polyclonal anti- | Thermo Fisher | Cat# A-21424  |        | 1:500 |
| Mouse IgG (H+L)       | Scientific    |               |        |       |
| Highly Cross-         |               |               |        |       |
| Adsorbed              |               |               |        |       |
| Secondary Antibody,   |               |               |        |       |
| Alexa Fluor 555       |               |               |        |       |

# Chapter 3. Result 1. Cyclin E expression induces endoreduplication through mitotic bypass

## 3.1 Introduction

Cancer genomics studies associate several genetic alterations including amplification of *CCNE1* which encodes cyclin E protein, with WGD. Using cells inducibly expressing cyclin E, Bartkova *et al* observed that a subset of cyclin E-expressing cells became polyploid with >4N DNA content, although they attributed this phenotype with partial re-replication rather than WGD (Bartkova et al., 2005). In this chapter doxycycline-inducible cells lines overexpressing cyclin E were established, and I used these cells to investigate whether cyclin E-induced polyploidisation is caused by WGD. I also tested whether the cyclin E-induced >4N cells are viable.

WGD can be generated experimentally in three ways: cell fusion, failures of mitosis or cytokinesis, mitotic bypass or endoreduplication. To investigate whether any of these occurs during cyclin E overexpression, I used FUCCI (fluorescent, ubiquitination-based cell cycle indicator) live cell imaging to visualise the cell cycle.

## 3.2 Results

## 3.2.1 Cyclin E1 expression induces whole genome duplication in U2OS cells

To study the effects of cyclin E overexpression, I used a tetracyclineinducible system (tetON) that enables rapid expression of genes-of-interest upon addition of tetracycline (tet), or a more stable analogue, doxycycline (Dox). The tetON promoter consists of a tet response element (TRE) placed upstream of a minimal CMV promoter. In the absence of tet, the tet repressor (tetR) binds to TRE and prevents transcription. Addition of doxycycline prevents tetR binding to TRE and therefore permits transcription of gene-ofinterest. For this chapter, I used the U-2 OS (U2OS) cell line, an epitheliallike osteosarcoma cell line that is commonly used in DNA damage studies. The cell line was modified by lab member Stephanie Hills to express the tetON expression plasmid containing full length human cyclin E1 with a hemagglutinin (HA) tag at the N-terminus (U2OS tetON cyclin E cells). Elevated expression of cyclin E could be seen 1 hour post Dox addition, with the expression level peaking after 6 hours (Figure 3.1A). Cyclin E expression in our U2OS tetON cyclin E cells was more rapid than in 'tet-off' cell line previously described in literature inducibly expressing a truncated version of cyclin E1 (U2OS tetOFF cyclin E cells) (Bartkova et al., 2005), though expression levels in both lines are similar (Figure 3.1B). The 'tet-off' cell line was shown to express cyclin E at a comparable level to a breast cancerderived cell line MDA-157 that contains amplified copies of CCNE1.

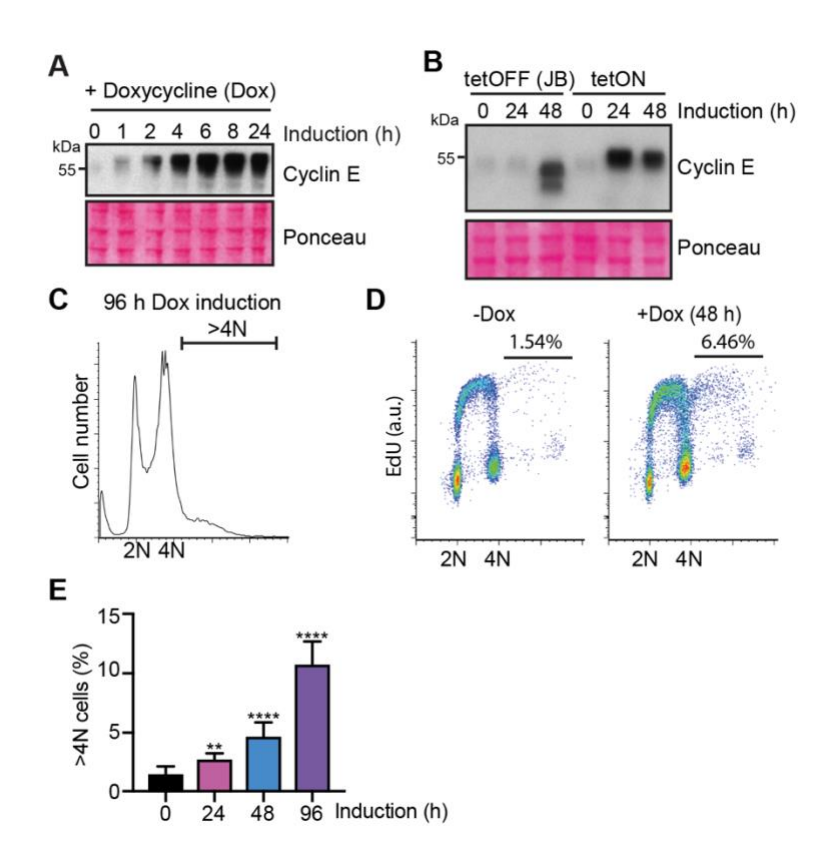


Figure 3.1 Cyclin E overexpression leads to whole genome duplication in U2OS cells.

- (A) Immunoblot showing expression of cyclin E1 over time upon addition of doxycycline (Dox) in U2OS tetON cyclin E cells. One representative experiment of three independent repeats is shown.
- (B) Immunoblot showing expression of cyclin E1 over time in U2OS tetOFF cyclin E cells and U2OS tetON cyclin E cells. U2OS tetOFF cyclin E cells were a gift from Jiri Bartek (JB) and only used in this experiment. One representative experiment of three independent repeats is shown.
- (C) Representative DNA content analysis by FACS of U2OS tetON cyclin E cells overexpressing cyclin E for 96 h. One representative experiment from three independent repeats is shown.
- (D) EdU incorporation and DNA content analysis by FACS of U2OS tetON cyclin E cells overexpressing cyclin E (+Dox) for 48 h. Numbers indicate the proportion of cells with greater than 4N DNA content. One representative experiment from three independent repeats is shown.
- (E) Quantification of FACS analysis of the percentage of cells in (D) with greater than 4N DNA content after overexpressing cyclin E over 96 h. Mean and standard deviations (SDs) from three independent experiments are shown. Statistical significance (\*\*p<0.005;\*\*\*\*<0.0001) was examined by unpaired t test.

Note: all experiments in Figure 3-1 were performed by Stephanie Hills.

A proportion of cells acquired greater than 4N DNA content (>4N) 96 h post cyclin E induction (Figure 3.1C), which was previously observed and attributed to partial genome re-replication (Bartkova et al., 2005). However, It was found that, by performing EdU incorporation analysis, distinct G1, S and G2 populations were seen at and beyond 4N DNA content, indicating an extra full cell cycle (Figure 3.1D). Therefore, these cells started from 4N DNA content to re-replicate, suggesting that cyclin E expression induces whole genome duplication (WGD). The proportion of WGD cells increased over time with ~10% seen at 96 h (Figure 3.1E). Viable single cell clones of WGD cells could be grown by sorting cells with >4N DNA content after cyclin E expression into 96-wells (Figure 3.2A). Clones were allowed to expand for at least a month, and were analysed by FACS for DNA content to identity WGD clones (Figure 3.2B). Six WGD clones were obtained. Their chromosome numbers were measured by metaphase spreading. The original U2OS cell line has 74 chromosomes (2N), so a WGD clone is expected to have on average 148 chromosomes (4N). However, the chromosome numbers of all 6 WGD clones isolated were counted to be considerably less than 148, indicating chromosome loss (Figure 3.2C). This is consistent with observations that a significantly proportion of cancers have sub-tetraploid chromosome numbers. Moreover, the WGD clones displayed highly variable chromosome numbers within each clone, indicating CIN during clonal expansion.

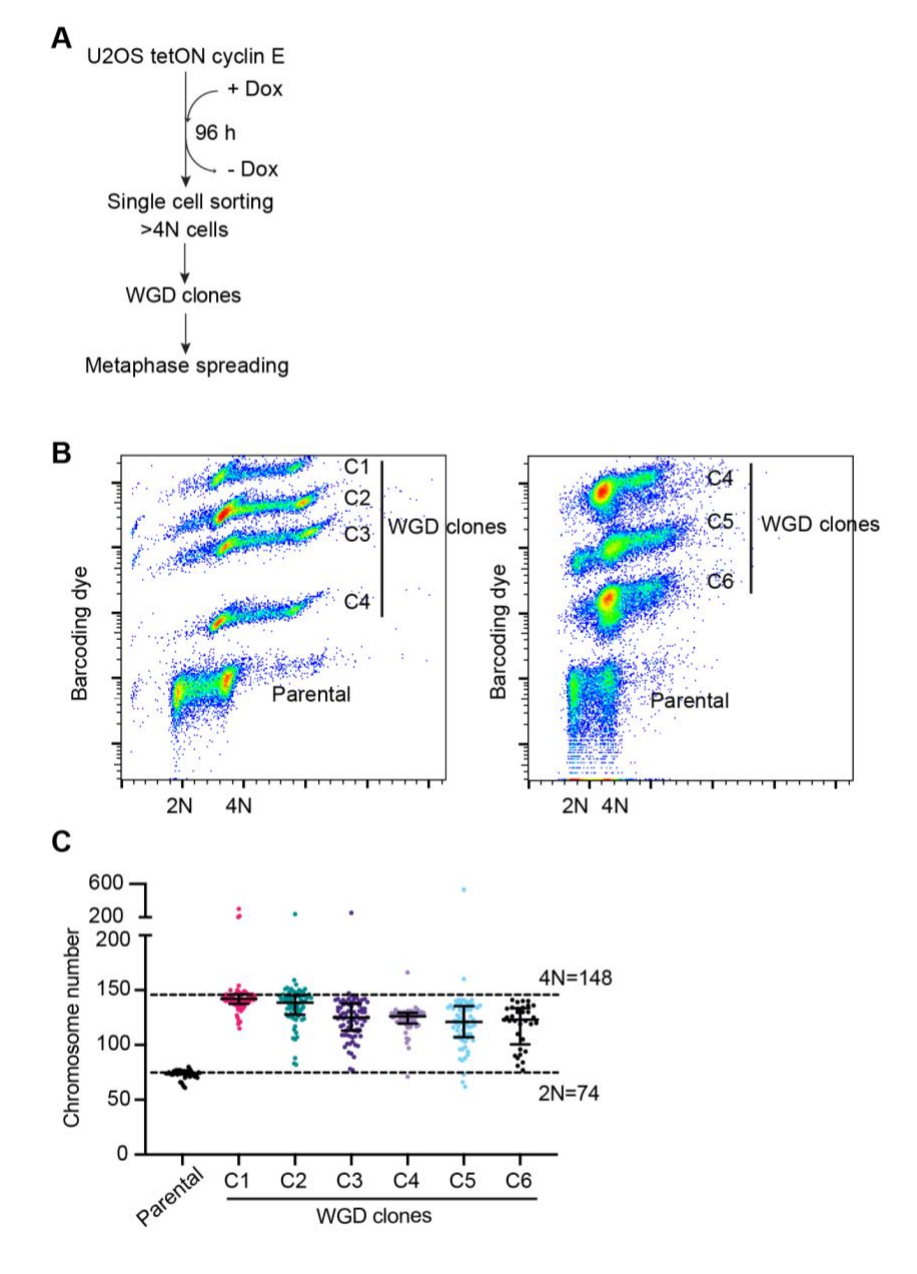


Figure 3.2 Karyotypes of cyclin E-induced U2OS WGD clones.

Schematic of the experimental approach is shown in (A). After 96 h Dox treatment, >4N cells were single cell sorted after staining with Hoechst. Single-cell clones were grown, and examined by FACS for DNA content shown in (B). In (B), the samples were barcoded together with the parental cell line and stained with DAPI for DNA content (n=1). Six WGD clones were obtained (U2OS WGD C1-6). In (B), clones were stained with different concentrations of barcoding dye and DAPI. Chromosome numbers of >50 individual cells of each WGD clone were counted by metaphase spreading shown in (C).

The tetON system gives rise to high levels of expression of genes under a strong CMV promoter in a matter of hours. Although our modelling system shows similar levels of cyclin E expression as the patient-derived MDA-157 cell line, the sudden increase does not look at adaptation over time to intermediate levels. To induce moderate to intermediate levels of cyclin E expression, cells were treated with dilutions of doxycycline. However, the expression levels remained high even until sub-nanomolar range of doxycycline (Figure 3.3A). It was difficult to produce reproducible levels of expression using picomolar range of the drug. A tumour suppressor protein, FBXW7, functions as the substrate recognition component of the SCF E3 ubiquitin ligase to control proteasome-mediated degradation of several prooncoproteins including cyclin E. Specific mutations of FBXW7 implicated in cancer can disrupt its ability to degrade cyclin E, resulting in chromosome instability and aneuploidy. I found that depleting FBXW7 could achieve a moderate increase in the expression of cyclin E (Figure 3.3B). Furthermore, it also caused WGD, to a lower extent than Dox-induced cyclin E expression, suggesting WGD can be induced by different levels of cyclin E (Figure 3.3C, D).

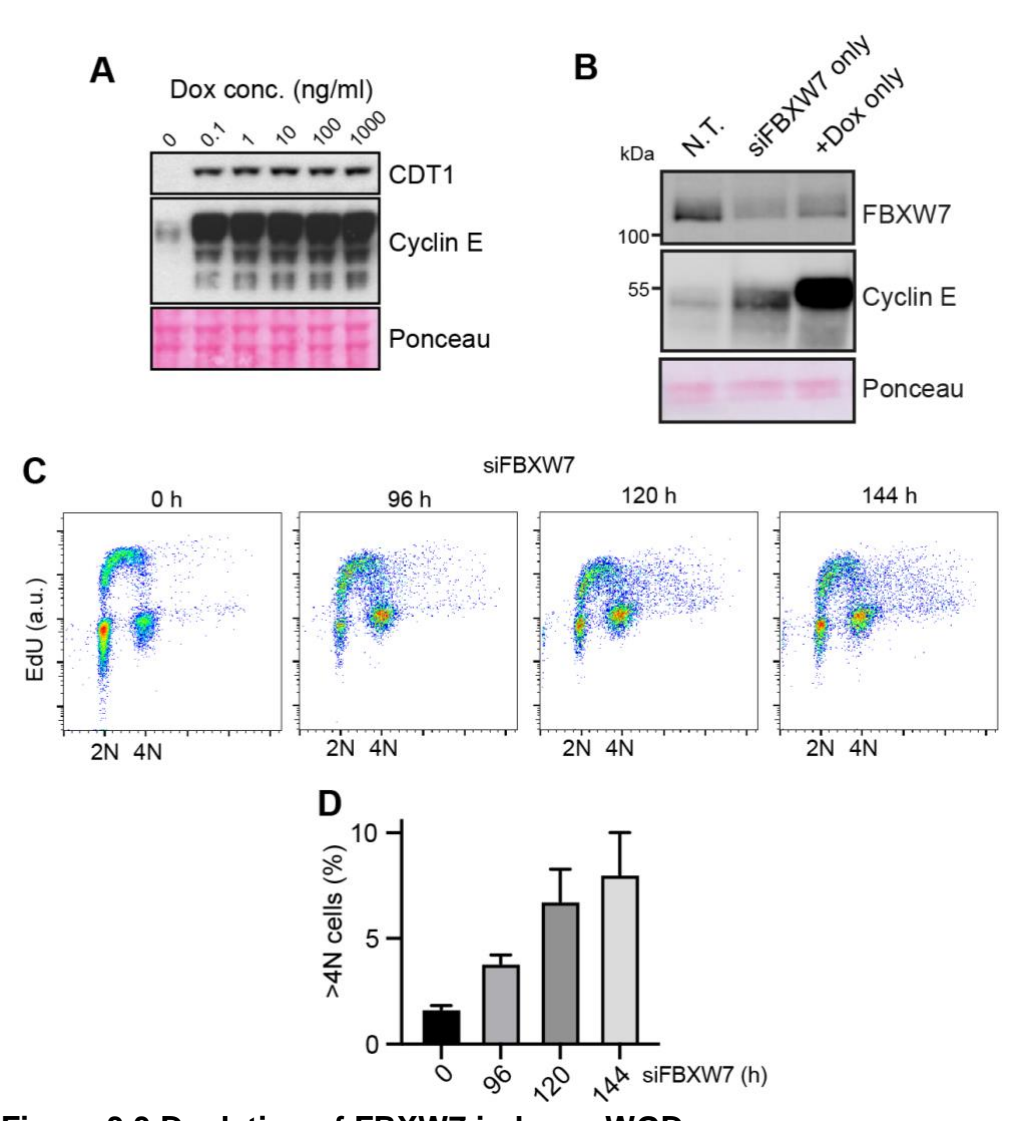


Figure 3.3 Depletion of FBXW7 induces WGD.

- (A) Immunoblots showing expression of cyclin E and CDT1 upon addition of titrations of doxycycline in the U2OS tetON cyclin E cell line. One representative experiment of three independent repeats is shown. Note: this experiment was performed by Stephanie Hills.
- (B) Immunoblots showing depletion of FBXW7 in the presence of FBXW7 siRNA. Representative immunoblots were selected from two independent experiments. The cell line used is U2OS tetON cyclin E without addition of doxycycline. N.T.: non-treated.
- (C-D) EdU incorporation and DNA content analysis of cells depleted with FBXW7 over time. Mean and standard deviations (SDs) of the percentage of cells with greater than 4N DNA content from three independent experiments are shown in D. The cell line used is U2OS tetON cyclin E without addition of doxycycline.

# 3.2.2 Cyclin E1-induced whole genome duplication occurs by mitotic bypass

To determine whether cyclin E-induced WGD occurs by mitotic defects, cell fusion or mitotic bypass, I applied FUCCI (fluorescent, ubiquitination-based cell cycle indicator) live cell imaging (Sakaue-Sawano et al., 2008). FUCCI technology relies on fluorescently tagged truncated versions of two cell cycle-regulated proteins, geminin and CDT1, to distinguish cell cycle stages. CDT1 is required for MCM loading during G1 but is degraded upon entry into S phase by SCF<sup>Skp2</sup> (active during S/G2/M phases) and CUL4<sup>Ddb1</sup> (active during S phase) mediated ubiquitination. Geminin (gene product of GMNN, hereafter referred to as geminin), an inhibitor of CDT1, is present during S and G2 phases to prevent MCM loading and is normally degraded upon mitotic exit by the anaphase-promoting complex/cyclosome (APC/C). These oscillations in CDT1 and geminin ensure the genome is replicated once and only once in each cell cycle. I used FUCCI(CA)2 probes which can distinguish between G1, S and G2 phases by using an APC/C-sensitive geminin probe and a CDT1 probe specifically sensitive to CUL4DDB1 (Sakaue-Sawano et al., 2017). With this system, G1 is defined by high CDT1, S by high geminin, and G2/M by high CDT1 and geminin (Figure 3.4A). The geminin fragment is tagged with mVenus (mVenus-Gem) and the CDT1 fragment is tagged with mCherry (mCherry-CDT1). I introduced the probes into U2OS cells by lentiviral transduction. I also introduced mTurquoise-tagged H2B, which labels the nucleus and generates clear

signal in all cell cycle phases. Single cell clones positive for mCherry, mVenus and mTurquoise were selected by FACS sorting (Figure 3.4B-E).

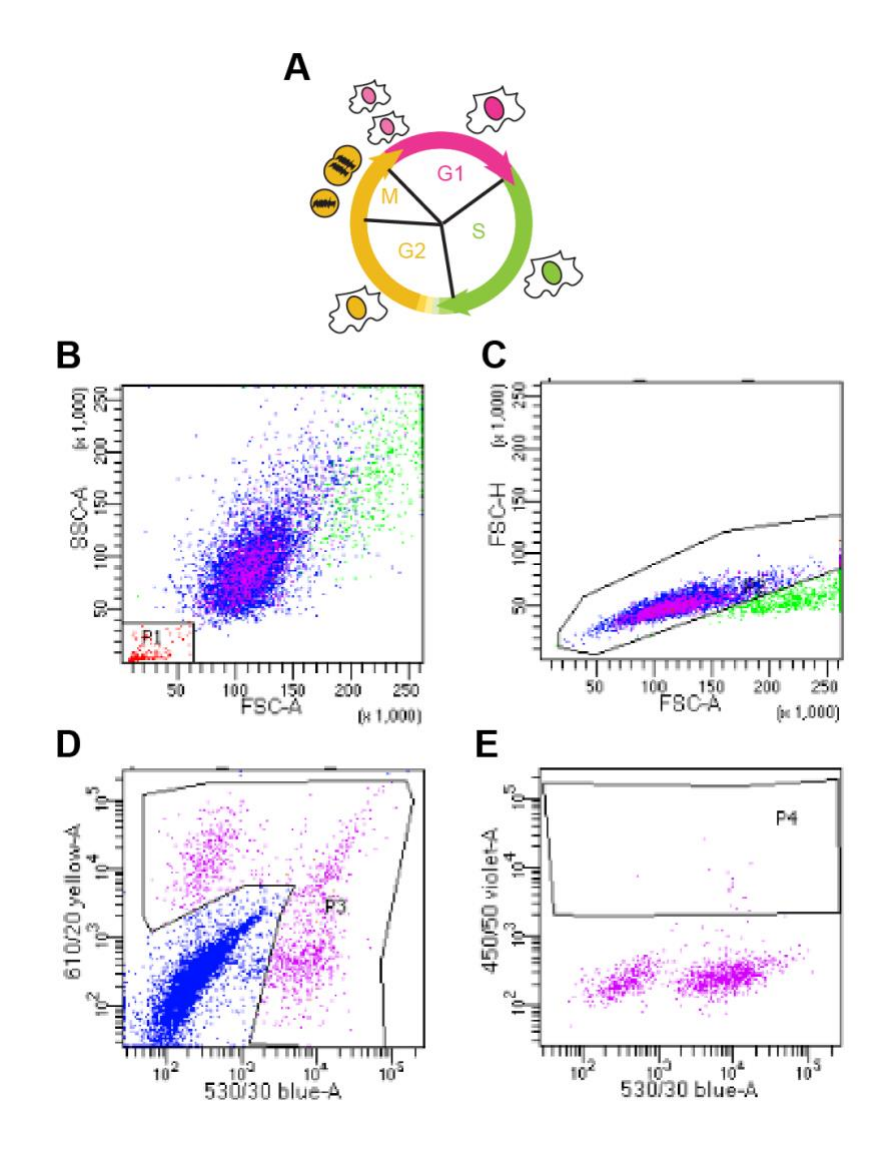


Figure 3.4 Establishment of FUCCI cells.

(A) Schematic showing colours of cell cycle phases of the FUCCI(CA)2 system. U2OS cells were transduced with lentivirus containing FUCCI(CA)2 plasmid and pCSII EF1a hH2B-Turq plasmid. Positive cells were selected by FACS sorting as in (B-E). In (B), dead cells and debris (P1) were excluded, the remaining population were selected for single cells using FSC-H and FSC-A as in (C). Cells positive for mCherry signal (positive in the 610/20 channel) or mVenus signal (positive in the 530/30 channel) were selected as in (D). Cells positive for mTurquoise (positive in the 450/50 channel) were then single-cell sorted into 96-wells.

Using the mTurquoise-H2B signal, I created an automatic single-cell tracking system based on TrackMate that can track single cells (Figure 3.5A, B) and simultaneously measure the fluorescence intensities for the corresponding FUCCI reporters over time (Figure 3.5C). In addition, I observed an abrupt increase in mTurquoise-H2B signal during mitosis due to chromosome condensation. This allowed me to clearly distinguish mitosis on the temporal profiles of single-cell tracks. As a result, the automatic single-cell tracking system can effectively distinguish all 4 phases, G1, S, G2 and M phases, of the cell cycle.

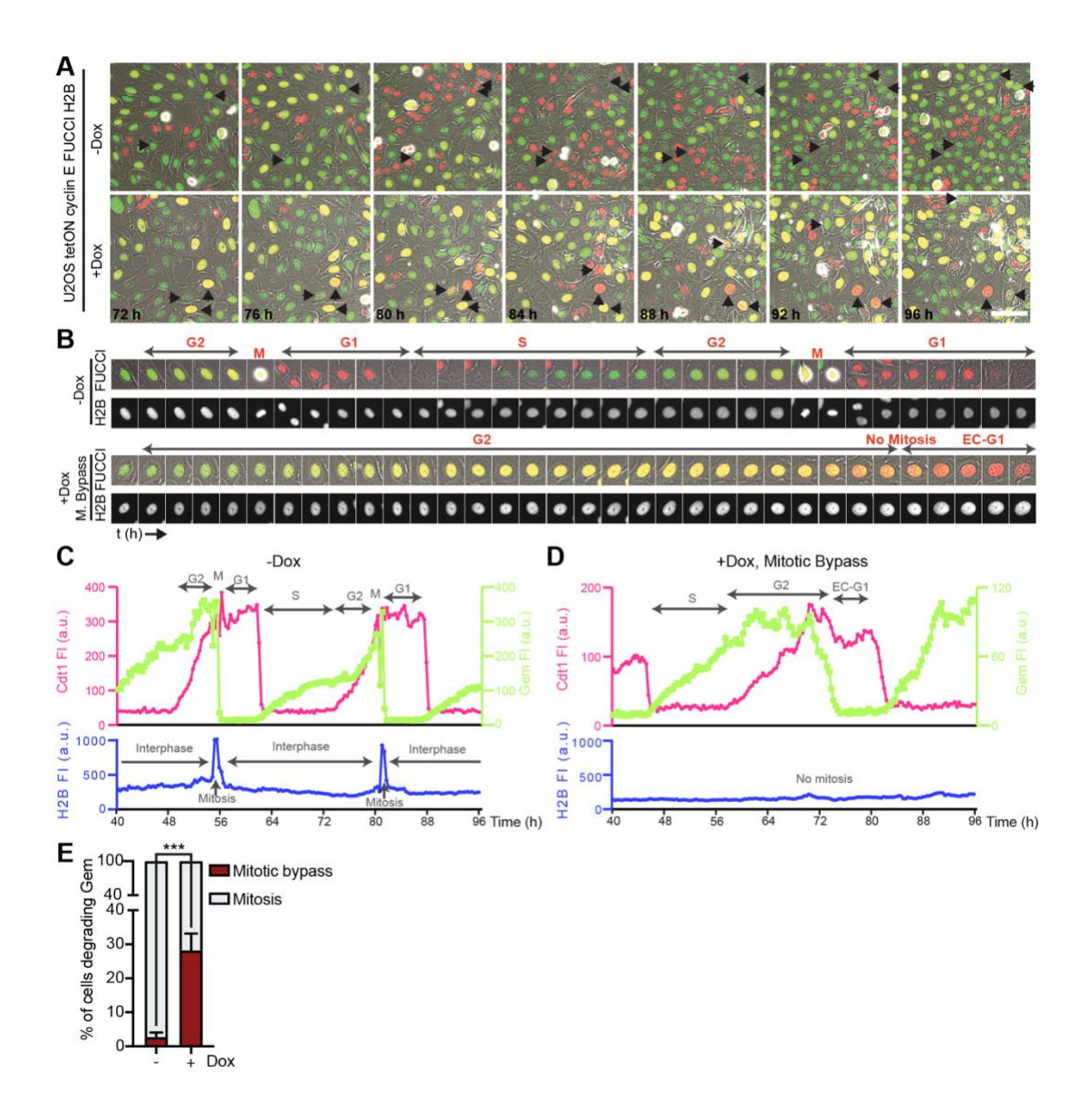


Figure 3.5 FUCCI imaging of U2OS cells overexpressing cyclin E.

- (A) Time-lapse imaging of U2OS tetON cyclin E FUCCI H2B cells treated with or without Dox. Every 20 min, images for FUCCI, H2B and phase contrast channels were acquired, for 72 h. FUCCI fluorescence and phase contrast images were merged. Selected images at indicated timepoints are shown from one representative experiment of three individual repeats. Example individual cells and their daughter cells after mitosis are indicated by arrows facing the same direction. Scale bar, 100 μm.
- (B) Tracking of an example cell in non-dox-treated (-Dox) and cyclin E-overexpressing (+Dox) conditions from (A) is shown.
- (C and D) Temporal profiles of fluorescence intensities (FI) of mCherry-CDT1, mVenus-Gem, and mTurquoise-H2B of a control cell (-Dox) and a Dox-treated cell bypassing mitosis. a.u., arbitrary unit.
- (E) The mean percentages of cells that bypassed mitosis, measured in % of cells that degraded geminin (% of cells completing S/G2) with SDs were

obtained from three independent experiments. At least 400 cells for each condition analysed. Statistical significance (\*\*\*p<0.001) was examined by unpaired t test.

I used this system to analyse U2OS cells expressing cyclin E. Control cells without cyclin E overexpression entered and exited mitosis, as demonstrated by the rapid degradation of mVenus-Gem and the spike of mTurquoise-H2B (Figure 3.5C). I found ~30% cyclin E-overexpressing cells degraded mVenus-Gem without evidence of mitosis (no chromosome condensation or nuclear envelope breakdown), entering G1 directly from G2 (Figure 3.5D, E). This G1 phase following mitotic bypass was termed by us as Endoreduplication Cycle G1 (EC-G1) phase to differentiate it from normal G1 phase (Figure 3.5D). After certain time in EC-G1, most cells degraded mCherry-CDT1 and started to accumulate mVenus-Gem, indicating these cells entered S phase and endoreduplicated (Figure 3.5D). Nocodazole is a chemical that inhibits polymerisation of microtubules and commonly used to arrest cells at metaphase of mitosis. These data suggest that cyclin E overexpression causes whole genome duplication through mitotic bypass and endoreduplication.

I noticed mVenus-Gem degradation was significantly slower during mitotic bypass in cyclin E-expressing cells than mitosis in control cells. mVenus-Gem degradation in mitosis is rapid, with an average half time ( $t_{1/2}$ ) of 64.4 ± 26.5 min (mean ± SD, median = 71.6 min), while it is significantly slower during mitotic bypass, with an average half time ( $t_{1/2}$ ) roughly 4 times longer (253.9 ± 97.3 min, median = 232.5 min) (Figure 3.6A). The length of time it costed to degrade mVenus-Gem was also highly variable during mitotic

bypass, ranging from ~2 h to 8 h. In addition, there were many aberrant events. ~3% of cells appeared to have G2 to S phase transition, where mCherry-CDT1 degradation began before complete degradation of mVenus-Gem (Figure 3.6B-D). These cells presumably entered S phase with incompletely licensed origins, as loading of the replication helicase MCM occurs in G1 phase. Therefore, unlike normal mitosis, mitotic bypass is a very variable and messy process.

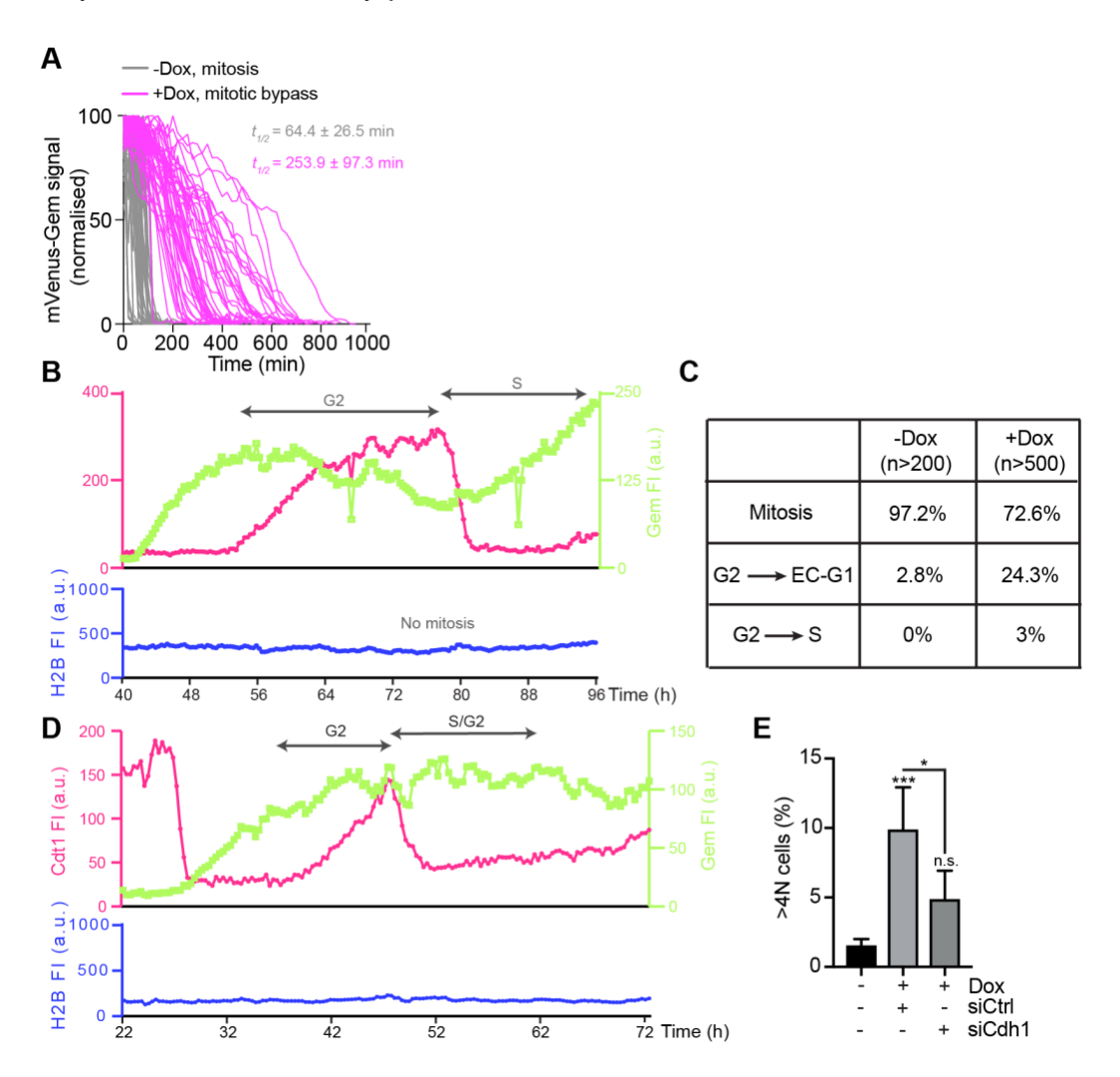


Figure 3.6 Abnormal cell cycle transitions in cyclin E-overexpressing cells.

(A) Normalised data of mVenus-Gem degradation over time in cells from a representative experiment in Figure 3.5A-E. Each line shows a tracking from a single cell (at least 50 cells for each condition were examined). Average

- half-life  $(t_{1/2})$  values with SDs of mVenus-Gem degradation calculated by logistic growth curve fitting are shown both in the figure and main text.
- (B) Temporal profiles of FUCCI channels and mTurquoise-H2B of a cyclin E-overexpressing U2OS cell that appeared to have a G2 to S transition in an experiment in Figure 3.5A-E.
- (C) Summary table of cell cycle transitions from G2 observed in control (-Dox) and cyclin E-overexpressing (+Dox) conditions from three independent experiments combined in Figure 3.5A-E. G2 to EC-G1 transition is classified as complete degradation of Venus-Gem without a spike in the H2B signal, followed by high mCherry-CDT1 signal. G2 to S transition is scored when mCherry-CDT1 degradation began before complete degradation of mVenus-Gem. Experimental details are described in Figure 3.5A-E.
- (D) Temporal profiles of a cyclin E-overexpressing U2OS cell that appeared to have a G2 to S/G2 transition in an experiment in Figure 3.5A-E.
- (E) U2OS cells overexpressing cyclin E (+Dox) for 96 h were supplemented with siRNAs at 48 h to knockdown CDH1. The percentage of cells with >4N DNA content analysed by FACS is shown. Mean percentages from 3 independent experiments with SDs are shown. Statistical significance (\*p<0.05; \*\*\*p<0.001; n.s., non-significant) was examined by Tukey's method.

The APC/C degrades various cell cycle factors, including geminin and cyclin B, to promote entry into, and progression through, G1. In a mitotic cell cycle, two activators of APC/C, CDC20 and CDH1, act one after the other in mitosis and G1 respectively (Clijsters et al., 2013). Given endoreduplicating cells never entered mitosis, I asked whether APC/CCDH1 is primarily responsible for G1 entry in these cells. Indeed, depleting CDH1 reduced WGD in cyclin E-overexpressing cells (Figure 3.6E). This is consistent with previous findings that CDH1 is crucial for endoreduplication cell cycles caused by persistent telomere damage or DSBs (Davoli et al., 2010). CDC20 could not be adequately assessed because depletion of CDC20 resulted in mitotic arrest and eventually extensive mitotic death (data not shown). It role in cyclin E-induced mitotic bypass was therefore inconclusive.

## 3.2.3 Role of the DNA damage checkpoint

Mitotic bypass has previously been shown to occur following activation of the G2 checkpoint (Davoli et al., 2010). Cyclin E expression led to an accumulation of G2 cells over time, as seen with an increase in the cyclin B-positive population (a marker of G2) (Figure 3.7A). Consistent with activation of the G2 checkpoint, FUCCI imaging revealed that the average length of G2 increased significantly from 8 ± 3 h (mean ± SD, median = 8 h) in control U2OS cells to 23 ± 14 h (mean ± SD, median = 21 h) in cyclin E-expressing cells that bypassed mitosis (Figure 3.7B). Upregulation of p-CHK1, p-p53, and p-RPA, inhibitory phosphorylations of CDK1 (Figure 3.7C) was observed. This is consistent with previous findings that cyclin E overexpression leads to replication stress (Spruck et al., 1999), presumably why the G2 checkpoint was activated; It reduces loading of the replication helicase MCM during G1, and alters replication origin usage during S phase (Ekholm-Reed et al., 2004, Bartkova et al., 2005, Bester et al., 2011, Matson et al., 2017).

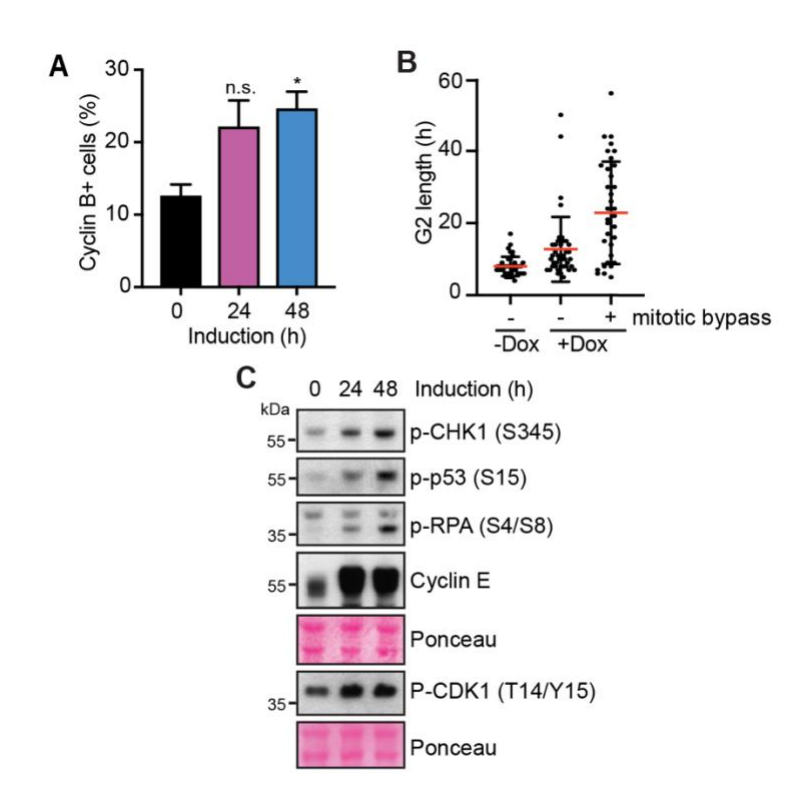


Figure 3.7 G2 arrest of cyclin E-overexpressing U2OS cells.

- (A) Quantification of FACS analysis of U2OS cells positive for cyclin B1 following doxycycline induction to overexpress cyclin E. Mean percentages with range from 2 independent experiments are shown. Statistical significance (\*p<0.05; n.s., non-significant) was examined by unpaired t test. Note: this experiment was performed by Stephanie Hills.
- (B) G2 lengths of cells measured from a representative FUCCI experiment in Figure 3.5A-E. Each dot represents a single cell. Mean length is labelled in red. At least 50 cells were measured for each group.
- (C) Immunoblots showing expression of DNA damage markers in cyclin Eoverexpressing cells. Note: this experiment was performed by Stephanie Hills.

Flow cytometry assays were used on whole cells to study protein dynamics throughout the cell cycle, measuring EdU incorporation to determine replication rate and extracted cells to examine the chromatin-bound fraction. As previously reported, cyclin E expression shortened the length of G1 phase (Figure 3.8A, B), caused cells to enter S phase with reduced MCM (Figure 3.8C-F), and led to a reduction of EdU incorporation in S phase and

higher levels of  $\gamma$ H2AX (Figure 3.8G, H), indicative of replication stress. Depleting FBXW7 which led to a moderate increase in cyclin E expression level also reduced EdU incorporation and upregulated phospho-CHK1 (Figure 3.8I, J).

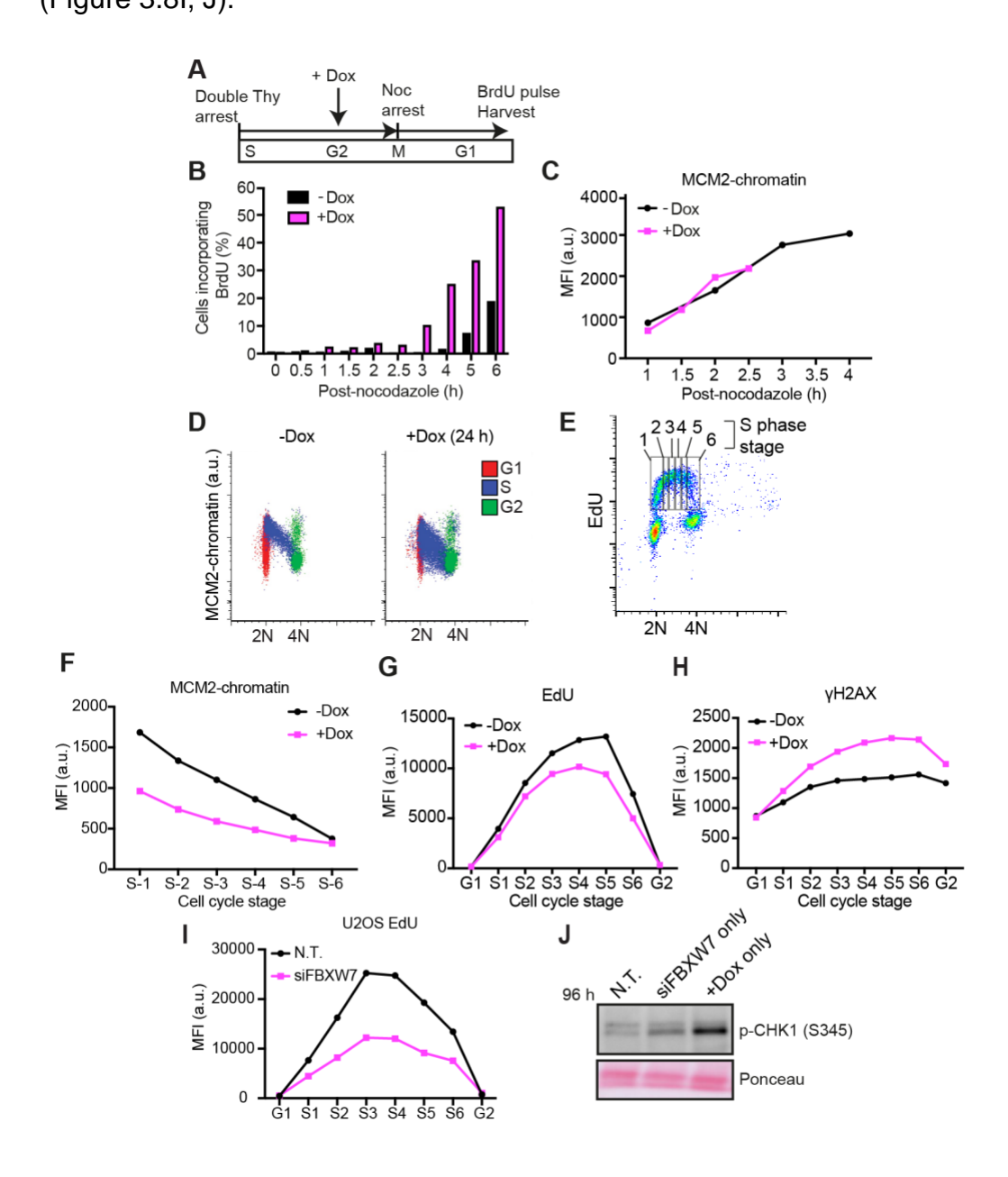


Figure 3.8 Replication stress in cyclin E-overexpressing U2OS cells.

(A-C) U2OS cells were synchronised and treated as in (A). Dox was added while synchronised cells were in G2. Cells released into G1 post nocodazole arrest were pulsed with a nucleotide analogue BrdU and harvested at different timepoints for FACS analysis. The percentage of BrdU-positive cells at different timepoints is shown in (B). Chromatin bound-MCM2 level is

- shown in (C). MFI: mean fluorescence intensity. a.u.: arbitrary unit. Note: this experiment was performed by Stephanie Hills in a single repeat.
- (D) Chromatin bound-MCM2 level in control and cyclin E-expressing U2OS cells (+ Dox), analysed by FACS. G1, S and G2 phases were coloured according to EdU incorporation and DNA content; G1: 2N, EdU negative. S: 2N-4N, EdU positive. G2: 4N, EdU negative. A representative experiment of three independent repeats is shown. Note: this experiment was performed by Stephanie Hills.
- (E) S phase was divided into 6 stages as shown for Figure 3.7F-I. Note: this experiment was performed by Stephanie Hills.
- (F) Mean fluorescence intensities of chromatin bound-MCM2 levels measured in FACS analysis of cells overexpressing cyclin E are shown. A representative experiment of three independent repeats is shown. Note: this experiment was performed by Stephanie Hills.
- (G) Mean fluorescence intensities of EdU incorporation levels measured in FACS analysis of cells overexpressing cyclin E are shown. A representative experiment of three independent repeats is shown. Note: this experiment was performed by Stephanie Hills.
- (H) Mean fluorescence intensities of gH2AX levels measured in FACS analysis of cells overexpressing cyclin E are shown. A representative experiment of three independent repeats is shown. Note: this experiment was performed by Stephanie Hills.
- (I) Mean fluorescence intensities of EdU incorporation levels measured in in FACS analysis of cells depleted with FBXW7 are shown. A representative experiment of three independent repeats is shown.
- (J) Immunoblot showing p-CHK1 (S345) expression in FBXW7-depleted U2OS cells. A representative immunoblot was selected from two independent experiments.

Note: the cell line used in Figure 3.8 is U2OS tetON cyclin E.

G2 arrest was seen in cells overexpressing cyclin E in the FUCCI experiments (Figure 3.5A, B; Figure 3.7B), indicating G2 checkpoint activation. As an independent validation experiment looking at G2 checkpoint activation, Figure 3.9A shows that the percentage of cyclin E-overexpressing cells entering mitosis decreases over time (Figure 3.9A black bars). As is the case after telomere damage, G2 checkpoint activation following cyclin E expression was CHK1-dependent; inhibition of CHK1 using a chemical inhibitor forced cells arresting at G2 into mitosis (Figure 3.9A) and elevated the frequency of abnormal mitosis (Figure 3.9B). Interestingly, I also saw

longer G2 in a subset of cyclin E-overexpressing cells that eventually completed mitosis, increasing to  $13 \pm 9 \text{ h}$  (mean  $\pm \text{SD}$ , median = 10 h) (Figure 3.7B). Therefore, it seems that most cyclin E-expressing cells experienced sufficient stress to activate the G2 checkpoint but some cells resolved replication issues adequately to enter mitosis; in these cells, mitosis appeared to have minor problems within 48 h of cyclin E overexpression (Figure 3.9B). In other cells, presumably those experiencing the most severe stress, the G2 checkpoint remained active, extending G2 to approximately three times the normal length, before cells eventually bypassed mitosis and entered EC-G1. Cells that entered EC-G1 could be separated from those that were still arrested in 4N G2 in flow cytometry assays (Figure 3.9C); cells that re-loaded MCM with 4N DNA content were identified as EC-G1 cells while cells that did not re-load MCM at 4N were assumed to be in G2. It was found cells that bypassed mitosis went into EC-G1 with a lower DNA content on average than their 4N G2 counterparts (Figure 3.9D, E). Those EC-G1 cells also had increased level of the DNA damage maker yH2AX (Figure 3.9F). These data show that cyclin E overexpression causes replication stress; cells with less stress can, resolve replicative issues and go into mitosis after some time arresting in G2. However, cells with higher levels of replication stress have extended G2 arrest; these cells eventually bypass mitosis, enter EC-G1 without under-replicated DNA and then enter S phase to endoreduplicate.

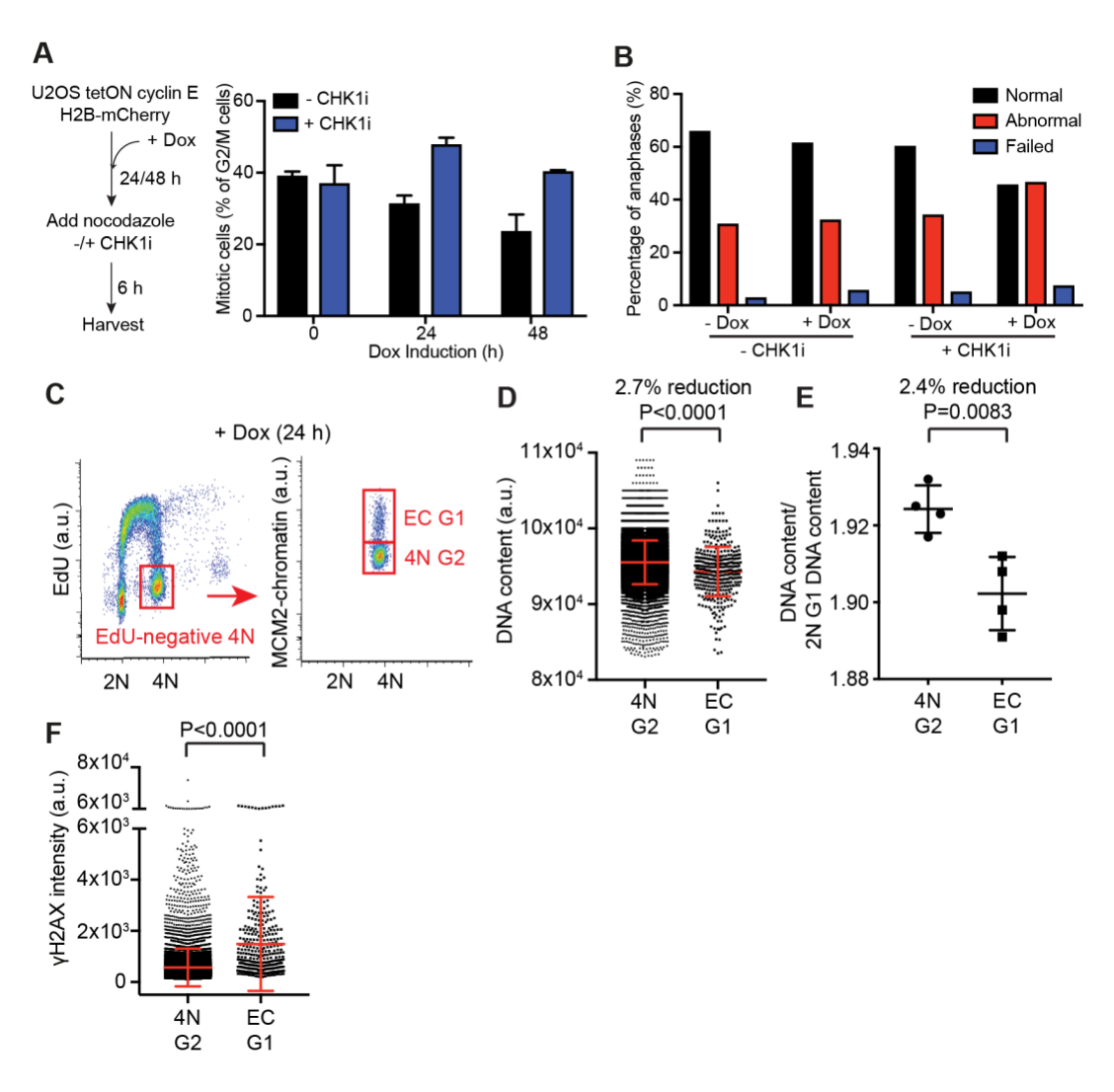


Figure 3.9 Endoreduplicating cells start with under-replicated DNA.

- (A) Schematic of the experiment approach is shown in the left. Quantification of FACS analysis of cells in mitosis (pH3+ cells) is shown. Mean percentages with range from two independent experiments are shown. Note: this experiment was performed by Stephanie Hills.
- (B) U2OS cells expressing cyclin E were treated with 100 nM CHK1 inhibitor and live imaged for 12 h. The percentages of abnormal mitosis and failed mitosis are shown. The experiment was performed in a single repeat. Note: This experiment was performed by Stephanie Hills.
- (C-F) EC-G1 cells were identified as cells with 4N DNA content, EdU- and MCM2+ as in (C). 4N G2 cells were identified as cells with 4N DNA content, EdU- and MCM2-. The DNA content of single cells in the 4N G2 and EC-G1 populations was measured using DAPI intensity as in (D) from a representative experiment. Average DNA content of 4N G2 and EC-G1 populations relative to 2N G1 DNA content from four independent experiments was calculated and shown in (E).  $\gamma$ H2AX levels were compared as in (F). Statistical significance was examined by unpaired t test. Note: These experiments were performed by Stephanie Hills.

Note: the cell line used in Figure 3.9 is U2OS tetON cyclin E.

WGD has been proposed as an intermediate on the pathway to aneuploidy during tumorigenesis. Whole genome duplicated cells tend to have supernumerary centrosomes which increases the chance of chromosome mis-segregation. They may also be more permissive to gain or loss of chromosomes due to a buffering effect of their extra chromosomes, and their increased genomic material may increase the chance of acquiring numerical aberrations (Ganem et al., 2007). I could grow up clones of sorted endoreduplicated cells following cyclin E expression and counted chromosomes in metaphase spreads. I found the endoreduplicated clones possessed a much wider range of chromosome numbers than the control (Figure 3.2). This extensive variation in individual cell karyotypes indicates that chromosomal instability occurred during expansion of the clone. To investigate the cause of this chromosomal instability in endoreduplicated cells. I sorted and isolated cells with >4N DNA content after cyclin E overexpression and analysed their first cell cycle after WGD (Figure 3.10A). These cells were live imaged, in the absence of cyclin E expression (-Dox). I found the lengths of G2 (20 h) and S phases (18 h) of these cells were significantly longer than in control cells (11 h and 8 h) (Figure 3.10B). I observed the first mitosis following WGD, and found 10% of the cells had multipolar mitosis, suggesting the presence of supernumerary centrosomes (Figure 3.10C, D) (Chen et al., 2016, Ganem et al., 2009). The other 90% of the cells underwent bipolar mitosis; however, these cells showed higher frequencies of failed cytokinesis, micronuclei, and nuclear fragmentation (Figure 3.10E, F). These results suggest that the first cell cycles of

endoreduplicated cells after mitotic bypass are particularly chaotic, which likely contributes to chromosomal instability.

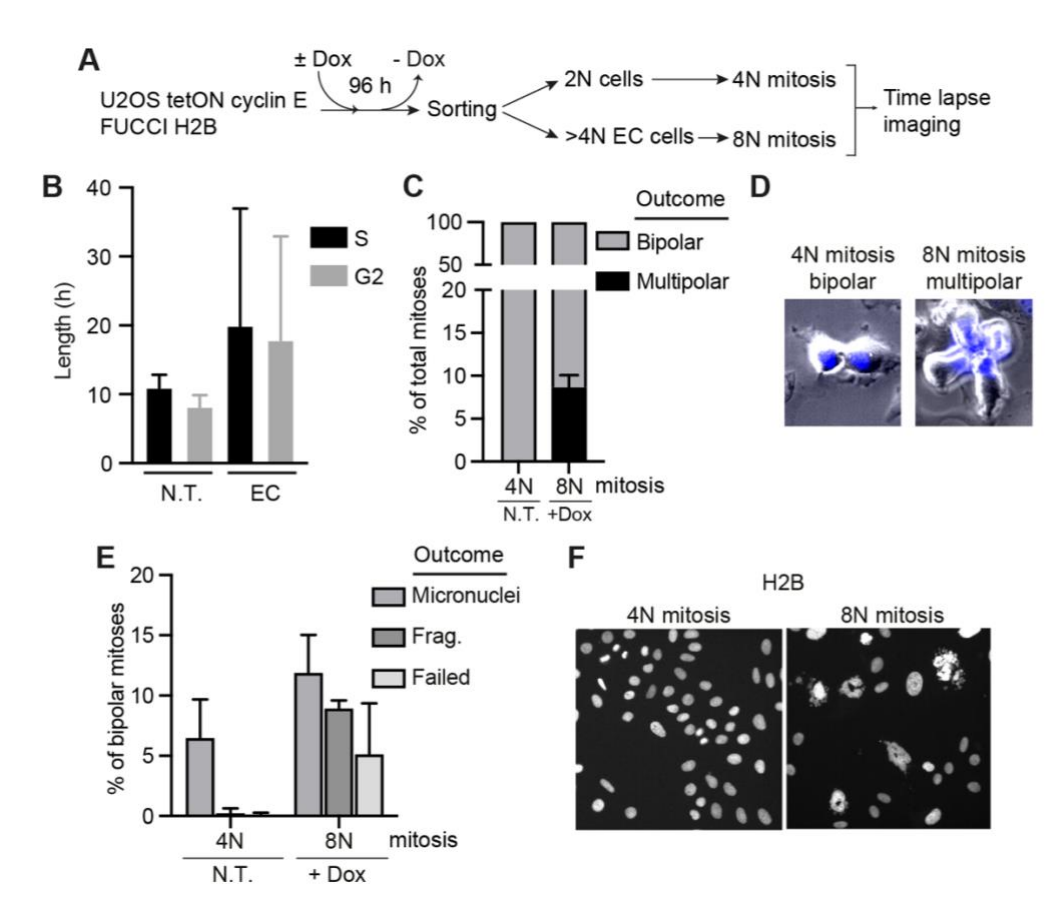


Figure 3.10 Whole genome duplicated cells undergo abnormal mitosis.

(A-F) Schematic of the experimental approach is shown in (A). Lengths of S and G2 phases of sorted 2N and >4N EC (endoreduplication cycle) cells are shown in (B), calculated from over 45 cells in 2 independent experiments. Mean lengths  $\pm$  SDs for Ctrl S, Ctrl G2, EC S and EC G2 are 11  $\pm$  2 h, 8  $\pm$  2 h, 20  $\pm$  17 h, 18  $\pm$  15 h respectively. Median lengths are 11 h, 8 h, 12 h and 11.5 h respectively. Quantification of mean percentages of bipolar and multipolar mitosis with SDs from three independent experiments is shown in (C). Selected H2B and phase contrast composite images of 4N bipolar mitosis and 8N multipolar mitosis are shown in (D). Mean percentages of abnormal mitosis with SDs from three independent experiments are shown in (E). Example still images of sorted cells' nuclei are shown in (F).

#### 3.3 Conclusions

The results from this chapter show that U2OS cells became whole genome duplicated when induced to overexpress cyclin E. Most notably, the data

from the FUCCI experiments show that cyclin E-overexpressing cells bypassed mitosis and endoreduplicated after an extended G2 arrest. I show that the G2 checkpoint was activated in cyclin E-overexpressing cells, presumably due to replication stress caused by abnormal origin licensing. In the FUCCI experiments, mitotic bypass is indicated by the degradation of mVenus-Gem without a spike in the mTurquoise-H2B signal. I found that the degradation of mVenus-Gem during mitotic bypass was slow and highly variable than normal mitosis, as its average half-time is longer and shows greater standard deviations. Using FACS experiments I show cells that bypassed mitosis were likely those with more replication stress and underreplicated DNA. Taken together, these results show cyclin E-overexpressing cells become whole genome duplicated through a highly abnormal pathway – mitotic bypass.

I could isolate WGD single cell clones from cyclin E overexpression, indicating endoreduplicated cells are viable. These clones displayed subtetraploid karyotypes with highly variable chromosome numbers within the population, indicating CIN after WGD. FUCCI imaging of newly endoreduplicated cells show these cells experienced extended S phase and chaotic mitosis, which likely contributes to CIN. This is consistent with a recent studying showing that the first S phase of newly whole genome duplicated cells is highly unstable that leads to genetic instability (Gemble et al., 2022).

# Chapter 4. Result 2. Replication stress drives mitotic bypass in U2OS and RPE1 cells

# 4.1 Introduction

Cyclin E overexpression causes replication stress and activates the G2 checkpoint, but the roles of replication stress and the checkpoint in mitotic bypass are unclear. In this chapter I use other forms of replication stress to investigate the relationship between replication stress and mitotic bypass. I use small molecule inhibitors to test whether mitotic bypass is dependent on different checkpoint kinases. I also test to extend our findings from the previous chapter to another cell line – RPE1, which a non-cancerous epithelial cell line immortalised by telomerase.

## 4.2 Results

# 4.2.1 Replication stress in general induces endoreduplication in U2OS cells

Given WGD occurs following cyclin E-induced replication stress, I asked if different types of replication stress are able to induce endoreduplication or cyclin E overexpression plays unique roles other than causing replication stress. To test this, I used aphidicolin, a reversible inhibitor of eukaryotic DNA replication, isolated from the mould *Cephalosporium aphidicola*, that specifically inhibits B-family DNA polymerases including Pol  $\alpha$ , Pol  $\delta$ , Pol  $\epsilon$  (Baranovskiy et al., 2014). Treating U2OS cells with aphidicolin induced

expression of DNA damage markers and expression of p21, consistent with replication stress (Figure 4.1A). I found aphidicolin was greatly effective in causing mitotic bypass without cyclin E overexpression; around 80% of the cells went into EC-G1 without mitosis after 72 h treatment of 1 μM aphidicolin, as shown by FUCCI live cell imaging (Figure 4.1B, C). During this process, cyclin B was degraded, so that there was an accumulation of cells with 4N DNA content and low cyclin B levels (Figure 4.1D, E), which were identified as EC-G1 cells in FACS analysis. The majority of these EC-G1 cells re-loaded MCM (Figure 4.1F).

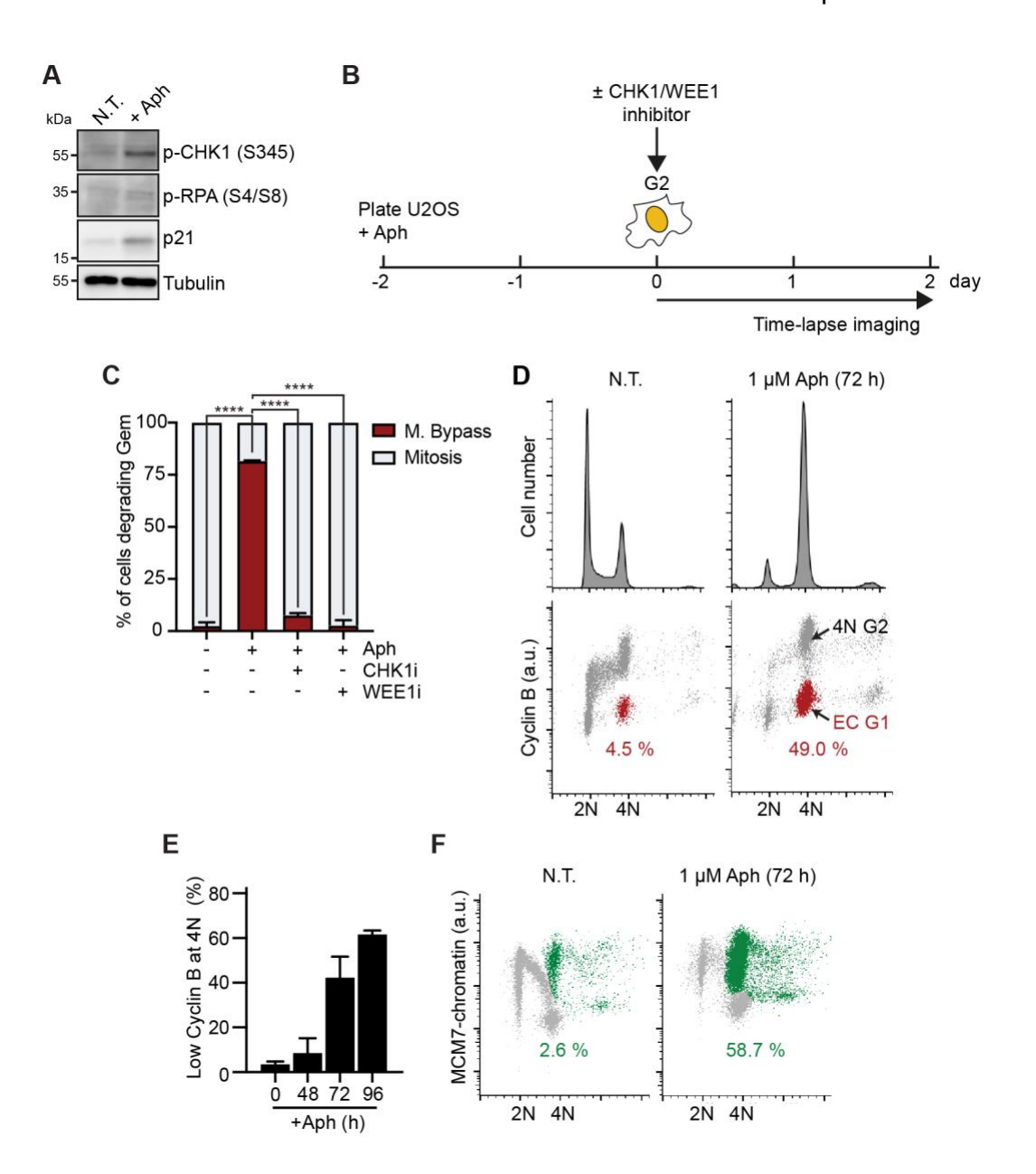


Figure 4.1 Aphidicolin induces mitotic bypass in U2OS cells.

- (A) Immunoblots showing expression of DNA damage markers in U2OS cells treated with 1  $\mu$ M aphidicolin (Aph). Representative immunoblots were selected from two independent experiments.
- (B and C) Schematic of the experiment approach is shown in (B). The mean percentage with range of U2OS cells that bypassed mitosis in 1  $\mu$ M aphidicolin, supplemented with CHK1 or WEE1 inhibitor, is shown in (C). At least 200 cells for each condition were analysed from two independent experiments. The U2OS cell line used is U2OS TetON cyclin E FUCCI H2B without doxycycline (Dox) supplement. Statistical significance (\*\*\*\*p<0.0001) was examined by Tukey's method.
- (D-F) Aph-treated U2OS cells were analysed for DNA content, cyclin B1, and chromatin-bound MCM7 by FACS. Cells with 4N DNA content and low cyclin B level were assumed to have entered EC-G1 (labelled in red in (D)), and

quantified from two independent experiments with mean and range shown in (E). Cells at 4N that re-loaded MCM7 are labelled in green in (F). One representative experiment of three independent repeats is shown for (D) and (F).

Like during cyclin E overexpression, degradation of geminin during Aphinduced mitotic bypass was a slow process, having a mean  $t_{1/2}$  of 229.8 ± 110 minutes (mean ± SD, median = 211 minutes) (Figure 4.2A). It was also variable, with  $t_{1/2}$  spanning from 2 h to 10 h. This suggests replication stressinduced mitotic bypass per se is slow and variable, regardless of cyclin E expression. I also saw extended G2 arrest in aphidicolin treated cells. As with cyclin E expression, adding CHK1 or WEE1 inhibitors almost abolished mitotic bypass and forced aphidicolin-treated cells into aberrant mitoses, with large numbers of micronuclei generated, suggesting the CHK1-dependent G2 checkpoint is required for replication stress-induced mitotic bypass (Figure 4.1B, C; Figure 4.2B). It also required CDH1; depleting CDH1 almost completely prevented cells entering EC-G1 (accumulation of 4N cyclin B negative cells) (Figure 4.2C-E) while depleting CDC20 showed a minor effect. Therefore, APC/CCDH1 was mainly responsible for cyclin B degradation during mitotic bypass, a role performed primarily by APC/CCDC20 in a diploid cell cycle. I found releasing U2OS EC-G1 cells from aphidicolin into fresh media allowed them to enter S phase. The endoreduplicated cells appeared to be viable, with up to approximately 40% of cells incorporating EdU with >4N DNA content 72 h post release from 1 µM aphidicolin (Figure 4.2F-H). Diplochromosomes were seen in metaphase samples of aph-treated U2OS cells (Figure 4.2I, J). These data suggest that aphidicolin-induced replication stress is sufficient to cause WGD in U2OS cells.

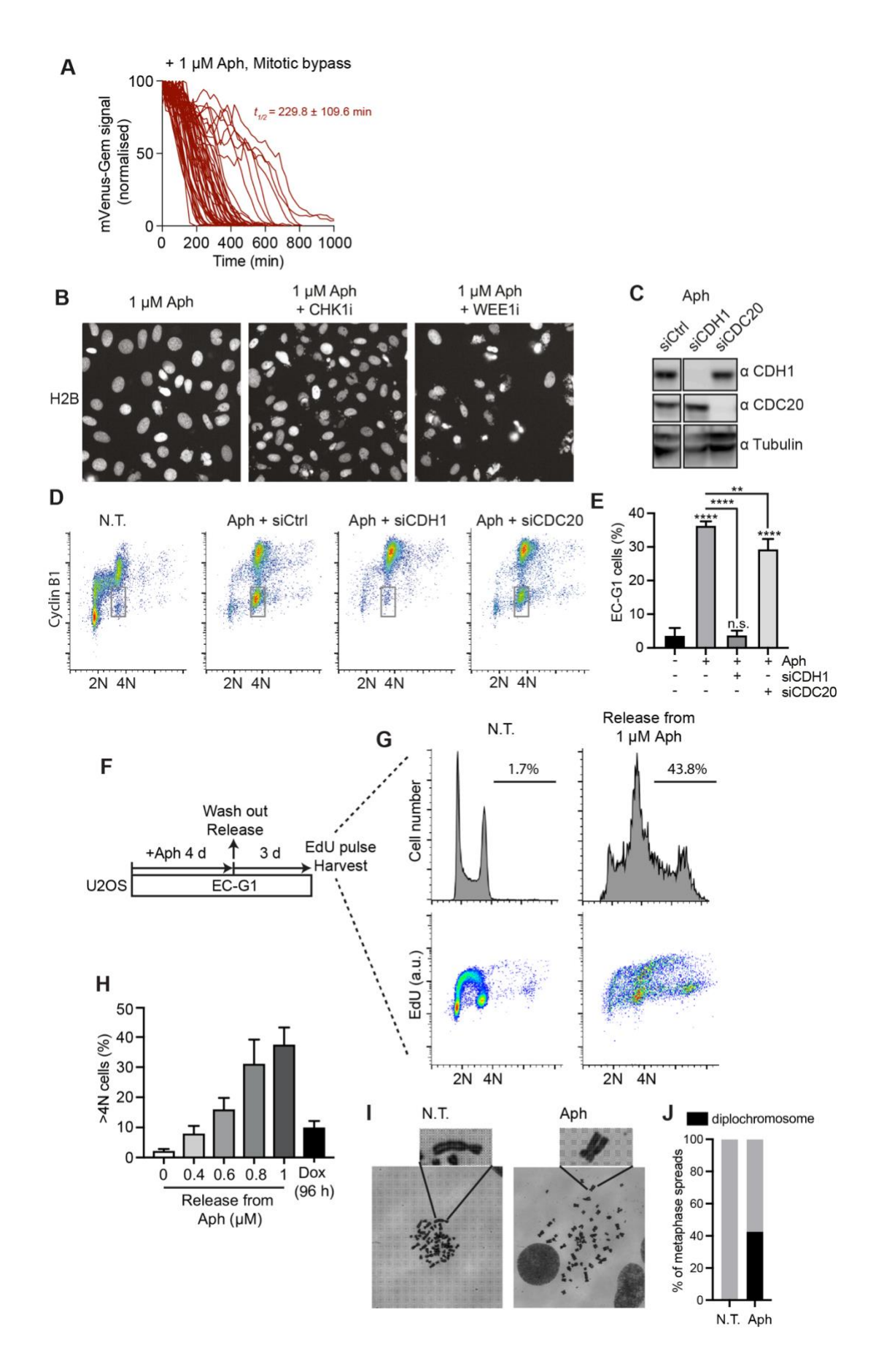


Figure 4.2 Aphidicolin induces whole genome duplicatiin in U2OS cells.

- (A) Normalised data of mVenus-Gem degradation in aph-treated cells over time in Figure 4.1B. Each line shows a tracking from a single cell (at least 50 cells were shown for each condition). Average half-life ( $t_{1/2}$ ) values with SDs of mVenus-Gem degradation calculated by logistic growth curve fitting are shown in the figure and main text.
- (B) Selected images of the H2B-mTurquiose channel after adding CHK1 or WEE1 inhibitor to Aph treated U2OS cells as in Figure 4.1B.
- (C-E) Aph-treated U2OS cells were depleted with CDH1 or CDC20 using siRNAs. Immunoblots showing knockdown of CDH1 and CDC20 are in (C). Cells were analysed by FACS for cyclin B level and DNA content as in (D). Cells with low cyclin B level at 4N DNA content were identified as EC-G1 cells and are quantified in (E). The mean percentage of EC-G1 cells from three independent experiments with SDs is shown. Statistical significance (\*\*\*\*p<0.0001; \*\*p<0.005; n.s., non-significant) was examined by Tukey's method.
- (F-H) Schematic of the experimental approach is shown in (F). Cells released from aphidicolin were analysed by FACS for EdU incorporation and DNA content as shown in (G). Numbers indicate cells with >4N DNA content. The mean percentages of >4N cells with SDs from three independent experiments are shown in (H) for cells released from aphidicolin titrations. (I and J) U2OS cells treated with 1  $\mu$ M aphidicolin were analysed by metaphase spreads. An example spread sample with diplochromosomes is shown in (I). The percentage of spread samples showing diplochromosomes from one independent experiment is shown in (J). N.T.: non-treated.

Next, I went on to test if replication stress caused by other oncogenes can induce mitotic bypass. U2OS cell lines that can inducibly express CDC25A, MYC and oncogenic RAS (HRAS<sup>V12</sup>) were established and they were all capable of inducing cells with >4N DNA content to some extent (Figure 4.3A, B). Ras<sup>V12</sup> has been shown to cause replication stress via elevating the level of ROS (Lee et al., 1999, Irani et al., 1997). Consistent with this, treating Ras-expressing cells with an anti-oxidant N-acetyl cysteine (NAC) reduced γH2AX level and WGD (Figure 4.3C, D). In contrast, cyclin E-induced γH2AX level and WGD were not affected by NAC, consistent with the fact that cyclin E causes replication stress by reducing origin licensing rather than generating ROS. In addition, unlike cyclin E overexpression, HRAS<sup>V12</sup>

overexpression did not affect origin licensing (Figure 4.3E). Altogether, these data suggest that replication stress in general acts as a driver of WGD. I also established a U2OS cell line that can inducibly express cyclin D (Figure 4.3F). In contrast to other oncogenes, cyclin D expression did not induce whole genome duplication (Figure 4.3G).

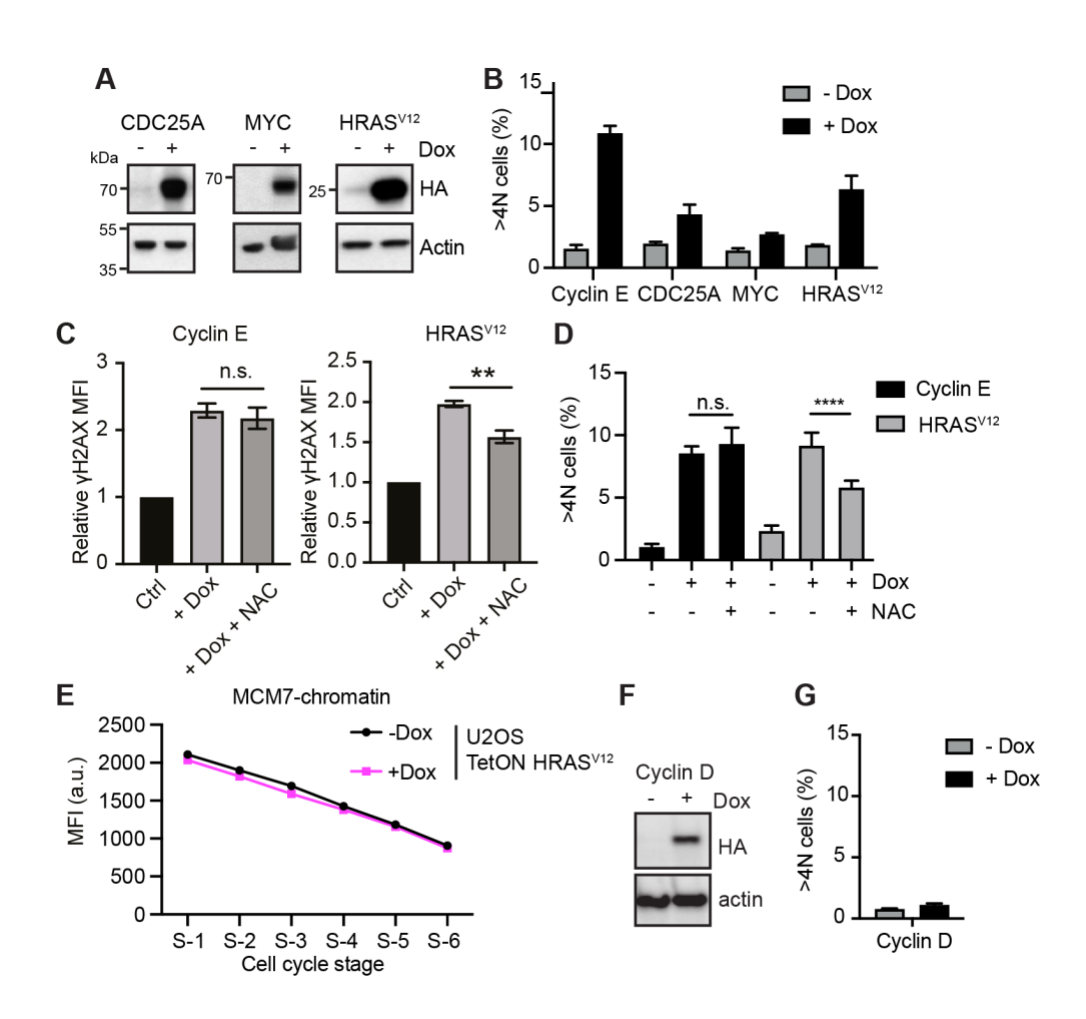


Figure 4.3 Other oncogenes can induce mitotic bypass in U2OS cells.

(A) Immunoblots showing overexpression of CDC25A, MYC or HRAS<sup>V12</sup> by addition of doxycycline (Dox) in U2OS tetON cell lines, probed by anti-HA antibody. A representative experiment of three independent repeats is shown. Note: this experiment was performed by Stephanie Hills.
(B) U2OS cells were induced to express oncogenes for 96 h and analysed for DNA content. The mean percentages of >4N cells with SDs from three independent experiments are shown. Note: this experiment was performed by Stephanie Hills.

- (C and D) U2OS cells induced to overexpress cyclin E or HRAS<sup>V12</sup> were treated with a reducing agent N-acetyl cysteine (NAC). Cells were analysed for γH2AX level and DNA content by FACS. The mean MFI with SDs of γH2AX level from there independent experiments is shown in (C). Statistical significance (\*\*p<0.01; n.s., non-significant, two-tailed) was examined by paired t test. The average percentage of >4N cells with SDs from four independent experiments is shown in (D). Data were obtained from three independent experiments. Statistical significance: \*\*\*\*p<0.0001, Tukey's method.
- (E) U2OS tetON HRAS<sup>V12</sup> were induced to overexpress HRAS<sup>V12</sup> before being analysed as in Figure 3.8F for MCM loading. One independent experiment is performed.
- (F) Immunoblots showing overexpression of cyclin D1 (cyclin D) by addition of doxycycline (Dox) in U2OS tetON cyclin D cells, probed by anti-HA antibody. A representative experiment of two independent repeats is shown. (G) U2OS tetON cyclin D cells were induced to overexpression cyclin D for 96 h (+Dox) before analysed for DNA content. The mean percentage with SDs of the fraction of >4N cells is shown, obtained from three independent experiments.

# 4.2.2 Replication Stress-Induced Mitotic Bypass in RPE1 Cells

U2OS cells are derived from a tumour and have already undergone a whole genome duplication event as indicated by their sub-tetraploid karyotype. They may have adapted to increased chromosome numbers and therefore can be more likely to survive after WGD. I wanted to investigate whether replication stress-induced WGD occurs in a more normal, diploid cell line. To this end, I used hTERT-RPE1 (hereafter RPE1), an non-cancer-derived, near diploid, retinal pigment epithelial (RPE) cell line that was immortalised by telomerase introduction (hTERT). RPE1 cells are genetically stable with wild type p53 background and are widely used to model cell cycle and DNA repair.

An RPE1 cell line that can inducibly express full-length cyclin E1 upon doxycycline addition was established (Figure 4.4A). Similar to the U2OS cells

described previously, cyclin E-expressing RPE1 cells had reduced MCM loading, lower rate of DNA synthesis and upregulated DNA damage markers, consistent with replication stress and G2 checkpoint activation (Figure 4.4B-D). Overtime, these cyclin E-overexpressing RPE1 cells also underwent whole genome duplication (Figure 4.4E, F), to a similar degree as the U2OS cell line.

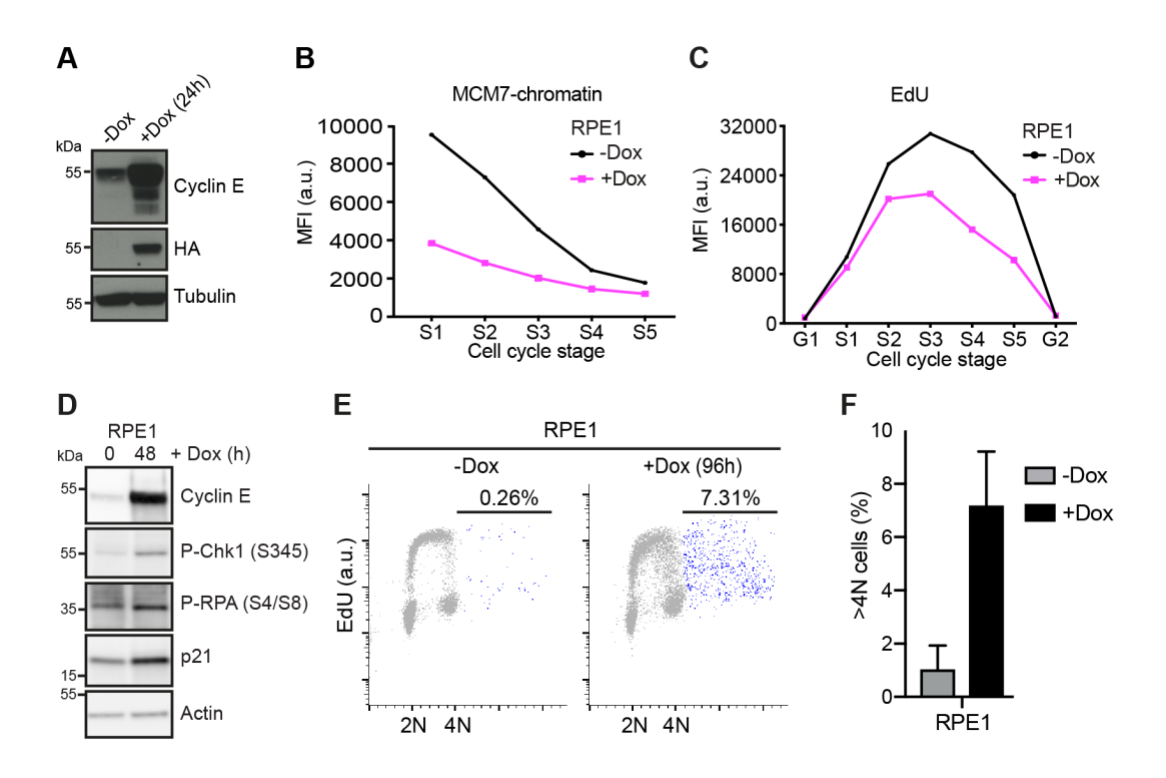


Figure 4.4 Cyclin E overexpression induces replication stress and WGD in RPE1 cells.

- (A) Immunoblots showing cyclin E induction by addition of Dox in RPE1 tetON cyclin E cells. A representative experiment of three independent repeats is shown. Note: this experiment was performed by Eiko Ozono. (B and C) RPE1 cells were induced to express cyclin E (+ Dox) before being analysed by FACS as in Figure 3.8F, G. S phase was divided into 5 stages. Average fluorescence intensities (MFI) for chromatin bound MCM7 and EdU incorporation for different S phase stages are shown in (B) and (C) respectively. A representative experiment of three independent repeats is shown.
- (D) Immunoblots showing expression of DNA damage markers in RPE1 cells overexpressing cyclin E. One independent experiment is performed and shown.

- (E) FACS analysis of EdU incorporation and DNA content for RPE1 cells overexpressing cyclin E for 96 h. Numbers indicate the percentage of cells with >4N DNA content. A representative experiment of three independent repeats is shown.
- (F) The mean percentage of >4N cells with SDs from three independent experiments shown in (E).

Note: the cell line used in experiments in Figure 4.4 is RPE1 tetON cyclin E.

I also introduced FUCCI probes into RPE1 cells. FUCCI live cell imaging showed that control RPE1 cells had normal cell cycle progression with entry and exit of mitosis (mVenus-Gem degradation with spike of mTurq-H2B signal), whereas approximately 50% of cyclin E-overexpressing RPE1 cells bypassed mitosis (mVenus-Gem degradation without spike of mTurq-H2B signal) (Figure 4.5A-C). I wondered whether mitotic bypass was dependent on ATM or ATR. To test this, I used an ATM inhibitor KU-55933 and an ATR inhibitor VE-822. Both inhibitors were able to reduce the level of an activating phosphorylation on p53 (S15) in the presence of a DNA double-strand break (DSB)-inducing agent zeocin, suggesting they were effective at indicated concentrations (Figure 4.5D). However, only ATR inhibition but not ATM inhibition reduced the level of mitotic bypass, indicating that mitotic bypass is mostly dependent on ATR-mediated G2 checkpoint activation (Figure 4.5E). Mitotic bypass in these RPE1 cells were also slow and variable, with a  $t_{1/2}$  of 261.1 ± 134.1 min (mean ± SD, median = 231.8 min) for mVenus-Gem degradation (Figure 4.5F). Some cells not only bypassed mitosis, but also seemed to jump from halfway in G2 into EC-G1 or S phase, where mVenus-Gem degradation did not complete before mCherry-CDT1 degradation (Figure 4.5G, H).

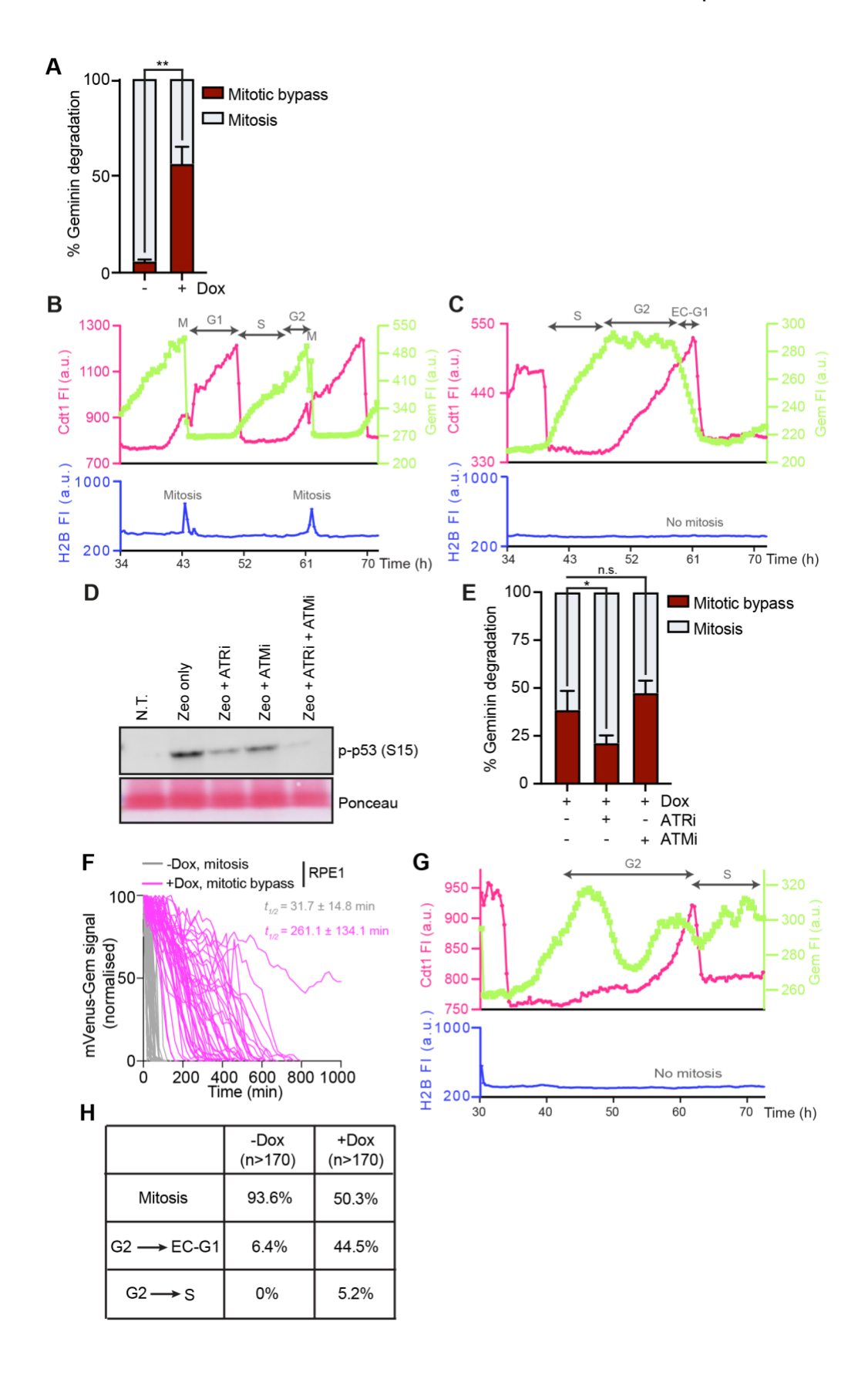


Figure 4.5 Mitotic bypass of cyclin E-overexpressing RPE1 cells is dependent on ATR.

- (A)The mean percentage of cyclin E-overexpressing RPE1 cells induced by Dox that bypassed mitosis from three independent FUCCI live cell imaging experiments with SDs is shown. At lease 150 cells for each condition were analysed. The RPE1 cell line used is RPE1 TetON cyclin E FUCCI H2B. Statistical significance (\*\*p<0.005) was measured by unpaired t test. (B and C) Temporal profiles of FIs of mCherry-CDT1, mVenus-Gem, and mTurquoise-H2B of an untreated RPE1 cell (B) and a cyclin E-overexpressing RPE1 cell (+Dox) bypassing mitosis (C). a.u., arbitrary unit. (D) Immunoblot showing expression of p-p53 (S15) in zeocin-treated cells, supplemented with an ATM inhibitor (KU-55933, 10  $\mu$ M) or an ATR inhibitor (VE-822, 200 nM). Zeocin concentration is 100  $\mu$ g/ml. One independent experiment is performed and shown.
- (E) Schematic of the experiment approach is shown in Figure 4.1B, except that cells were treated with Dox instead of Aph at the beginning of the experiment. ATM inhibitor: KU-55933, 10  $\mu$ M. ATR inhibitor: VE-822, 200 nM. The mean percentage with SDs of RPE1 cells that bypassed mitosis is shown. Data were obtained from three independent FUCCI experiments. At lease 200 cells for each condition were analysed. The RPE1 cell line used is RPE1 TetON cyclin E FUCCI. Statistical significance (\*p<0.05; n.s., nonsignificant) was examined by unpaired t test.
- (F) Normalised data of mVenus-Gem degradation in cells from a representative experiment in Figure 4.5A over time. Each line shows a tracking from a single cell (n>50 for each condition). Average half-life (t<sub>1/2</sub>) values with SDs of mVenus-Gem degradation calculated by logistic growth curve fitting are shown in the figure and main text.
- (G) Temporal profiles of FIs of mCherry-CDT1, mVenus-Gem, and mTurquoise-H2B of a cyclin-overexpressing RPE1 cell that appeared to have a G2-S transition.
- (H) Summary table showing the percentages of abnormal cell cycle transitions from G2 in cyclin E-overexpressing RPE1 cells.

I wondered whether other forms of replication stress could also cause mitotic bypass in RPE1 cells. I treated RPE1 with aphidicolin for 72 h and found most cells arrested with low cyclin B levels at 4N, indicative of EC-G1 entry (Figure 4.6A). Consistent with this, FUCCI imaging showed that almost all aphidicolin-treated RPE1 cells bypassed mitosis and entered EC-G1.

Treatment with the ATR inhibitor VE-822 but not the ATM inhibitor decreased mitotic bypass and increased abnormal mitosis, indicating that aphidicolin-

induced mitotic bypass is dependent on ATR, consistent with that observed

with cyclin E overexpression (Figure 4.6B). These results show that replication stress is sufficient to lead to mitotic bypass in p53-positive cells after extended G2 checkpoint activation. However, unlike U2OS, MCM-reloading was not seen in aph-induced RPE1 EC-G1 cells after release from aphidicolin, with most of the cells remaining blocked in EC-G1 (Figure 4.6A). This growth suppression could be due to a p53-dependent tetraploid G1 checkpoint (Andreassen et al., 2001). Mitotic bypass has been shown to be sufficient for senescence induction, with cells exiting the cell cycle from EC-G1 (Johmura et al., 2014). Indeed, the senescence-associated beta-galactosidase assay revealed these cells were in fact positive for the senescence marker (Figure 4.6C).

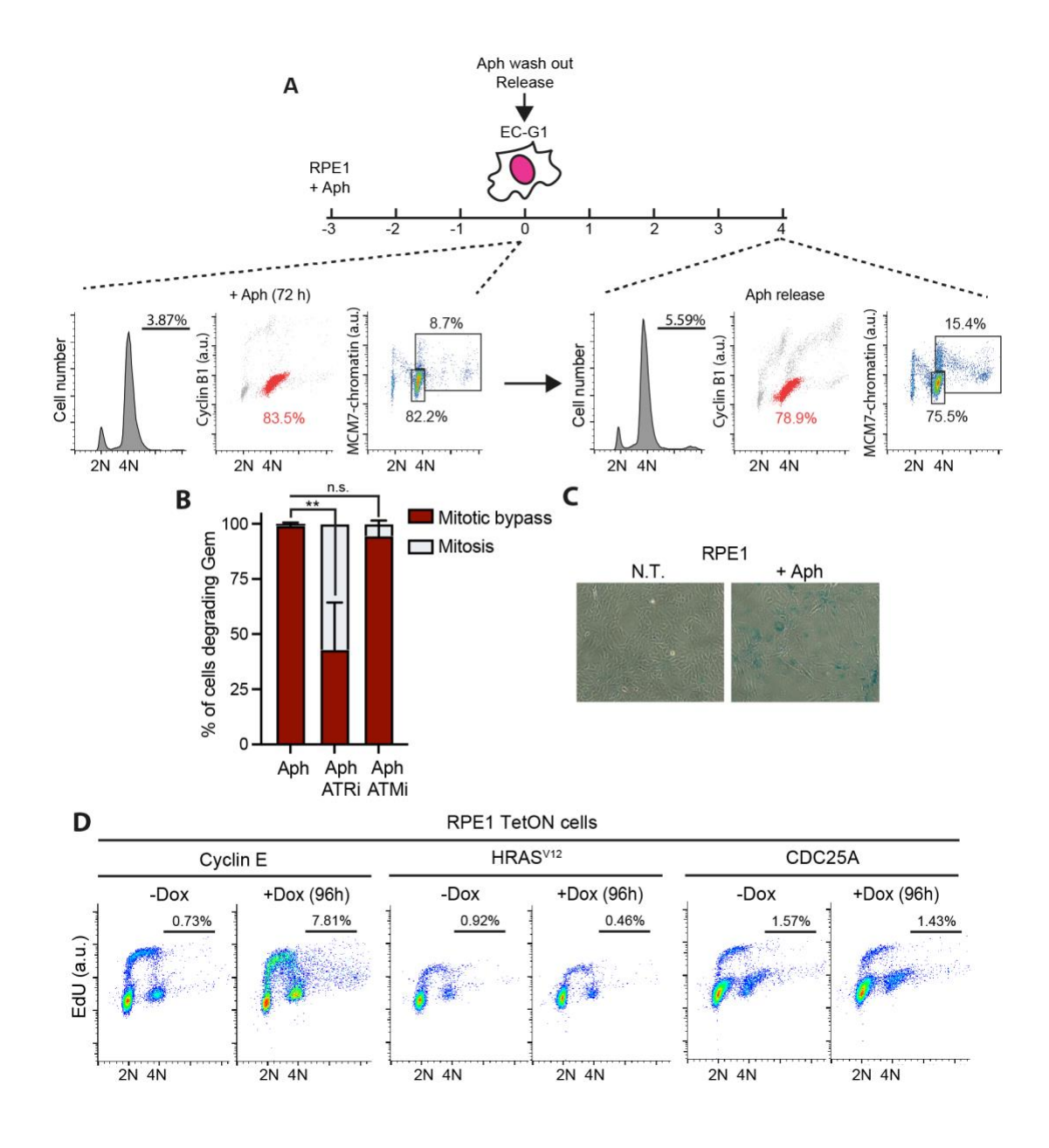


Figure 4.6 Aph-induced RPE1 EC-G1 cells enter a senescence-like state.

(A) Schematic of the experiment approach is shown at the top. RPE1 cells were treated with 1  $\mu$ M aphidicolin and released into fresh media, analysed by FACS to see EC-G1 entry and MCM re-loading. Cells with low cyclin B level at 4N were assumed to be EC-G1 cells (labelled in red). One representative experiment of four independent repeats is shown. (B) Schematic of the experiment approach is shown in Figure 4.1B. The mean percentage with SDs of RPE1 cells that bypassed mitosis is shown.

Data were obtained from three independent FUCCI experiments. At lease 200 cells for each condition were analysed. Aph concentration was 1  $\mu$ M. ATM inhibitor: KU-55933, 10  $\mu$ M. ATR inhibitor: VE-822, 200 nM. The RPE1 cell line used is RPE1 TetON cyclin E FUCCI. Statistical significance (\*\*p<0.005; n.s., non-significant) was examined by Tukey's method.

- (C) Wide-field images of RPE1 cells after treatment with 1  $\mu$ M aphidicolin, measured for  $\beta$ -galactosidase activity. Blue colour indicates positive  $\beta$ -galactosidase activity.
- (D) RPE1 tetON cells were induced by Dox to overexpress cyclin E, Ras<sup>V12</sup>, or Cdc25A for 96 h. FACS analysis of EdU incorporation and DNA content is shown. Numbers indicate the percentage of >4N cells. One representative experiment of two independent repeats is shown.

I also established RPE1 cells that can inducibly express other oncogenes, CDC25A and HRAS<sup>V12</sup>. Addition of doxycycline efficiently induced expression of the oncogenes. However, unlike in U2OS cells, only cyclin E induced WGD in RPE1 cells but not CDC25A or HRAS<sup>V12</sup> (Figure 4.6D). This likely suggests that diploid, untransformed cells such as RPE1 may have better protective mechanisms against WGD than cancer cells like U2OS.

## 4.3 Conclusions

In this chapter I show that aphidicolin, a general inducer of replication stress, led to mitotic bypass in both U2OS and RPE1 cells efficiently. After removing aphidicolin, U2OS EC-G1 cells were able to re-license their origins and endoreduplicate, whilst RPE1 EC-G1 cells stayed arrested. This growth suppression could be p53-dependent as p53 is proposed to maintain diploid genome and clear tetraploid cells (Andreassen et al., 2001). In contrast, cyclin E overexpression caused endoreduplication in both cell lines. This suggests cyclin E may be able to bypass p53-dependent cell cycle block in EC-G1 cells.

Using small molecule inhibitors, I found that only ATR inhibition but not ATM inhibition reduced mitotic bypass induced by cyclin E or aphidicolin. This is in contrast with telomere attrition- or DSB-induced mitotic bypass, which is shown to depend on both ATM and ATR (Davoli et al., 2010). Studies by Davoli et al and us both found the G2 marker cyclin B was degraded during mitotic bypass, by the E3 ubiquitin ligase APC/CCDH1. In normal mitosis, the CDH1 form of APC/C is activated at anaphase, and degradation cyclin B is initiated by the CDC20 form. However, since mitosis is not initiated during mitotic bypass, the order of activation of CDH1 and CDC20 could be changed. As our result shows, depletion of CDH1 but not CDC20 prevented cyclin B degradation during mitotic bypass.

# Chapter 5. Result 3. Role of the p53-p21 pathway in replication stress-induced mitotic bypass

### 5.1 Introduction

In the previous chapter I found that aphidicolin-induced RPE1 EC-G1 cells had permanent cell cycle arrest. I speculate this could be due to p53-dependent suppression of tetraploid cells. In this chapter, I investigate the role of p53 and its downstream targets in replication stress-induced WGD using CRISPR knockout cell lines.

### 5.2 Results

#### 5.2.1 p53 is required for replication stress-induced mitotic bypass

Mitotic bypass in response to telomere damage has been shown to occur in p53-deficient cells (Davoli et al., 2010). The p53 status of U2OS cells is complicated; they have wild type p53, but p53 expression may be reduced due to silencing of *CDKN2A* (Park et al., 2002). RPE1 cells are genetically stable with wild type p53 background. The results in the previous chapter show that cyclin E-expressing RPE1 cells underwent endoreduplication but aphidicolin-treated RPE1 cells entered senescence after bypassing mitosis. I asked whether removing p53 could promote WGD in RPE1 cells in response to replication stress. To this end, I generated p53-knockout (p53KO) RPE1 cells using CRISPR-Cas9 (Figure 5.1A). The cells were validated by western

blotting, PCR and sanger sequencing for successful knockout (Figure 5.1A-



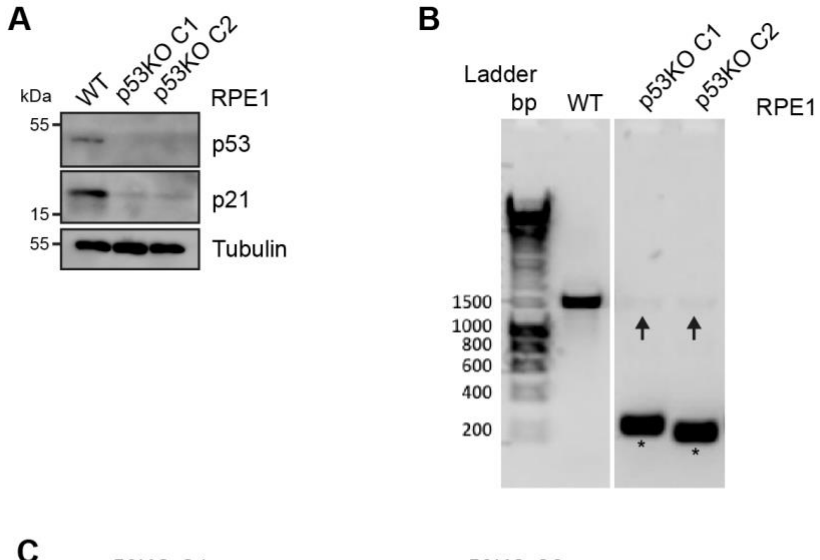




Figure 5.1 Establishment of p53-knockout cells.

- (A) Immunoblots showing expression of p53 and p21 in RPE1 tetON cyclin E p53KO C1 & C2 cells.
- (B) PCR validation of p53KO cells. Genomic DNA was extracted from p53KO C1 and p53KO C2 cells. Regions around the p53 gene were amplified by PCR. PCR products were run by agarose gel. The bands marked by asterisks indicate large excision of a p53 allele by CRISPR-cas9 targeting two exons at the same time. The bands marked by arrows indicate the other p53 allele that was cut only at one position.
- (C) Sanger sequencing validation of p53KO cells. The bands marked by arrows were excised from the gel and amplified using PCR and sent for sanger sequencing. Sequencing results were mapped to p53 gene sequence. In p53KO C1, the allele had a single adenine insertion. In p53KO C2, the allele had a 20-bp deletion.

Aphidicolin treatment increased DNA damage markers to similar levels in both p53-positive and p53-knockout cells, indicative of replication stress

(Figure 5,2A). However, treatment with aphidicolin in p53-knockout cells did not result in accumulation of cells in EC-G1 (4N DNA content, low cyclin B) but an increase in cells with <2N DNA content, indicative of cell death (Figure 5.2B). FUCCI live cell imaging revealed that, instead of bypassing mitosis, as seen in almost all RPE1 p53-positive cells, a great fraction of p53-knockout cells went into catastrophic mitosis, leading to either cell death or nuclear fragmentation (Figure 5.2C, D).

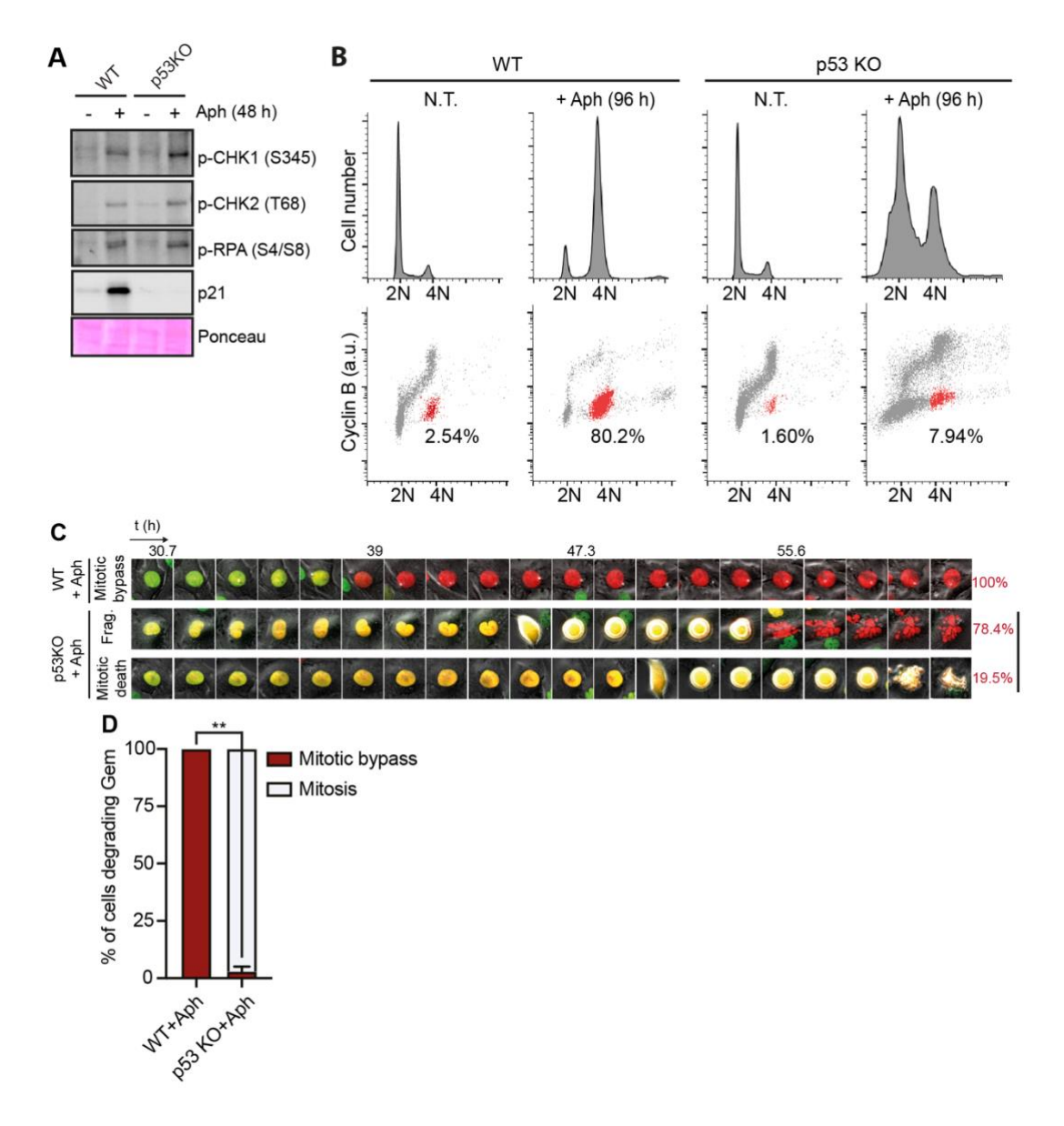


Figure 5.2 p53 knockout in RPE1 cells abolishes aphidicolin-induced mitotic bypass.

- (A) Immunoblots showing expression of DNA damage markers in Aphtreated wild-type (WT) and p53-knockout RPE1 cells. One representative experiment of two independent repeats in shown. The cell lines are RPE1 TetON cyclin E and RPE1 TetON cyclin E p53KO C1.
- (B) DNA content analysis by FACS of RPE1 WT and p53KO cells treated with 1  $\mu$ M aphidicolin. EC-G1 cells were identified and labelled in red. One representative experiment of three independent repeats in shown.
- (C) Example time-course FUCCI images of RPE1 WT and p53KO treated with 1  $\mu$ M aphidicolin. Numbers indicate the percentage of different mitotic outcomes. Examples cells are selected from one representative experiment of three independent repeats. The cell lines used are RPE1 TetON cyclin E FUCCI and RPE1 TetON cyclin E p53KO FUCCI.

(D) The mean percentage with SDs of RPE1 WT and p53KO cells that bypassed mitosis in 1  $\mu$ M aphidicolin is shown. Data were obtained from three independent FUCCI experiments.

I observed very similar results when I induced cyclin E expression in p53-knockout RPE1 cells. Cyclin E expression induced DNA damage markers and reduced EdU incorporation to similar levels in both p53-positive and p53-knockout cells (Figure 5.3A, B). Whereas p53-positive cells eventually bypassed mitosis and entered endoreduplication cell cycle, mitotic bypass was almost abolished in cells lacking p53 (Figure 5.3C). As is the case with aphidicolin treatment, a great fraction of cyclin E-expressing p53-knockout cells went into catastrophic mitosis (Figure 5.3D, E).

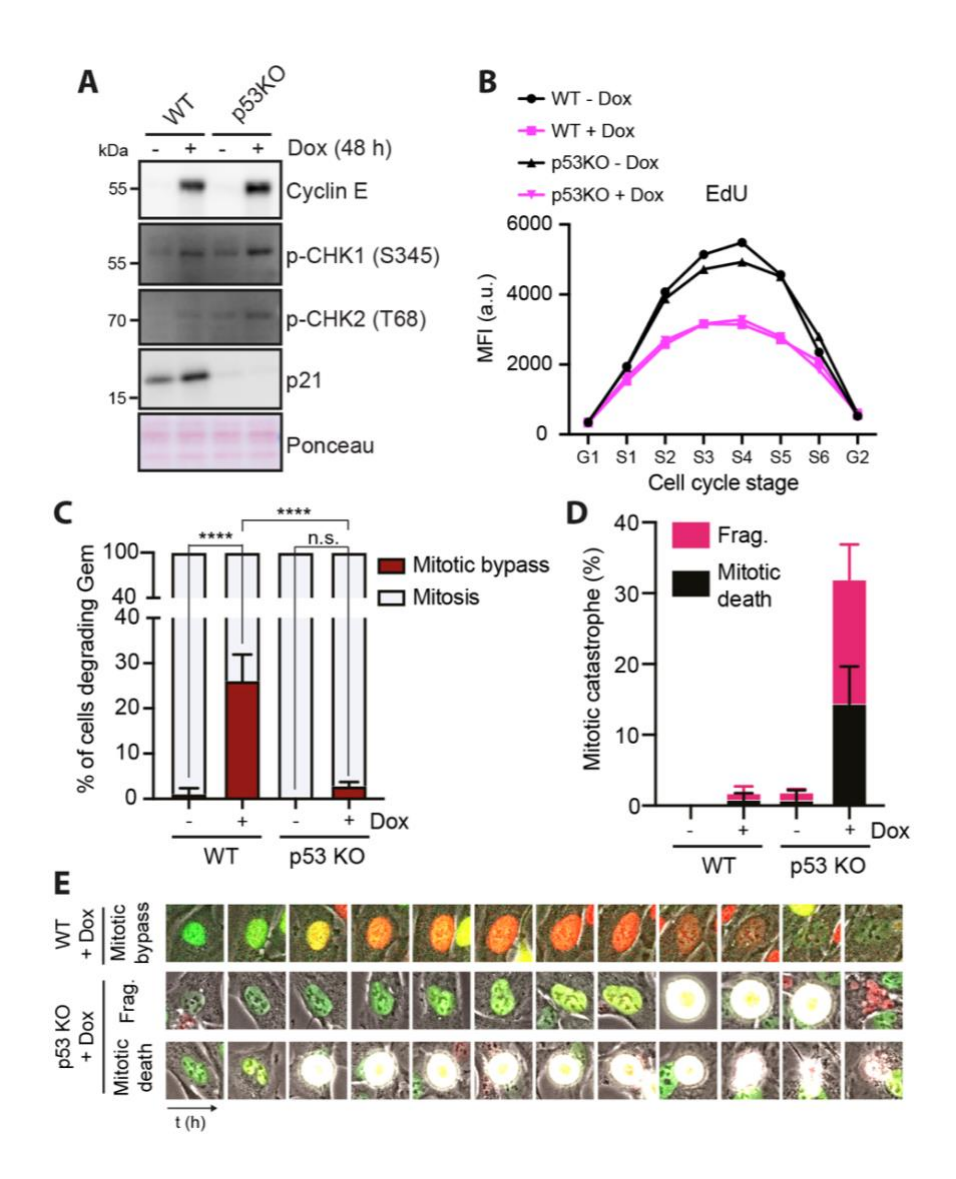


Figure 5.3 p53 knockout in RPE1 cells abolishes cyclin E-induced mitotic bypass.

- (A) Immunoblots showing expression of DNA damage markers in cyclin E-overexpressing RPE1 WT and p53KO cells. One representative experiment of two independent repeats in shown. The cell lines are RPE1 TetON cyclin E and RPE1 TetON cyclin E p53KO C1.
- (B) FACS analysis of EdU incorporation in RPE1 WT and p53KO cell overexpressing cyclin E for 96 h. Mean fluorescence intensity (MFI) of EdU signal at different cell stages is shown. One representative experiment of two independent repeats in shown.
- (C-E) RPE1 WT and p53 KO cells were treated with doxycycline (Dox) to induce cyclin E expression and live cell imaged for 96 h. Average percentages of cells that had mitotic bypass from three independent experiments with SDs are shown in (C). Mean percentages with SDs of mitosis that resulted in nuclear fragmentation (Frag.) and mitotic death is shown in (D). At lease 300 cells for each condition were analysed. Selected images of example cells are shown in (E). The RPE1 WT and p53 KO cell

lines used are RPE1 TetON cyclin E FUCCI H2B and RPE1 TetON cyclin E p53KO FUCCI. Statistical significance (\*\*\*\*p<0.0001; n.s., non-significant) was examined by Šidák's method.

Since p53-knockout cells behaved similarly to CHK1-inhibited cells in response to replication stress, preventing mitotic bypass and allowing cells into aberrant mitoses, I wondered whether p53, like CHK1, might be involved in activation and maintenance of the G2 checkpoint, a prerequisite for mitotic bypass. To assess this, I used FUCCI imaging to measure the length of G2 in p53-knockout cells following replication stress, either induced by cyclin E or aphidicolin. Analysis of FUCCI images revealed G2 length was longer in p53-KO cells that went into mitosis than in p53-WT cells that had mitotic bypass, suggesting the G2 checkpoint was still activated without p53 (Figure 5.4).

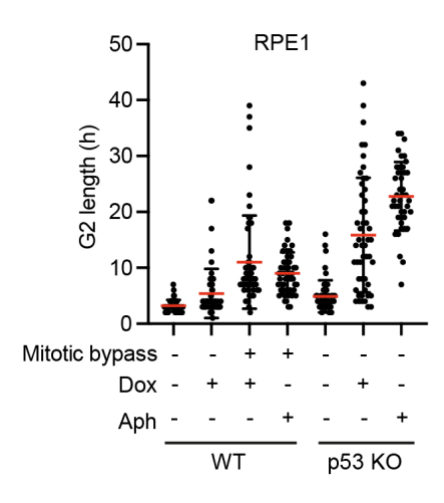


Figure 5.4 p53-knockout cells can have extended G2 arrest in replication stress.

G2 lengths of individual cells in representative FUCCI experiments in Figure 5.2C and Figure 5.3E. Mean values are shown labelled by red lines (n>50 for each group). Error bars represent SDs.

### 5.2.2 p21 is essential for mitotic bypass by inhibiting CDK

p53 is a transcription factor that is reported to directly target about 500 genes (Aubrey et al., 2018). I wondered which p53 target is responsible for replication stress-induced mitotic bypass. To investigate this, I depleted p21, GADD45A and 14-3-3σ, three main downstream effectors of p53 involved in G2/M regulation in response to DNA damage (Hermeking et al., 1997), in aphidicolin-treated RPE1 cells (Figure 5.5A). Only depletion of p21 decreased accumulation of EC-G1 cells (4N DNA content, cyclin B negative) as depletion of p53 did. I also knocked out p21 in RPE1 cells using CRISPR-Cas9 (Figure 5.5B-D) and found p21 knockout behaved very similarly to p53 knockout: p21-knockout RPE1 cells had reduced WGD in response to cyclin E expression; they also had increased cell death (accumulation of cells with <2N DNA content) instead of entering EC-G1 when treated with aphidicolin (Figure 5.5E-G).

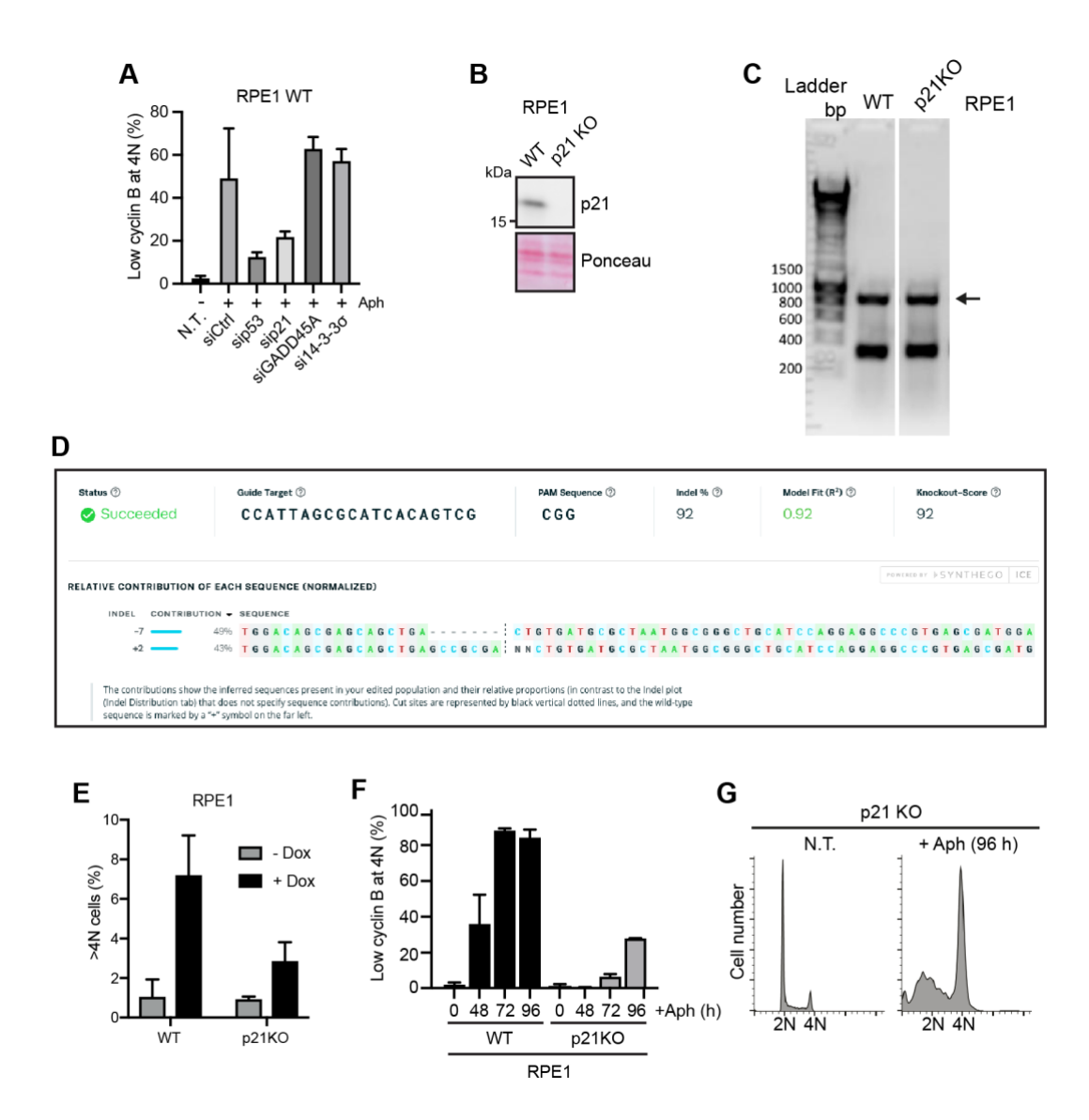


Figure 5.5 p21 is required for replication stress-induced mitotic bypass in RPE1 cells.

- (A) RPE1 WT cells treated with 0.5  $\mu$ M aphidicolin were supplemented with siRNAs for p53 downstream effectors for 72 h. Mean percentage of cells with low cyclin B level and 4N DNA content from two independent experiments with range is shown.
- (B) Immunoblot showing expressing of p21 in p21-knockout RPE1 cells. (C, D) Genomic regions around the p21 gene in RPE1 p21 KO cells were amplified by PCR and the band of right size (indicated by arrows) was excised after running on agarose gel (C). The bands were sequenced by sanger sequencing and the result was resolved by Synthego for indel information on the two alleles. Both alleles were inactivated by deletions (D). (E) RPE1 WT and p21KO cells were induced to overexpress p21 for 96 h and analysed by FACS for DNA content. Mean percentages with SDs of >4N cells from three independent experiments are shown.

- (F) RPE1 WT and p21KO cells were treated with 1  $\mu$ M aphidicolin over time and analysed by FACS. Mean percentages with range of EC-G1 cells from two independent experiments are shown.
- (G) RPE1 p21KO cells treated with 1  $\mu$ M aphidicolin were analysed by FACS for DNA content. One representative experiment of two independent repeats is shown.

I quantified the number of cells entering EC-G1 following aphidicolin treatment in a panel of p53- and p21-negative cell lines. In p53-positive U2OS, RPE1, IMR90 and HCT116 cells, I saw an accumulation of EC-G1 cells whereas in p53-knockout RPE1, p53-knockout U2OS, p53-depleted IMR90 and p53-depleted HCT116 cells, I saw barely any EC-G1 cells (Figure 5.6A-I). Instead, I saw an increase in cells with <2N DNA content and an increase in cells with fragmented nuclei (p53-depleted HCT116 cells and p53-knockout RPE1 cells) (Figure 5.6J-L; Figure 5.2B). In addition, knockout of p53 reduced the proportion of whole genome duplicated cells in response to cyclin E expression in both RPE1 and U2OS cells (Figure 5.6M, N). This was also similar in p21-knockout U2OS cells, p21-depleted IMR90 cells and p21-depleted HCT116 cells: p21 deficiency reduced WGD in response to cyclin E in U2OS cells (Figure 5.6N) and almost abolished accumulation of EC-G1 cells in response to aphidicolin in U2OS, IMR90 and HCT116 cells (Figure 5.6D-H); depletion of p21 in aph-treated HCT116 cells increased cell death (increase in <2N cells and nuclear fragmentation) (Figure 5.6J, L). These data suggest that p21 is a major effector mediating p53's function in mitotic bypass.

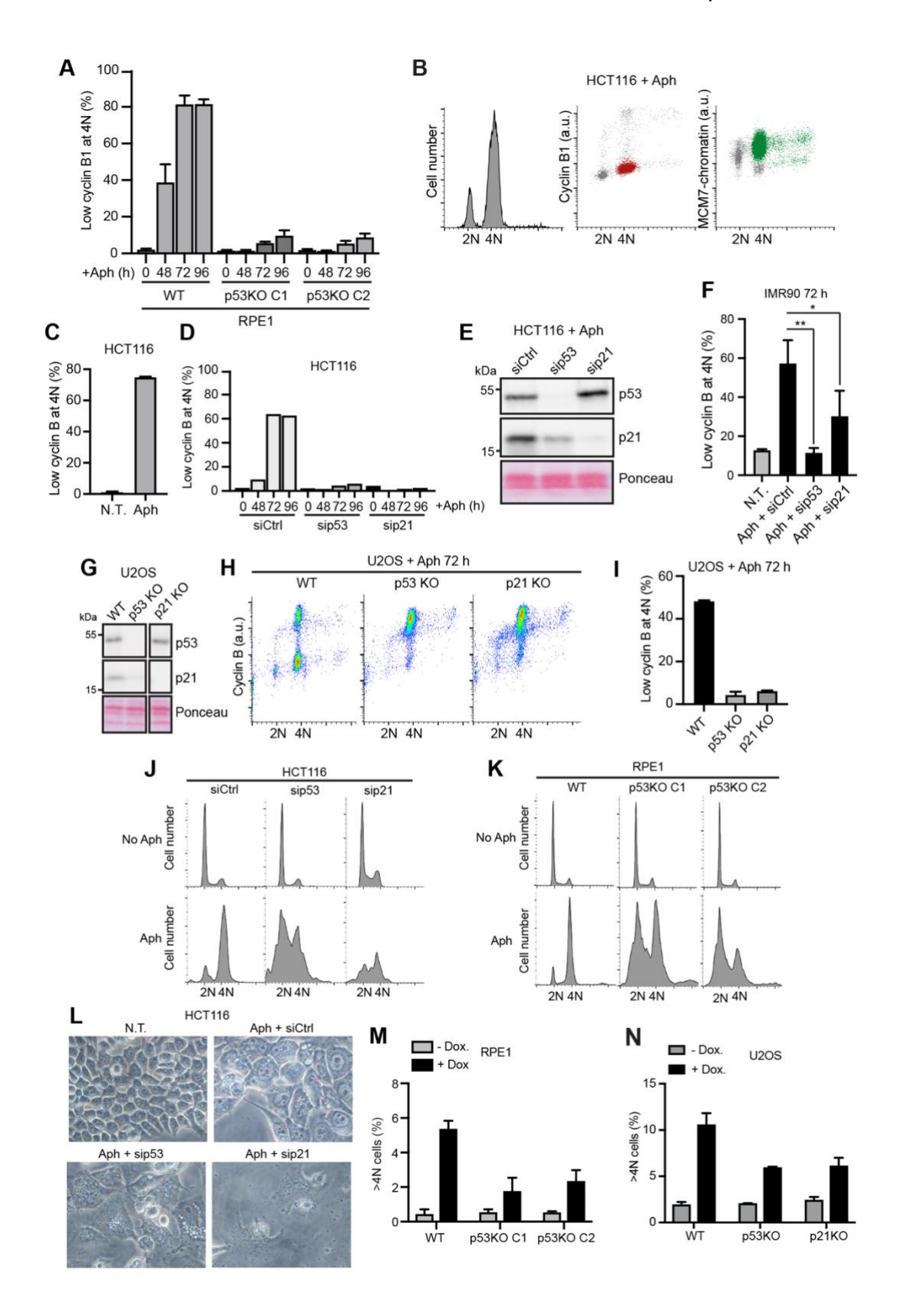


Figure 5.6 Replication stress-induced mitotic bypass is dependent on p53 and p21 in a panel of cell lines.

(A) RPE1 WT and p53 KO cells were treated with 1  $\mu$ M aphidicolin for 96 h and analysed by FACS for cyclin B level and DNA content. EC-G1 cells were

identified as cells with low cyclin B at 4N DNA content. Mean percentages with range of EC-G1 cells are shown from two independent experiments. (B and C) HCT116 cells were treated with 1  $\mu$ M aphidicolin for 96 h and analysed by FACS for levels of cyclin B, chromatin-bound MCM7 and DNA content. Identified EC-G1 cells are labelled in red and EC-G1 cells that reloaded MCM are labelled in green in (B). Mean percentages with range of EC-G1 cells are shown in (C).

- (D and E) HCT116 cells treated with 1  $\mu$ M aphidicolin were depleted with p53 or p21. The average percentage of EC-G1 cells from one independent experiment is shown in (D). Immunoblots showing knockdown of p53 or p21 are in (E).
- (F) IMR90 cells were treated with 1  $\mu$ M aphidicolin and depleted with p53 or p21. Mean percentages with SDs of EC-G1 cells from three independent experiments are shown. Statistical significance (\*p < 0.05 and \*\*p < 0.005) was examined by Tukey's method.
- (G-I) Immunoblots showing expression of p53 and p21 in U2OS p53KO and p21KO cells (G). Cells were incubated with 1  $\mu$ M Aph for 72 h and analysed by FACS for cyclin B level and DNA content (H), with a representative experiment of two independent repeats shown. Cells with low cyclin B level at 4N were assumed to be EC-G1 cells. Mean percentages with range of EC-G1 cells are in (I).
- (J) DNA content analysis by FACS of p53-depleted or p21-depleted HCT116 cells treated with 1  $\mu$ M Aph for 96 h. One representative experiment of two independent repeats is shown.
- (K) DNA content analysis by FACS of p53-knockout RPE1 cells treated with 1  $\mu$ M Aph. One representative experiment of two independent repeats is shown.
- (L) Wide-field images of HCT116 cells in (J). One independent experiment is performed and shown.
- (M) RPE1 p53KO cells were induced to overexpress cyclin E for 96 h and analysed by FACS for DNA content. Mean percentages with SDs of >4N cells from three independent are shown.
- (N) U2OS p53KO and p21KO cells were induced to overexpress cyclin E for 96 h and analysed by FACS for DNA content. Mean percentages with SDs of >4N cells from three independent are shown.

p21 is an inhibitor of CDK and has been shown to inhibit several CDKs including CDK1, CDK2 and CDK4/6. I asked whether p21 mediates mitotic bypass through CDK inhibition. To test this, I used chemical inhibitors of CDKs, RO-3306 for CDK1 inhibition, CVT-313 for CDK2 inhibition and Abemaciclib for CDK4/6 inhibition. I added these CDK inhibitors to aph-

treated p21-knockout RPE1 cells arresting at G2. Figure 5.7A shows that adding inhibitors of CDK1 or CDK2 significantly increased the fraction of p53-knockout cells in EC-G1, indicative of mitotic bypass, whereas cells treated with CDK4/6 inhibitor or vehicle control had little mitotic bypass. Adding two or all of the CDK inhibitors together further increased accumulation of EC-G1 cells. These data indicate that low CDK activity in G2 is required for replication stress-induced mitotic bypass to occur, primarily through inhibition of CDK1 and CDK2 by p21. Addition of Nutlin, a p53 stabiliser, could increase p21 expression and fraction of EC-G1 cells (4N DNA content, cyclin B negative) in aphidicolin-treated U2OS (Figure 5.7B, C). Also, the level of p21 and the fraction of aphidicolin-induced U2OS EC-G1 cells both increased proportionally to increasing concentrations of Nutlin (Figure 5.7B, C). This suggests that the extent of replication stress-induced mitotic bypass is correlated with the level of p53 activity.

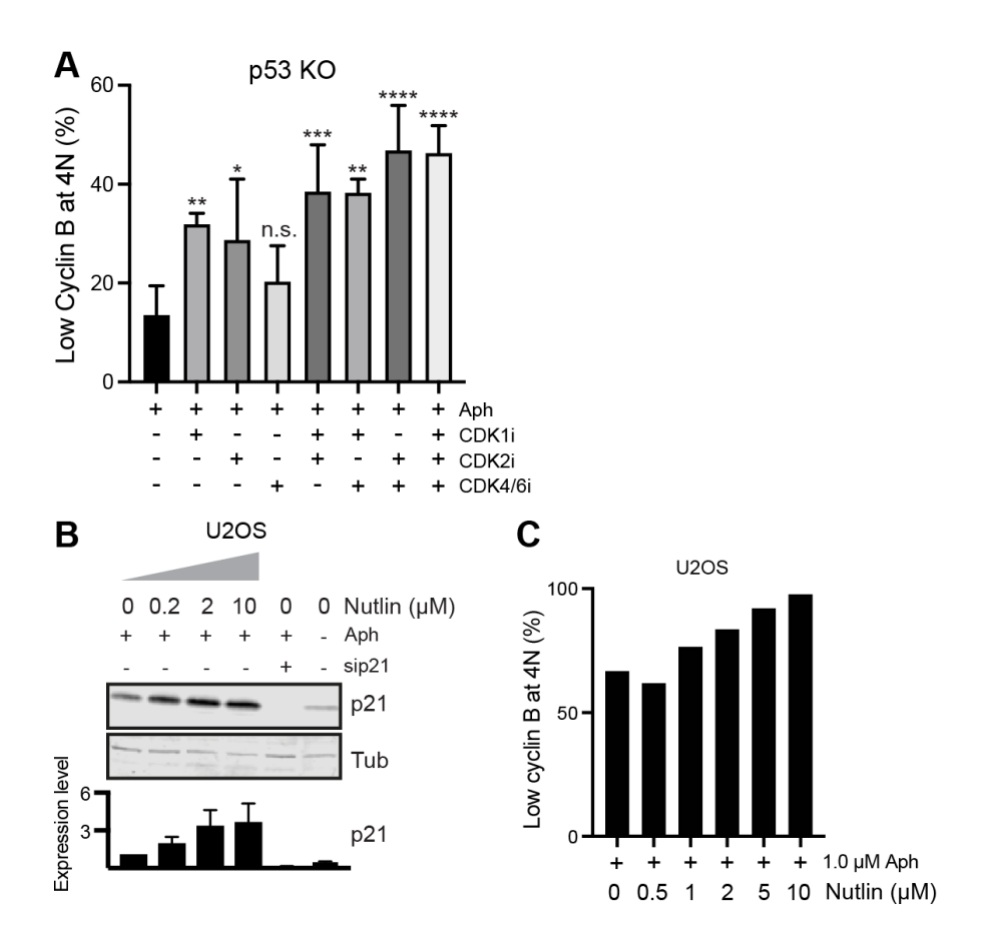


Figure 5.7 p21 promotes replication stress-induced mitotic bypass by inhibiting CDK levels.

(A) RPE1 p53KO cells were first treated with 1  $\mu$ M aphidicolin for 48 h when they were mostly in G2 phase, then they were treated with inhibitors of CDK1, CDK2 or CDK4/6 for a further 24 h. Cells were analysed by FACS for cyclin B level and DNA content. The average percentage of EC-G1 cells (low cyclin B1 at 4N) with SDs from three independent experiments is shown. Statistical significance (\*p<0.05; \*\*p<0.005; \*\*\*p<0.001; \*\*\*\*p<0.0001; n.s., non-significant) was examined by Tukey's method. The cell line used is RPE1 tetON cyclin E p53KO C1.

(B and C) U2OS cells treated with 1  $\mu$ M aphidicolin were supplemented with increasing concentrations of Nutlin. Immunoblots showing expression of p21 are shown in (B). Mean expression levels with SDs are quantified from three independent experiments. Cells were analysed by FACS and the fraction of the cell population with low cyclin B at 4N from a single experiment is shown in (C).

My results showing mitotic bypass requires p53 seem to be clashing with previous research showing that mitotic bypass occurred in p53-deficient cells after telomere attrition or prolonged treatment of DSB-inducing agents

(Davoli et al., 2010). In this study, mouse embryonic fibroblast (MEF) cells or human BJ cells transformed by SV40 large T antigen (SV40LT) or HPV-E6/E7 were used. SV40LT is widely used for cell immortalisation due to its ability to efficiently inhibit p53 and RB1, and p53 activity is generally assumed to be deficient in SV40LT-transformed cells. I therefore went on to assess mitotic bypass in SV40LT-transformed BJ cells (BJ-LT) in replication stress and DNA damage. Both zeocin and aphidicolin caused mitotic bypass in BJ-LT cells (Figure 5.8A). I found p21 was upregulated in response to both aphidicolin and zeocin in BJ-LT cells, indicating p53 is active to some extent (Figure 5.8B). This is consistent with previous work showing that SV40LT is not an efficient inhibitor of human p53 (Sheppard et al., 1999). Moreover, addition of Nutlin could further increase p21 expression and accumulation of cells in EC-G1 (4N DNA content, cyclin B negative) in aphidicolin-treated BJ-LT, whereas depletion of p53 led to a decrease in both p21 expression and EC-G1 entry (Figure 5.8A, B). In contrast, zeocin-induced mitotic bypass in BJ-LT cells was unaffected by Nutlin or p53 depletion, suggesting DNA damage-induced mitotic bypass is independent of p53. I also tested whether telomere attrition or DSBs could induce mitotic bypass in U2OS and RPE1 cell. POT1 is a component of the shelterin complex involved in telomere protection (de Lange, 2005, Denchi and de Lange, 2007). Most cancers extend telomeres by activating telomerase while around 10% cancers use the alternative-lengthening (ALT) mechanism (Heaphy et al., 2011). The shelterin complex is shown to be important for telomere protection regardless of the ALT status (Zhang and Zou, 2020). In U2OS, an ALT+ cell line, it has been shown that loss of POT1, or TRF2, another component of the shelterin

complex, results in telomere de-protection (Episkopou et al., 2019, Stagno D'Alcontres et al., 2007). I found that U2OS cells efficiently bypassed mitosis in zeocin and underwent WGD when POT1 was depleted (Figure 5.8C-F). In a clear contrast, zeocin-treated or POT1-depleted RPE1 cells primarily had a 2N G1 arrest (Figure 5.8G, H). This could be attributed to activation of the G1 DNA damage checkpoint. Nevertheless, a small fraction of RPE1 cells bypassed mitosis in zeocin or POT1 depletion as indicated by an increase in EC-G1 cells (4N DNA content, cyclin B negative).

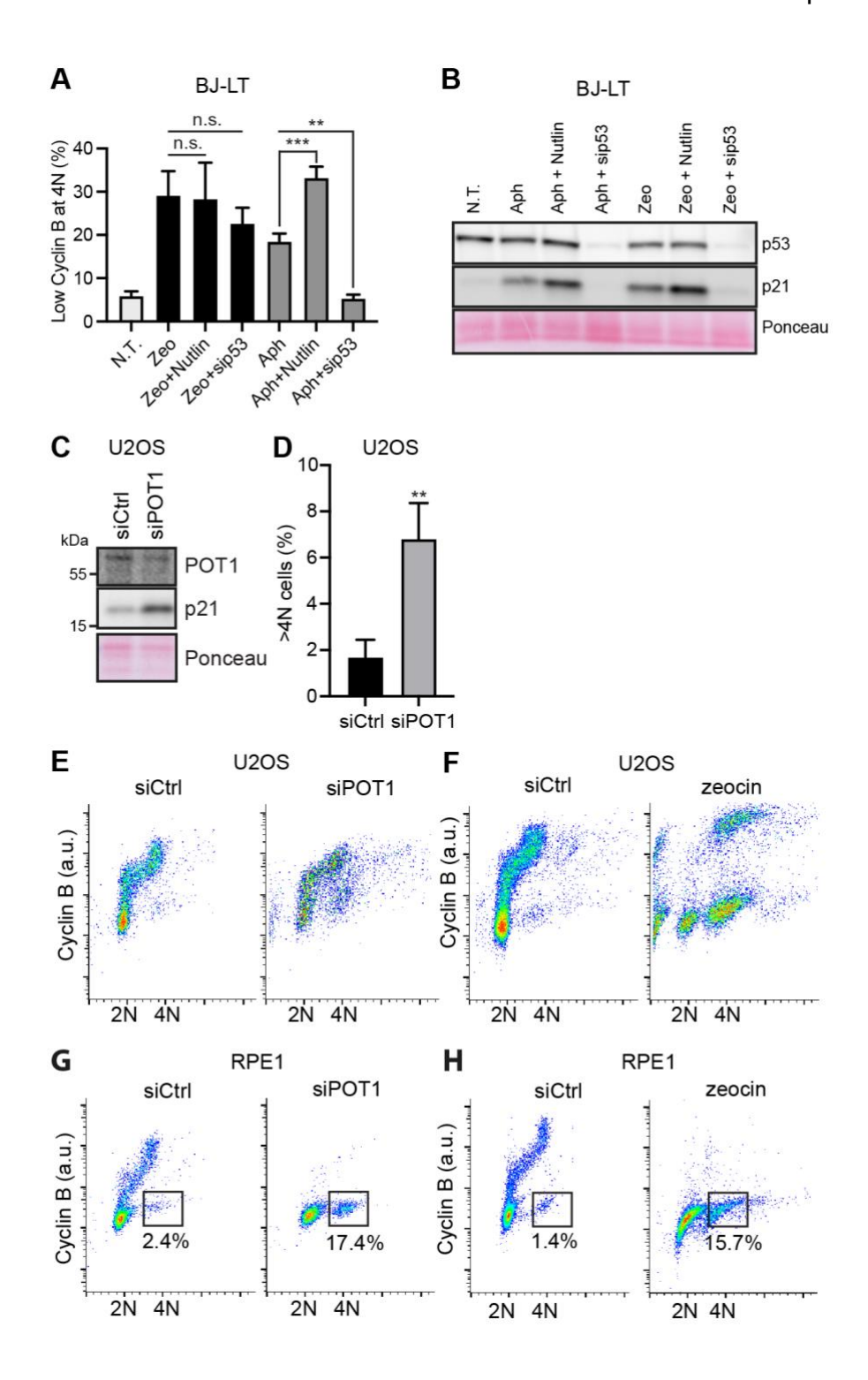


Figure 5.8 Difference between DNA damage- and replication stress-induced whole genome duplication.

(A and B) BJ-LT cells were treated with either 0.5  $\mu$ M aph or 50  $\mu$ g/ml zeocin for 72 h. On top of that, at time 24 h of Aph treatment, 2  $\mu$ M Nutlin (at time 24 h) was added or p53 (at time 0) was depleted. Then cells were analysed by western blotting and FACS. Immunoblots showing expression of p53 and p21 are shown in (I), with one representative experiment of two independent repeats shown. Average percentages of EC-G1 cells (cyclin B1 negative at

- 4N DNA) with SDs from three independent FACS experiments are shown in (H). Statistical significance (\*\*p<0.005; \*\*\*p<0.001) was examined by Tukey's method.
- (C-E) U2OS were depleted with POT1 and analysed by FACS for DNA content. Immunoblots showing POT1 depletion are shown in (C), with one representative experiment of two independent repeats shown. Mean percentages with SDs of >4N cells from three independent experiments are in (D).
- (E-H) U2OS or RPE1 cells were depleted with POT1 or treated with 100  $\mu$ g/ml zeocin for 96 h before being analysed for cyclin B level and DNA content by FACS. One representative experiment of three independent repeats is shown.

## 5.2.3 Cyclin E overexpression prevents EC-G1 arrest and reverses senescence

Aphidicolin treatment can induce both RPE1 and U2OS cells to bypass mitosis and enter EC-G1. The difference between the two cell lines was their ability to re-load MCMs while arrested in EC-G1; in U2OS cells, the majority of EC-G1 cells re-loaded MCMs (Figure 4.1F), whereas in RPE1 cells, there was negligible MCM re-loading (Figure 4.6A). In addition, releasing U2OS cells from aphidicolin into fresh media drove arrested EC-G1 cells into S phase (Figure 4.2G), whereas the vast majority of released RPE1 EC-G1 cells remained arrested in EC-G1 without any MCMs re-loaded (Figure 4.6A). These aph-induced RPE1 EC-G1 cells showed β-galactosidase activity, suggesting they have entered senescence (Figure 4.6C). In these cells, CDC6 and CDT1, licensing factors required for MCM loading, were not expressed, indicative of withdrawal from the cell cycle (Figure 5.9A).

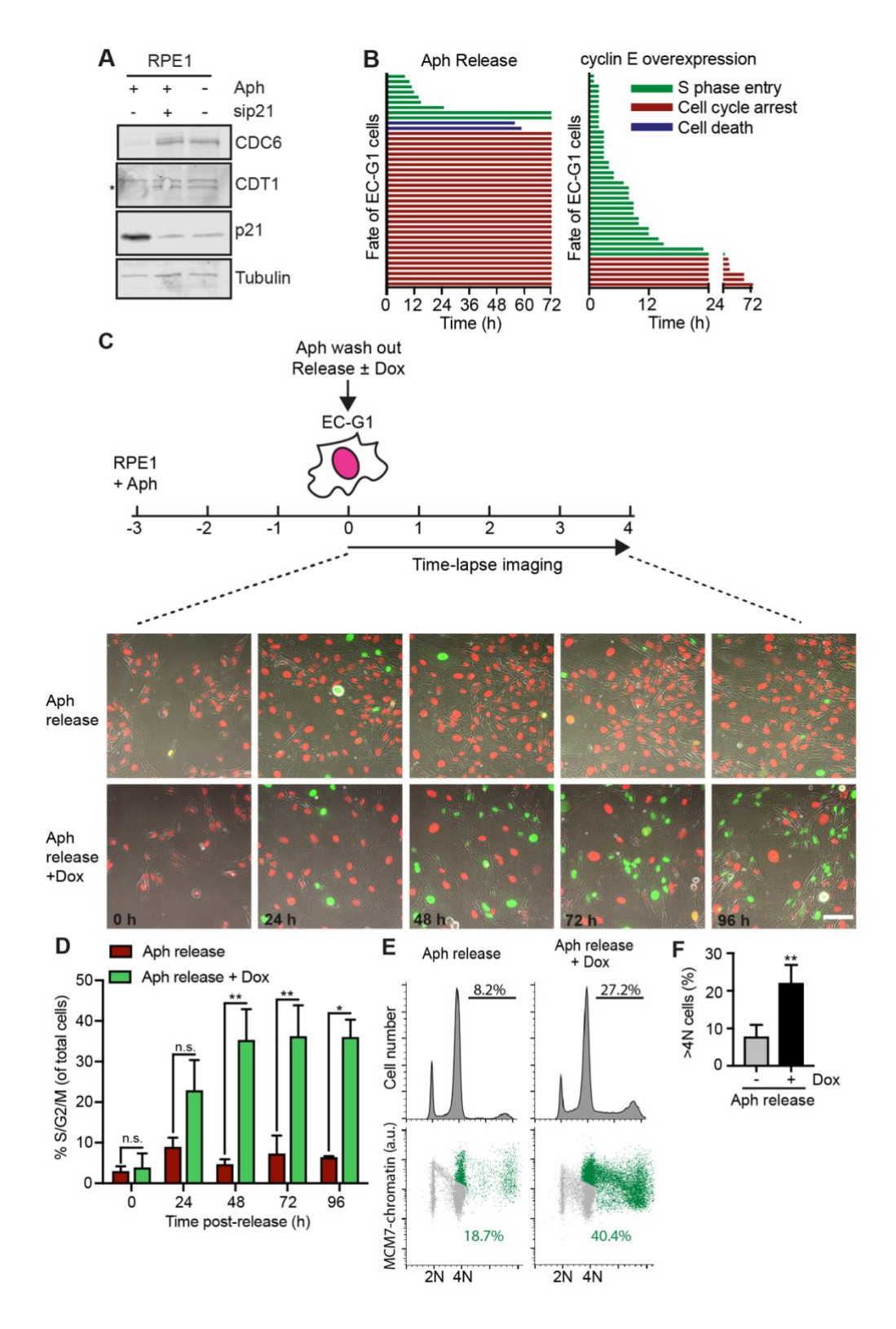


Figure 5.9 cyclin E overexpression restores endoreduplication of EC-G1 cells in senescence.

(A) Immunoblots showing expression of CDC6, CDT1 and p21 in RPE1 cells treated with 1  $\mu$ M aph. One representative experiment of two independent repeats is shown.

- (B) Fates of individual RPE1 EC-G1 cells after release from 0.5  $\mu$ M Aph in Figure 5.9C vs. fates of individual RPE1 EC-G1 cells from overexpressing cyclin E alone in Figure 5.3E. The length of each line represents the time of e single cell (n>40 for each condition) staying in EC-G1. Tracking stops when cells enter S phase (green), die (blue) or staying in EC-G1 until the end of 72 h imaging (red).
- (C and D) Schematic of the experimental approach is shown at the top in (C). RPE1 cells were treated with 0.5  $\mu$ M Aph for 72 h before release into fresh media without aphidicolin. Doxycycline (Dox) was supplemented at the time of release to induce cyclin E expression. Selected images at indicated timepoints are shown in (C). Scale bar, 100  $\mu$ m. The RPE1 cell line used is RPE1 TetON cyclin E FUCCI. The average percentage with SEMs of cells in S/G2/M phase at indicated timepoints from 3 independent experiments is shown in (D). Statistical significance (\*p<0.05; \*\*p<0.005; n.s., non-significant) was examined by Šidák's method.

(E and F) RPE1 cells were treated with aph and released into fresh media as in (C) and analysed for DNA content and MCM loading as shown in (E). Cells with >4N DNA content or with high level of MCM loading at 4N are labelled in green. Mean percentages of cells incorporating EdU with >4N DNA content from four independent experiments with SDs is shown in (F). Statistical significance (\*\*p<0.005) was examined by unpaired t test.

In contrast to aphidicolin treatment, which led RPE1 EC-G1 cells into senescent cell cycle arrest, cyclin E expression alone induced efficient S phase entry in RPE1 p53-wild type cells that bypassed mitosis (Figure 5.9B). Since cyclin E/CDK2 is responsible for the G1/S transition in the diploid cell cycle, and cyclin E is known to promote S phase entry, I wondered whether cyclin E expression might be able to drive senescent cells back into cell cycle. To test this, I induced cyclin E expression in aphidicolin-treated cells already arrested in EC-G1. A large proportion of these cells were driven to re-load MCM, enter S phase and re-replicate (Figure 5.9C-F). Viable single cell clones of RPE1 WGD cells could be grown by sorting cyclin E-induced >4N cells or senescent cells driven back into cycle by cyclin E overexpression. Karyotyping of these RPE1 WGD clones showed that their chromosome numbers are sub-tetraploid and highly variable between

individual cells, similar to that seen with U2OS WGD clones (Figure 5.10A). These results suggest that the senescent state of EC-G1 cells can be reversed. This conclusion is further supported by our results showing that depleting p53 or p21 in RPE1 EC-G1 cells greatly promoted cell cycle reentry and replication (Figure 5.10B, C). Depleting RB1 in these EC-G1 cells also promoted MCM re-loading although it was less efficient at driving cell cycle re-entry (Figure 5.10D).

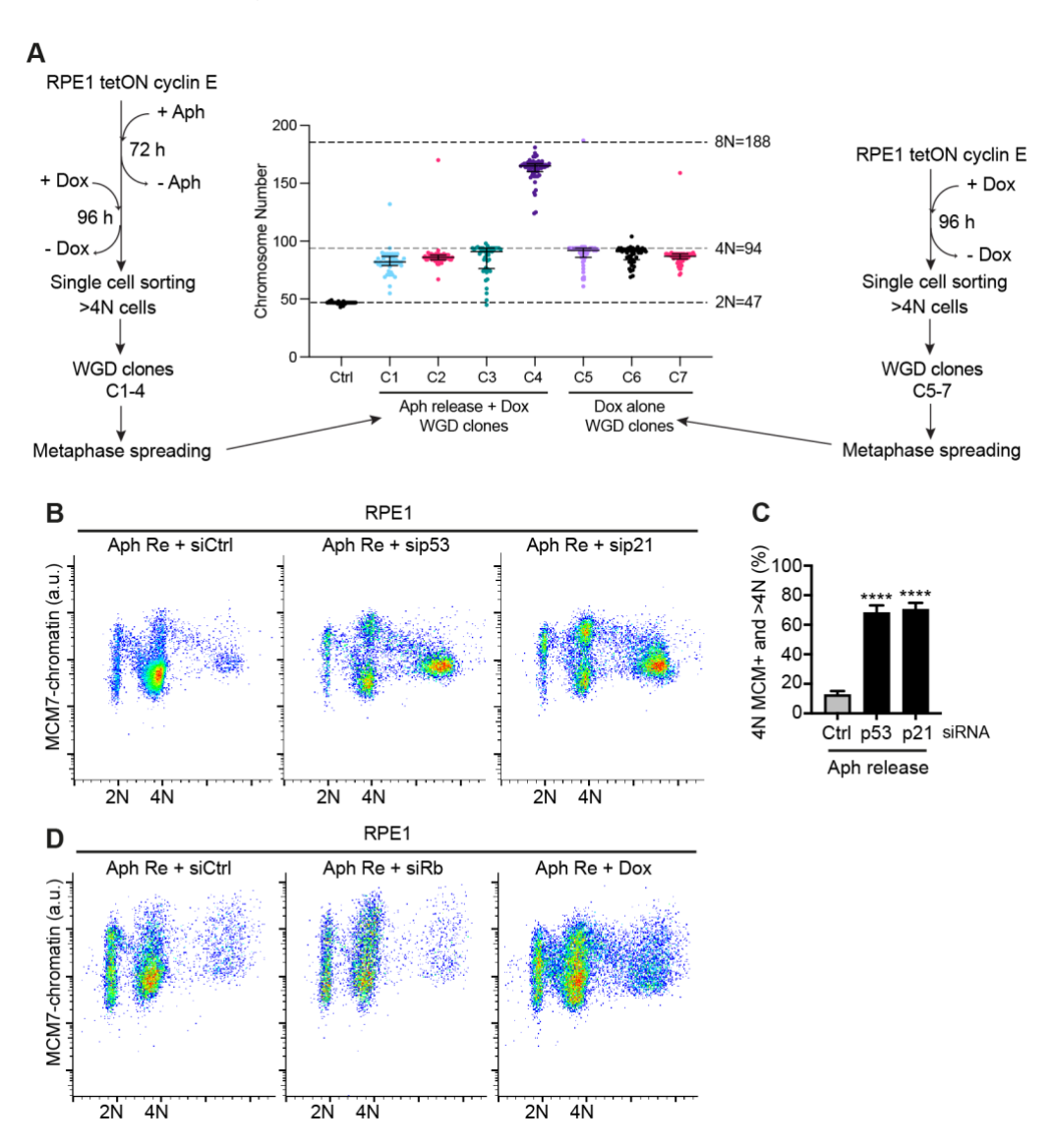


Figure 5.10 Reversal of senescent EC-G1

(A) RPE1 WGD clones were grown as the schematic shows on the left and right. Karyotypes of the clones are shown in the middle.

(B and C) RPE1 cells were treated with 0.5 μM Aph for 72 h to generate EC-G1 cells and then released into fresh media. siRNAs were supplemented at the point of release to knockdown p53 or p21. Cells were analysed by FACS at 96 h post Aph release (Aph Re) for MCM loading and DNA content (B). Average percentages with SDs of cells with high chromatin-bound MCM level at 4N DNA content or with >4N DNA content from three independent experiments is shown in (C). Statistical significance (\*\*\*\*p<0.0001) was examined by Tukey's method.

(D) RPE1 cells were treated as in (B). siRNA for RB1 was supplemented at the point of Aph release. One representative experiment of two independent repeats is shown.

The cell line used in Figure 5.10 is RPE1 tetON cycin E.

Some chemotherapeutic agents are known to cause replication stress and induce permanent cell cycle arrest. Can chemotherapeutics-induced arrest be reversed by cyclin E expression? To test this, I used camptothecin (CPT) and etoposide, two commonly used anti-tumour drugs, and found they induced RPE1 cells to arrest in EC-G1 (Figure 5.11A). Induction of cyclin E in these EC-G1 cells promoted cell cycle re-entry and re-replication (Figure 5.11B).

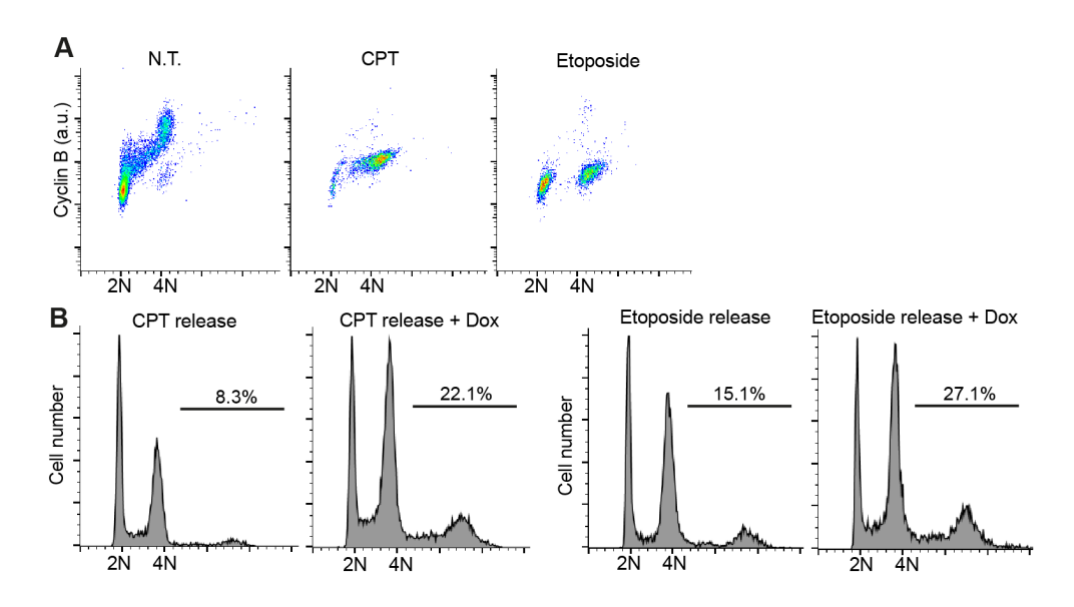


Figure 5.11 cyclin E overexpression re-establishes replication of senescent cells induced by chemotherapeutic agents.

(A) RPE1 cells were treated with 10 nM camptothecin (CPT) or 1  $\mu$ M etoposide for 72 h before FACS analysis for cyclin B level and DNA content.

Cells with low cyclin B level at 4N DNA content were identified as EC-G1 cells. One representative experiment of two independent repeats is shown. (B) CPT- or etoposide-treated cells in (A) were released into fresh media for 96 h, ± cyclin E induction at the point of release. Cells were analysed for DNA content by FACS. Numbers indicate the percentage of >4N cells. One representative experiment of two independent repeats is shown. The cell line used in Figure 5.11 is RPE1 tetON cycin E.

### 5.3 Conclusions

In this chapter, I found that p53 knockout almost abolished mitotic bypass in cyclin E-overexpressing or aphidicolin-treated cells, suggesting replication stress-induced mitotic bypass is dependent on p53. These p53-knockout cells did not lose the ability to activate the G2 checkpoint, as FUCCI experiments show they still had extended G2 arrest. This suggests p53 loss is not sufficient to abolish G2 arrest, consistent with previously published work (Kastan et al., 1991, Taylor and Stark, 2001, Smits and Medema, 2001). The CHK1 and p53 pathways work semi-redundantly to inhibit CDK, with CHK1 delivering a fast response and p53 adding an additional push. The p53 arm of CDK inhibition seems particularly important for establishing mitotic bypass, as p53-knockout cells eventually entered catastrophic mitosis after extended G2 arrest following replication stress. These results were somewhat surprising, as Davoli et al show that p53-knockout mouse cells and human cells transformed by SV40LT or E6/E7 endoreduplicate in zeocin and telomere damage (Davoli et al., 2010). I tested BJ cells transformed with SV40LT (BJ-LT), which were used in the Davoli et al study. I found SV40 large T antigen did not completely inactivate p53, as BJ-LT cells still upregulated p21 in response to aphidicolin and zeocin, consistent with

previous study showing SV40LT is a poor inhibitor of human p53 (Sheppard et al., 1999). In these cells, p53 deletion reduced aphidicolin-induced mitotic bypass but not zeocin-induced mitotic bypass, suggesting mitotic bypass is dependent on p53 in replication stress but not in DNA damage.

I found the p53 downstream target p21 is required for mitotic bypass as the absence of p21 also almost abolished mitotic bypass in aphidicolin. p21 is a CDK inhibitor, so p21 presumably promotes mitotic bypass by inhibiting CDK. Indeed, inhibiting CDK2 or CDK1 using chemical inhibitors rescued mitotic bypass phenotype in p53-knockout cells in aphidicolin. As CDK and APC/CCDH1 inhibit each other, p21 inhibition of CDK may thus allow activation of APC/CCDH1 and subsequent degradation of cyclin B.

p53 promoted mitotic bypass in aphidicolin, but also supressed the growth of RPE1 EC-G1 cells which showed hallmarks of senescence. In contrast, cyclin E-overexpressing RPE1 cells were able to bypass mitosis and continue endoreduplication. I found expressing cyclin E could overcome p53-dependent cell cycle block in aphidicolin-induced EC-G1 cells. Single cell WGD clones could be isolated from cells induced to re-enter the cell cycle this way, or from cyclin E overexpression alone. Altogether, these data suggest that p53-dependent bypass of mitosis in replication stress does not lead to permanent withdrawal from the cell cycle, but rather results in a state with some characteristics of senescence that can be reserved by cyclin E expression.

### **Chapter 6. Discussion**

Previous studies have demonstrated that whole genome duplication can occur due to cell fusion, mitotic failures or endoreduplication following telomere attrition. p53-dependent tumour suppression pathways appear to exist to prevent proliferation of the resultant tetraploid cells (Andreassen et al., 2001, Ganem et al., 2014). It is generally accepted that loss of the p53 pathway is required for efficient polyploidisation. Indeed, studies have shown that p53 deficient cells are genomically unstable and are tumorigenic in animal models (Davoli and de Lange, 2012). However, large-scale genomics studies on cancer patients reveal that almost half polyploid tumours have wild type p53 background (Zack et al., 2013, Bielski et al., 2018). In such p53 proficient tumours, alterations in genes that affect the G1 RB1-E2F pathway, such as CCNE1 amplification and RB1 deletion, are frequently seen. It therefore appears that p53 deficiency is not an obligatory requirement for polyploidisation. However, early driver events that lead to polyploidisation in p53 proficient cells have been poorly documented and are controversial. Our model, summarised in figure 6.1, demonstrates that cyclin E overexpression alone is sufficient to induce whole genome duplication in p53 proficient cells. Replication stress caused by cyclin E overexpression leads to extended G2 arrest, and cells eventually bypass mitosis, entering the endoreduplication cycle G1 phase (EC-G1). Other forms of replication stress can also cause mitotic bypass, as I demonstrated with aphidicolin and oncogenic RAS induction. For newly endoreduplicated RPE1 cells induced by aphidicolin, p53-dependent EC-G1 arrest is imposed to prevent

proliferation. I show that cyclin E overexpression can overcome the EC-G1 cell cycle block, enable cells to replicate and undergo 8N mitosis that is prone to chromosome segregation errors, providing a plausible route for aneuploidy. In addition, oncogene-induced replication stress occurs early in tumorigenesis (Hills and Diffley, 2014, Negrini et al., 2010). Taken together, I reason that, cyclin E overexpression can drive whole genome duplication in early tumorigenesis before or without p53 dysfunction.

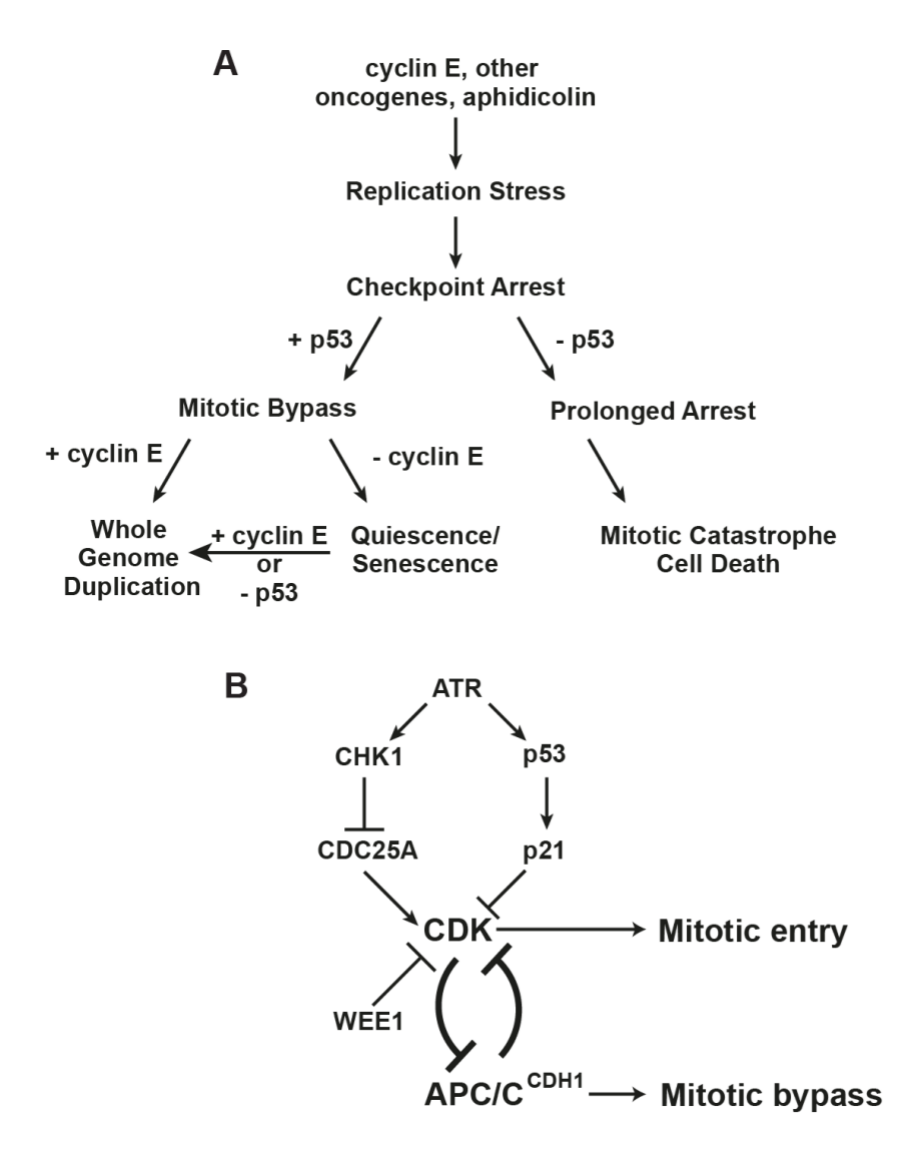


Figure 6.1 Model of WGD driven by cyclin E-induced replication stress.

Replication stress activates the CHK1-dependent G2 checkpoint, causing G2 arrest (Sorensen et al., 2003, Zhao et al., 2002). Without p53, I showed that cells can still undergo G2 arrest following replication stress but the G2 length is longer than p53-positive cells, consistent with previous studies showing p53 loss is not sufficient to abolish G2 arrest (Taylor and Stark, 2001, Kastan et al., 1991, Smits and Medema, 2001). The difference lies in that after replication stress, p53-proficient cells eventually bypass mitosis, while p53deficient cells force through mitosis that often ends catastrophically. In some ways activation of the p53-p21 pathway in G2 helps cells avoid disastrous mitosis by inducing mitotic bypass, and effectively resets the cell cycle at the same time. It is interesting that p53 triggers mitotic bypass before the G2 checkpoint can no longer maintain the G2 arrest. My findings are supported by other studies that show p53 deficiency leads to increased mitotic errors (Narkar et al., 2021) or mitotic catastrophe in IR-induced DNA damage (Johmura et al., 2014). My observations are also consistent with previous studies that show transient activation of p53 or ectopic expression of p21 in G2 causes mitotic bypass and endoreduplication (Bates et al., 1998, Shen et al., 2008, Krenning et al., 2014). It is possible p53-dependent mitotic bypass is a protective mechanism to prevent mitosis-induced genome instability in response to substantial genotoxic stress, but also predisposes WGD, as a double-edged sword. It will be interesting to investigate p53-independent WGD further in the future given that p53 is frequently perturbed in cancer. It is possible that p53 negative cells undergo WGD mainly via failed mitosis following replication stress. At high levels of replication stress shown in my

work here, most of the p53 negative cells die of catastrophic mitosis, but at low levels of stress some cells may have a survivable mitotic failure.

For mitotic bypass to occur, cyclin B needs to be degraded. Cyclin B-CDK1 and cyclin A-CDK2 have been shown to inhibit APC/CCDH1 (Chang et al., 2015, Lukas et al., 1999). Therefore, inhibition of CDK activity by p21 likely creates a permissive setting for CDH1 activation, which eventually degrades cyclin B, resulting in cells shifting to a state resembling G1. This unscheduled CDH1 activation is slow and gradual, as I observed that geminin degradation is 20 times slower during mitotic bypass than in normal mitosis, with approximately a half time ( $t_{1/2}$ ) of 213.1 min and 10.3 min respectively. How this slow activation of APC/CCDH1 during prolonged G2 arrest occurs is unclear. The bypass of mitosis that occurs after sustained expression of cyclin E displays similar characteristics to the bypass caused by aphidicolin. In both conditions, geminin degradation is slow and variable. This suggests the cyclin E-CDK2 activity does not need to oscillate to allow endoreduplication. This is different from the natural endoreplication cycles in fruit flies, which need a period of low cyclin E levels for replication origin licensing and a period of high cyclin E levels for DNA replication (Zielke et al., 2013). In mammalian cells, origin licensing does not seem to be directly impeded by cyclin E overexpression. For instance, in U2OS cells, elevated expression of cyclin E does not reduce MCM loading speed in the G1 phase (Figure 3.7C). Furthermore, cyclin E can promote licensing by protecting the licensing factor CDC6 from APC/C degradation (Mailand and Diffley, 2005). The decrease in loaded MCM level in these cells is because cyclin E

overexpression accelerates the G1 phase, reducing the time for licensing. These data also align with biochemical studies using purified proteins indicating that human cyclin E-CDK2 does not inhibit APC/C<sup>CDH1</sup> activity (Lukas et al., 1999). Thus, my findings support the notion that increased expression of cyclin E does not directly affect either origin licensing or APC/C<sup>CDH1</sup> activity.

Previous studies show p53 deficient mouse cells and human cells transformed by SV40LT or E6/E7 can bypass mitosis following DSBs or telomere attrition (Davoli et al., 2010, Davoli and de Lange, 2012) while in contrast my data show that replication stress-induced mitotic bypass requires p53. Although these results seem contradictory, the underlying mechanism of WGD in both p53-proficient and p53-deficient background should be the same—prolonged CDK inactivation leads to activation of APC/CCDH1 and results in mitotic bypass (Figure 6.2). However, the DSB-driven pathway needs p53 to be absent as telomere attrition or DSBs triggers p53-dependent G1 arrest, which hinders WGD. On the other hand, p53 can be absent because checkpoint activation by DSBs is strong enough to cause mitotic bypass without the need for p21. In contrast, the replication stress mechanism needs p53 because extra CDK inhibition is needed from p21 for mitotic bypass. It is not necessary to lose p53 in my cells as replication stress does not cause p53-dependent G1 arrest. The two pathways start from different checkpoint signals—telomere attrition in Davoli et al and cyclin E-induced replication stress in my case. These genetic changes are frequently observed in cancer, and therefore both mechanisms could play

important roles in the development of cancer. The discrepancy could also be by contributed by the difference between organisms or cell line models used in different studies.

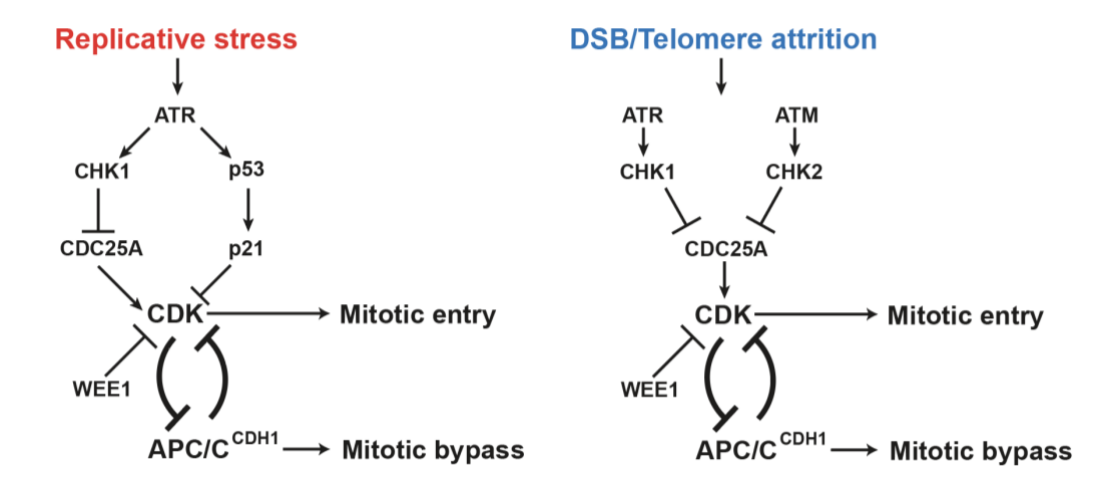


Figure 6.2 Models of WGD driven by replication stress and DSB/Telomere attrition.

Our findings indicate that oncoproteins from viruses may not completely deactivate p53. For instance, BJ cells that have been transformed by SV40-LT can still upregulate p21 when exposed to zeocin or aphidicolin, presumably at a diminished level. Additionally, both DSBs and replication stress can drive mitotic bypass in BJ-LT cells. It would be interesting to examine the capability of p53 mutations to activate both DSB-driven and replication stress-driven endoreduplication. It would also be interesting to study whether mutations causing a diminished p53 response confer tumour cells higher propensity to polyploidisation and more survival advantage compared to a complete loss of p53 response during early tumorigenesis. p53 is typically regarded as a tumour suppressor gene; however, homozygous p53 deletions are rare in cancer (Donehower et al., 2019) and research on p53 mutations in cancer has led to a long-lasting speculation

that mutant p53 is oncogenic (Soussi and Wiman, 2015). p53 functions as a tetramer. Mutant forms of p53 can inhibit the wild type through dominant negative effect (DNE) (Friedman et al., 1993, Gaglia et al., 2013). This DNE confers p53 some oncogenic properties as overexpression of p53 mutants could transform cells and was tumorigenic in mice (Hinds et al., 1990, Hinds et al., 1989, Levine and Oren, 2009, Linzer and Levine, 1979, Lane and Crawford, 1979, Oren and Levine, 1983). The mutant/wild type co-tetramer is not always inactive. Residual transactivation activities may exit (Kakudo et al., 2005, Kawaguchi et al., 2005). My results align with the oncogene perspective on p53 and suggest that p53 may actually play a role in cancer evolution by promoting replication stress-driven WGD. It will be interesting to test how p53 mutants may promote WGD in the future.

The RB1-E2F pathway is critical in controlling G1 phase progression and regulating DNA replication initiation in the human cell cycle. Alterations in the pathway promote hyperproliferation and are observed in virtually all human cancers. Recent genomics studies also associate alterations in many factors of the pathway with whole genome duplication in human tumours, regardless of p53 status. In p53 wild-type tumours, in order to whole genome duplicate, the p53-dependent tetraploid G1 block must be overcome. It is unlikely that p53 can sense the number of chromosomes *per se*, as many aneuploid tumours have wild type p53. It is more likely that p53 is activated by errors in the cell cycle prior to tetraploid G1. Such errors can be the ones that cause replication stress, DNA damage or mitotic failure which activates p53 and leads to p21 upregulation. Since p21 is a cyclin-dependent kinase inhibitor

(Harper et al., 1993), the tetraploid G1 block presumably functions by inhibiting CDKs including CDK4/6 and CDK2. Hyperactivity of G1 CDKs, which can be induced by overexpression of oncogenes in the RB1-E2F pathway, can therefore potentially overcome the p53-dependent tetraploid G1 block in p53 proficient tumours. This is supported by my data with cyclin E overexpression, and partially supported by work on proliferation-quiescence decision (Spencer et al., 2013) that shows high CDK2 activity can prevent cells from entering p21-regulated quiescence and promote proliferation.

Our study provides interesting insights about cancer treatment. Many antitumour drugs induce replication stress by interfering with DNA replication. Actively replicating tumour cells treated with anti-tumour drugs should either die or enter senescence. However, drug resistance can occur. It is shown cells can escape drug-induced senescence if CDK activity is high (Hsu et al., 2019). Since deregulation of the RB1-E2F pathway frequently leads to high CDK activity, it is possible that cyclin E-overexpressing tumour cells can escape senescence and whole genome duplicate in drug treatments, even with wild type p53, as our data show that cyclin E-overexpressing cells can endoreduplicate in anti-cancer drugs (Figure 5.10). Indeed, studies show that drug resistance in several cancers is related to high levels of cyclin E (Scaltriti et al., 2011, Gorski et al., 2020). It is thus interesting to explore the relationship between oncogene expression and chemotherapy resistance in animal models.

### 6.1 Statement of limitations

The conclusion of this work is based on cell biology experiments. No animal models or genetic analysis have been used to test the relevance of the mechanism of WGD proposed for tumorigenesis. The TetON system induces acute cyclin E expression which may differ from the gradual accumulation of *CCNE1* gene amplifications in cancer.

Most of the experiments presented in this work were repeated independently at least three times. In cases where it falls short of three independent repeats, the data volume has been stated in figure legends. More than one independent clone was selected for most of the established cell lines. The U2OS/RPE1 TetON cyclin E, U2OS TetON HRAS<sup>12V</sup>, U2OS TetON MYC, U2OS TetON CDC25A cell lines had a least two independent clones initially tested by Stephanie Hills and Eiko Ozono. One representative clone of each of these cell lines is used in this study. U2OS TetON cyclin D had two clones generated but only one tested. RPE1 TetON cyclin E p53KO had four clones tested and two representative clones were used in the study. RPE1 TetON cyclin E p21KO had four clones tested and one representative clone was used in the study. U2OS TetON cyclin E p53KO had four clones generated but only one clone was tested. U2OS TetON cyclin E p21KO had two clones tested and one representative clone was used in the study. U2OS TetON cyclin E FUCCI H2B had two clones generated and only one clone was tested in the study. RPE1 TetON cyclin E FUCCI and RPE1 TetON cyclin E FUCCI H2B are two independent clones of each other with the only difference being the H2B tag. Only one clone of BJ-LT cells was tested.

Chemical inhibition of ATM, ATR and CDKs was not conducted using chemically unrelated inhibitors for the same target or accompanied with a genetic strategy. Gene depletion experiments used pools of siRNAs targeting different regions of the target gene.

### **Reference List**

- ABBAS, T. & DUTTA, A. 2009. p21 in cancer: intricate networks and multiple activities. *Nat Rev Cancer*, 9, 400-14.
- ABBAS, T., SIVAPRASAD, U., TERAI, K., AMADOR, V., PAGANO, M. & DUTTA, A. 2008. PCNA-dependent regulation of p21 ubiquitylation and degradation via the CRL4Cdt2 ubiquitin ligase complex. *Genes Dev*, 22, 2496-506.
- AHN, J. Y., SCHWARZ, J. K., PIWNICA-WORMS, H. & CANMAN, C. E. 2000. Threonine 68 phosphorylation by ataxia telangiectasia mutated is required for efficient activation of Chk2 in response to ionizing radiation. *Cancer Res*, 60, 5934-6.
- ALBANESE, C., JOHNSON, J., WATANABE, G., EKLUND, N., VU, D., ARNOLD, A. & PESTELL, R. G. 1995. Transforming p21ras mutants and c-Ets-2 activate the cyclin D1 promoter through distinguishable regions. *J Biol Chem*, 270, 23589-97.
- ANDERS, L., KE, N., HYDBRING, P., CHOI, Y. J., WIDLUND, H. R., CHICK, J. M., ZHAI, H., VIDAL, M., GYGI, S. P., BRAUN, P. & SICINSKI, P. 2011. A systematic screen for CDK4/6 substrates links FOXM1 phosphorylation to senescence suppression in cancer cells. *Cancer Cell*, 20, 620-34.
- ANDREASSEN, P. R., LOHEZ, O. D., LACROIX, F. B. & MARGOLIS, R. L. 2001. Tetraploid state induces p53-dependent arrest of nontransformed mammalian cells in G1. *Mol Biol Cell*, 12, 1315-28.
- APPELLA, E. & ANDERSON, C. W. 2001. Post-translational modifications and activation of p53 by genotoxic stresses. *Eur J Biochem*, 268, 2764-72.
- AUBREY, B. J., KELLY, G. L., JANIC, A., HEROLD, M. J. & STRASSER, A. 2018. How does p53 induce apoptosis and how does this relate to p53-mediated tumour suppression? *Cell Death Differ*, 25, 104-113.
- BALACHANDRAN, R. S., HEIGHINGTON, C. S., STAROSTINA, N. G., ANDERSON, J. W., OWEN, D. L., VASUDEVAN, S. & KIPREOS, E. T. 2016. The ubiquitin ligase CRL2ZYG11 targets cyclin B1 for degradation in a conserved pathway that facilitates mitotic slippage. *J Cell Biol*, 215, 151-166.
- BANIN, S., MOYAL, L., SHIEH, S., TAYA, Y., ANDERSON, C. W., CHESSA, L., SMORODINSKY, N. I., PRIVES, C., REISS, Y., SHILOH, Y. & ZIV, Y. 1998. Enhanced phosphorylation of p53 by ATM in response to DNA damage. *Science*, 281, 1674-7.

- BARAK, Y., JUVEN, T., HAFFNER, R. & OREN, M. 1993. mdm2 expression is induced by wild type p53 activity. *EMBO J*, 12, 461-8.
- BARANOVSKIY, A. G., BABAYEVA, N. D., SUWA, Y., GU, J., PAVLOV, Y. I. & TAHIROV, T. H. 2014. Structural basis for inhibition of DNA replication by aphidicolin. *Nucleic Acids Res*, 42, 14013-21.
- BARBER, T. D., MCMANUS, K., YUEN, K. W., REIS, M., PARMIGIANI, G., SHEN, D., BARRETT, I., NOUHI, Y., SPENCER, F., MARKOWITZ, S., VELCULESCU, V. E., KINZLER, K. W., VOGELSTEIN, B., LENGAUER, C. & HIETER, P. 2008. Chromatid cohesion defects may underlie chromosome instability in human colorectal cancers. *Proc Natl Acad Sci U S A*, 105, 3443-8.
- BARTEK, J., BARTKOVA, J. & LUKAS, J. 1996. The retinoblastoma protein pathway and the restriction point. *Curr Opin Cell Biol*, 8, 805-14.
- BARTEK, J., BARTKOVA, J., VOJTESEK, B., STASKOVA, Z., LUKAS, J., REJTHAR, A., KOVARIK, J., MIDGLEY, C. A., GANNON, J. V. & LANE, D. P. 1991. Aberrant expression of the p53 oncoprotein is a common feature of a wide spectrum of human malignancies. *Oncogene*, 6, 1699-703.
- BARTKOVA, J., HOREJSI, Z., KOED, K., KRAMER, A., TORT, F., ZIEGER, K., GULDBERG, P., SEHESTED, M., NESLAND, J. M., LUKAS, C., ORNTOFT, T., LUKAS, J. & BARTEK, J. 2005. DNA damage response as a candidate anti-cancer barrier in early human tumorigenesis. *Nature*, 434, 864-70.
- BATES, S., RYAN, K. M., PHILLIPS, A. C. & VOUSDEN, K. H. 1998. Cell cycle arrest and DNA endoreduplication following p21Waf1/Cip1 expression. *Oncogene*, 17, 1691-703.
- BAUS, F., GIRE, V., FISHER, D., PIETTE, J. & DULIC, V. 2003. Permanent cell cycle exit in G2 phase after DNA damage in normal human fibroblasts. *EMBO J*, 22, 3992-4002.
- BENCHIMOL, S., PIM, D. & CRAWFORD, L. 1982. Radioimmunoassay of the cellular protein p53 in mouse and human cell lines. *EMBO J*, 1, 1055-62.
- BESTER, A. C., RONIGER, M., OREN, Y. S., IM, M. M., SARNI, D., CHAOAT, M., BENSIMON, A., ZAMIR, G., SHEWACH, D. S. & KEREM, B. 2011. Nucleotide deficiency promotes genomic instability in early stages of cancer development. *Cell*, 145, 435-46.
- BIEGING, K. T., MELLO, S. S. & ATTARDI, L. D. 2014. Unravelling mechanisms of p53-mediated tumour suppression. *Nat Rev Cancer*, 14, 359-70.
- BIELSKI, C. M., ZEHIR, A., PENSON, A. V., DONOGHUE, M. T. A., CHATILA, W., ARMENIA, J., CHANG, M. T., SCHRAM, A. M.,

- JONSSON, P., BANDLAMUDI, C., RAZAVI, P., IYER, G., ROBSON, M. E., STADLER, Z. K., SCHULTZ, N., BASELGA, J., SOLIT, D. B., HYMAN, D. M., BERGER, M. F. & TAYLOR, B. S. 2018. Genome doubling shapes the evolution and prognosis of advanced cancers. *Nat Genet*, 50, 1189-1195.
- BLACKFORD, A. N. & JACKSON, S. P. 2017. ATM, ATR, and DNA-PK: The Trinity at the Heart of the DNA Damage Response. *Mol Cell*, 66, 801-817.
- BRACKEN, A. P., CIRO, M., COCITO, A. & HELIN, K. 2004. E2F target genes: unraveling the biology. *Trends Biochem Sci*, 29, 409-17.
- BRITO, D. A. & RIEDER, C. L. 2006. Mitotic checkpoint slippage in humans occurs via cyclin B destruction in the presence of an active checkpoint. *Curr Biol*, 16, 1194-200.
- BROWN, E. J. & BALTIMORE, D. 2000. ATR disruption leads to chromosomal fragmentation and early embryonic lethality. *Genes Dev*, 14, 397-402.
- BUNZ, F., DUTRIAUX, A., LENGAUER, C., WALDMAN, T., ZHOU, S., BROWN, J. P., SEDIVY, J. M., KINZLER, K. W. & VOGELSTEIN, B. 1998. Requirement for p53 and p21 to sustain G2 arrest after DNA damage. *Science*, 282, 1497-501.
- BURRELL, R. A., MCGRANAHAN, N., BARTEK, J. & SWANTON, C. 2013. The causes and consequences of genetic heterogeneity in cancer evolution. *Nature*, 501, 338-45.
- BYUN, T. S., PACEK, M., YEE, M. C., WALTER, J. C. & CIMPRICH, K. A. 2005. Functional uncoupling of MCM helicase and DNA polymerase activities activates the ATR-dependent checkpoint. *Genes Dev,* 19, 1040-52.
- CAHILL, D. P., LENGAUER, C., YU, J., RIGGINS, G. J., WILLSON, J. K., MARKOWITZ, S. D., KINZLER, K. W. & VOGELSTEIN, B. 1998. Mutations of mitotic checkpoint genes in human cancers. *Nature*, 392, 300-3.
- CAPPELL, S. D., CHUNG, M., JAIMOVICH, A., SPENCER, S. L. & MEYER, T. 2016. Irreversible APC(Cdh1) Inactivation Underlies the Point of No Return for Cell-Cycle Entry. *Cell*, 166, 167-80.
- CAPPELL, S. D., MARK, K. G., GARBETT, D., PACK, L. R., RAPE, M. & MEYER, T. 2018. EMI1 switches from being a substrate to an inhibitor of APC/C(CDH1) to start the cell cycle. *Nature*, 558, 313-317.
- CHAN, W. M., SIU, W. Y., LAU, A. & POON, R. Y. 2004. How many mutant p53 molecules are needed to inactivate a tetramer? *Mol Cell Biol*, 24, 3536-51.

- CHANG, L., ZHANG, Z., YANG, J., MCLAUGHLIN, S. H. & BARFORD, D. 2015. Atomic structure of the APC/C and its mechanism of protein ubiquitination. *Nature*, 522, 450-454.
- CHELLAPPAN, S. P., HIEBERT, S., MUDRYJ, M., HOROWITZ, J. M. & NEVINS, J. R. 1991. The E2F transcription factor is a cellular target for the RB protein. *Cell*, 65, 1053-61.
- CHEN, J., SAHA, P., KORNBLUTH, S., DYNLACHT, B. D. & DUTTA, A. 1996a. Cyclin-binding motifs are essential for the function of p21CIP1. *Mol Cell Biol.* 16, 4673-82.
- CHEN, L., WEI, T., SI, X., WANG, Q., LI, Y., LENG, Y., DENG, A., CHEN, J., WANG, G., ZHU, S. & KANG, J. 2013. Lysine acetyltransferase GCN5 potentiates the growth of non-small cell lung cancer via promotion of E2F1, cyclin D1, and cyclin E1 expression. *J Biol Chem*, 288, 14510-14521.
- CHEN, Q. & AMES, B. N. 1994. Senescence-like growth arrest induced by hydrogen peroxide in human diploid fibroblast F65 cells. *Proc Natl Acad Sci U S A*, 91, 4130-4.
- CHEN, S., STOUT, J. R., DHARMAIAH, S., YDE, S., CALVI, B. R. & WALCZAK, C. E. 2016. Transient endoreplication down-regulates the kinesin-14 HSET and contributes to genomic instability. *Mol Biol Cell*, 27, 2911-23.
- CHEN, X., KO, L. J., JAYARAMAN, L. & PRIVES, C. 1996b. p53 levels, functional domains, and DNA damage determine the extent of the apoptotic response of tumor cells. *Genes Dev*, 10, 2438-51.
- CHU, C., GENG, Y., ZHOU, Y. & SICINSKI, P. 2021. Cyclin E in normal physiology and disease states. *Trends Cell Biol*, 31, 732-746.
- CLIJSTERS, L., OGINK, J. & WOLTHUIS, R. 2013. The spindle checkpoint, APC/C(Cdc20), and APC/C(Cdh1) play distinct roles in connecting mitosis to S phase. *J Cell Biol*, 201, 1013-26.
- CLURMAN, B. E., SHEAFF, R. J., THRESS, K., GROUDINE, M. & ROBERTS, J. M. 1996. Turnover of cyclin E by the ubiquitin-proteasome pathway is regulated by cdk2 binding and cyclin phosphorylation. *Genes Dev,* 10, 1979-90.
- COSTANTINO, L., SOTIRIOU, S. K., RANTALA, J. K., MAGIN, S., MLADENOV, E., HELLEDAY, T., HABER, J. E., ILIAKIS, G., KALLIONIEMI, O. P. & HALAZONETIS, T. D. 2014. Break-induced replication repair of damaged forks induces genomic duplications in human cells. *Science*, 343, 88-91.
- CRNCEC, A. & HOCHEGGER, H. 2019. Triggering mitosis. *FEBS Lett*, 593, 2868-2888.

- CROOK, T., TIDY, J. A. & VOUSDEN, K. H. 1991. Degradation of p53 can be targeted by HPV E6 sequences distinct from those required for p53 binding and trans-activation. *Cell*, 67, 547-56.
- D'ADDA DI FAGAGNA, F., REAPER, P. M., CLAY-FARRACE, L., FIEGLER, H., CARR, P., VON ZGLINICKI, T., SARETZKI, G., CARTER, N. P. & JACKSON, S. P. 2003. A DNA damage checkpoint response in telomere-initiated senescence. *Nature*, 426, 194-8.
- DAVOLI, T. & DE LANGE, T. 2011. The causes and consequences of polyploidy in normal development and cancer. *Annu Rev Cell Dev Biol*, 27, 585-610.
- DAVOLI, T. & DE LANGE, T. 2012. Telomere-driven tetraploidization occurs in human cells undergoing crisis and promotes transformation of mouse cells. *Cancer Cell*, 21, 765-76.
- DAVOLI, T., DENCHI, E. L. & DE LANGE, T. 2010. Persistent telomere damage induces bypass of mitosis and tetraploidy. *Cell*, 141, 81-93.
- DE KLEIN, A., MUIJTJENS, M., VAN OS, R., VERHOEVEN, Y., SMIT, B., CARR, A. M., LEHMANN, A. R. & HOEIJMAKERS, J. H. 2000. Targeted disruption of the cell-cycle checkpoint gene ATR leads to early embryonic lethality in mice. *Curr Biol*, 10, 479-82.
- DE LANGE, T. 2005. Shelterin: the protein complex that shapes and safeguards human telomeres. *Genes Dev,* 19, 2100-10.
- DEGREGORI, J., KOWALIK, T. & NEVINS, J. R. 1995. Cellular targets for activation by the E2F1 transcription factor include DNA synthesis- and G1/S-regulatory genes. *Mol Cell Biol*, 15, 4215-24.
- DEHART, C. J., CHAHAL, J. S., FLINT, S. J. & PERLMAN, D. H. 2014. Extensive post-translational modification of active and inactivated forms of endogenous p53. *Mol Cell Proteomics*, 13, 1-17.
- DEN ELZEN, N. & PINES, J. 2001. Cyclin A is destroyed in prometaphase and can delay chromosome alignment and anaphase. *J Cell Biol*, 153, 121-36.
- DENCHI, E. L. & DE LANGE, T. 2007. Protection of telomeres through independent control of ATM and ATR by TRF2 and POT1. *Nature*, 448, 1068-71.
- DENOYELLE, C., ABOU-RJAILY, G., BEZROOKOVE, V., VERHAEGEN, M., JOHNSON, T. M., FULLEN, D. R., POINTER, J. N., GRUBER, S. B., SU, L. D., NIKIFOROV, M. A., KAUFMAN, R. J., BASTIAN, B. C. & SOENGAS, M. S. 2006. Anti-oncogenic role of the endoplasmic reticulum differentially activated by mutations in the MAPK pathway. *Nat Cell Biol*, 8, 1053-63.

- DI COMO, C. J. & PRIVES, C. 1998. Human tumor-derived p53 proteins exhibit binding site selectivity and temperature sensitivity for transactivation in a yeast-based assay. *Oncogene*, 16, 2527-39.
- DI LEONARDO, A., LINKE, S. P., CLARKIN, K. & WAHL, G. M. 1994. DNA damage triggers a prolonged p53-dependent G1 arrest and long-term induction of Cip1 in normal human fibroblasts. *Genes Dev*, 8, 2540-51.
- DIFFLEY, J. F. 2004. Regulation of early events in chromosome replication. *Curr Biol*, 14, R778-86.
- DIMRI, G. P., LEE, X., BASILE, G., ACOSTA, M., SCOTT, G., ROSKELLEY, C., MEDRANO, E. E., LINSKENS, M., RUBELJ, I., PEREIRA-SMITH, O. & ET AL. 1995. A biomarker that identifies senescent human cells in culture and in aging skin in vivo. *Proc Natl Acad Sci U S A*, 92, 9363-7.
- DITTMER, D., PATI, S., ZAMBETTI, G., CHU, S., TERESKY, A. K., MOORE, M., FINLAY, C. & LEVINE, A. J. 1993. Gain of function mutations in p53. *Nat Genet*, 4, 42-6.
- DONEHOWER, L. A., SOUSSI, T., KORKUT, A., LIU, Y., SCHULTZ, A., CARDENAS, M., LI, X., BABUR, O., HSU, T. K., LICHTARGE, O., WEINSTEIN, J. N., AKBANI, R. & WHEELER, D. A. 2019. Integrated Analysis of TP53 Gene and Pathway Alterations in The Cancer Genome Atlas. *Cell Rep*, 28, 1370-1384 e5.
- DUELLI, D. M., PADILLA-NASH, H. M., BERMAN, D., MURPHY, K. M., RIED, T. & LAZEBNIK, Y. 2007. A virus causes cancer by inducing massive chromosomal instability through cell fusion. *Curr Biol*, 17, 431-7.
- DYSON, N. 1998. The regulation of E2F by pRB-family proteins. *Genes Dev,* 12, 2245-62.
- EKHOLM-REED, S., MENDEZ, J., TEDESCO, D., ZETTERBERG, A., STILLMAN, B. & REED, S. I. 2004. Deregulation of cyclin E in human cells interferes with prereplication complex assembly. *J Cell Biol*, 165, 789-800.
- EL-DEIRY, W. S., KERN, S. E., PIETENPOL, J. A., KINZLER, K. W. & VOGELSTEIN, B. 1992. Definition of a consensus binding site for p53. *Nat Genet*, 1, 45-9.
- EL-DEIRY, W. S., TOKINO, T., VELCULESCU, V. E., LEVY, D. B., PARSONS, R., TRENT, J. M., LIN, D., MERCER, W. E., KINZLER, K. W. & VOGELSTEIN, B. 1993. WAF1, a potential mediator of p53 tumor suppression. *Cell*, 75, 817-25.
- EPISKOPOU, H., DIMAN, A., CLAUDE, E., VICECONTE, N. & DECOTTIGNIES, A. 2019. TSPYL5 Depletion Induces Specific Death

- of ALT Cells through USP7-Dependent Proteasomal Degradation of POT1. *Mol Cell*, 75, 469-482 e6.
- ESPINOSA, J. M. & EMERSON, B. M. 2001. Transcriptional regulation by p53 through intrinsic DNA/chromatin binding and site-directed cofactor recruitment. *Mol Cell*, 8, 57-69.
- ETEMADMOGHADAM, D., DEFAZIO, A., BEROUKHIM, R., MERMEL, C., GEORGE, J., GETZ, G., TOTHILL, R., OKAMOTO, A., RAEDER, M. B., HARNETT, P., LADE, S., AKSLEN, L. A., TINKER, A. V., LOCANDRO, B., ALSOP, K., CHIEW, Y. E., TRAFICANTE, N., FEREDAY, S., JOHNSON, D., FOX, S., SELLERS, W., URASHIMA, M., SALVESEN, H. B., MEYERSON, M., BOWTELL, D. & GROUP, A. S. 2009. Integrated genome-wide DNA copy number and expression analysis identifies distinct mechanisms of primary chemoresistance in ovarian carcinomas. *Clin Cancer Res*, 15, 1417-27.
- FAGUNDES, R. & TEIXEIRA, L. K. 2021. Cyclin E/CDK2: DNA Replication, Replication Stress and Genomic Instability. *Front Cell Dev Biol*, 9, 774845.
- FALCK, J., MAILAND, N., SYLJUASEN, R. G., BARTEK, J. & LUKAS, J. 2001. The ATM-Chk2-Cdc25A checkpoint pathway guards against radioresistant DNA synthesis. *Nature*, 410, 842-7.
- FINN, R. S., DERING, J., CONKLIN, D., KALOUS, O., COHEN, D. J., DESAI, A. J., GINTHER, C., ATEFI, M., CHEN, I., FOWST, C., LOS, G. & SLAMON, D. J. 2009. PD 0332991, a selective cyclin D kinase 4/6 inhibitor, preferentially inhibits proliferation of luminal estrogen receptor-positive human breast cancer cell lines in vitro. *Breast Cancer Res*, 11, R77.
- FISHER, R. P. & MORGAN, D. O. 1994. A novel cyclin associates with MO15/CDK7 to form the CDK-activating kinase. *Cell*, 78, 713-24.
- FOX, P. M., VOUGHT, V. E., HANAZAWA, M., LEE, M. H., MAINE, E. M. & SCHEDL, T. 2011. Cyclin E and CDK-2 regulate proliferative cell fate and cell cycle progression in the C. elegans germline. *Development*, 138, 2223-34.
- FREED-PASTOR, W. A. & PRIVES, C. 2012. Mutant p53: one name, many proteins. *Genes Dev.* 26, 1268-86.
- FRIEDMAN, P. N., CHEN, X., BARGONETTI, J. & PRIVES, C. 1993. The p53 protein is an unusually shaped tetramer that binds directly to DNA. *Proc Natl Acad Sci U S A*, 90, 3319-23.
- GAGLIA, G., GUAN, Y., SHAH, J. V. & LAHAV, G. 2013. Activation and control of p53 tetramerization in individual living cells. *Proc Natl Acad Sci U S A*, 110, 15497-501.

- GALIPEAU, P. C., COWAN, D. S., SANCHEZ, C. A., BARRETT, M. T., EMOND, M. J., LEVINE, D. S., RABINOVITCH, P. S. & REID, B. J. 1996. 17p (p53) allelic losses, 4N (G2/tetraploid) populations, and progression to aneuploidy in Barrett's esophagus. *Proc Natl Acad Sci U S A*, 93, 7081-4.
- GANEM, N. J., CORNILS, H., CHIU, S. Y., O'ROURKE, K. P., ARNAUD, J., YIMLAMAI, D., THERY, M., CAMARGO, F. D. & PELLMAN, D. 2014. Cytokinesis failure triggers hippo tumor suppressor pathway activation. *Cell*, 158, 833-848.
- GANEM, N. J., GODINHO, S. A. & PELLMAN, D. 2009. A mechanism linking extra centrosomes to chromosomal instability. *Nature*, 460, 278-82.
- GANEM, N. J., STORCHOVA, Z. & PELLMAN, D. 2007. Tetraploidy, aneuploidy and cancer. *Curr Opin Genet Dev*, 17, 157-62.
- GAO, J., AKSOY, B. A., DOGRUSOZ, U., DRESDNER, G., GROSS, B., SUMER, S. O., SUN, Y., JACOBSEN, A., SINHA, R., LARSSON, E., CERAMI, E., SANDER, C. & SCHULTZ, N. 2013. Integrative analysis of complex cancer genomics and clinical profiles using the cBioPortal. *Sci Signal*, 6, pl1.
- GEMBLE, S., WARDENAAR, R., KEUPER, K., SRIVASTAVA, N., NANO, M., MACE, A. S., TIJHUIS, A. E., BERNHARD, S. V., SPIERINGS, D. C. J., SIMON, A., GOUNDIAM, O., HOCHEGGER, H., PIEL, M., FOIJER, F., STORCHOVA, Z. & BASTO, R. 2022. Genetic instability from a single S phase after whole-genome duplication. *Nature*, 604, 146-151.
- GENG, Y., MICHOWSKI, W., CHICK, J. M., WANG, Y. E., JECROIS, M. E., SWEENEY, K. E., LIU, L., HAN, R. C., KE, N., ZAGOZDZON, A., SICINSKA, E., BRONSON, R. T., GYGI, S. P. & SICINSKI, P. 2018. Kinase-independent function of E-type cyclins in liver cancer. *Proc Natl Acad Sci U S A*, 115, 1015-1020.
- GENG, Y., YU, Q., SICINSKA, E., DAS, M., SCHNEIDER, J. E., BHATTACHARYA, S., RIDEOUT, W. M., BRONSON, R. T., GARDNER, H. & SICINSKI, P. 2003. Cyclin E Ablation in the Mouse. *Cell*, 114, 431-443.
- GIACOMELLI, A. O., YANG, X., LINTNER, R. E., MCFARLAND, J. M., DUBY, M., KIM, J., HOWARD, T. P., TAKEDA, D. Y., LY, S. H., KIM, E., GANNON, H. S., HURHULA, B., SHARPE, T., GOODALE, A., FRITCHMAN, B., STEELMAN, S., VAZQUEZ, F., TSHERNIAK, A., AGUIRRE, A. J., DOENCH, J. G., PICCIONI, F., ROBERTS, C. W. M., MEYERSON, M., GETZ, G., JOHANNESSEN, C. M., ROOT, D. E. & HAHN, W. C. 2018. Mutational processes shape the landscape of TP53 mutations in human cancer. *Nat Genet*, 50, 1381-1387.

- GIRE, V. & DULIC, V. 2015. Senescence from G2 arrest, revisited. *Cell Cycle*, 14, 297-304.
- GOLAN, A., YUDKOVSKY, Y. & HERSHKO, A. 2002. The cyclin-ubiquitin ligase activity of cyclosome/APC is jointly activated by protein kinases Cdk1-cyclin B and Plk. *J Biol Chem*, 277, 15552-7.
- GORSKI, J. W., UELAND, F. R. & KOLESAR, J. M. 2020. CCNE1
  Amplification as a Predictive Biomarker of Chemotherapy Resistance in Epithelial Ovarian Cancer. *Diagnostics (Basel)*, 10.
- GOULD, K. L. & NURSE, P. 1989. Tyrosine phosphorylation of the fission yeast cdc2+ protein kinase regulates entry into mitosis. *Nature*, 342, 39-45.
- GREENMAN, C., STEPHENS, P., SMITH, R., DALGLIESH, G. L., HUNTER, C., BIGNELL, G., DAVIES, H., TEAGUE, J., BUTLER, A., STEVENS, C., EDKINS, S., O'MEARA, S., VASTRIK, I., SCHMIDT, E. E., AVIS, T., BARTHORPE, S., BHAMRA, G., BUCK, G., CHOUDHURY, B., CLEMENTS, J., COLE, J., DICKS, E., FORBES, S., GRAY, K., HALLIDAY, K., HARRISON, R., HILLS, K., HINTON, J., JENKINSON, A., JONES, D., MENZIES, A., MIRONENKO, T., PERRY, J., RAINE, K., RICHARDSON, D., SHEPHERD, R., SMALL, A., TOFTS, C., VARIAN, J., WEBB, T., WEST, S., WIDAA, S., YATES, A., CAHILL, D. P., LOUIS, D. N., GOLDSTRAW, P., NICHOLSON, A. G., BRASSEUR, F., LOOIJENGA, L., WEBER, B. L., CHIEW, Y. E., DEFAZIO, A., GREAVES, M. F., GREEN, A. R., CAMPBELL, P., BIRNEY, E., EASTON, D. F., CHENEVIX-TRENCH, G., TAN, M. H., KHOO, S. K., TEH, B. T., YUEN, S. T., LEUNG, S. Y., WOOSTER, R., FUTREAL, P. A. & STRATTON, M. R. 2007. Patterns of somatic mutation in human cancer genomes. Nature, 446, 153-8.
- GUO, X. & HARTLEY, R. S. 2006. HuR contributes to cyclin E1 deregulation in MCF-7 breast cancer cells. *Cancer Res*, 66, 7948-56.
- GUO, Z., KUMAGAI, A., WANG, S. X. & DUNPHY, W. G. 2000. Requirement for Atr in phosphorylation of Chk1 and cell cycle regulation in response to DNA replication blocks and UV-damaged DNA in Xenopus egg extracts. *Genes Dev,* 14, 2745-56.
- GUPTA-ROSSI, N., LE BAIL, O., GONEN, H., BROU, C., LOGEAT, F., SIX, E., CIECHANOVER, A. & ISRAEL, A. 2001. Functional interaction between SEL-10, an F-box protein, and the nuclear form of activated Notch1 receptor. *J Biol Chem*, 276, 34371-8.
- HAFNER, A., BULYK, M. L., JAMBHEKAR, A. & LAHAV, G. 2019. The multiple mechanisms that regulate p53 activity and cell fate. *Nat Rev Mol Cell Biol*, 20, 199-210.

- HAFNER, A., KUBLO, L., TSABAR, M., LAHAV, G. & STEWART-ORNSTEIN, J. 2020. Identification of universal and cell-type specific p53 DNA binding. *BMC Mol Cell Biol*, 21, 5.
- HALAZONETIS, T. D., GORGOULIS, V. G. & BARTEK, J. 2008. An oncogene-induced DNA damage model for cancer development. *Science*, 319, 1352-5.
- HARPER, J. W., ADAMI, G. R., WEI, N., KEYOMARSI, K. & ELLEDGE, S. J. 1993. The p21 Cdk-interacting protein Cip1 is a potent inhibitor of G1 cyclin-dependent kinases. *Cell.* 75, 805-16.
- HARPER, J. W., ELLEDGE, S. J., KEYOMARSI, K., DYNLACHT, B., TSAI, L. H., ZHANG, P., DOBROWOLSKI, S., BAI, C., CONNELL-CROWLEY, L., SWINDELL, E. & ET AL. 1995. Inhibition of cyclin-dependent kinases by p21. *Mol Biol Cell*, 6, 387-400.
- HAUPT, Y., MAYA, R., KAZAZ, A. & OREN, M. 1997. Mdm2 promotes the rapid degradation of p53. *Nature*, 387, 296-9.
- HAYFLICK, L. 1965. The Limited in Vitro Lifetime of Human Diploid Cell Strains. *Exp Cell Res*, 37, 614-36.
- HEALD, R., MCLOUGHLIN, M. & MCKEON, F. 1993. Human wee1 maintains mitotic timing by protecting the nucleus from cytoplasmically activated Cdc2 kinase. *Cell*, 74, 463-74.
- HEAPHY, C. M., SUBHAWONG, A. P., HONG, S. M., GOGGINS, M. G., MONTGOMERY, E. A., GABRIELSON, E., NETTO, G. J., EPSTEIN, J. I., LOTAN, T. L., WESTRA, W. H., SHIH IE, M., IACOBUZIO-DONAHUE, C. A., MAITRA, A., LI, Q. K., EBERHART, C. G., TAUBE, J. M., RAKHEJA, D., KURMAN, R. J., WU, T. C., RODEN, R. B., ARGANI, P., DE MARZO, A. M., TERRACCIANO, L., TORBENSON, M. & MEEKER, A. K. 2011. Prevalence of the alternative lengthening of telomeres telomere maintenance mechanism in human cancer subtypes. *Am J Pathol*, 179, 1608-15.
- HEKMAT-NEJAD, M., YOU, Z., YEE, M. C., NEWPORT, J. W. & CIMPRICH, K. A. 2000. Xenopus ATR is a replication-dependent chromatin-binding protein required for the DNA replication checkpoint. *Curr Biol*, 10, 1565-73.
- HERMEKING, H., LENGAUER, C., POLYAK, K., HE, T. C., ZHANG, L., THIAGALINGAM, S., KINZLER, K. W. & VOGELSTEIN, B. 1997. 14-3-3sigma is a p53-regulated inhibitor of G2/M progression. *Mol Cell*, 1, 3-11.
- HILLS, S. A. & DIFFLEY, J. F. 2014. DNA replication and oncogene-induced replicative stress. *Curr Biol*, 24, R435-44.

- HINDS, P., FINLAY, C. & LEVINE, A. J. 1989. Mutation is required to activate the p53 gene for cooperation with the ras oncogene and transformation. *J Virol*, 63, 739-46.
- HINDS, P. W., FINLAY, C. A., QUARTIN, R. S., BAKER, S. J., FEARON, E. R., VOGELSTEIN, B. & LEVINE, A. J. 1990. Mutant p53 DNA clones from human colon carcinomas cooperate with ras in transforming primary rat cells: a comparison of the "hot spot" mutant phenotypes. *Cell Growth Differ,* 1, 571-80.
- HOEIJMAKERS, J. H. 2001. Genome maintenance mechanisms for preventing cancer. *Nature*, 411, 366-74.
- HOLLAND, A. J. & CLEVELAND, D. W. 2009. Boveri revisited: chromosomal instability, aneuploidy and tumorigenesis. *Nat Rev Mol Cell Biol*, 10, 478-87.
- HONDA, R., TANAKA, H. & YASUDA, H. 1997. Oncoprotein MDM2 is a ubiquitin ligase E3 for tumor suppressor p53. *FEBS Lett*, 420, 25-7.
- HSU, C. H., ALTSCHULER, S. J. & WU, L. F. 2019. Patterns of Early p21 Dynamics Determine Proliferation-Senescence Cell Fate after Chemotherapy. *Cell*, 178, 361-373 e12.
- HU, L., PLAFKER, K., VOROZHKO, V., ZUNA, R. E., HANIGAN, M. H., GORBSKY, G. J., PLAFKER, S. M., ANGELETTI, P. C. & CERESA, B. P. 2009. Human papillomavirus 16 E5 induces bi-nucleated cell formation by cell-cell fusion. *Virology*, 384, 125-34.
- HUANG, J. N., PARK, I., ELLINGSON, E., LITTLEPAGE, L. E. & PELLMAN, D. 2001. Activity of the APC(Cdh1) form of the anaphase-promoting complex persists until S phase and prevents the premature expression of Cdc20p. *J Cell Biol*, 154, 85-94.
- HWANG, H. C. & CLURMAN, B. E. 2005. Cyclin E in normal and neoplastic cell cycles. *Oncogene*, 24, 2776-86.
- IRANI, K., XIA, Y., ZWEIER, J. L., SOLLOTT, S. J., DER, C. J., FEARON, E. R., SUNDARESAN, M., FINKEL, T. & GOLDSCHMIDT-CLERMONT, P. J. 1997. Mitogenic signaling mediated by oxidants in Rastransformed fibroblasts. *Science*, 275, 1649-52.
- JACKSON, S. P. & BARTEK, J. 2009. The DNA-damage response in human biology and disease. *Nature*, 461, 1071-8.
- JASPERSEN, S. L., CHARLES, J. F. & MORGAN, D. O. 1999. Inhibitory phosphorylation of the APC regulator Hct1 is controlled by the kinase Cdc28 and the phosphatase Cdc14. *Curr Biol*, 9, 227-36.
- JAZAYERI, A., FALCK, J., LUKAS, C., BARTEK, J., SMITH, G. C., LUKAS, J. & JACKSON, S. P. 2006. ATM- and cell cycle-dependent regulation

- of ATR in response to DNA double-strand breaks. *Nat Cell Biol*, 8, 37-45.
- JOHMURA, Y., SHIMADA, M., MISAKI, T., NAIKI-ITO, A., MIYOSHI, H., MOTOYAMA, N., OHTANI, N., HARA, E., NAKAMURA, M., MORITA, A., TAKAHASHI, S. & NAKANISHI, M. 2014. Necessary and sufficient role for a mitosis skip in senescence induction. *Mol Cell*, 55, 73-84.
- JOHNSON, A. & SKOTHEIM, J. M. 2013. Start and the restriction point. *Curr Opin Cell Biol*, 25, 717-23.
- JONES, D. L. & MUNGER, K. 1996. Interactions of the human papillomavirus E7 protein with cell cycle regulators. *Semin Cancer Biol*, 7, 327-37.
- JONES, R. M., MORTUSEWICZ, O., AFZAL, I., LORVELLEC, M., GARCIA, P., HELLEDAY, T. & PETERMANN, E. 2013. Increased replication initiation and conflicts with transcription underlie Cyclin E-induced replication stress. *Oncogene*, 32, 3744-53.
- JORDAN, J. J., MENENDEZ, D., INGA, A., NOUREDDINE, M., BELL, D. A. & RESNICK, M. A. 2008. Noncanonical DNA motifs as transactivation targets by wild type and mutant p53. *PLoS Genet,* 4, e1000104.
- JORDAN, M. A., THROWER, D. & WILSON, L. 1992. Effects of vinblastine, podophyllotoxin and nocodazole on mitotic spindles. Implications for the role of microtubule dynamics in mitosis. *J Cell Sci*, 102 ( Pt 3), 401-16.
- KAKUDO, Y., SHIBATA, H., OTSUKA, K., KATO, S. & ISHIOKA, C. 2005. Lack of correlation between p53-dependent transcriptional activity and the ability to induce apoptosis among 179 mutant p53s. *Cancer Res*, 65, 2108-14.
- KAPOOR, M. & LOZANO, G. 1998. Functional activation of p53 via phosphorylation following DNA damage by UV but not gamma radiation. *Proc Natl Acad Sci U S A*, 95, 2834-7.
- KASTAN, M. B., ONYEKWERE, O., SIDRANSKY, D., VOGELSTEIN, B. & CRAIG, R. W. 1991. Participation of p53 protein in the cellular response to DNA damage. *Cancer Res*, 51, 6304-11.
- KATO, S., HAN, S. Y., LIU, W., OTSUKA, K., SHIBATA, H., KANAMARU, R. & ISHIOKA, C. 2003. Understanding the function-structure and function-mutation relationships of p53 tumor suppressor protein by high-resolution missense mutation analysis. *Proc Natl Acad Sci U S A*, 100, 8424-9.
- KAWAGUCHI, T., KATO, S., OTSUKA, K., WATANABE, G., KUMABE, T., TOMINAGA, T., YOSHIMOTO, T. & ISHIOKA, C. 2005. The relationship among p53 oligomer formation, structure and

- transcriptional activity using a comprehensive missense mutation library. *Oncogene*, 24, 6976-81.
- KHANNA, K. K. & JACKSON, S. P. 2001. DNA double-strand breaks: signaling, repair and the cancer connection. *Nat Genet*, 27, 247-54.
- KNOBLICH, J. A., SAUER, K., JONES, L., RICHARDSON, H., SAINT, R. & LEHNER, C. F. 1994. Cyclin E controls S phase progression and its down-regulation during Drosophila embryogenesis is required for the arrest of cell proliferation. *Cell*, 77, 107-20.
- KOBAYASHI, H., STEWART, E., POON, R., ADAMCZEWSKI, J. P., GANNON, J. & HUNT, T. 1992. Identification of the domains in cyclin A required for binding to, and activation of, p34cdc2 and p32cdk2 protein kinase subunits. *Mol Biol Cell*, 3, 1279-94.
- KOEPP, D. M., SCHAEFER, L. K., YE, X., KEYOMARSI, K., CHU, C., HARPER, J. W. & ELLEDGE, S. J. 2001. Phosphorylation-dependent ubiquitination of cyclin E by the SCFFbw7 ubiquitin ligase. *Science*, 294, 173-7.
- KOPS, G. J., FOLTZ, D. R. & CLEVELAND, D. W. 2004. Lethality to human cancer cells through massive chromosome loss by inhibition of the mitotic checkpoint. *Proc Natl Acad Sci U S A*, 101, 8699-704.
- KOSSATZ, U., BREUHAHN, K., WOLF, B., HARDTKE-WOLENSKI, M., WILKENS, L., STEINEMANN, D., SINGER, S., BRASS, F., KUBICKA, S., SCHLEGELBERGER, B., SCHIRMACHER, P., MANNS, M. P., SINGER, J. D. & MALEK, N. P. 2010. The cyclin E regulator cullin 3 prevents mouse hepatic progenitor cells from becoming tumorinitiating cells. *J Clin Invest*, 120, 3820-33.
- KRAFT, C., HERZOG, F., GIEFFERS, C., MECHTLER, K., HAGTING, A., PINES, J. & PETERS, J. M. 2003. Mitotic regulation of the human anaphase-promoting complex by phosphorylation. *EMBO J*, 22, 6598-609.
- KRAISS, S., QUAISER, A., OREN, M. & MONTENARH, M. 1988. Oligomerization of oncoprotein p53. *J Virol*, 62, 4737-44.
- KRAMER, E. R., SCHEURINGER, N., PODTELEJNIKOV, A. V., MANN, M. & PETERS, J. M. 2000. Mitotic regulation of the APC activator proteins CDC20 and CDH1. *Mol Biol Cell*, 11, 1555-69.
- KRENNING, L., FERINGA, F. M., SHALTIEL, I. A., VAN DEN BERG, J. & MEDEMA, R. H. 2014. Transient activation of p53 in G2 phase is sufficient to induce senescence. *Mol Cell*, 55, 59-72.
- KUBBUTAT, M. H., JONES, S. N. & VOUSDEN, K. H. 1997. Regulation of p53 stability by Mdm2. *Nature*, 387, 299-303.

- KUILMAN, T., MICHALOGLOU, C., MOOI, W. J. & PEEPER, D. S. 2010. The essence of senescence. *Genes Dev*, 24, 2463-79.
- KUMAGAI, A. & DUNPHY, W. G. 1991. The cdc25 protein controls tyrosine dephosphorylation of the cdc2 protein in a cell-free system. *Cell*, 64, 903-14.
- KUMAGAI, A., LEE, J., YOO, H. Y. & DUNPHY, W. G. 2006. TopBP1 activates the ATR-ATRIP complex. *Cell*, 124, 943-55.
- KURZ, D. J., DECARY, S., HONG, Y. & ERUSALIMSKY, J. D. 2000. Senescence-associated (beta)-galactosidase reflects an increase in lysosomal mass during replicative ageing of human endothelial cells. *J Cell Sci*, 113 ( Pt 20), 3613-22.
- LAN, K. H., SHEU, M. L., HWANG, S. J., YEN, S. H., CHEN, S. Y., WU, J. C., WANG, Y. J., KATO, N., OMATA, M., CHANG, F. Y. & LEE, S. D. 2002. HCV NS5A interacts with p53 and inhibits p53-mediated apoptosis. *Oncogene*, 21, 4801-11.
- LAND, H., PARADA, L. F. & WEINBERG, R. A. 1983. Tumorigenic conversion of primary embryo fibroblasts requires at least two cooperating oncogenes. *Nature*, 304, 596-602.
- LANE, D. P. & CRAWFORD, L. V. 1979. T antigen is bound to a host protein in SV40-transformed cells. *Nature*, 278, 261-3.
- LARA-GONZALEZ, P., WESTHORPE, F. G. & TAYLOR, S. S. 2012. The spindle assembly checkpoint. *Curr Biol*, 22, R966-80.
- LEE, A. C., FENSTER, B. E., ITO, H., TAKEDA, K., BAE, N. S., HIRAI, T., YU, Z. X., FERRANS, V. J., HOWARD, B. H. & FINKEL, T. 1999. Ras proteins induce senescence by altering the intracellular levels of reactive oxygen species. *J Biol Chem*, 274, 7936-40.
- LEE, B. Y., HAN, J. A., IM, J. S., MORRONE, A., JOHUNG, K., GOODWIN, E. C., KLEIJER, W. J., DIMAIO, D. & HWANG, E. S. 2006. Senescence-associated beta-galactosidase is lysosomal beta-galactosidase. *Aging Cell*, 5, 187-95.
- LEE, J. H. & PAULL, T. T. 2005. ATM activation by DNA double-strand breaks through the Mre11-Rad50-Nbs1 complex. *Science*, 308, 551-4.
- LEHMAN, N. L., VERSCHUREN, E. W., HSU, J. Y., CHERRY, A. M. & JACKSON, P. K. 2006. Overexpression of the anaphase promoting complex/cyclosome inhibitor Emi1 leads to tetraploidy and genomic instability of p53-deficient cells. *Cell Cycle*, 5, 1569-73.
- LENGAUER, C., KINZLER, K. W. & VOGELSTEIN, B. 1997. Genetic instability in colorectal cancers. *Nature*, 386, 623-7.

- LENTINI, L., AMATO, A., SCHILLACI, T. & DI LEONARDO, A. 2007. Simultaneous Aurora-A/STK15 overexpression and centrosome amplification induce chromosomal instability in tumour cells with a MIN phenotype. *BMC Cancer*, 7, 212.
- LEVINE, A. J. 2009. The common mechanisms of transformation by the small DNA tumor viruses: The inactivation of tumor suppressor gene products: p53. *Virology*, 384, 285-93.
- LEVINE, A. J. & OREN, M. 2009. The first 30 years of p53: growing ever more complex. *Nat Rev Cancer*, 9, 749-58.
- LI, D., MARCHENKO, N. D., SCHULZ, R., FISCHER, V., VELASCO-HERNANDEZ, T., TALOS, F. & MOLL, U. M. 2011. Functional inactivation of endogenous MDM2 and CHIP by HSP90 causes aberrant stabilization of mutant p53 in human cancer cells. *Mol Cancer Res*, 9, 577-88.
- LINDAHL, T. 1993. Instability and decay of the primary structure of DNA. *Nature*, 362, 709-15.
- LINDAHL, T. & BARNES, D. E. 2000. Repair of endogenous DNA damage. Cold Spring Harb Symp Quant Biol, 65, 127-33.
- LINDAHL, T. & NYBERG, B. 1972. Rate of depurination of native deoxyribonucleic acid. *Biochemistry*, 11, 3610-8.
- LINZER, D. I. & LEVINE, A. J. 1979. Characterization of a 54K dalton cellular SV40 tumor antigen present in SV40-transformed cells and uninfected embryonal carcinoma cells. *Cell*, 17, 43-52.
- LOPES, M., COTTA-RAMUSINO, C., PELLICIOLI, A., LIBERI, G., PLEVANI, P., MUZI-FALCONI, M., NEWLON, C. S. & FOIANI, M. 2001. The DNA replication checkpoint response stabilizes stalled replication forks. *Nature*, 412, 557-61.
- LUKAS, C., SORENSEN, C. S., KRAMER, E., SANTONI-RUGIU, E., LINDENEG, C., PETERS, J. M., BARTEK, J. & LUKAS, J. 1999. Accumulation of cyclin B1 requires E2F and cyclin-A-dependent rearrangement of the anaphase-promoting complex. *Nature*, 401, 815-8.
- LUKASHCHUK, N. & VOUSDEN, K. H. 2007. Ubiquitination and degradation of mutant p53. *Mol Cell Biol*, 27, 8284-95.
- MACHERET, M. & HALAZONETIS, T. D. 2018. Intragenic origins due to short G1 phases underlie oncogene-induced DNA replication stress. *Nature*, 555, 112-116.
- MADDEN, S. L., GALELLA, E. A., ZHU, J., BERTELSEN, A. H. & BEAUDRY, G. A. 1997. SAGE transcript profiles for p53-dependent growth regulation. *Oncogene*, 15, 1079-85.

- MAILAND, N. & DIFFLEY, J. F. 2005. CDKs promote DNA replication origin licensing in human cells by protecting Cdc6 from APC/C-dependent proteolysis. *Cell*, 122, 915-26.
- MAKELA, T. P., TASSAN, J. P., NIGG, E. A., FRUTIGER, S., HUGHES, G. J. & WEINBERG, R. A. 1994. A cyclin associated with the CDK-activating kinase MO15. *Nature*, 371, 254-7.
- MAKI, C. G. & HOWLEY, P. M. 1997. Ubiquitination of p53 and p21 is differentially affected by ionizing and UV radiation. *Mol Cell Biol*, 17, 355-63.
- MANTOVANI, F., COLLAVIN, L. & DEL SAL, G. 2019. Mutant p53 as a guardian of the cancer cell. *Cell Death Differ*, 26, 199-212.
- MARECHAL, A. & ZOU, L. 2013. DNA damage sensing by the ATM and ATR kinases. *Cold Spring Harb Perspect Biol*, 5.
- MARTINERIE, L., MANTEROLA, M., CHUNG, S. S., PANIGRAHI, S. K., WEISBACH, M., VASILEVA, A., GENG, Y., SICINSKI, P. & WOLGEMUTH, D. J. 2014. Mammalian E-type cyclins control chromosome pairing, telomere stability and CDK2 localization in male meiosis. *PLoS Genet*, 10, e1004165.
- MARTINEZ-ZAPIEN, D., RUIZ, F. X., POIRSON, J., MITSCHLER, A., RAMIREZ, J., FORSTER, A., COUSIDO-SIAH, A., MASSON, M., VANDE POL, S., PODJARNY, A., TRAVE, G. & ZANIER, K. 2016. Structure of the E6/E6AP/p53 complex required for HPV-mediated degradation of p53. *Nature*, 529, 541-5.
- MATSON, J. P., DUMITRU, R., CORYELL, P., BAXLEY, R. M., CHEN, W., TWAROSKI, K., WEBBER, B. R., TOLAR, J., BIELINSKY, A. K., PURVIS, J. E. & COOK, J. G. 2017. Rapid DNA replication origin licensing protects stem cell pluripotency. *Elife*, 6.
- MATSUOKA, S., HUANG, M. & ELLEDGE, S. J. 1998. Linkage of ATM to cell cycle regulation by the Chk2 protein kinase. *Science*, 282, 1893-7.
- MATTHEWS, H. K., BERTOLI, C. & DE BRUIN, R. A. M. 2022. Cell cycle control in cancer. *Nat Rev Mol Cell Biol*, 23, 74-88.
- MAY, P. & MAY, E. 1999. Twenty years of p53 research: structural and functional aspects of the p53 protein. *Oncogene*, 18, 7621-36.
- MCGOWAN, C. H. & RUSSELL, P. 1993. Human Wee1 kinase inhibits cell division by phosphorylating p34cdc2 exclusively on Tyr15. *EMBO J*, 12, 75-85.
- MEI, L., KEDZIORA, K. M., SONG, E. A., PURVIS, J. E. & COOK, J. G. 2022. The consequences of differential origin licensing dynamics in distinct chromatin environments. *Nucleic Acids Res*, 50, 9601-9620.

- MEIER, A., FIEGLER, H., MUNOZ, P., ELLIS, P., RIGLER, D., LANGFORD, C., BLASCO, M. A., CARTER, N. & JACKSON, S. P. 2007. Spreading of mammalian DNA-damage response factors studied by ChIP-chip at damaged telomeres. *EMBO J*, 26, 2707-18.
- MENGHI, F., BARTHEL, F. P., YADAV, V., TANG, M., JI, B., TANG, Z., CARTER, G. W., RUAN, Y., SCULLY, R., VERHAAK, R. G. W., JONKERS, J. & LIU, E. T. 2018. The Tandem Duplicator Phenotype Is a Prevalent Genome-Wide Cancer Configuration Driven by Distinct Gene Mutations. *Cancer Cell*, 34, 197-210 e5.
- MIRON, K., GOLAN-LEV, T., DVIR, R., BEN-DAVID, E. & KEREM, B. 2015. Oncogenes create a unique landscape of fragile sites. *Nat Commun*, 6, 7094.
- MIRZA, A., WU, Q., WANG, L., MCCLANAHAN, T., BISHOP, W. R., GHEYAS, F., DING, W., HUTCHINS, B., HOCKENBERRY, T., KIRSCHMEIER, P., GREENE, J. R. & LIU, S. 2003. Global transcriptional program of p53 target genes during the process of apoptosis and cell cycle progression. *Oncogene*, 22, 3645-54.
- MOMAND, J., JUNG, D., WILCZYNSKI, S. & NILAND, J. 1998. The MDM2 gene amplification database. *Nucleic Acids Res*, 26, 3453-9.
- MOORE, J. D., YANG, J., TRUANT, R. & KORNBLUTH, S. 1999. Nuclear import of Cdk/cyclin complexes: identification of distinct mechanisms for import of Cdk2/cyclin E and Cdc2/cyclin B1. *J Cell Biol*, 144, 213-24.
- MUELLER, P. R., COLEMAN, T. R., KUMAGAI, A. & DUNPHY, W. G. 1995. Myt1: a membrane-associated inhibitory kinase that phosphorylates Cdc2 on both threonine-14 and tyrosine-15. *Science*, 270, 86-90.
- MULLINS, J. M. & BIESELE, J. J. 1977. Terminal phase of cytokinesis in D-98s cells. *J Cell Biol*, 73, 672-84.
- MUSSMAN, J. G., HORN, H. F., CARROLL, P. E., OKUDA, M., TARAPORE, P., DONEHOWER, L. A. & FUKASAWA, K. 2000. Synergistic induction of centrosome hyperamplification by loss of p53 and cyclin E overexpression. *Oncogene*, 19, 1635-46.
- MYERS, J. S. & CORTEZ, D. 2006. Rapid activation of ATR by ionizing radiation requires ATM and Mre11. *J Biol Chem*, 281, 9346-50.
- NARASIMHA, A. M., KAULICH, M., SHAPIRO, G. S., CHOI, Y. J., SICINSKI, P. & DOWDY, S. F. 2014. Cyclin D activates the Rb tumor suppressor by mono-phosphorylation. *Elife*, 3.
- NARITA, M., NARITA, M., KRIZHANOVSKY, V., NUNEZ, S., CHICAS, A., HEARN, S. A., MYERS, M. P. & LOWE, S. W. 2006. A novel role for high-mobility group a proteins in cellular senescence and heterochromatin formation. *Cell.* 126, 503-14.

- NARKAR, A., JOHNSON, B. A., BHARNE, P., ZHU, J., PADMANABAN, V., BISWAS, D., FRASER, A., IGLESIAS, P. A., EWALD, A. J. & LI, R. 2021. On the role of p53 in the cellular response to aneuploidy. *Cell Rep*, 34, 108892.
- NATERI, A. S., RIERA-SANS, L., DA COSTA, C. & BEHRENS, A. 2004. The ubiquitin ligase SCFFbw7 antagonizes apoptotic JNK signaling. *Science*, 303, 1374-8.
- NEGRINI, S., GORGOULIS, V. G. & HALAZONETIS, T. D. 2010. Genomic instability--an evolving hallmark of cancer. *Nat Rev Mol Cell Biol*, 11, 220-8.
- OHRT, T., MERKLE, D., BIRKENFELD, K., ECHEVERRI, C. J. & SCHWILLE, P. 2006. In situ fluorescence analysis demonstrates active siRNA exclusion from the nucleus by Exportin 5. *Nucleic Acids Res*, 34, 1369-80.
- OLIVIER, M., HOLLSTEIN, M. & HAINAUT, P. 2010. TP53 mutations in human cancers: origins, consequences, and clinical use. *Cold Spring Harb Perspect Biol*, 2, a001008.
- OREN, M. & LEVINE, A. J. 1983. Molecular cloning of a cDNA specific for the murine p53 cellular tumor antigen. *Proc Natl Acad Sci U S A*, 80, 56-9.
- OU, Y. H., CHUNG, P. H., SUN, T. P. & SHIEH, S. Y. 2005. p53 C-terminal phosphorylation by CHK1 and CHK2 participates in the regulation of DNA-damage-induced C-terminal acetylation. *Mol Biol Cell*, 16, 1684-95.
- OZENNE, P., EYMIN, B., BRAMBILLA, E. & GAZZERI, S. 2010. The ARF tumor suppressor: structure, functions and status in cancer. *Int J Cancer*, 127, 2239-47.
- PARISI, T., BECK, A. R., ROUGIER, N., MCNEIL, T., LUCIAN, L., WERB, Z. & AMATI, B. 2003. Cyclins E1 and E2 are required for endoreplication in placental trophoblast giant cells. *EMBO J*, 22, 4794-803.
- PARK, Y. B., PARK, M. J., KIMURA, K., SHIMIZU, K., LEE, S. H. & YOKOTA, J. 2002. Alterations in the INK4a/ARF locus and their effects on the growth of human osteosarcoma cell lines. *Cancer Genet Cytogenet*, 133, 105-11.
- PARKER, L. L. & PIWNICA-WORMS, H. 1992. Inactivation of the p34cdc2-cyclin B complex by the human WEE1 tyrosine kinase. *Science*, 257, 1955-7.
- PETERS, J. M. 2006. The anaphase promoting complex/cyclosome: a machine designed to destroy. *Nat Rev Mol Cell Biol*, 7, 644-56.

- PIETENPOL, J. A., TOKINO, T., THIAGALINGAM, S., EL-DEIRY, W. S., KINZLER, K. W. & VOGELSTEIN, B. 1994. Sequence-specific transcriptional activation is essential for growth suppression by p53. *Proc Natl Acad Sci U S A*, 91, 1998-2002.
- PINES, J. & HUNT, T. 1987. Molecular cloning and characterization of the mRNA for cyclin from sea urchin eggs. *EMBO J*, 6, 2987-95.
- PLUMMER, M., DE MARTEL, C., VIGNAT, J., FERLAY, J., BRAY, F. & FRANCESCHI, S. 2016. Global burden of cancers attributable to infections in 2012: a synthetic analysis. *Lancet Glob Health*, 4, e609-16.
- POMERANTZ, J., SCHREIBER-AGUS, N., LIEGEOIS, N. J., SILVERMAN, A., ALLAND, L., CHIN, L., POTES, J., CHEN, K., ORLOW, I., LEE, H. W., CORDON-CARDO, C. & DEPINHO, R. A. 1998. The Ink4a tumor suppressor gene product, p19Arf, interacts with MDM2 and neutralizes MDM2's inhibition of p53. *Cell*, 92, 713-23.
- QIAO, R., WEISSMANN, F., YAMAGUCHI, M., BROWN, N. G., VANDERLINDEN, R., IMRE, R., JARVIS, M. A., BRUNNER, M. R., DAVIDSON, I. F., LITOS, G., HASELBACH, D., MECHTLER, K., STARK, H., SCHULMAN, B. A. & PETERS, J. M. 2016. Mechanism of APC/CCDC20 activation by mitotic phosphorylation. *Proc Natl Acad Sci U S A*, 113, E2570-8.
- QUELLE, D. E., ZINDY, F., ASHMUN, R. A. & SHERR, C. J. 1995.
  Alternative reading frames of the INK4a tumor suppressor gene encode two unrelated proteins capable of inducing cell cycle arrest. *Cell*, 83, 993-1000.
- QUINTON, R. J., DIDOMIZIO, A., VITTORIA, M. A., KOTYNKOVA, K., TICAS, C. J., PATEL, S., KOGA, Y., VAKHSHOORZADEH, J., HERMANCE, N., KURODA, T. S., PARULEKAR, N., TAYLOR, A. M., MANNING, A. L., CAMPBELL, J. D. & GANEM, N. J. 2021. Wholegenome doubling confers unique genetic vulnerabilities on tumour cells. *Nature*, 590, 492-497.
- RADERSCHALL, E., GOLUB, E. I. & HAAF, T. 1999. Nuclear foci of mammalian recombination proteins are located at single-stranded DNA regions formed after DNA damage. *Proc Natl Acad Sci U S A*, 96, 1921-6.
- REID, B. J., BARRETT, M. T., GALIPEAU, P. C., SANCHEZ, C. A., NESHAT, K., COWAN, D. S. & LEVINE, D. S. 1996. Barrett's esophagus: ordering the events that lead to cancer. *Eur J Cancer Prev*, 5 Suppl 2, 57-65.
- RESNICK, M. A. & INGA, A. 2003. Functional mutants of the sequencespecific transcription factor p53 and implications for master genes of diversity. *Proc Natl Acad Sci U S A*, 100, 9934-9.

- RIEDER, C. L., COLE, R. W., KHODJAKOV, A. & SLUDER, G. 1995. The checkpoint delaying anaphase in response to chromosome monoorientation is mediated by an inhibitory signal produced by unattached kinetochores. *J Cell Biol*, 130, 941-8.
- RODRIGUEZ-MARTINEZ, M., HILLS, S. A., DIFFLEY, J. F. X. & SVEJSTRUP, J. Q. 2020. Multiplex Cell Fate Tracking by Flow Cytometry. *Methods Protoc*, 3.
- SAKAUE-SAWANO, A., KUROKAWA, H., MORIMURA, T., HANYU, A., HAMA, H., OSAWA, H., KASHIWAGI, S., FUKAMI, K., MIYATA, T., MIYOSHI, H., IMAMURA, T., OGAWA, M., MASAI, H. & MIYAWAKI, A. 2008. Visualizing spatiotemporal dynamics of multicellular cell-cycle progression. *Cell*, 132, 487-98.
- SAKAUE-SAWANO, A., YO, M., KOMATSU, N., HIRATSUKA, T., KOGURE, T., HOSHIDA, T., GOSHIMA, N., MATSUDA, M., MIYOSHI, H. & MIYAWAKI, A. 2017. Genetically Encoded Tools for Optical Dissection of the Mammalian Cell Cycle. *Mol Cell*, 68, 626-640 e5.
- SALDIVAR, J. C., CORTEZ, D. & CIMPRICH, K. A. 2017. The essential kinase ATR: ensuring faithful duplication of a challenging genome. *Nat Rev Mol Cell Biol*, 18, 622-636.
- SANIDAS, I., MORRIS, R., FELLA, K. A., RUMDE, P. H., BOUKHALI, M., TAI, E. C., TING, D. T., LAWRENCE, M. S., HAAS, W. & DYSON, N. J. 2019. A Code of Mono-phosphorylation Modulates the Function of RB. *Mol Cell*, 73, 985-1000 e6.
- SARNOW, P., HO, Y. S., WILLIAMS, J. & LEVINE, A. J. 1982. Adenovirus E1b-58kd tumor antigen and SV40 large tumor antigen are physically associated with the same 54 kd cellular protein in transformed cells. *Cell*, 28, 387-94.
- SATO, Y., SHIRATA, N., KUDOH, A., IWAHORI, S., NAKAYAMA, S., MURATA, T., ISOMURA, H., NISHIYAMA, Y. & TSURUMI, T. 2009. Expression of Epstein-Barr virus BZLF1 immediate-early protein induces p53 degradation independent of MDM2, leading to repression of p53-mediated transcription. *Virology*, 388, 204-11.
- SATYANARAYANA, A., HILTON, M. B. & KALDIS, P. 2008. p21 Inhibits Cdk1 in the absence of Cdk2 to maintain the G1/S phase DNA damage checkpoint. *Mol Biol Cell*, 19, 65-77.
- SAVIC, V., YIN, B., MAAS, N. L., BREDEMEYER, A. L., CARPENTER, A. C., HELMINK, B. A., YANG-IOTT, K. S., SLECKMAN, B. P. & BASSING, C. H. 2009. Formation of dynamic gamma-H2AX domains along broken DNA strands is distinctly regulated by ATM and MDC1 and dependent upon H2AX densities in chromatin. *Mol Cell*, 34, 298-310.

- SAVITSKY, K., BAR-SHIRA, A., GILAD, S., ROTMAN, G., ZIV, Y., VANAGAITE, L., TAGLE, D. A., SMITH, S., UZIEL, T., SFEZ, S., ASHKENAZI, M., PECKER, I., FRYDMAN, M., HARNIK, R., PATANJALI, S. R., SIMMONS, A., CLINES, G. A., SARTIEL, A., GATTI, R. A., CHESSA, L., SANAL, O., LAVIN, M. F., JASPERS, N. G., TAYLOR, A. M., ARLETT, C. F., MIKI, T., WEISSMAN, S. M., LOVETT, M., COLLINS, F. S. & SHILOH, Y. 1995. A single ataxia telangiectasia gene with a product similar to PI-3 kinase. *Science*, 268, 1749-53.
- SCALTRITI, M., EICHHORN, P. J., CORTÉS, J., PRUDKIN, L., AURA, C., JIMÉNEZ, J., CHANDARLAPATY, S., SERRA, V., PRAT, A., IBRAHIM, Y. H., GUZMÁN, M., GILI, M., RODRÍGUEZ, O., RODRÍGUEZ, S., PÉREZ, J., GREEN, S. R., MAI, S., ROSEN, N., HUDIS, C. & BASELGA, J. 2011. Cyclin E amplification/overexpression is a mechanism of trastuzumab resistance in HER2

breast cancer patients. *Proceedings of the National Academy of Sciences*, 108, 3761-3766.

- SCHLERETH, K., BEINORAVICIUTE-KELLNER, R., ZEITLINGER, M. K., BRETZ, A. C., SAUER, M., CHARLES, J. P., VOGIATZI, F., LEICH, E., SAMANS, B., EILERS, M., KISKER, C., ROSENWALD, A. & STIEWE, T. 2010. DNA binding cooperativity of p53 modulates the decision between cell-cycle arrest and apoptosis. *Mol Cell*, 38, 356-68.
- SERRANO, M., LIN, A. W., MCCURRACH, M. E., BEACH, D. & LOWE, S. W. 1997. Oncogenic ras provokes premature cell senescence associated with accumulation of p53 and p16INK4a. *Cell*, 88, 593-602.
- SHARPLESS, N. E. 2005. INK4a/ARF: a multifunctional tumor suppressor locus. *Mutat Res*, 576, 22-38.
- SHEAFF, R. J., GROUDINE, M., GORDON, M., ROBERTS, J. M. & CLURMAN, B. E. 1997. Cyclin E-CDK2 is a regulator of p27Kip1. *Genes Dev*, 11, 1464-78.
- SHELTON, D. N., CHANG, E., WHITTIER, P. S., CHOI, D. & FUNK, W. D. 1999. Microarray analysis of replicative senescence. *Curr Biol*, 9, 939-45.
- SHEN, H., MORAN, D. M. & MAKI, C. G. 2008. Transient nutlin-3a treatment promotes endoreduplication and the generation of therapy-resistant tetraploid cells. *Cancer Res*, 68, 8260-8.
- SHEPPARD, H. M., CORNEILLIE, S. I., ESPIRITU, C., GATTI, A. & LIU, X. 1999. New insights into the mechanism of inhibition of p53 by simian virus 40 large T antigen. *Mol Cell Biol*, 19, 2746-53.

- SHERR, C. J. & WEBER, J. D. 2000. The ARF/p53 pathway. *Curr Opin Genet Dev*, 10, 94-9.
- SHIEH, S. Y., IKEDA, M., TAYA, Y. & PRIVES, C. 1997. DNA damage-induced phosphorylation of p53 alleviates inhibition by MDM2. *Cell*, 91, 325-34.
- SIGAL, A. & ROTTER, V. 2000. Oncogenic mutations of the p53 tumor suppressor: the demons of the guardian of the genome. *Cancer Res*, 60, 6788-93.
- SILICIANO, J. D., CANMAN, C. E., TAYA, Y., SAKAGUCHI, K., APPELLA, E. & KASTAN, M. B. 1997. DNA damage induces phosphorylation of the amino terminus of p53. *Genes Dev,* 11, 3471-81.
- SINGER, J. D., GURIAN-WEST, M., CLURMAN, B. & ROBERTS, J. M. 1999. Cullin-3 targets cyclin E for ubiquitination and controls S phase in mammalian cells. *Genes Dev*, 13, 2375-87.
- SIU, K. T., ROSNER, M. R. & MINELLA, A. C. 2012. An integrated view of cyclin E function and regulation. *Cell Cycle*, 11, 57-64.
- SKOTHEIM, J. M., DI TALIA, S., SIGGIA, E. D. & CROSS, F. R. 2008. Positive feedback of G1 cyclins ensures coherent cell cycle entry. *Nature*, 454, 291-6.
- SMITS, V. A., KLOMPMAKER, R., VALLENIUS, T., RIJKSEN, G., MAKELA, T. P. & MEDEMA, R. H. 2000. p21 inhibits Thr161 phosphorylation of Cdc2 to enforce the G2 DNA damage checkpoint. *J Biol Chem*, 275, 30638-43.
- SMITS, V. A. & MEDEMA, R. H. 2001. Checking out the G(2)/M transition. *Biochim Biophys Acta*, 1519, 1-12.
- SORENSEN, C. S., SYLJUASEN, R. G., FALCK, J., SCHROEDER, T., RONNSTRAND, L., KHANNA, K. K., ZHOU, B. B., BARTEK, J. & LUKAS, J. 2003. Chk1 regulates the S phase checkpoint by coupling the physiological turnover and ionizing radiation-induced accelerated proteolysis of Cdc25A. *Cancer Cell*, 3, 247-58.
- SOTILLO, R., HERNANDO, E., DIAZ-RODRIGUEZ, E., TERUYA-FELDSTEIN, J., CORDON-CARDO, C., LOWE, S. W. & BENEZRA, R. 2007. Mad2 overexpression promotes aneuploidy and tumorigenesis in mice. *Cancer Cell*, 11, 9-23.
- SOTO, M., RAAIJMAKERS, J. A., BAKKER, B., SPIERINGS, D. C. J., LANSDORP, P. M., FOIJER, F. & MEDEMA, R. H. 2017. p53 Prohibits Propagation of Chromosome Segregation Errors that Produce Structural Aneuploidies. *Cell Rep*, 19, 2423-2431.
- SOUSSI, T. & MAY, P. 1996. Structural aspects of the p53 protein in relation to gene evolution: a second look. *J Mol Biol.* 260, 623-37.

- SOUSSI, T. & WIMAN, K. G. 2015. TP53: an oncogene in disguise. *Cell Death & Differentiation*, 22, 1239-1249.
- SPENCER, S. L., CAPPELL, S. D., TSAI, F. C., OVERTON, K. W., WANG, C. L. & MEYER, T. 2013. The proliferation-quiescence decision is controlled by a bifurcation in CDK2 activity at mitotic exit. *Cell*, 155, 369-83.
- SPRUCK, C. H., STROHMAIER, H., SANGFELT, O., MULLER, H. M., HUBALEK, M., MULLER-HOLZNER, E., MARTH, C., WIDSCHWENDTER, M. & REED, S. I. 2002. hCDC4 gene mutations in endometrial cancer. *Cancer Res*, 62, 4535-9.
- SPRUCK, C. H., WON, K. A. & REED, S. I. 1999. Deregulated cyclin E induces chromosome instability. *Nature*, 401, 297-300.
- STAGNO D'ALCONTRES, M., MENDEZ-BERMUDEZ, A., FOXON, J. L., ROYLE, N. J. & SALOMONI, P. 2007. Lack of TRF2 in ALT cells causes PML-dependent p53 activation and loss of telomeric DNA. *J Cell Biol*, 179, 855-67.
- STEIN, G. H., DRULLINGER, L. F., SOULARD, A. & DULIC, V. 1999.

  Differential roles for cyclin-dependent kinase inhibitors p21 and p16 in the mechanisms of senescence and differentiation in human fibroblasts. *Mol Cell Biol*, 19, 2109-17.
- STOTT, F. J., BATES, S., JAMES, M. C., MCCONNELL, B. B., STARBORG, M., BROOKES, S., PALMERO, I., RYAN, K., HARA, E., VOUSDEN, K. H. & PETERS, G. 1998. The alternative product from the human CDKN2A locus, p14(ARF), participates in a regulatory feedback loop with p53 and MDM2. *EMBO J*, 17, 5001-14.
- STROHMAIER, H., SPRUCK, C. H., KAISER, P., WON, K. A., SANGFELT, O. & REED, S. I. 2001. Human F-box protein hCdc4 targets cyclin E for proteolysis and is mutated in a breast cancer cell line. *Nature*, 413, 316-22.
- SUNG, H., FERLAY, J., SIEGEL, R. L., LAVERSANNE, M., SOERJOMATARAM, I., JEMAL, A. & BRAY, F. 2021. Global Cancer Statistics 2020: GLOBOCAN Estimates of Incidence and Mortality Worldwide for 36 Cancers in 185 Countries. *CA Cancer J Clin*, 71, 209-249.
- TADA, S., LI, A., MAIORANO, D., MECHALI, M. & BLOW, J. J. 2001.

  Repression of origin assembly in metaphase depends on inhibition of RLF-B/Cdt1 by geminin. *Nat Cell Biol*, 3, 107-13.
- TANAKA, S. & DIFFLEY, J. F. 2002. Deregulated G1-cyclin expression induces genomic instability by preventing efficient pre-RC formation. *Genes Dev*, 16, 2639-49.

- TAYLOR, A. M., METCALFE, J. A., OXFORD, J. M. & HARNDEN, D. G. 1976. Is chromatid-type damage in ataxia telangiectasia after irradiation at G0 a consequence of defective repair? *Nature*, 260, 441-3.
- TAYLOR, A. M., SHIH, J., HA, G., GAO, G. F., ZHANG, X., BERGER, A. C., SCHUMACHER, S. E., WANG, C., HU, H., LIU, J., LAZAR, A. J., CANCER GENOME ATLAS RESEARCH, N., CHERNIACK, A. D., BEROUKHIM, R. & MEYERSON, M. 2018. Genomic and Functional Approaches to Understanding Cancer Aneuploidy. *Cancer Cell*, 33, 676-689 e3.
- TAYLOR, W. R. & STARK, G. R. 2001. Regulation of the G2/M transition by p53. *Oncogene*, 20, 1803-15.
- TEIXEIRA, L. K., WANG, X., LI, Y., EKHOLM-REED, S., WU, X., WANG, P. & REED, S. I. 2015. Cyclin E deregulation promotes loss of specific genomic regions. *Curr Biol*, 25, 1327-33.
- THOMPSON, S. L., BAKHOUM, S. F. & COMPTON, D. A. 2010. Mechanisms of chromosomal instability. *Curr Biol*, 20, R285-95.
- THOMPSON, S. L. & COMPTON, D. A. 2008. Examining the link between chromosomal instability and aneuploidy in human cells. *J Cell Biol*, 180, 665-72.
- TIBBETTS, R. S., BRUMBAUGH, K. M., WILLIAMS, J. M., SARKARIA, J. N., CLIBY, W. A., SHIEH, S. Y., TAYA, Y., PRIVES, C. & ABRAHAM, R. T. 1999. A role for ATR in the DNA damage-induced phosphorylation of p53. *Genes Dev*, 13, 152-7.
- TINEVEZ, J. Y., PERRY, N., SCHINDELIN, J., HOOPES, G. M., REYNOLDS, G. D., LAPLANTINE, E., BEDNAREK, S. Y., SHORTE, S. L. & ELICEIRI, K. W. 2017. TrackMate: An open and extensible platform for single-particle tracking. *Methods*, 115, 80-90.
- TORNESELLO, M. L., ANNUNZIATA, C., TORNESELLO, A. L., BUONAGURO, L. & BUONAGURO, F. M. 2018. Human Oncoviruses and p53 Tumor Suppressor Pathway Deregulation at the Origin of Human Cancers. *Cancers (Basel)*, 10.
- UHLMANN, F., LOTTSPEICH, F. & NASMYTH, K. 1999. Sister-chromatid separation at anaphase onset is promoted by cleavage of the cohesin subunit Scc1. *Nature*, 400, 37-42.
- UZIEL, T., LERENTHAL, Y., MOYAL, L., ANDEGEKO, Y., MITTELMAN, L. & SHILOH, Y. 2003. Requirement of the MRN complex for ATM activation by DNA damage. *EMBO J*, 22, 5612-21.
- VASSILEV, L. T. 2006. Cell cycle synchronization at the G2/M phase border by reversible inhibition of CDK1. *Cell Cycle*, 5, 2555-6.

- VERFAILLIE, A., SVETLICHNYY, D., IMRICHOVA, H., DAVIE, K., FIERS, M., KALENDER ATAK, Z., HULSELMANS, G., CHRISTIAENS, V. & AERTS, S. 2016. Multiplex enhancer-reporter assays uncover unsophisticated TP53 enhancer logic. *Genome Res*, 26, 882-95.
- VIJAYAKUMARAN, R., TAN, K. H., MIRANDA, P. J., HAUPT, S. & HAUPT, Y. 2015. Regulation of Mutant p53 Protein Expression. *Front Oncol*, 5, 284.
- VOUSDEN, K. H. & LU, X. 2002. Live or let die: the cell's response to p53. Nat Rev Cancer, 2, 594-604.
- WALKER, J. R., CORPINA, R. A. & GOLDBERG, J. 2001. Structure of the Ku heterodimer bound to DNA and its implications for double-strand break repair. *Nature*, 412, 607-14.
- WANG, X. W., ZHAN, Q., COURSEN, J. D., KHAN, M. A., KONTNY, H. U., YU, L., HOLLANDER, M. C., O'CONNOR, P. M., FORNACE, A. J., JR. & HARRIS, C. C. 1999. GADD45 induction of a G2/M cell cycle checkpoint. *Proc Natl Acad Sci U S A*, 96, 3706-11.
- WEE, P. & WANG, Z. 2017. Epidermal Growth Factor Receptor Cell Proliferation Signaling Pathways. *Cancers (Basel)*, 9.
- WEI, C. L., WU, Q., VEGA, V. B., CHIU, K. P., NG, P., ZHANG, T., SHAHAB, A., YONG, H. C., FU, Y., WENG, Z., LIU, J., ZHAO, X. D., CHEW, J. L., LEE, Y. L., KUZNETSOV, V. A., SUNG, W. K., MILLER, L. D., LIM, B., LIU, E. T., YU, Q., NG, H. H. & RUAN, Y. 2006. A global map of p53 transcription-factor binding sites in the human genome. *Cell*, 124, 207-19.
- WELCKER, M. & CLURMAN, B. E. 2008. FBW7 ubiquitin ligase: a tumour suppressor at the crossroads of cell division, growth and differentiation. *Nat Rev Cancer*, 8, 83-93.
- WELCKER, M., SINGER, J., LOEB, K. R., GRIM, J., BLOECHER, A., GURIEN-WEST, M., CLURMAN, B. E. & ROBERTS, J. M. 2003. Multisite phosphorylation by Cdk2 and GSK3 controls cyclin E degradation. *Mol Cell*, 12, 381-92.
- WOHLSCHLEGEL, J. A., DWYER, B. T., DHAR, S. K., CVETIC, C., WALTER, J. C. & DUTTA, A. 2000. Inhibition of eukaryotic DNA replication by geminin binding to Cdt1. *Science*, 290, 2309-12.
- WOLF, D., HARRIS, N. & ROTTER, V. 1984. Reconstitution of p53 expression in a nonproducer Ab-MuLV-transformed cell line by transfection of a functional p53 gene. *Cell*, 38, 119-26.
- YADA, M., HATAKEYAMA, S., KAMURA, T., NISHIYAMA, M., TSUNEMATSU, R., IMAKI, H., ISHIDA, N., OKUMURA, F., NAKAYAMA, K. & NAKAYAMA, K. I. 2004. Phosphorylation-

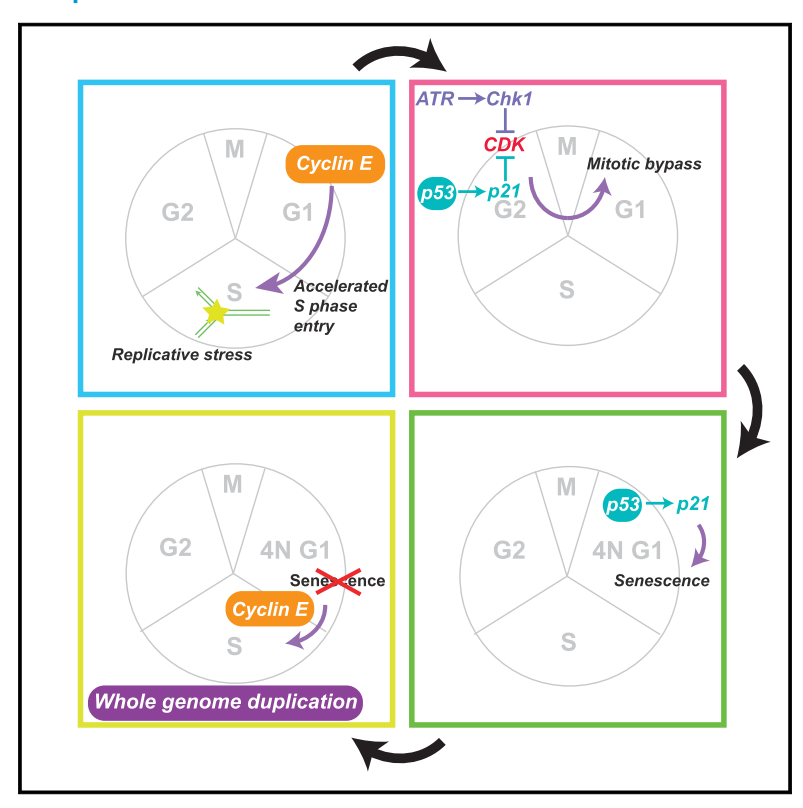
- dependent degradation of c-Myc is mediated by the F-box protein Fbw7. *EMBO J*, 23, 2116-25.
- YANG, X., YU, K., HAO, Y., LI, D. M., STEWART, R., INSOGNA, K. L. & XU, T. 2004. LATS1 tumour suppressor affects cytokinesis by inhibiting LIMK1. *Nat Cell Biol*, 6, 609-17.
- YEH, C. H., BELLON, M. & NICOT, C. 2018. FBXW7: a critical tumor suppressor of human cancers. *Mol Cancer*, 17, 115.
- YOSHIDA, A. & DIEHL, J. A. 2015. CDK4/6 inhibitor: from quiescence to senescence. *Oncoscience*, 2, 896-7.
- ZACHARIAE, W., SCHWAB, M., NASMYTH, K. & SEUFERT, W. 1998. Control of cyclin ubiquitination by CDK-regulated binding of Hct1 to the anaphase promoting complex. *Science*, 282, 1721-4.
- ZACK, T. I., SCHUMACHER, S. E., CARTER, S. L., CHERNIACK, A. D., SAKSENA, G., TABAK, B., LAWRENCE, M. S., ZHSNG, C. Z., WALA, J., MERMEL, C. H., SOUGNEZ, C., GABRIEL, S. B., HERNANDEZ, B., SHEN, H., LAIRD, P. W., GETZ, G., MEYERSON, M. & BEROUKHIM, R. 2013. Pan-cancer patterns of somatic copy number alteration. *Nat Genet*, 45, 1134-40.
- ZANE, L., YASUNAGA, J., MITAGAMI, Y., YEDAVALLI, V., TANG, S. W., CHEN, C. Y., RATNER, L., LU, X. & JEANG, K. T. 2012. Wip1 and p53 contribute to HTLV-1 Tax-induced tumorigenesis. *Retrovirology*, 9, 114.
- ZENG, J., HILLS, S. A., OZONO, E. & DIFFLEY, J. F. X. 2023. Cyclin E-induced replicative stress drives p53-dependent whole-genome duplication. *Cell*, 186, 528-542.e14.
- ZHAN, Q., ANTINORE, M. J., WANG, X. W., CARRIER, F., SMITH, M. L., HARRIS, C. C. & FORNACE, A. J., JR. 1999. Association with Cdc2 and inhibition of Cdc2/Cyclin B1 kinase activity by the p53-regulated protein Gadd45. *Oncogene*, 18, 2892-900.
- ZHANG, J. M. & ZOU, L. 2020. Alternative lengthening of telomeres: from molecular mechanisms to therapeutic outlooks. *Cell Biosci*, 10, 30.
- ZHANG, N., GE, G., MEYER, R., SETHI, S., BASU, D., PRADHAN, S., ZHAO, Y. J., LI, X. N., CAI, W. W., EL-NAGGAR, A. K., BALADANDAYUTHAPANI, V., KITTRELL, F. S., RAO, P. H., MEDINA, D. & PATI, D. 2008. Overexpression of Separase induces aneuploidy and mammary tumorigenesis. *Proc Natl Acad Sci U S A*, 105, 13033-8.
- ZHAO, H. & PIWNICA-WORMS, H. 2001. ATR-mediated checkpoint pathways regulate phosphorylation and activation of human Chk1. *Mol Cell Biol*, 21, 4129-39.

- ZHAO, H., WATKINS, J. L. & PIWNICA-WORMS, H. 2002. Disruption of the checkpoint kinase 1/cell division cycle 25A pathway abrogates ionizing radiation-induced S and G2 checkpoints. *Proc Natl Acad Sci U S A*, 99, 14795-800.
- ZIELKE, N., EDGAR, B. A. & DEPAMPHILIS, M. L. 2013. Endoreplication. *Cold Spring Harb Perspect Biol*, 5, a012948.
- ZOU, L. & ELLEDGE, S. J. 2003. Sensing DNA damage through ATRIP recognition of RPA-ssDNA complexes. *Science*, 300, 1542-8.



## Cyclin E-induced replicative stress drives p53dependent whole-genome duplication

## **Graphical abstract**



## **Authors**

Jingkun Zeng, Stephanie A. Hills, Eiko Ozono, John F.X. Diffley

## Correspondence

john.diffley@crick.ac.uk

## In brief

DNA replication stress-induced wholegenome duplication (WGD) requires p53 function, in contrast to WGD induced by DNA damage; these findings provide mechanistic insight into cancer genome evolution in p53<sup>+/+</sup> tumors.

## **Highlights**

- Replicative stress from elevated cyclin E drives p53dependent mitotic bypass
- p53, via p21, promotes mitotic bypass by inhibiting cyclindependent kinase
- Elevated cyclin E drives p53<sup>+/+</sup> G1-arrested cells to complete endoreduplication
- Cyclin E can therefore drive WGD in p53-proficient cells









## **Article**

# Cyclin E-induced replicative stress drives p53-dependent whole-genome duplication

Jingkun Zeng,<sup>1,2</sup> Stephanie A. Hills,<sup>1,2</sup> Eiko Ozono,<sup>1</sup> and John F.X. Diffley<sup>1,3,\*</sup>

<sup>1</sup>Chromosome Replication Laboratory, The Francis Crick Institute, London NW1 1AT, UK

\*Correspondence: john.diffley@crick.ac.uk https://doi.org/10.1016/j.cell.2022.12.036

## **SUMMARY**

Whole-genome duplication (WGD) is a frequent event in cancer evolution and an important driver of aneuploidy. The role of the p53 tumor suppressor in WGD has been enigmatic: p53 can block the proliferation of tetraploid cells, acting as a barrier to WGD, but can also promote mitotic bypass, a key step in WGD via endoreduplication. In wild-type (WT) p53 tumors, WGD is frequently associated with activation of the E2F pathway, especially amplification of *CCNE1*, encoding cyclin E1. Here, we show that elevated cyclin E1 expression causes replicative stress, which activates ATR- and Chk1-dependent G2 phase arrest. p53, via its downstream target p21, together with Wee1, then inhibits mitotic cyclin-dependent kinase activity sufficiently to activate APC/C<sup>Cdh1</sup> and promote mitotic bypass. Cyclin E expression suppresses p53-dependent senescence after mitotic bypass, allowing cells to complete endoreduplication. Our results indicate that p53 can contribute to cancer evolution through the promotion of WGD.

## **INTRODUCTION**

Almost 90% of human cancers exhibit aneuploidy. In many cancers, small numbers of chromosomes are gained or lost as a result of the mis-segregation of individual chromosomes in mitosis. However, in many other cancers, chromosome numbers are much higher, and their karyotypes are often described as being hypertriploid or sub-tetraploid. Such extensive aneuploidies are likely generated from a tetraploid intermediate. Approximately 30%–40% of human tumors have undergone whole-genome duplication (WGD) during their history, making it one of the most common single genomic events in oncogenesis, and WGD is generally associated with poor prognosis. Thus, understanding the causes and consequences of WGD is important for cancer biology.

WGD can occur by a variety of mechanisms. Cell-cell fusion can be induced by viruses including human papilloma virus (HPV), the causative agent of most cervical cancers. Failing to complete or exit mitosis (mitotic slippage) or defects in cytokinesis can also lead to WGD. Telomere attrition or persistent double-strand DNA breaks can promote WGD by mitotic bypass and endoreduplication. The relative importance of each of these pathways in different cancers is still largely unknown.

The tumor suppressor p53 protects cells from WGD by preventing the cell-cycle progression of G1 cells with a 4N DNA content. How this "tetraploid checkpoint" works is unknown, <sup>10</sup> but it can be activated by mitotic slippage, cytokinesis blockage, and endoreduplication; moreover, WGD via endoreduplication after

telomere attrition occurs only in cells lacking p53. One might, therefore, expect the loss of p53 to be essential for WGD to occur; however, large-scale genomics studies have shown that approximately half of the WGD events in cancer happen with wild-type (WT) p53 background. Also, p53 has been shown to promote mitotic bypass after genotoxic or oncogene stress. Although this generates tetraploid cells, these cells are senescent and therefore do not proliferate. How WGD happens in p53 proficient cells is still unclear. Deregulation of the E2F pathway is relatively common in p53-proficient tumors with WGD ( $\sim$ 32%), especially amplification of the gene encoding cyclin E1 (CCNE1), suggesting a causal connection.

Replicative stress is an early event in oncogenesis, resulting in the activation of DNA damage checkpoints after the acquisition of early cancer driver mutations. <sup>13,14</sup> Among these drivers, deregulation of the E2F pathway, for example, by cyclin E expression, has been shown to induce replicative stress. <sup>14–18</sup> The relationship between oncogene-induced replicative stress and WGD has not been explored. In this paper, we show how cyclin E can promote WGD in p53-proficient cells and how p53 can contribute to the generation of WGD.

## **RESULTS**

# Cyclin E expression induces WGD by mitotic bypass in U2OS cells

To study the consequences of elevated cyclin E levels, we established a U2OS cell line expressing doxycycline-inducible

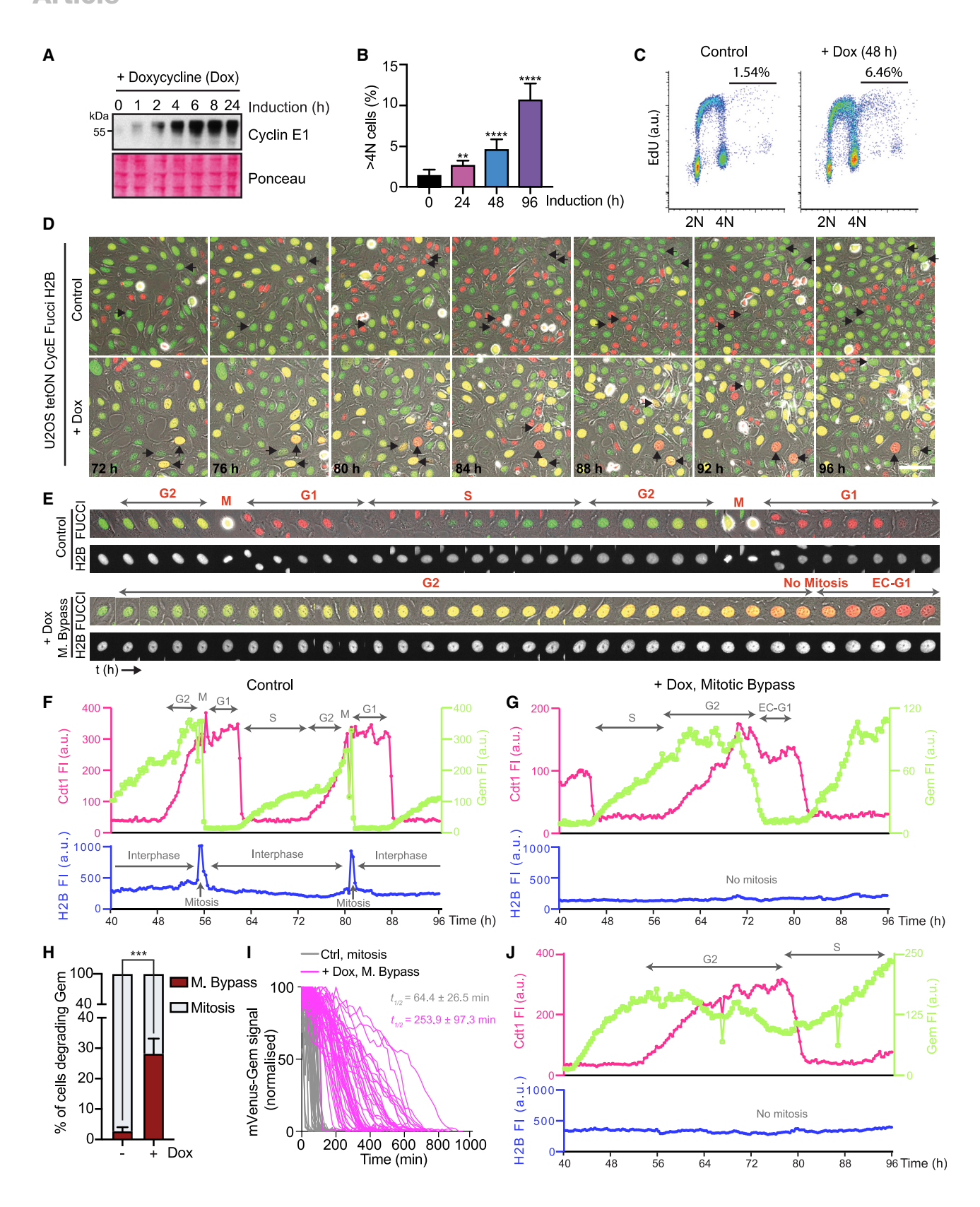


<sup>&</sup>lt;sup>2</sup>These authors contributed equally

<sup>3</sup>Lead contact

## Cell Article





(legend on next page)





("tetON") full-length cyclin E1 (Figure 1A). U2OS is an osteosarcoma-derived cell line commonly used in DNA damage studies. Cyclin E expression in this cell line was somewhat faster than in a previously described "tetOFF" U2OS cell line expressing a cyclin E truncation (Figure S1A), 14 but both cell lines express cyclin E to comparable levels (Figure S1A), which has previously been shown to be similar to levels seen in breast cancer cell lines containing increased copies of CCNE1.14 It was previously shown that a proportion of cells became >4N when expressing cyclin E, 14 which was ascribed to partial genome re-replication. We confirmed this observation (Figures 1B and S1B), but by examining EdU incorporation (Figure 1C), we found that discrete G1, S, and G2 phases could be delineated at and above the 4N DNA content, apparently leading to complete replication. Therefore, these cells are undergoing a full cell cycle starting from a 4N DNA content, indicating that cyclin E expression can induce WGD. As an alternative approach to increasing cyclin E levels, we knocked down the FBXW7 (F box and WD repeat domaincontaining 7) tumor suppressor that is required for cyclin E degradation and is frequently lost in cancer. 19 We found that depletion of FBXW7 led to an increase in cyclin E expression, as well as to a small increase in c-Myc but not c-Jun or JunB expression (Figures S1C and S1D). Over a slightly longer time frame, FBXW7-depleted cells also underwent WGD (Figure S1E), indicating that even a moderate increase in cyclin E expression can also induce WGD.

To determine how WGD was generated following cyclin E expression, we used fluorescent ubiquitination-based cell-cycle indicator (FUCCI) live-cell imaging.<sup>20</sup> In cells expressing fluorescently tagged, truncated versions of Cdt1 and geminin,<sup>21</sup> one can distinguish G1 (high mCherry-Cdt1), S (high mVenus-Gem), and G2 (high mCherry-Cdt1 and high mVenus-Gem) phases of the cell cycle (Figure S1F). We also introduced the mTurquoise-H2B protein, which generates robust fluorescence throughout the cell cycle; this allows us to identify mitotic cells and enables better automated single-cell tracking. Control cells not expressing cyclin E entered and exited mitosis, as evidenced by the spike of mTurquoise-H2B fluorescence from chromosome condensation and by the rapid degradation of mVenus-Gem (Figures 1D-1F; Video S1). We saw no evidence of cell fusion, mitotic slippage, or cytokinesis defects in cyclin E-expressing cells. However, in roughly one-third of cyclin E-expressing cells, mVenus-Gem degradation occurred without mitosis (Figures 1D, 1E, 1G, and 1H; Video S1). In these cells, there was no evidence of chromosome condensation (mTurquoise-H2B spike) and no evidence of nuclear envelope breakdown (dispersal or leakage of the FUCCI markers from the nucleus), indicating that they transited directly from G2 to G1 phase. We call this G1 phase after mitotic bypass endoreduplication cycle G1 (EC-G1) (Figure 1G) to distinguish it from normal G1 phase. After a period of EC-G1, most cells then entered S phase, as seen by the degradation of mCherry-Cdt1 (Figure 1G). Taken together, these results indicate that cyclin E expression induces WGD via mitotic bypass and endoreduplication.

In contrast to the rapid mVenus-Gem degradation in mitosis of control cells (Figures 1F and 1I), mVenus-Gem degradation was much slower during mitotic bypass (Figures 1G and 1I): the half-time ( $t_{1/2}$ ) of degradation was 253.9  $\pm$  97.3 min (median = 232.5 min) during mitotic bypass, roughly 4 times longer than control mitosis (64.4  $\pm$  26.5 min mean  $t_{1/2}$ , 71.6 min median  $t_{1/2}$ ). We found that there was also great variability in the length of time it took to degrade mVenus-Gem, ranging from  $\sim$ 2 to  $\sim$ 8 h (Figure 1I). Additionally, we saw many aberrant events, for example, where mVenus-Gem degradation either did not begin (Figure S1G) or began but did not go to completion (Figure 1J) before cells entered S phase (mCherry-Cdt1 degradation) (Figures 1J, S1G, and S1H). Thus, in contrast to normal mitosis, mitotic bypass is highly variable in length and often aberrant

In mitotic cell cycles, two activators of the anaphase-promoting complex/cyclosome (APC/C)—Cdc20 and Cdh1—act sequentially in mitosis and G1, respectively, <sup>22</sup> to degrade important cell-cycle substrates including geminin and cyclin B. In mitotic cell-cycle progression, Cdc20 is essential while Cdh1 plays a relatively minor role, but in endoreduplication cell cycles, including those generated by double-strand breaks (DSBs) or eroded telomeres, Cdh1 is crucial. <sup>9</sup> Consistent with this, we found that depleting Cdh1 significantly reduced WGD in cyclin E-expressing cells (Figure S1I).

## The DNA damage checkpoint is required for WGD

Cyclin E expression caused cells to accumulate in G2 phase over time, with an increase in cyclin B-positive cells (a marker of G2) (Figures 2A and S2A). In these cells, we saw increases in DNA damage markers (phospho-Chk1, phospho-p53, and phospho-RPA), increased inhibitory phosphorylation of the mitotic cyclin-dependent kinases 1 (CDK1) (Figure 2B), and a reduction in the proportion of G2 cells entering mitosis (Figure 2C black bars).

## Figure 1. Cyclin ${\bf E}$ expression induces endoreduplication in U2OS cells

(A) Immunoblots showing cyclin E1 (CycE) expression by doxycycline (Dox) treatment in U2OS tetON CycE cell line.

(B) Quantification of cells with >4N DNA content following cyclin E induction over 96 h in U2OS, measured in % of total cells. Mean and standard deviations (SD) are shown (n = 3). Statistical significance: \*\*p < 0.005 and \*\*\*\*p < 0.0001, unpaired t test.

(C) FACS analysis of U2OS cells incorporating EdU after cyclin E induction.

(D and E) Time-lapse imaging of U2OS cells expressing cyclin E. FUCCI and phase contrast images were merged. Selected still images are shown in (D) (see also Video S1). Black arrows of the same direction indicate individual tracked cells and their daughter cells. Tracking of example cells is shown in (E). Scale bars, 100 μm.

(F and G) Temporal profiles of fluorescence intensities (FI) of mCherry-cdt1 and mVenus-Gem of cells. a.u., arbitrary unit.

(H) Quantification of mitotic bypass, measured in % of cells that degraded geminin (% of cells completing S/G2). Mean and SDs were shown (n = 3), with >400 cells for each condition analyzed. Statistical significance: \*\*\*p < 0.001, unpaired t test.

(I) Normalized time-course degradation of mVenus-Gem. Each line represents a single-cell tracking (n > 50 for each condition). Mean half-life  $(t_{1/2})$  with SDs are shown in the figure and main text.

(J) Temporal profiles of a cyclin E-expressing U2OS cell that degraded mCherry-Cdt1 while maintaining high levels of mVenus-Gem.



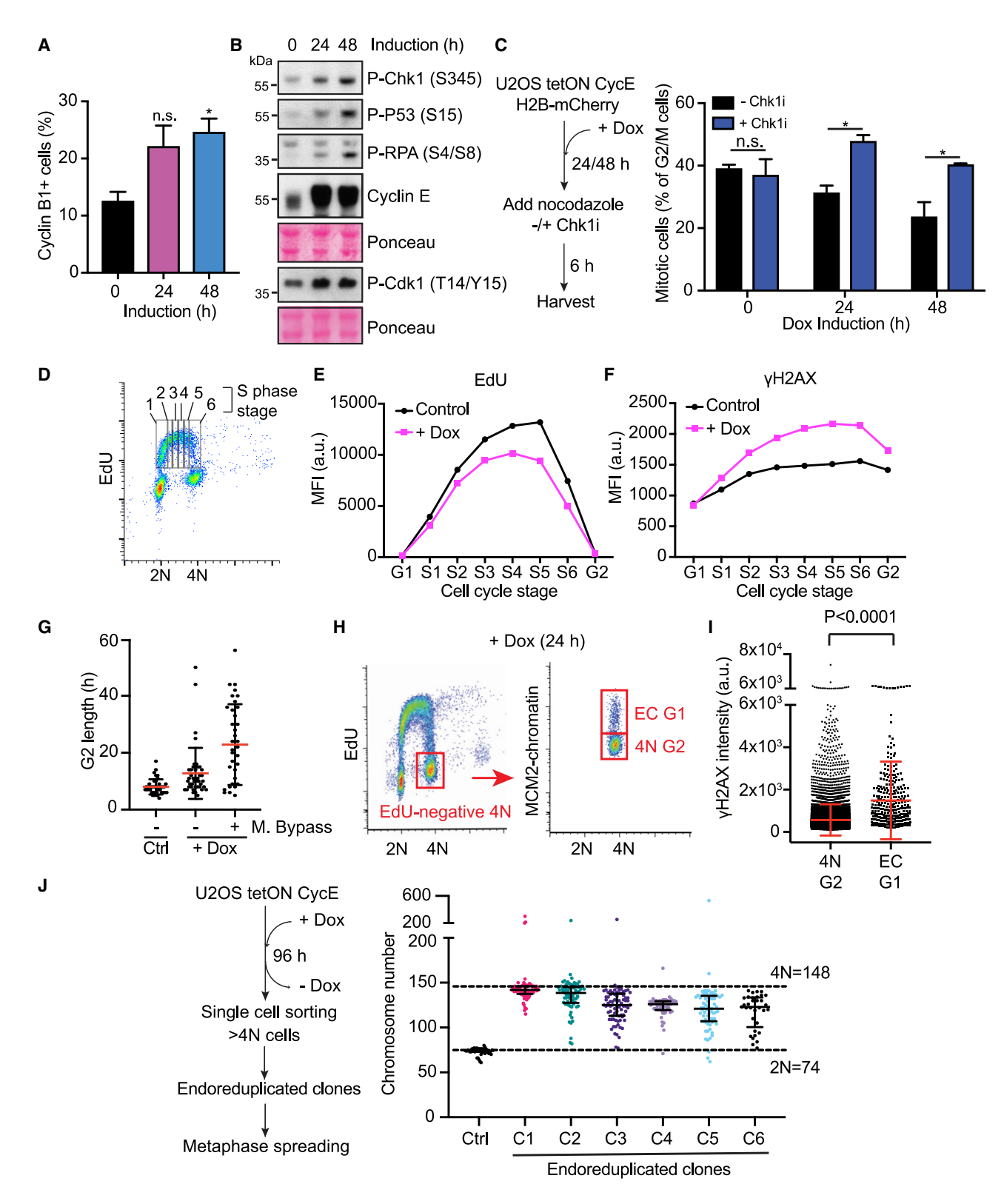


Figure 2. Replicative stress in cyclin E-expressing cells

(A) Quantification of U2OS cells positive for cyclin B1 following cyclin E induction by FACS analysis. Mean and range are shown (n = 2). Statistical significance (\*p < 0.05; n.s., non-significant) was examined by unpaired t test.

(B) Immunoblots showing DNA damage markers after cyclin E induction in U2OS cells.





This is all consistent with previous work showing that cyclin E expression causes replicative stress. 14-18,23,24 Cyclin E expression accelerates passage through G1 phase, causing cells to enter S phase prematurely (Figures S2B-S2D), before completion of the origin licensing program (Figures 2D, S2E, and S2F; Ekholm-Reed et al., 2004;<sup>16</sup> Matson et al., 2017; <sup>18</sup> Tanaka and Diffley, 2002<sup>25</sup>)—this, in turn, reduces the rate of EdU incorporation during S phase (Figures 2D and 2E), prevents clearance of the minichromosome maintenance complex (MCM) from intragenic deposition sites<sup>17</sup> and induces replication stress (Figures 2D and 2F), making S phase longer (Figure S2G). Similarly, depletion of FBXW7 reduces the rate of DNA synthesis and increases Chk1 phosphorylation (Figures S2H and S2I). The addition of a Chk1 inhibitor AZD7762 forced cyclin E-overexpressing G2-arrested cells into mitosis (Figure 2C) and increased the frequency of cells exhibiting aberrant mitosis (Figure S2J), indicating that the G2 arrest is dependent upon Chk1.

The mean length of G2 phase was  $8 \pm 3 \text{ h}$  (median = 8 h) in control U2OS cells not expressing cyclin E, determined from live-cell imaging. G2 length was longer (13  $\pm$  9 h; median = 10 h) in the subset of cyclin E-expressing cells that subsequently entered mitosis (Figure 2G). We did not observe EdU incorporation in these cells when they entered mitosis (phospho-histone H3 positive; Figure S2K), suggesting that DNA replication was completed before mitotic entry. Mean G2 length was even longer  $(23 \pm 14 \text{ h}; \text{ median} = 21 \text{ h})$  in the subset of cells that subsequently bypassed mitosis and entered EC-G1 (Figure 2G), and these cells also bore higher levels of DNA damage markers (Figures 2H and 2I). Taken together, these results show that cyclin E expression induces replicative stress; cells with less stress can complete replication and enter mitosis after a transient G2 arrest. However, cells with more replicative stress remain arrested in G2 for extended periods; these cells ultimately undergo mitotic bypass, enter EC-G1 and then enter S phase to complete endoreduplication.

To characterize the outcome of endoreduplication, cells with >4N DNA content after cyclin E expression were separated by cell sorting, and individual clones were isolated, grown, and analyzed. Figure 2J shows that these clones had chromosome numbers between 74 (the diploid karyotype of U2OS cells) and 148 (the predicted chromosome number for U2OS cells after WGD) consistent with endoreduplication followed by chromosome loss. The chromosome number in individual cells from the clones shown in Figure 2L exhibited extensive variation compared with the control. This large variation in individual cell karyotypes suggests that changes in chromosome number (primarily chromosome loss) continued to occur during the growth of the clone. We also analyzed the first cell cycles after

mitotic bypass by isolating cells with >4N DNA content after cyclin E expression by cell sorting. In these cells, the lengths of G2 and S phases were considerably longer (20 and 18 h, respectively) than in control cells (11 and 8 h) (Figures S2L and S2M). During the first mitosis following endoreduplication, 90% of the mitotic cells had bipolar spindles; these cells exhibited high levels of micronuclei, fragmented nuclei, and failed cytokinesis (Figures S2L, S2N, and S2O). Among the mitotic cells, 10% had multipolar spindles consistent with the presence of supernumerary centrosomes (Figures S2L, S2P, and S2Q), 26,27 which likely also contributes to chromosome instability. These results suggest that in addition to progressive chromosome loss during colony growth, the first cell cycle after mitotic bypass is especially chaotic. The DNA content of EC-G1 cells was slightly less than G2 cells (Figures S2R and S2S), suggesting that replication was incomplete before mitotic bypass. Thus, some of the replicative stress may arise from the second round of replication occurring on an incompletely replicated genome. Regardless, these results are consistent with a recent publication showing that cells undergo high rates of replicative stress and DNA damage in the first S phase after induction of tetraploidy.<sup>28</sup>

## Replicative stress is a general inducer of endoreduplication in U2OS cells

Results presented so far show that replicative stress caused by cyclin E expression induces WGD. To determine whether other forms of replicative stress could also induce endoreduplication or whether cyclin E expression plays any role in this process, in addition to generating replicative stress, we treated cells with the DNA polymerase inhibitor aphidicolin. Figures 3A and 3B and Video S2 show that this treatment is highly effective in inducing mitotic bypass in U2OS cells, even without cyclin E expression; nearly 80% of cells entered EC-G1 without mitosis after 72 h, as judged by mVenus-Gem degradation (Figure 3B; Video S2). This was accompanied by the accumulation of 4N cells with low cyclin B levels (Figures 3C and 3D) and re-loaded MCM (Figure 3E). mVenus-Gem degradation during aphidicolininduced mitotic bypass was very slow with an average  $t_{1/2}$  of 229.8  $\pm$  110 min (median = 211 min) (Figure S3A), similar to that seen with cyclin E expression (Figure S1D). Therefore, the slow G2 to EC-G1 transition seen in Figure 1G does not require continuous cyclin E expression. We saw an increase in DNA damage markers and an upregulation of p21 (Figure S3B), consistent with the generation of replicative stress. As with cyclin E expression, aphidicolin-induced bypass of mitosis required a Chk1-dependent G2 checkpoint since treatment with Chk1 or Wee1 inhibitors greatly reduced mitotic bypass and increased aberrant mitosis and micronucleus generation (Figures 3A, 3B,

<sup>(</sup>C) Left: schematic of the experimental approach. Mean percentages of mitotic cells with range are shown (n = 2). Statistical significance: \*p < 0.05, unpaired

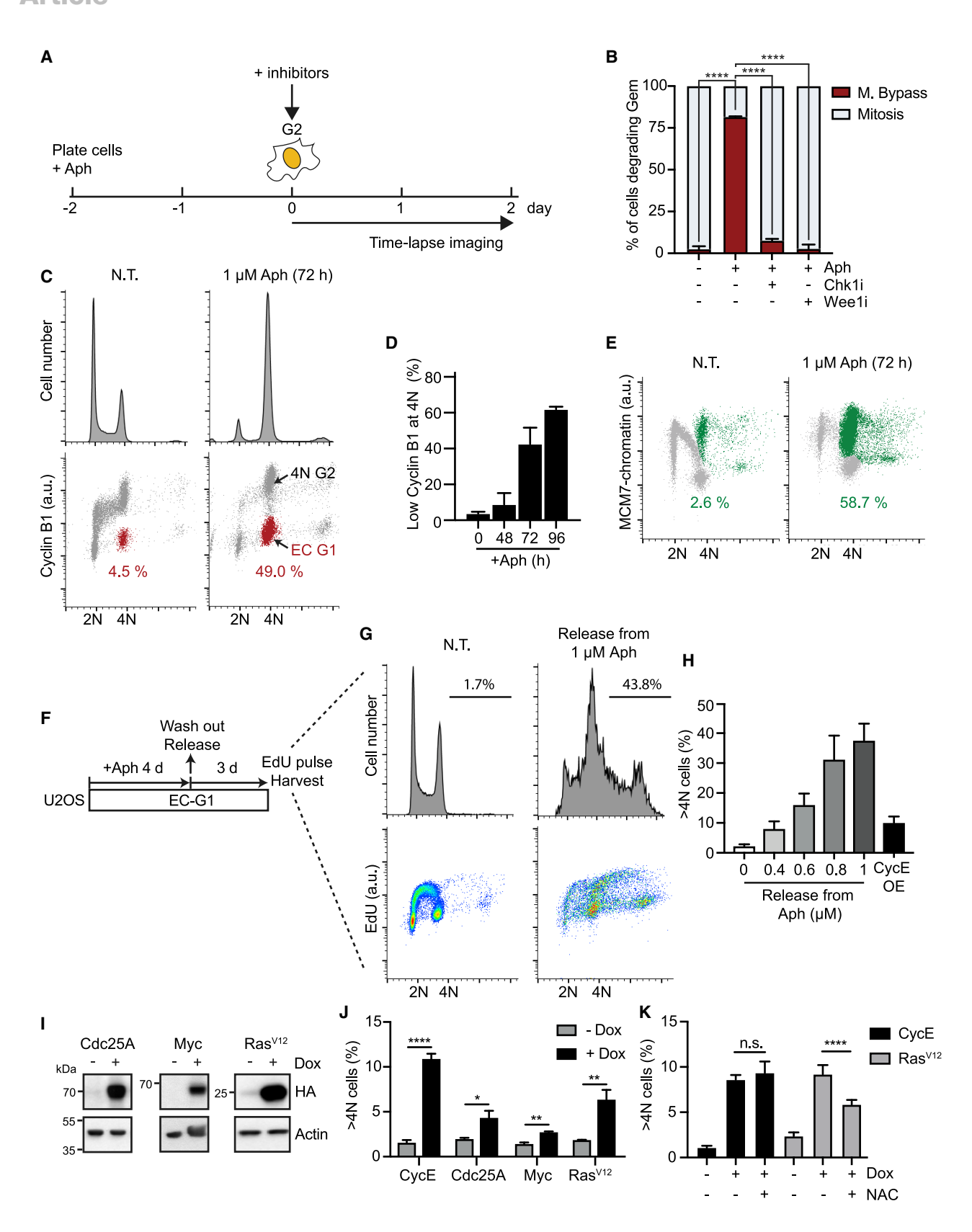
<sup>(</sup>D-F) Replicative stress in cyclin E-expressing cells. S phase (EdU+) was divided into 6 stages as shown in (D). The mean fluorescence intensities (MFI) of EdU and  $\gamma$ H2AX were measured for each cell-cycle stage as shown in (E) and (F), respectively. a.u., arbitrary unit.

<sup>(</sup>G) G2 lengths of individual cells from a representative FUCCI experiment in Figure 1D.

<sup>(</sup>H and I) After 24-h cyclin E induction, EC-G1 and 4N G2 populations were identified by FACS analysis as illustrated in (H). EdU-negative cells at 4N DNA content were assumed to have finished replication and should be either in G2 or EC-G1. EC-G1 cells were then identified as those having loaded MCM. YH2AX level for individual cells in a representative experiment is shown in (I). Statistical significance: unpaired t test. (J) Karyotypes of endoreduplicated clones.

## **Cell** Article





(legend on next page)





and S3C; Video S2). Like mitotic bypass after cyclin E expression, mitotic bypass after aphidicolin treatment also required Cdh1 (Figures S3D-S3F). When aphidicolin was removed after 96 h, >40% of the cells underwent endoreduplication (Figures 3F-3H). Thus, replicative stress induced by aphidicolin is sufficient to induce WGD in U2OS cells.

To explore the role of replicative stress in WGD further, we next tested whether replicative stress induced by other oncogenes could also induce WGD. To this end, we established U2OS cell lines (Figure 3I) in which expression of Cdc25A, Myc, or oncogenic Ras (Ras<sup>V12</sup>) can be induced. Figure 3J shows that all oncogenes tested generated elevated levels of WGD. Oncogenic Ras has been shown to induce replicative stress via the generation of reactive oxygen species. 29,30 Consistent with this, the anti-oxidant N-acetyl cysteine (NAC) reduced DNA damage in Ras-expressing cells but not in cyclin E-expressing cells (Figure 3G). NAC also reduced WGD in Ras-expressing cells, but not cyclin E-expressing cells, consistent with the idea that it is Ras<sup>V12</sup>-induced replicative stress that drives WGD (Figure 3K). In addition, unlike cyclin E expression that reduced origin licensing (Figures 2D, S2E, and S2F), oncogenic Ras did not affect MCM loading (Figure 3H). Taken together, these results show that replicative stress acts as a general driver of WGD, with different forms of replicative stress, including oncogene-induced replicative stress, capable of inducing endoreduplication.

## Cyclin E drives WGD in hTERT-RPE1 cells

U2OS cells are transformed and have likely already undergone a WGD event as evident from their hypertriploid karyotype (see Figure 2J). Moreover, although U2OS cells express WT p53, their actual p53 status is complicated at least in part due to the absence of CDKN2A expression,31 which encodes the alternative reading frame (ARF) Mdm2 inhibitor in addition to the p16 CDK inhibitor.<sup>32</sup> We therefore wanted to determine whether cyclin E could induce WGD in a more normal, diploid cell line. hTERT-RPE1 (hereafter RPE1) cells are untransformed, neardiploid, retinal epithelial cells with WT p53 that have been immortalized by telomerase expression. We established an RPE1 cell line expressing doxycycline-inducible (tetON) full-length cyclin E1 (Figure 4A), analogous to the U2OS cell line described above. We found that cyclin E-expressing RPE1 cells underwent WGD with similar kinetics to the U2OS cell line (Figures 4B and 4C). These RPE1 cells expressing cyclin E1 had reduced origin

licensing, reduced rate of DNA synthesis, and increased DNA damage markers (Figures S4A-S4C) similar to U2OS cells (Figures 2B, 2D, 2E, S2F, and S2G), indicative of replicative stress and G2 checkpoint activation.

Control RPE1 cells not expressing cyclin E entered and exited mitosis, whereas roughly half of cyclin E-expressing RPE1 cells bypassed mitosis (Figures 4D-4F). mVenus-Gem degradation during mitotic bypass in cyclin E-expressing RPE1 cells was also very slow with a  $t_{1/2}$  of 261.1  $\pm$  134.1 min (mean  $\pm$  SD, median = 231.8 min) (Figure S4D). We also saw many aberrant events, where mVenus-Gem degradation began but did not go to completion before cells entered S phase (mCherry-Cdt1 degradation) (Figures 4G and S4E). The addition of an ATR inhibitor but not an ATM inhibitor significantly reduced mitotic bypass, indicating that mitotic bypass is primarily dependent upon ATR (Figures S4F and 4H). Together, these experiments show that expression of cyclin E can induce WGD via mitotic bypass in an untransformed, p53-proficient, diploid cell line.

#### p53 is required for mitotic bypass

The results in the previous section show that cyclin E expression can drive WGD in p53-proficient RPE1 cells. To test whether this is also true in p53-deficient cells, we inactivated the TP53 gene in the RPE1 cyclin E-expressing cell line using CRISPR-Cas9 (Figure S5A). We found similar cyclin E expression levels, DNA damage marker upregulation, and reduction in the rate of DNA synthesis in p53-positive and p53-knockout RPE1 cells, following doxycycline induction (Figures S5B and S5C). Whereas approximately 25% of cyclin E-expressing p53-positive cells bypassed mitosis, mitotic bypass and WGD were almost completely suppressed in the p53-knockout RPE1 cells (Figures 5A and S5D; Videos S3 and S4). Instead of bypassing mitosis, a high proportion of these p53-knockout cells entered into catastrophic mitosis (Figures 5B and 5C). Therefore, the presence of p53 is not only permissive for mitotic bypass and endoreduplication following replicative stress, but it is in fact essential for the process.

Similar to U2OS cells, RPE1 cells treated with aphidicolin efficiently bypassed mitosis (mVenus-Gem degradation) and accumulated in EC-G1 (high mCherry-Cdt1), with 4N DNA content and low cyclin B levels (Figures 5D, 5E, and S5E; Video S5). Therefore, replicative stress is sufficient to cause mitotic bypass in p53-proficient cells. Similar to cyclin E expression, the addition of an ATR inhibitor but not an ATM inhibitor

## Figure 3. Mitotic bypass in aphidicolin-treated and oncogene-expressing cells

(A and B) Schematic of the experiment approach is shown in (A). Quantification of U2OS cells that bypassed mitosis, measured in % of cells that degraded geminin (% of cells completing S/G2), is shown in (B) (see also Video S2). Mean and range are shown (n = 2, >200 cells for each condition analyzed). Statistical significance: \*\*\*\*p < 0.0001, Tukey's method.

(C-E) (C and E) U2OS cells treated with 1 µM aphidicolin (Aph) for 72 h were analyzed for DNA content, cyclin B1 level, and chromatin-bound MCM7 level. EC-G1 cells were identified and labeled in red (C). Mean percentage of EC-G1 cells with range is shown in (D) (n = 2). Cells with >4N DNA content or cells with high levels of MCM loading at 4N are labeled in green (E).

(F-H) Schematic of the experiment approach is shown in (F). Released cells were analyzed for DNA content and DNA synthesis (EdU) (G). Quantification of >4N cells incorporating EdU is shown with SDs in (H) (n = 3).

- (I) Immunoblots showing Cdc25A, Myc, or Ras<sup>V12</sup> induction by Dox treatment in U2OS tetON cell lines.
- (J) Quantification of U2OS cells with >4N DNA content by FACS analysis after 96-h induction (Dox) of cyclin E (CycE), Cdc25A, Myc, or Ras<sup>V12</sup>. Mean percentages with SDs (n = 3) are shown. Statistical significance:  $^*p < 0.05$ ,  $^{**}p < 0.005$ , and  $^{****}p < 0.0001$ , unpaired t test.
- (K) U2OS cells induced to express CycE or Ras<sup>V12</sup> (+Dox) were incubated with 5mM N-acetyl cysteine (NAC). Quantification of cells with >4N DNA content by FACS analysis with SDs (n = 4) is shown. Statistical significance: \*\*\*\*p < 0.0001, Tukey's method.



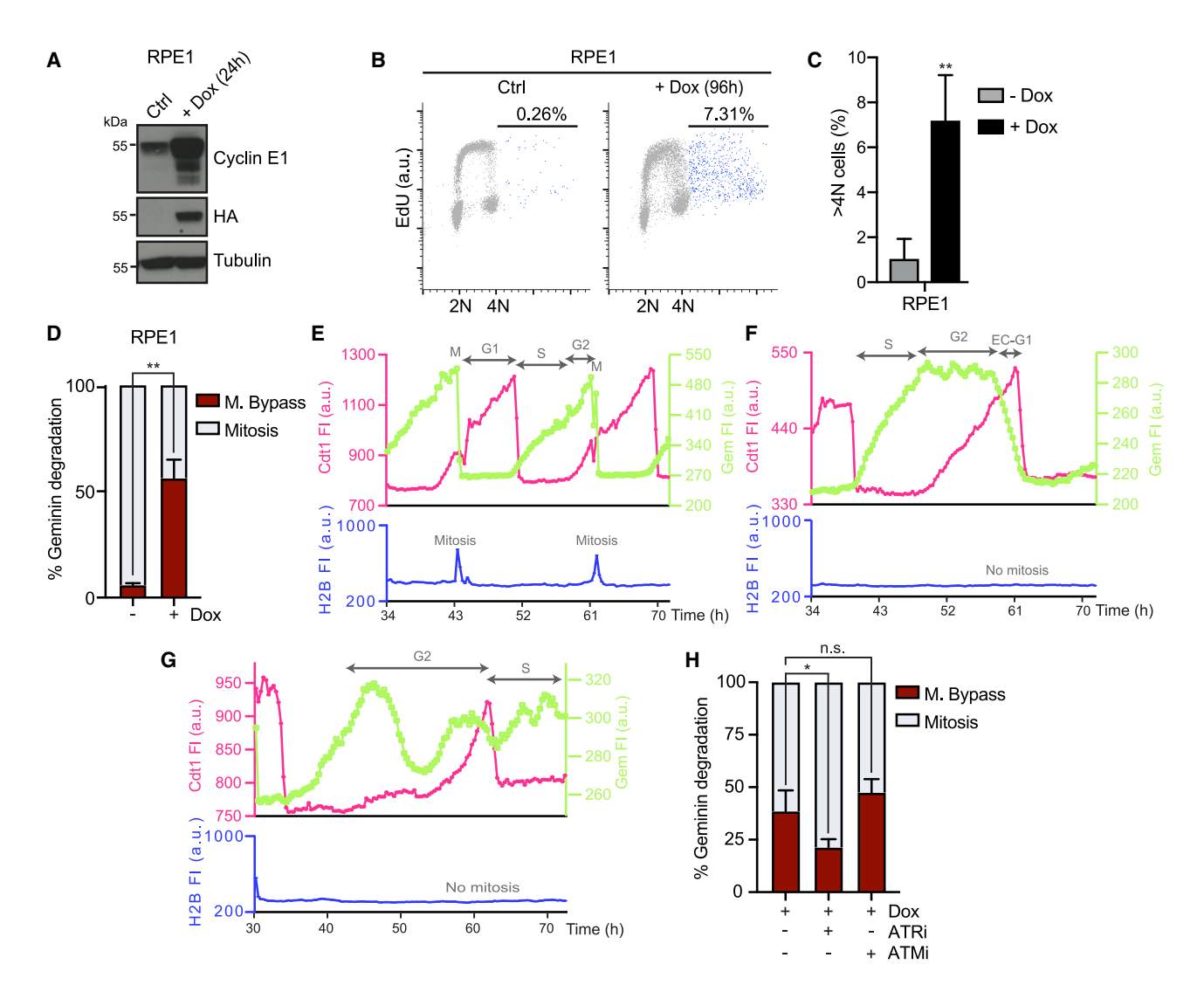


Figure 4. Cyclin E expression induces endoreduplication in RPE1 cells

(A) Immunoblots showing cyclin E induction (+Dox) in RPE1 tetON CycE cells.

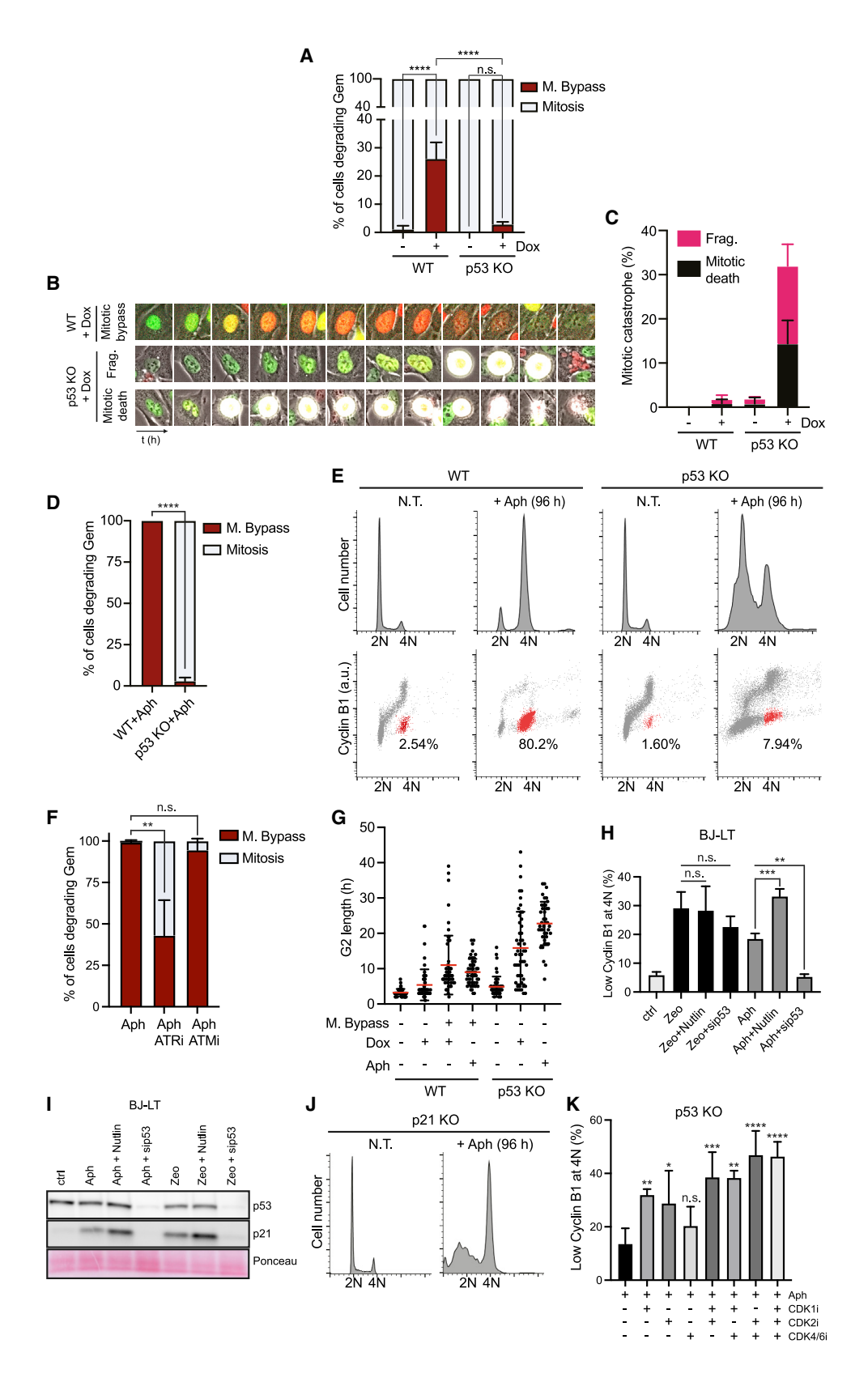
- (B) FACS analysis of RPE1 cells incorporating EdU after 96-h cyclin E expression.
- (C) Quantification of cells with >4N DNA content, measured in % of total cells, in (B) with SDs (n = 4). Statistical significance: \*\*p < 0.005, unpaired t test.
- (D) Quantification of cyclin E-expressing RPE1 cells (+Dox) that bypassed mitosis, measured in % of cells that degraded geminin (% of cells completing S/G2), with SDs is shown (n = 3, >150 cells for each condition analyzed).
- (E and F) Temporal profiles of the fluorescence intensities (FI) of mCherry-cdt1 and mVenus-Gem of a control RPE1 cell and a Dox-treated RPE1 cell bypassing mitosis. a.u., arbitrary unit. Statistical significance: \*\*p < 0.005, unpaired t test.
- (G) Temporal profiles of an example Dox-treated RPE1 cell degrading mCherry-cdt1 with high levels of mVenus-Gem.
- (H) Schematic of the experiment approach is shown in Figure 3A, except that the initial treatment was Dox instead of Aph. Mean percentages of RPE1 cells that bypassed mitosis with SDs are shown (n = 3, >200 cells analyzed for each condition). Statistical significance: \*p < 0.05, unpaired t test.

significantly reduced mitotic bypass in aphidicolin (Figure 5F). In RPE1 cells lacking p53, aphidicolin treatment induced similar levels of DNA damage markers as in p53-proficient cells (Figure S5F) but did not result in mitotic bypass (Figures 5D and S5E). Instead, there was an increase in cells with <2N DNA content; cells entered catastrophic mitosis resulting in nuclear fragmentation and death (Figures 5E, S5G, and S5H; Video S5). Taken together, these results show that replicative stressdriven mitotic bypass, whether caused by cyclin E or aphidicolin, requires p53.

This requirement is not restricted to RPE1 cells: p53-positive HCT116 cells accumulated in EC-G1 (4N DNA content with low cyclin B) (Figures S5I and S5J), while cells lacking p53 including p53-knockout U2OS, p53-depleted HCT116, and HeLa cells, which are p53 deficient, exhibited either prolonged G2 arrest with high cyclin B levels (p53-knockout U2OS) or an increase in cells with <2N DNA content and nuclear fragmentation (p53depleted HCT116 cells and HeLa cells) (Figures S5K-S5Q). We also found that aphidicolin-induced mitotic bypass occurred in a non-transformed fibroblast cell line IMR90 and that this mitotic







(legend on next page)





bypass was greatly reduced after the knockdown of p53 (Figure S5R).

One could explain the aberrant mitotic entry described above if p53 contributed to the G2 checkpoint arrest after replicative stress. However, we found by live-cell imaging that both cyclin E-expressing cells and aphidicolin-treated cells remained in G2 phase much longer in the p53-knockout cells before they entered aberrant mitosis than in the p53-positive cells before they bypassed mitosis, indicating that the G2 checkpoint was still activated and maintained in the absence of p53 (Figure 5G). Therefore, rather than being involved in maintaining the G2 arrest, our results indicate that p53 is actively required for replicative stress-driven mitotic bypass.

A requirement for p53 in WGD appears at odds with previous work showing that mitotic bypass and endoreduplication after telomere attrition or double-strand DNA breaks (DSB-driven mitotic bypass) occurred in p53-deficient cells. For their work, Davoli et al. used p53<sup>-/-</sup> MEFs and human cells in which p53 was inactivated by viral oncoproteins such as SV40 large T antigen (SV40LT).9 Indeed, we could confirm that zeocin induced mitotic bypass in BJ cells immortalized with SV40LT (Figure 5H). Moreover, the amount of mitotic bypass induced by zeocin in these cells was not enhanced by Nutlin, an Mdm2 inhibitor, and was not significantly decreased by p53 siRNA, indicating that zeocin-induced mitotic bypass does not require p53 (Figure 5H), consistent with the work of Davoli et al.<sup>9</sup>. Aphidicolin also induced mitotic bypass in these cells, but in sharp contrast to zeocin treatment, mitotic bypass induced by aphidicolin was markedly increased by Nutlin treatment and eliminated by p53 siRNA (Figure 5H). Despite the expression of SV40LT, it is clear these cells can still mount a p53 response since they exhibited an increase in p21 after zeocin or aphidicolin treatment, which was enhanced by Nutlin treatment and eliminated by p53 siRNA (Figure 5I). Thus, in the same cell line, DSB-driven mitotic bypass is independent of p53, whereas replicative stress-driven mitotic bypass absolutely requires p53. Zeocin or POT1 depletion also induced mitotic bypass or WGD in U2OS cells (Figures S6A-S6D), which likely has a dampened p53 response. By contrast, in p53-positive RPE1 cells, zeocin treatment or POT1 depletion primarily induced a G1 arrest (Figures S6E and S6F), consistent with DNA damage-induced G1 checkpoint activation. Nonetheless, there was also an increase in mitotic bypass as evidenced by the increase in cells with a 4N DNA content and low cyclin B (Figures S6E and S6F).

## p53 promotes mitotic bypass via p21 inhibition of CDK

p21, GADD45 $\alpha$ , and 14-3-3 $\sigma$  are key downstream G2/M targets of p53,34 so we depleted each individually in RPE1 cells treated with aphidicolin. Only p21 depletion reduced the accumulation of cells in EC-G1 (4N DNA content, low cyclin B) as p53 depletion did (Figure S6G). We also generated p21-knockout RPE1 cells (Figure S6H) and found that they behaved very similarly to p53-knockout cells: instead of the accumulation of cells in EC-G1 (Figure S6I), there was an increase in cells with <2N DNA content in aphidicolin (Figure 5J). Knockout of p21 in U2OS cells or depletion of p21 in IMR90 cells and HCT116 also almost completely abolished the accumulation of EC-G1 cells (Figures S5K-S5O and S5R). Depletion of p21 in HCT116 cells treated with aphidicolin caused accumulation of <2N cells and increased nuclear fragmentation, consistent with cells being forced into aberrant mitoses (Figures S5P and S5Q). Therefore, p21 is the major mediator of p53's function in mitotic bypass.

p21 is an inhibitor of CDK. We wondered whether chemical inhibition of CDK could bypass the requirement for p53 in inducing mitotic bypass. To test this, we added inhibitors of CDK1, CDK2, or CDK4/6 to G2-arrested p53-knockout RPE1 cells treated with aphidicolin. Figure 5K shows that inhibition of CDK1 or CDK2 significantly increased the accumulation of cells in EC-G1. Coincubation of two or three of the CDK inhibitors further increased EC-G1 accumulation (Figure 5K). Taken together, these results support the idea that mitotic bypass is initiated when CDK activities are inhibited in G2 by Wee1 and p21 to a sufficiently low level to allow activation of APC/ $C^{Cdh1}$ .

# **Cyclin E expression prevents and reverses senescence entry**

Aphidicolin-induced RPE1 EC-G1 cells did not reload MCM or proliferate after release from aphidicolin (Figures 6A and S7A), in contrast to U2OS (Figures 3F-3H) or RPE1 cells expressing cyclin E (Figure 4B). RPE1 EC-G1 cells generated by aphidicolin treatment were positive for  $\beta$ -galactosidase activity (Figure 7B), suggesting that they have become senescent. Previous work

## Figure 5. p53 knockout abolishes mitotic bypass in aphidicolin-treated and cyclin E-expressing RPE1 cells

(A–C) RPE1 WT and p53 KO cells were induced to express cyclin E (+ Dox) and imaged for 96 h. Quantification of cells that bypassed mitosis with SDs is shown in (A) (n = 3). Selected images of example cells are shown in (B) (see also Videos S3 and S4). Quantification of nuclear fragmentation (Frag.) and mitotic death is shown with SDs in (C). At least 300 cells for each condition were analyzed. Statistical significance: \*\*\*\*p < 0.0001, Šidák's method.

(D) RPE1 WT and p53 KO cells were treated with 1  $\mu$ M aphidicolin (Aph) and imaged for 72 h (see also Video S5). Quantification of mitotic bypass with SDs is shown (n = 3, >200 cells for each condition analyzed). Statistical significance: \*\*\*\*p < 0.0001, unpaired t test.

(E) RPE1 WT and p53 KO cells treated with 1 μM Aph were analyzed by FACS at 96 h. EC-G1 cells were identified and labeled in red.

(F) Schematic of the experiment approach is shown in Figure 3A. Quantification of RPE1 cells that bypassed mitosis with SDs is shown (n = 3, >200 cells for each condition analyzed). Statistical significance: \*\*p < 0.005, Tukey's method.

(G) Measured G2 length of cells in (A) and (D) from single representative experiments.

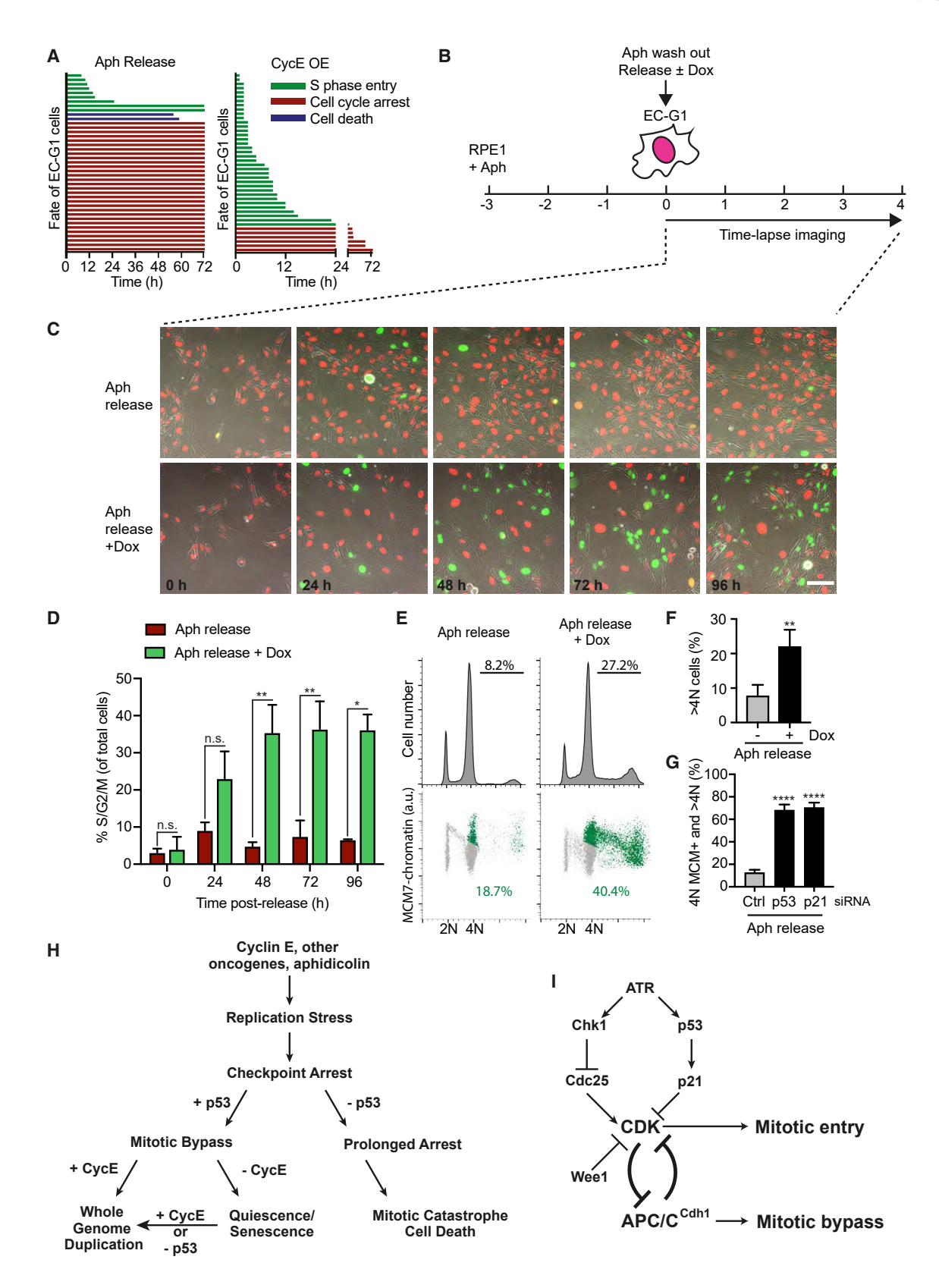
(H and I) BJ-LT cells treated with  $0.5 \,\mu\text{M}$  aphidicolin (Aph) or  $50 \,\mu\text{g}$ /ml zeocin (Zeo) for  $72 \,\text{h}$  were supplemented with  $2 \,\mu\text{M}$  Nutlin (at time  $24 \,\text{h}$ ) or  $p53 \,\text{siRNA}$  (at time 0) before being analyzed by immunoblots and FACS. Immunoblots showing  $p53 \,\text{and}\, p21 \,\text{expression}$  are shown in (I). Mean percentages of cells with low cyclin B1 at 4N DNA content with SDs are shown in (H) (n = 3). Statistical significance: \*\*p < 0.005 and \*\*\*p < 0.001, Tukey's method.

(J) RPE1 p21 KO cells treated with 1  $\mu M$  Aph were analyzed by FACS for DNA content.

(K) RPE1 p53KO cells treated with 1  $\mu$ M Aph for 48 h were supplemented with inhibitors of CDK1, CDK2, or CDK4/6 for a further 24 h before FACS analysis. Mean percentages of cells with low cyclin B1 at 4N DNA content with SDs are shown (n = 3). Statistical significance: \*p < 0.05, \*\*p < 0.005, \*\*\*p < 0.001, and \*\*\*\*p < 0.0001, Tukey's method.







(legend on next page)





has shown that transient activation of p53 in G2 can cause mitotic bypass and promote entry into senescence. 11,12 Since cyclin E expression, in contrast to aphidicolin treatment, induces WGD in p53-proficient RPE1 cells (Figure 6A), cyclin E must prevent this entry into senescence; but, can cyclin E expression drive cells that have already entered senescence back into the cycle? To test this, we asked whether the expression of cyclin E after mitotic bypass induced by aphidicolin could drive the senescent EC-G1 cells into the cell cycle. Figures 6B-6H show that a large fraction of these EC-G1 cells were induced to enter the cell cycle (Figures 6C and 6D; Video S6), re-license and rereplicate their genomes (Figure 6E), and accumulate as endoreduplicated cells (Figure 6F). Knocking down Rb in these EC-G1 cells was less efficient than cyclin E expression at driving them into cycle, but it did result in the re-licensing of DNA (Figure S7C). Senescent EC-G1 cells generated by aphidicolin treatment and then driven back into cell cycle by cyclin E expression, or cells with >4N DNA content after cyclin E expression alone, were separated by cell sorting, and individual clones could be isolated. All but one of these clones exhibited sub-tetraploid chromosome numbers and extensive chromosome number variation (Figure S7D), similar to that seen in U2OS endoreduplicated clones. One clone (C4) had clearly undergone an additional round of endoreplication and had a sub-octaploid chromosome number. These results indicate that the senescent EC-G1 state is not irreversible. This conclusion is reinforced by the fact that the knockdown of either p53 or p21 in EC-G1 cells also greatly induced cell-cycle re-entry and re-replication (Figures 6G and S7E). Taken together, these results indicate that p53-dependent mitotic bypass induced by replicative stress does not induce an irreversible arrest, but it rather induces a state with some hallmarks of senescence that can be reversed by alterations in the Rb or p53 pathways.

#### **DISCUSSION**

Our results, summarized in Figures 6H and 6I, describe a pathway for WGD via endoreduplication that requires p53. The pathway begins with the generation of replicative stress, a common consequence of oncogene expression. In the case of cyclin E expression, replicative stress arises from perturbation of the replication origin licensing system caused by the shortened G1 phase (Macheret and Halazonetis, 2018;17 Matson et al., 2017;<sup>18</sup> and this study). However, Ras<sup>V12</sup> does not reduce origin licensing (Figure S3H); instead, it generates replicative stress through the generation of reactive oxygen species.<sup>29,30</sup> Our results show that both types of stress can induce mitotic bypass and WGD. Moreover, exogenous sources of replicative stress like aphidicolin can also induce mitotic bypass. Since many anti-cancer drugs work by interfering with DNA replication, we speculate that drug treatments may promote WGD, even in p53-proficient cells, which may have implications for cancer evolution after chemotherapy.

Replicative stress induces mitotic bypass after a prolonged checkpoint-dependent G2 arrest, with ATR being primarily responsible for the DNA damage signal. This mitotic bypass requires the activation of the G1 form of the APC/C, APC/CCdh1, which is normally repressed by CDK activity. The DNA damage checkpoint in human cells blocks entry into mitosis via Wee1dependent inhibition of mitotic CDK. This inhibition of CDK is sufficient to prevent mitotic entry and is essential for mitotic bypass, but it is not sufficient to activate APC/CCdh1. Instead, mitotic bypass requires an additional CDK inhibitor, p21, whose accumulation is also dependent upon checkpoint activation, in this case, via p53 in a pathway parallel to Wee1. The time taken to transit from G2 (high mVenus-Gem) to G1 (low mVenus-Gem) varied widely in our experiments, suggesting that some or all of the feedback loops involved in the switch-like activation of the APC/C at the metaphase to anaphase transition in a normal cell cycle are not fully operational.35

The mitotic bypass seen after continued cyclin E expression has similar kinetics to the bypass induced by aphidicolin, indicating that oscillations in cyclin E-CDK2 are not essential for endoreduplication. This contrasts with naturally occurring endoreduplication cycles in Drosophila, which require a low cyclin E period to promote origin licensing and a high cyclin E period to drive replication.<sup>36</sup> In human cells, it appears that cyclin E expression does not directly inhibit licensing. For example, overexpression of cyclin E in U2OS cells does not affect the rate of MCM loading during G1 phase (Figures S2B and S2D). Moreover, cyclin E plays a positive role in licensing by preventing APC/C-dependent degradation of Cdc6.<sup>37</sup> The reduced MCM loading seen in these cells when they enter S phase is because cyclin E expression shortens G1 phase and therefore reduces the time available for licensing (Figures S2B and S2C). These results are also consistent with biochemical experiments showing that human cyclin A-CDK2 but not cyclin E-CDK2 phosphorylation can inhibit APC/C<sup>Cdh1</sup> activity in vitro. <sup>38</sup> Thus, our results are consistent with the idea that cyclin E overexpression directly inhibits neither replication origin licensing nor APC/C<sup>Cdh1</sup> activity.

After mitotic bypass induced by aphidicolin, p53-proficient RPE1 cells arrest in a senescence-like state. This is very likely

# Figure 6. CycE expression re-establishes endoreduplication of senescent EC-G1 cells

(A) Individual cell fates of RPE1 EC-G1 cells released from 0.5 μM aphidicolin (Aph) treatment or generated with CycE expression (represented by single-colored lines) are shown.

(B–D) Schematic of the experiment approach is shown in (B). 0.5 μM Aph was used. Still images at indicated time points are shown in (C) (see also Video S6). Scale bars, 100 µm. The mean percentage with SEMs of cells in S/G2/M phase at indicated time points is shown in (D) (n = 3). Statistical significance: \*p < 0.05 and \*\*p < 0.005, Šidák's method.

(E and F) RPE1 cells were treated as in (B) and analyzed by FACS at 96 h post Aph release for DNA content and MCM loading. Cells with >4N DNA content or with high levels of MCM loading at 4N are labeled in green. Quantification of >4N cells incorporating EdU is shown with SDs in (F) (n = 4). Statistical significance:

(G) Cells were treated as in (B) and released with siRNAs for 96 h. Mean percentages with SDs of cells with a high MCM level at 4N DNA content or with >4N DNA content are shown (n = 3). Statistical significance: \*\*\*\*p < 0.0001, Tukey's method.

(H and I) Model of whole-genome duplication driven by oncogene-induced replicative stress in p53-positive cells. Details of the model are described in the text.





related to previous work showing that transient induction of p53 in G2 triggers entry into senescence after mitotic bypass. 11,12 Cyclin E expression prevents this entry into senescence and can drive these senescent cells to complete endoreduplication. Cancers that have deregulated the E2F pathway, for example, by amplifying *CCNE1*, should, based on our findings, be primed to endoreduplicate without entering senescence. In other cases, where mitotic bypass and senescence occur before driver acquisition, subsequent E2F deregulation or p53 loss might drive cells back into cycle from senescence as tetraploid cells.

Previous work has shown that DSBs can drive WGD in cells lacking p53, whereas our results show that WGD driven by replicative stress requires p53. In both cases, the underlying mechanism of WGD is the same-extended checkpoint-dependent CDK inactivation allows APC/CCdh1 activation and subsequent mitotic bypass. However, the DSB-driven mechanism requires p53 deficiency because DSBs cause p53-dependent G1-arrest, which prevents WGD; p53 is not required because DSBs generate a strong enough checkpoint signal to cause mitotic bypass without p21. The mechanism we describe here for replicative stress requires p53 proficiency because the additional CDK inhibition from p21 is essential for mitotic bypass; p53 loss is not required because replicative stress does not induce p53-dependent G1 arrest. The DSB-driven mechanism requires telomere attrition to generate the checkpoint signal and requires p53 inactivation; the mechanism we describe requires genetic alteration in the cyclin E pathway to generate the checkpoint signal and to prevent senescence. These genetic events are all common in cancer and thus both pathways may play important roles in cancer.

Our results show that viral oncogenes may not always fully inactivate p53. For example, BJ cells transformed by SV40 large T antigen can still express p21 when treated with zeocin or aphidicolin (Figure 5H). Also, both DSB-driven and replicative stress-driven mechanisms can work in cells like BJ-LT that have dampened p53 function. It will be interesting to assess the ability of common p53 mutants to promote both DSB-driven as well as replicative stress-driven endoreduplication. p53 is classically considered to be a tumor suppressor gene; however, p53 null mutants are rare in cancer, and studies on the distribution of p53 mutations in cancer have led to a more nuanced vision in which p53 mutants can also contribute to oncogenesis. Our results fit into this view of p53 and suggest that p53 may actually contribute to cancer evolution by promoting replicative stress-driven WGD.

#### **Limitations of the study**

The relevance for tumorigenesis of the mechanism for WGD described in this study has not been directly addressed either in animal models or by human cancer genetics. This study primarily used acute cyclin E expression, which may be different from the gradual accumulation of *CCNE1* gene expression during amplification over several generations.

# **STAR**\*METHODS

Detailed methods are provided in the online version of this paper and include the following:

- KEY RESOURCES TABLE
- RESOURCE AVAILABILITY
  - Lead contact
  - Materials availability
  - Data and code availability
- EXPERIMENTAL MODEL AND SUBJECT DETAILS
  - O Cell lines and culture conditions
- METHOD DETAILS
  - O Plasmids and cell lines
  - O RNA Interference and small molecule inhibitors
  - Metaphase spreading
  - Live-Cell imaging
  - Automated cell tracking
  - Numerical analysis
  - Flow cytometry and cell sorting
  - Antibodies
- QUANTIFICATION AND STATISTICAL ANALYSIS

#### **SUPPLEMENTAL INFORMATION**

Supplemental information can be found online at https://doi.org/10.1016/j.cell. 2022.12.036.

#### **ACKNOWLEDGMENTS**

We thank Frank Uhlmann, Charles Swanton, and Karen Vousden for comments on the manuscript; Joe Padgett and Silvia Santos for help with generating FUCCI cell lines; Ilirjana Bajrami, Anaid Benitez, and Steve West for help with metaphase spreads; Mariia Yuneva for providing BJ-LT cells; and Matt Renshaw from the Crick Advanced Light Microscopy for help with developing FUCCI analysis scripts. We are also grateful to the Crick Flow Cytometry and Cell Services facilities. This work was supported by the Francis Crick Institute, which receives its core funding from Cancer Research UK (FC001066), the UK Medical Research Council (FC001066), and the Wellcome Trust (FC001066). This work was also funded by a Wellcome Trust Senior Investigator Award (106252/Z/14/Z) and a European Research Council Advanced Grant (669424-CHROMOREP) to J.F.X.D. J.Z. has received a Boehringer Ingelheim Fonds fellowship.

# **AUTHOR CONTRIBUTIONS**

J.F.X.D., J.Z., and S.A.H. conceived the project. J.Z., S.A.H., and J.F.X.D. designed the experiments. J.Z. and S.A.H. conducted the experiments and analyzed the data. E.O. contributed to making some cell lines and conducting some experiments. J.Z., S.A.H., and J.F.X.D. wrote the manuscript with input from all authors.

# **DECLARATION OF INTERESTS**

The authors declare no competing interests.

Received: March 20, 2022 Revised: November 8, 2022 Accepted: December 20, 2022 Published: January 20, 2023

#### **REFERENCES**

Taylor, A.M., Shih, J., Ha, G., Gao, G.F., Zhang, X., Berger, A.C., Schumacher, S.E., Wang, C., Hu, H., Liu, J., et al. (2018). Genomic and functional approaches to understanding cancer aneuploidy. Cancer Cell 33, 676–689.e3. https://doi.org/10.1016/j.ccell.2018.03.007.





- 2. Davoli, T., and de Lange, T. (2011). The causes and consequences of polyploidy in normal development and cancer. Annu. Rev. Cell Dev. Biol. 27, 585-610. https://doi.org/10.1146/annurev-cellbio-092910-154234.
- 3. Zack, T.I., Schumacher, S.E., Carter, S.L., Cherniack, A.D., Saksena, G., Tabak, B., Lawrence, M.S., Zhsng, C.-Z., Wala, J., Mermel, C.H., et al. (2013). Pan-cancer patterns of somatic copy number alteration. Nat. Genet. 45, 1134-1140. https://doi.org/10.1038/ng.2760.
- 4. Bielski, C.M., Zehir, A., Penson, A.V., Donoghue, M.T.A., Chatila, W., Armenia, J., Chang, M.T., Schram, A.M., Jonsson, P., Bandlamudi, C., et al. (2018). Genome doubling shapes the evolution and prognosis of advanced cancers. Nat. Genet. 50, 1189-1195. https://doi.org/10.1038/ s41588-018-0165-1.
- 5. Quinton, R.J., DiDomizio, A., Vittoria, M.A., Kotýnková, K., Ticas, C.J., Patel, S., Koga, Y., Vakhshoorzadeh, J., Hermance, N., Kuroda, T.S., et al. (2021). Whole-genome doubling confers unique genetic vulnerabilities on tumour cells. Nature 590, 492-497. https://doi.org/10.1038/s41586-020-03133-3.
- 6. Duelli, D.M., Padilla-Nash, H.M., Berman, D., Murphy, K.M., Ried, T., and Lazebnik, Y. (2007). A virus causes cancer by inducing massive chromosomal instability through cell fusion. Curr. Biol. 17, 431-437. https://doi. org/10.1016/j.cub.2007.01.049.
- 7. Sotillo, R., Hernando, E., Díaz-Rodríguez, E., Teruya-Feldstein, J., Cordón-Cardo, C., Lowe, S.W., and Benezra, R. (2007). Mad2 overexpression promotes aneuploidy and tumorigenesis in mice. Cancer Cell 11, 9-23. https://doi.org/10.1016/j.ccr.2006.10.019.
- 8. Lens, S.M.A., and Medema, R.H. (2019). Cytokinesis defects and cancer. Nat. Rev. Cancer 19, 32-45. https://doi.org/10.1038/s41568-018-0084-6.
- 9. Davoli, T., Denchi, E.L., and de Lange, T. (2010). Persistent telomere damage induces bypass of mitosis and tetraploidy. Cell 141, 81-93. https:// doi.org/10.1016/j.cell.2010.01.031.
- 10. Ganem, N.J., and Pellman, D. (2007). Limiting the proliferation of polyploid cells. Cell 131, 437-440. https://doi.org/10.1016/j.cell.2007.10.024.
- 11. Krenning, L., Feringa, F.M., Shaltiel, I.A., van den Berg, J., and Medema, R.H. (2014). Transient activation of p53 in G2 phase is sufficient to induce senescence. Mol. Cell 55, 59-72. https://doi.org/10.1016/j.molcel.2014. 05.007.
- 12. Johmura, Y., Shimada, M., Misaki, T., Naiki-Ito, A., Miyoshi, H., Motoyama, N., Ohtani, N., Hara, E., Nakamura, M., Morita, A., et al. (2014). Necessary and sufficient role for a mitosis skip in senescence induction. Mol. Cell 55, 73-84. https://doi.org/10.1016/j.molcel.2014.05.003.
- 13. Gorgoulis, V.G., Vassiliou, L.V., Karakaidos, P., Zacharatos, P., Kotsinas, A., Liloglou, T., Venere, M., Ditullio, R.A., Kastrinakis, N.G., Levy, B., et al. (2005). Activation of the DNA damage checkpoint and genomic instability in human precancerous lesions. Nature 434, 907–913. https://doi.org/10. 1038/nature03485.
- 14. Bartkova, J., Horejsí, Z., Koed, K., Krämer, A., Tort, F., Zieger, K., Guldberg, P., Sehested, M., Nesland, J.M., Lukas, C., et al. (2005). DNA damage response as a candidate anti-cancer barrier in early human tumorigenesis. Nature 434, 864-870. https://doi.org/10.1038/nature03482.
- 15. Bester, A.C., Roniger, M., Oren, Y.S., Im, M.M., Sarni, D., Chaoat, M., Bensimon, A., Zamir, G., Shewach, D.S., and Kerem, B. (2011). Nucleotide deficiency promotes genomic instability in early stages of cancer development. Cell 145, 435-446. https://doi.org/10.1016/j.cell.2011.03.044.
- 16. Ekholm-Reed, S., Méndez, J., Tedesco, D., Zetterberg, A., Stillman, B., and Reed, S.I. (2004). Deregulation of cyclin E in human cells interferes with prereplication complex assembly. J. Cell Biol. 165, 789-800. https://doi.org/10.1083/jcb.200404092.
- 17. Macheret, M., and Halazonetis, T.D. (2018). Intragenic origins due to short G1 phases underlie oncogene-induced DNA replication stress. Nature 555, 112-116. https://doi.org/10.1038/nature25507.
- 18. Matson, J.P., Dumitru, R., Coryell, P., Baxley, R.M., Chen, W., Twaroski, K., Webber, B.R., Tolar, J., Bielinsky, A.-K., Purvis, J.E., et al. (2017). Rapid

- DNA replication origin licensing protects stem cell pluripotency. eLife 6. https://doi.org/10.7554/eLife.30473.
- 19. Yeh, C.H., Bellon, M., and Nicot, C. (2018). FBXW7: a critical tumor suppressor of human cancers. Mol. Cancer 17, 115. https://doi.org/10. 1186/s12943-018-0857-2.
- 20. Sakaue-Sawano, A., Kurokawa, H., Morimura, T., Hanyu, A., Hama, H., Osawa, H., Kashiwagi, S., Fukami, K., Miyata, T., Miyoshi, H., et al. (2008). Visualizing spatiotemporal dynamics of multicellular cell-cycle progression. Cell 132, 487-498. https://doi.org/10.1016/j.cell.2007.12.033.
- 21. Sakaue-Sawano, A., Yo, M., Komatsu, N., Hiratsuka, T., Kogure, T., Hoshida, T., Goshima, N., Matsuda, M., Miyoshi, H., and Miyawaki, A. (2017). Genetically encoded tools for optical dissection of the mammalian cell cycle. Mol. Cell 68, 626-640.e5. https://doi.org/10.1016/j.molcel.2017. 10.001.
- 22. Clijsters, L., Ogink, J., and Wolthuis, R. (2013). The spindle checkpoint, APC/C(Cdc20), and APC/C(Cdh1) play distinct roles in connecting mitosis to S phase. J. Cell Biol. 201, 1013-1026. https://doi.org/10.1083/jcb. 201211019
- 23. Jones, R.M., Mortusewicz, O., Afzal, I., Lorvellec, M., García, P., Helleday, T., and Petermann, E. (2013). Increased replication initiation and conflicts with transcription underlie cyclin E-induced replication stress. Oncogene 32, 3744-3753. https://doi.org/10.1038/onc.2012.387.
- 24. Neelsen, K.J., Zanini, I.M., Herrador, R., and Lopes, M. (2013). Oncogenes induce genotoxic stress by mitotic processing of unusual replication intermediates. J. Cell Biol. 200, 699-708. https://doi.org/10.1083/jcb. 201212058.
- 25. Tanaka, S., and Diffley, J.F. (2002). Deregulated G1-cyclin expression induces genomic instability by preventing efficient pre-RC formation. Genes Dev. 16, 2639-2649. https://doi.org/10.1101/gad.1011002.
- 26. Ganem, N.J., Godinho, S.A., and Pellman, D. (2009). A mechanism linking extra centrosomes to chromosomal instability. Nature 460, 278-282. https://doi.org/10.1038/nature08136.
- 27. Chen, S., Stout, J.R., Dharmaiah, S., Yde, S., Calvi, B.R., and Walczak, C.E. (2016). Transient endoreplication down-regulates the kinesin-14 HSET and contributes to genomic instability. Mol. Biol. Cell 27, 2911-2923. https://doi.org/10.1091/mbc.E16-03-0159.
- 28. Gemble, S., Wardenaar, R., Keuper, K., Srivastava, N., Nano, M., Macé, A.S., Tijhuis, A.E., Bernhard, S.V., Spierings, D.C.J., Simon, A., et al. (2022). Genetic instability from a single S phase after whole-genome duplication. Nature 604, 146-151. https://doi.org/10.1038/s41586-022-04578-4.
- 29. Irani, K., Xia, Y., Zweier, J.L., Sollott, S.J., Der, C.J., Fearon, E.R., Sundaresan, M., Finkel, T., and Goldschmidt-Clermont, P.J. (1997). Mitogenic signaling mediated by oxidants in Ras-transformed fibroblasts. Science 275, 1649-1652. https://doi.org/10.1126/science.275.5306.1649.
- 30. Lee, A.C., Fenster, B.E., Ito, H., Takeda, K., Bae, N.S., Hirai, T., Yu, Z.X., Ferrans, V.J., Howard, B.H., and Finkel, T. (1999). Ras proteins induce senescence by altering the intracellular levels of reactive oxygen species. J. Biol. Chem. 274, 7936–7940. https://doi.org/10.1074/jbc.274.12.7936.
- 31. Park, Y.B., Park, M.J., Kimura, K., Shimizu, K., Lee, S.H., and Yokota, J. (2002). Alterations in the INK4a/ARF locus and their effects on the growth of human osteosarcoma cell lines. Cancer Genet. Cytogenet. 133, 105-111. https://doi.org/10.1016/s0165-4608(01)00575-1.
- 32. Sherr, C.J. (2001). The INK4a/ARF network in tumour suppression. Nat. Rev. Mol. Cell Biol. 2, 731-737. https://doi.org/10.1038/35096061.
- 33. Bunz, F., Dutriaux, A., Lengauer, C., Waldman, T., Zhou, S., Brown, J.P., Sedivy, J.M., Kinzler, K.W., and Vogelstein, B. (1998). Requirement for p53 and p21 to sustain G2 arrest after DNA damage. Science 282, 1497-1501. https://doi.org/10.1126/science.282.5393.1497.
- 34. Taylor, W.R., and Stark, G.R. (2001). Regulation of the G2/M transition by p53. Oncogene 20, 1803–1815. https://doi.org/10.1038/sj.onc.1204252.
- 35. Rata, S., Suarez Peredo Rodriguez, M.F., Joseph, S., Peter, N., Echegaray Iturra, F., Yang, F., Madzvamuse, A., Ruppert, J.G., Samejima, K., Platani,





- M., et al. (2018). Two interlinked bistable switches govern mitotic control in mammalian cells. Curr. Biol. 28, 3824-3832.e6. https://doi.org/10.1016/j. cub.2018.09.059.
- 36. Zielke, N., Edgar, B.A., and DePamphilis, M.L. (2013). Endoreplication. Cold Spring Harb. Perspect. Biol. 5, a012948. https://doi.org/10.1101/ cshperspect.a012948.
- 37. Mailand, N., and Diffley, J.F. (2005). CDKs promote DNA replication origin licensing in human cells by protecting Cdc6 from APC/C-dependent proteolysis. Cell 122, 915–926. https://doi.org/10.1016/j.cell.2005.08.013.
- 38. Lukas, C., Sørensen, C.S., Kramer, E., Santoni-Rugiu, E., Lindeneg, C., Peters, J.M., Bartek, J., and Lukas, J. (1999). Accumulation of cyclin B1 requires E2F and cyclin-A-dependent rearrangement of the anaphasepromoting complex. Nature 401, 815–818. https://doi.org/10.1038/44611.
- 39. Soussi, T., and Wiman, K.G. (2015). TP53: an oncogene in disguise. Cell Death Differ. 22, 1239-1249. https://doi.org/10.1038/cdd.2015.53.
- 40. Ohrt, T., Merkle, D., Birkenfeld, K., Echeverri, C.J., and Schwille, P. (2006). In situ fluorescence analysis demonstrates active siRNA exclusion from the nucleus by Exportin 5. Nucleic Acids Res. 34, 1369-1380. https:// doi.org/10.1093/nar/gkl001.
- 41. Tinevez, J.Y., Perry, N., Schindelin, J., Hoopes, G.M., Reynolds, G.D., Laplantine, E., Bednarek, S.Y., Shorte, S.L., and Eliceiri, K.W. (2017). TrackMate: an open and extensible platform for single-particle tracking. Methods 115, 80-90. https://doi.org/10.1016/j.ymeth.2016.09.016.
- 42. Rodríguez-Martínez, M., Hills, S.A., Diffley, J.F.X., and Svejstrup, J.Q. (2020). Multiplex cell fate tracking by flow cytometry. Methods Protoc. 3, 50. https://doi.org/10.3390/mps3030050.





# **STAR**\***METHODS**

# **KEY RESOURCES TABLE**

| REAGENT or RESOURCE   | SOURCE                      | IDENTIFIER                          |
|---|-----------------------------|-------------------------------------|
| Antibodies  |                             |                                     |
| Mouse monoclonal anti-Cyclin E1   | Santa Cruz Biotechnology    | Cat# sc-247, RRID:AB_627357         |
| Mouse monoclonal anti-beta Actin  | Santa Cruz Biotechnology    | Cat# sc-81178, RRID:AB_2223230      |
| Rabbit polyclonal anti-Phospho-p53 (Ser15)  | Cell Signaling Technology   | Cat# 9284, RRID:AB_331464           |
| Rabbit monoclonal anti-Phospho-Chk1 (Ser345)  | Cell Signaling Technology   | Cat# 2348, RRID:AB_331212           |
| Rabbit polyclonal anti-Phospho-RPA32 (S4/S8)  | Bethyl                      | Cat# A300-245A, RRID:AB_210547      |
| Mouse monoclonal anti-HA.11 Epitope Tag   | BioLegend                   | Cat# 901533, RRID:AB_2801249        |
| Rabbit polyclonal anti-HA Epitope Tag   | Santa Cruz Biotechnology    | Cat# sc-805, RRID:AB_631618         |
| Mouse monoclonal anti-p53   | Santa Cruz Biotechnology    | Cat# sc-126, RRID:AB_628082         |
| Mouse monoclonal anti-alpha-Tubulin   | Sigma-Aldrich               | Cat# T5168, RRID:AB_477579          |
| Mouse monoclonal anti-MCM7  | Santa Cruz Biotechnology    | Cat# sc-56324, RRID:AB_1125697      |
| Rabbit monoclonal anti-Cyclin B1  | Abcam                       | Cat# ab32053, RRID:AB_731779        |
| Mouse monoclonal anti-phospho-Histone H2A.X (Ser139)  | Millipore                   | Cat# 05-636, RRID:AB_309864         |
| Rabbit polyclonal anti-POT1   | Novus Biologicals           | Cat# NB500-176,<br>RRID:AB_10000829 |
| Rabbit polyclonal anti-FBXW7  | Proteintech                 | Cat# 55290-1-AP<br>RRID:AB_2881300  |
| Anti-p-CDK1 T14/Y15   | In-house by Julian Gannon   | N/A                                 |
| Anti-Cdh1   | In-house by Julian Gannon   | N/A                                 |
| Goat polyclonal Anti-Mouse Immunoglobulins  | Agilent                     | Cat# P0447, RRID:AB_2617137         |
| Oonkey polyclonal Anti-Rabbit IgG (H+L)   | Jackson ImmunoResearch Labs | Cat# 711-035-152, RRID:AB_10015282  |
| Goat polyclonal anti-Rabbit IgG (H+L) Cross-  | Thermo Fisher Scientific    | Cat# A-21428, RRID:AB_2535849       |
| Adsorbed Secondary Antibody, Alexa Fluor 555  |                             |                                     |
| Goat polyclonal anti-Mouse IgG (H+L) Highly<br>Cross-Adsorbed Secondary Antibody, Alexa Fluor 555 | Thermo Fisher Scientific    | Cat# A-21424, RRID:AB_141780        |
| Chemicals, peptides, and recombinant proteins   |                             |                                     |
| Dulbecco's Modified Eagle's Medium (DMEM) - high glucose  | Gibco                       | Cat# 41966052                       |
| ipofectamine RNAiMAX  | ThermoFisher                | Cat# 13778150                       |
| Opti-MEM Reduced Serum Medium, GlutaMAX Supplement  | ThermoFisher                | Cat# 51985034                       |
| Aphidicolin   | Sigma Aldrich               | Cat# A0781                          |
| AZD 7762  | Axon MEDCHEM                | Cat# 1399                           |
| MK 1775   | Axon MEDCHEM                | Cat# 1494                           |
| (U-55933  | Selleckchem                 | Cat# S1092                          |
| /E-822  | Selleckchem                 | Cat# S7102                          |
| Abemaciclib   | Selleckchem                 | Cat# S7158                          |
| RO-3306   | Merck                       | Cat# SML0569                        |
| CVT-313   | Cambridge Bioscience        | Cat# B1137                          |
| Nocodazole  | Sigma Aldrich               | Cat# M1404                          |
| Colcemid  | ThermoFisher                | Cat# 15212012                       |
| Doxycycline   | Sigma Aldrich               | Cat# D9891                          |
| DyeCycle Ruby   | ThermoFisher                | Cat# V10309                         |
| Hoechst 33342   | ThermoFisher                | Cat# 62249                          |
| DAPI  | Sigma Aldrich               | Cat# D9542                          |
| Alexa Fluor 488 NHS Ester   | ThermoFisher                | Cat# A20000                         |
| /ectashield Antifade Mounting Medium with DAPI  | Vector Laboratories         | Cat# H-1200                         |
| Protease Inhibitor Cocktail   | Sigma Aldrich               | Cat# 11873580001                    |

(Continued on next page)





| Continued  |                                    |                        |
|--|------------------------------------|------------------------|
| REAGENT or RESOURCE  | SOURCE                             | IDENTIFIER             |
| JetPRIME   | Polyplus                           | Cat# 114-15            |
| Lipofectamine 3000   | ThermoFisher                       | Cat# L3000008          |
| Zeocin   | Invivogen                          | Cat# ant-zn-1          |
| Blasticidin  | Invivogen                          | Cat# ant-bl-05         |
| Oritical commercial assays   |                                    |                        |
| QIAquick Gel Extract kit   | QIAGEN                             | Cat# 28706             |
| QIAprep Spin Miniprep Kit  | QIAGEN                             | Cat# 27106             |
| Click-iT® EdU Alexa Fluor® 647 Flow Cytometry Assay Kit                        | ThermoFisher                       | Cat# C10424            |
| Experimental models: Cell lines  |                                    |                        |
| Human: U2OS  | ATCC                               | HTB-96                 |
| Human: hTERT RPE1  | ATCC                               | CRL-4000               |
| Human: HCT116  | ATCC                               | CCL-247                |
| Human: IMR90   | ATCC                               | CCL-186                |
| Human: U2OS TetON CycE   | This paper                         | Available upon request |
| Human: U2OS TetON Ras <sup>12V</sup>   | This paper                         | Available upon request |
| Human: U2OS TetON c-Myc  | This paper                         | Available upon request |
| Human: U2OS TetON cdc25A   | This paper                         | Available upon request |
| Human: U2OS TetON CycE p53KO   | This paper                         | Available upon request |
| Human: U2OS TetON CycE p21KO   | This paper                         | Available upon request |
| Human: U2OS TetON CycE Fucci H2B   | This paper                         | Available upon request |
| Human: RPE1 TetON CycE   | This paper                         | Available upon request |
| Human: RPE1 TetON CycE p53KO C1 & C2   | This paper                         | Available upon request |
| Human: RPE1 TetON CycE p21KO   | This paper                         | Available upon request |
| Human: RPE1 TetON CycE Fucci   | This paper                         | Available upon request |
| Human: RPE1 TetON CycE Fucci H2B   | This paper                         | Available upon request |
| Human: RPE1 TetON CycE p53KO Fucci   | This paper                         | Available upon request |
| Human: U2OS CycE TetOFF  | Laboratory of Jiri Bartek          | N/A                    |
| Human: BJ-LT   | Laboratory of Mariia Yuneva        | N/A                    |
| Oligonucleotides   |                                    |                        |
| SMARTpool On-TARGETplus FZR1 (Cdh1) siRNA                                      | Dharmacon                          | L-015377-00            |
| siGENOME TP53 siRNA  | Dharmacon                          | D-003329-26            |
| SMARTpool siGENOME CDKN1A siRNA (p21)  | Dharmacon                          | M-003471-00            |
| SMARTpool siGENOME RB1 siRNA   | Dharmacon                          | M-003296-03            |
| SMARTpool siGENOME GADD45A siRNA   | Dharmacon                          | M-003893-02            |
| SMARTpool siGENOME SFN siRNA (14-3-3sigma)                                     | Dharmacon                          | M-005180-00            |
| SMARTpool siGENOME FBXW7 siRNA   | Dharmacon                          | M-004264-02            |
| SMARTpool siGENOME POT1 siRNA  | Dharmacon                          | M-004205-01            |
| Control siRNA siGL2 against Firefly luciferase:<br>CGU ACG CGG AAU ACU UCG AUU | Ohrt et al. <sup>40</sup>          | N/A                    |
| RNA for TP53 knockout targeting exon 4: CCATTGTTCAATATCGTCCG                   | This paper                         | N/A                    |
| gRNA for TP53 knockout targeting exon 5: CCTCAGCATCTTATCCGAG                   | This paper                         | N/A                    |
| RNA for CDKN1A knockout:<br>CCATTAGCGCATCACAGTCG                               | This paper                         | N/A                    |
| Recombinant DNA  |                                    |                        |
| Plasmid: Fucci(CA)2  | Sakaue-Sawano et al. <sup>21</sup> | N/A                    |
| Plasmid: pCSII EF1a hH2B-Turg  | Silvia Santos                      | N/A                    |

(Continued on next page)





| Continued                                 |                  |   |  |
|---|------------------|---|--|
| REAGENT or RESOURCE                       | SOURCE           | IDENTIFIER  |  |
| Plasmid: psPax2                           | Addgene          | 12260   |  |
| Plasmid: pMD2.G                           | Addgene          | 12259   |  |
| Plasmid: pSpCas9(BB)-2A-Puro (PX459) V2.0 | Addgene          | 62988   |  |
| Plasmid: PX459-TP53-exon4                 | This paper       | Available upon request                              |  |
| Plasmid: PX459-TP53-exon5                 | This paper       | Available upon request                              |  |
| Plasmid: PX459-CDKN1A                     | This paper       | Available upon request                              |  |
| Plasmid: pcDNA4/TO                        | Invitrogen       | V102020   |  |
| Plasmid: pcDNA4/TO-CycE                   | This paper       | Available upon request                              |  |
| Plasmid: pcDNA4/TO-Ras                    | This paper       | Available upon request                              |  |
| Plasmid: pcDNA4/TO-cMyc                   | This paper       | Available upon request                              |  |
| Plasmid: pcDNA4/TO-cdc25A                 | This paper       | Available upon request                              |  |
| Software and algorithms                   |                  |   |  |
| FlowJo 10.8                               | FlowJo, LLC      | https://www.flowjo.com/                             |  |
| MATLAB                                    | Mathworks        | https://www.mathworks.com/                          |  |
| mageJ 1.53                                | NIH              | RRID:SCR_001935                                     |  |
| FIJI                                      | NIH              | RRID: SCR_002285                                    |  |
| TrackMate plugin for FIJI                 | Tinevez et al.41 | https://github.com/fiji/TrackMate                   |  |
| Prism 8                                   | GraphPad         | https://www.graphpad.com/scientific-software/prism/ |  |
| FUCCI imaging analysis FIJI macro         | This paper       | https://github.com/zeng-j-k/Cell-FUCCI analysis.git |  |

#### **RESOURCE AVAILABILITY**

# **Lead contact**

Further information and requests for resources and reagents should be directed to and will be fulfilled by the lead contact, John F.X. Diffley (john.diffley@crick.ac.uk).

#### **Materials availability**

All unique/stable reagents generated in this study will be made available on request to the lead contact but may require a completed Materials Transfer Agreement.

## Data and code availability

Original immunoblot images have been deposited at Figshare and are publicly available (DOI: https://doi.org/10.6084/m9.figshare.c. 6284868.v1).

FIJI macro for FUCCI analysis has been deposited at GitHub (https://github.com/zeng-j-k/Cell-FUCCI-analysis.git) and is publicly available as of the date of publication.

Any additional information required to reanalyse the data reported in this paper is available from the lead contact upon request.

#### **EXPERIMENTAL MODEL AND SUBJECT DETAILS**

# **Cell lines and culture conditions**

All cells in this study were cultured using DMEM (Gibco, 41966052) supplemented with 10% fetal bovine serum in an ambientcontrolled incubator at 37 °C and 5% CO<sub>2</sub>. No antibiotics were supplemented unless specified. U2OS, hTERT RPE1, HCT116 and Hela cells were used in this study. U2OS TetON CycE, U2OS TetON Ras<sup>12V</sup>, U2OS TetON c-Myc, U2OS TetON cdc25A, U2OS TetON CycE p53KO, U2OS TetON CycE p21KO, U2OS TetON CycE Fucci H2B, RPE1 TetON CycE, RPE1 TetON CycE p53KO (clone #1&2, clone 1 was used unless specified), RPE1 TetON CycE p21KO, RPE1 TetON CycE Fucci, RPE1 TetON CycE Fucci H2B and RPE1 TetON CycE p53KO Fucci were generated for this study. U2OS CycE TetOFF was previously described in 14 and was kindly gifted from Thanos D. Halazonetis. See Plasmids and Cell Lines for details of construction of cell lines.





#### **METHOD DETAILS**

#### **Plasmids and cell lines**

Stable TetON cell lines were constructed by random plasmid integration. Human coding sequences of Cyclin E1, c-Myc, H-Ras<sup>V12</sup> and cdc25A were cloned in to the pcDNA4/TO vector (Invitrogen) respectively with a hemagglutinin (HA) tag at the N-terminus. T-REx-U2OS cells were obtained from Invitrogen. T-REx-RPE1 cells stably expressing the Tet repressor were constructed by transfecting hTERT RPE1 cells with the pcDNA6/TR plasmid (Invitrogen) and cells were selected in medium containing 5 µg/ml Blasticidin. For creation of TetON cells, T-REx-U2OS cells or T-REx-RPE1 cells were transfected with Lipofectamine 3000 (Invitrogen) or JetPRIME (Polyplus) using the pcDNA4/TO constructs carrying genes of interest. Transformed cells were selected in 200-500 μg/ml Zeocin and clones were tested for Doxycycline dependent gene expression.

For creation of TP53 knockout cells, we used the following gRNA sequences: 5' CCATTGTTCAATATCGTCCG 3' targeting exon 4 and 5' TCCTCAGCATCTTATCCGAG 3' targeting exon 6, cloned into the pSpCas9(BB)-2A-Puro (PX459) V2.0 vector (Addgene, 62988). The resultant constructs were co-transfected into U2OS TetON CycE or RPE1 TetON CycE cells. Transfected cells were single cell sorted into 96-well plates four days post puromycin selection. Successful TP53 knockout in single cell clones was verified by immunoblotting, PCR and sanger sequencing. For CDKN1A knockout, we used a gRNA sequence 5' CCATTAGCGCATCACAGTCG 3' and followed procedures described above.

The Fucci(CA)2 plasmid<sup>21</sup> carrying a Cdt1 fragment, mCherry tagged, and a geminin fragment, mVenus tagged, was introduced into U2OS TetON CycE, RPE1 TetON CycE and RPE1 TetON CycE p53KO C1 by lentiviral transduction. Stable clonal transformants positive for fluorescent signals were obtained by single cell sorting into 96-well plates. The pCSII EF1a hH2B-Turq plasmid carrying mTurquoise-tagged human H2B, provided by Dr. Silvia Santos, was introduced into U2OS TetON CycE Fucci and RPE1 TetON CycE Fucci cells by lentiviral transduction.

#### **RNA Interference and small molecule inhibitors**

Knockdown studies were performed using SMARTpool On-TARGETplus FZR1(Cdh1) siRNA (Dharmacon, L-015377-00), siGENOME TP53 siRNA (Dharmacon, D-003329-26), SMARTpool siGENOME CDKN1A siRNA (Dharmacon, M-003471-00), SMARTpool siGENOME GADD45A siRNA (Dharmacon, M-003893-02), SMARTpool siGENOME SFN siRNA (Dharmacon, M-005180-00), SMARTpool siGENOME FBXW7 siRNA (Dharmacon, M-004264-02), SMARTpool siGENOME POT1 siRNA (Dharmacon, M-004205-01), SMARTpool siGENOME RB1 siRNA (Dharmacon, M-003296-03) and a control siRNA siGL2 against Firefly luciferase<sup>40</sup> with sequence CGU ACG CGG AAU ACU UCG AUU. siRNAs were transfected at 40 nM final concentration using Lipofectamine RNAiMAX (Invitrogen) and OptiMEM (Invitrogen). The following small molecule compounds were used: aphidicolin from Nigrospora sphaerica (Sigma Aldrich), AZD 7762 (CHK1 inhibitor, Axon MedChem, used at 50 nM working concentration), MK 1775 (WEE1 inhibitor, Axon MedChem, used at 1 μM working concentration), KU-55933 (ATM inhibitor, Selleckchem, used at 10 μM working concentration), VE-822 (ATR inhibitor, Selleckchem, used at 200 nM working concentration), Abemaciclib (CDK4/ 6 inhibitor, Selleckchem, used at 500 nM working concentration), RO-3306 (CDK1 inhibitor, Merck, used at 7 μM working concentration), CVT-313 (CDK2 inhibitor, Cambridge Bioscience, used at 10 μM working concentration), nocodazole (Sigma Aldrich), colcemid (Thermo), Doxycycline (Sigma Aldrich).

# Metaphase spreading

Cells were stained with Hoechst and FACS-sorted for DNA content. Single-cell clones were selected, and chromosome numbers were counted by metaphase spreading. Endoreduplicated clones were grown in medium supplemented with 167 ng/ml colcemid (Thermo) for 3 h. Cells were trypsinised, re-suspended in 75 mM KCl at 37 °C for 10 min with gentle vortexing, and fixed in Carnoy's fixative (3:1 methanol:glacial acetic acid). Cells were washed two more times with Carnoy's fixative before spreading on slides. Mitotic samples were mounted in a mounting medium containing DAPI (Vector Laboratories) to visualise chromosomes.

# **Live-Cell imaging**

Cells were grown on 4-well polymer bottom slides (80446, Ibidi) in DMEM (Gibco, 41966052) containing 10% FBS with 1% Pen/Strep. Sorted cells were allowed to settle for at least 5 h prior to imaging. Time-lapse live-cell imaging was performed using a Nikon Eclipse Ti inverted microscope equipped with a custom humidified enclosure (Okolabs) that maintains temperature at 37 °C and CO<sub>2</sub> at 5%. The Nikon Perfect Focus System (PFS) was used for autofocus. Phase-contrast and fluorescent images were taken every 20 min using ImageJ-µManager software with a 20x objective. Filter sets and exposure times were optimised so that no phototoxicity or photobleaching was observed in cells. Medium in wells was replenished every 2 or 3 days. Image processing was performed using FIJI software. Cell lines used are: U2OS tetON CycE Fucci H2B-mTurQ in Figures 1D and 3A; RPE1 TetON CycE Fucci H2B in Figure 4D; RPE1 TetON CycE Fucci in Figure 4H; RPE1 TetON CycE Fucci and RPE1 TetON CycE p53KO Fucci in Figure 5A; RPE1 TetON CycE Fucci and RPE1 TetON CycE p53KO Fucci in Figure 5D; RPE1 TetON CycE Fucci in Figure 5F; RPE1 TetON CycE Fucci in Figure 6B.





## **Automated cell tracking**

Image analyses for U2OS cells in Figures 1D-1J and RPE1 cells in Figures 4D-4G were analysed by an in-house script-based automated cell tracking pipeline. Acquired images were filtered and background subtracted in FIJI (1.53c) before tracking using a plugin, Trackmate. 41 H2B-mTurquoise channel was used for tracking cell nuclei, and parameters were optimised for effective tracking of nuclei as following: the LoG detector was used with default parameters except using a radius of 11 μm for U2OS cells, and a radius of 9 µm for RPE1 cells. The Simple LAP Tracker was used with a max linking distance of 15, a max gap closing distance of 15 and a max frame gap of 2.

Fluorescence intensities were calculated on identified nuclear regions of H2B-mTurquiose, cdt1-mCherry and geminin-mVenus images. Cells showing red (mCherry+, mVenus-), green (mCherry-, mVenus+) and yellow (mCherry+, mVenus+) were assigned to G1, S and G2 phases respectively. Upon mitosis, one of the daughter cells is selected for tracking. MATLAB was used to plot fluorescence intensity changes over time for individual identified cells with tracks longer than 36 h. Mitosis was characterised as an abrupt increase in H2B-mTurquiose signal caused by condensation of chromosomes, in parallel with abrupt disappearance of mVenus-geminin signal. Mitotic bypass was characterised as disappearance of mVenus-geminin with no increase in H2B-mTurquiose signal. Image analyses for U2OS cells in Figures 3A and 3B and RPE1 cells in Figures 5A-5D and 5F were performed by manual tracking of cells.

#### **Numerical analysis**

To estimate degradation rates of mVenus-Gem, FUCCI datasets were exported, and time courses were excised around local maxima and minima. Excised intensity data were normalised and scaled to 0-100, and fitted to the logistic growth equation below<sup>21</sup>:

Normalised Intensity = 
$$\frac{100}{1 + e^{\left(-k\left(t - t_{1/2}\right)\right)}}$$

k is the rate of degradation of mVenus-Gem signal with a unit of 1/minute.  $t_{1/2}$  is half-life of mVenus-Gem degradation with a unit of minute, at which the signal reaches half of the maximum. Curves were fitted using Isocurvefit function in MATLAB.

#### Flow cytometry and cell sorting

Multiplexed flow cytometry analysis using fluorescent cell barcoding, combined with EdU, antibody and DNA staining, was performed as previously described. 42 Up to 6 samples treated with different conditions were barcoded in each experiment to allow unbiased subsequent staining of the combined samples. For detection of S phase progression, cells pulsed with 10 μM EdU for 30 min were harvested and stained with Click-iT chemistry using Click-iT EdU Alexa Fluor 647 Flow Cytometry Assay Kit (Thermo, C10424) according to the manufacturer's instructions. For DNA content analysis, cells were treated with 100 μg/mL RNase A and stained with 1  $\mu$ g/mL DAPI. For MCM loading analysis, cell chromatin fractions were extracted using CSK buffer (10 mM HEPES-KOH pH 7.9, 100 mM NaCl, 3 mM MgCl<sub>2</sub>, 1 mM EGTA, 300 mM sucrose, 1% BSA, 0.2% Triton X-100, 1 mM DTT, 1X Roche Complete protease inhibitor cocktail) before fixation and staining. Data were analysed using FlowJo software. Cell doublets were excluded for all analyses. See Antibodies for details of epitope staining. EC-G1 cells are identified as cells having low cyclin B1 level at 4N DNA content.

Non-EC and EC cells were isolated by sorting for 2N DNA content or >4N DNA content using a BD FCASAria Fusion flow cytometer after incubation with Hoechst 33342 (5 μg/ml, Thermo) at 37 °C for 30 min, or DyeCycle Ruby (1:10,000, Thermo, V10309) for Fucci cells at 37 °C for 15 min.

# **Antibodies**

Immunoblotting was performed using the following antibodies diluted in TBS supplemented with 0.1% Tween 20 and 5% milk powder or 3% BSA: cyclin E1 (1:1000, Santa Cruz, sc-247), beta-actin (1:1000, Santa Cruz, sc-81178), p-p53 S15 (1:1000, Cell Signalling, 9284), p-CHK1 S345 (1:1000, Cell Signalling, 2348), p-RPA S4/S8 (1:5000, Bethyl Laboratories, A300-245), HA.11 (1:1000, BioLegend, 16B12), p53 (1:1000, Santa Cruz, sc-126), p21 (1:1000, Cell Signalling, 2947), HA (1:1000, Santa Cruz, sc-805), alpha-Tubulin (1:4000, Sigma, T5168), POT1 (1:1000, Novus Biologicals, NB500-176), FBXW7 (1:1000, Proteintech, 55290-1-AP), p-CDK1 T14/Y15 (in-house by Julian Gannon), Cdh1 (1:1000, in-house by Julian Gannon, AR38.2), anti-Mouse HRP (1:5000, Dako, P0447) and anti-Rabbit HRP (1:5000, Jackson Immuno, 711-035-152). The following antibodies were used for FACS and diluted in PBS supplemented with 1% BSA: MCM7 (1:200, Santa Cruz, sc-56324), cyclin B1 (1:200, Abcam, ab32053), p-H2A.X S139 (1:200, Millipore, 05-636), anti-Rabbit Alexa Fluor 555 (1:500, Thermo, A21428) and anti-Mouse Alexa Fluor 555 (1:500, Thermo, A21424).

## **QUANTIFICATION AND STATISTICAL ANALYSIS**

Graphpad Prism were used for all statistical analyses. Statistical methods are described in the figure legends as appropriate.





# Supplemental figures

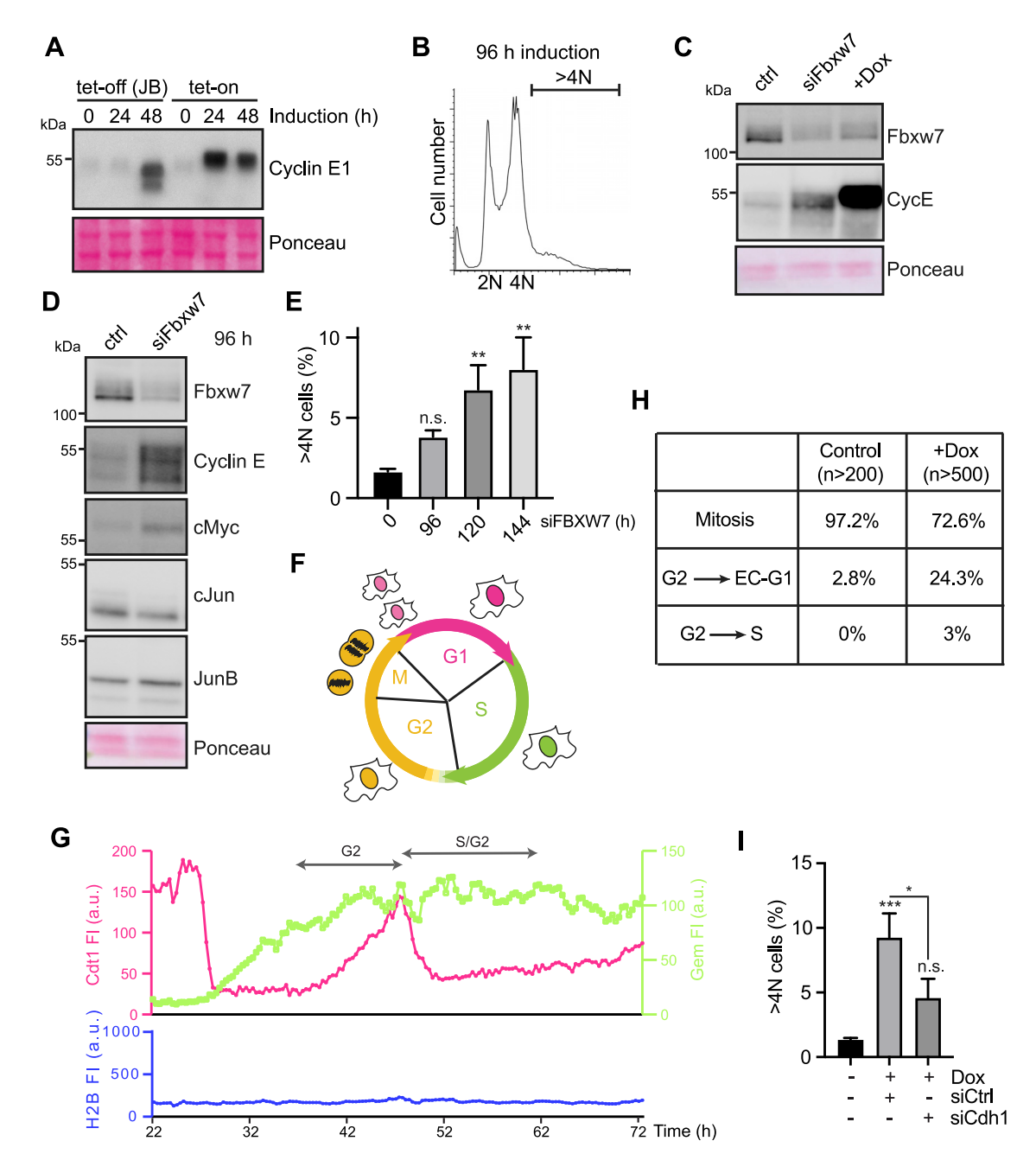


Figure S1. Aberrant G2 transitions in cyclin E-expressing cells; involvement of Cdh1 in CycE-induced endoreduplication, related to Figure 1

(A) Immunoblots showing cyclin E1 induction in U2OS tetON CycE cell line and U2OS tetOFF CycE cell line.

(B) FACS DNA content analysis of U2OS cells expressing cyclin E.

(C and D) Immunoblots showing expression of oncogenes after knockdown of Fbxw7 in U2OS cells.

(E) U2OS cells depleted with Fbxw7 were analyzed by FACS over time. Quantification of >4N cells with SDs is shown (n = 3). Statistical significance: \*\*p < 0.005, Tukey's method.

(F) Schematic showing colors of cell-cycle phases of the FUCCI system.

(G) Temporal profiles of a cyclin E-expressing U2OS cell that degraded mCherry-Cdt1 while maintaining high level of mVenus-Gem.

(H) The percentages of cell-cycle transitions from G2 in control and cyclin E-expressing (+ Dox) U2OS cells.

(I) U2OS cells were induced to express cyclin E by Dox for 96 h and were treated with siRNAs at 48 h to knock down Cdh1. Quantification of the percentage of >4N cells by FACS analysis with SDs is shown (n = 3). Statistical significance:  $^*p < 0.05$ ;  $^{***}p < 0.001$ , Tukey's method.

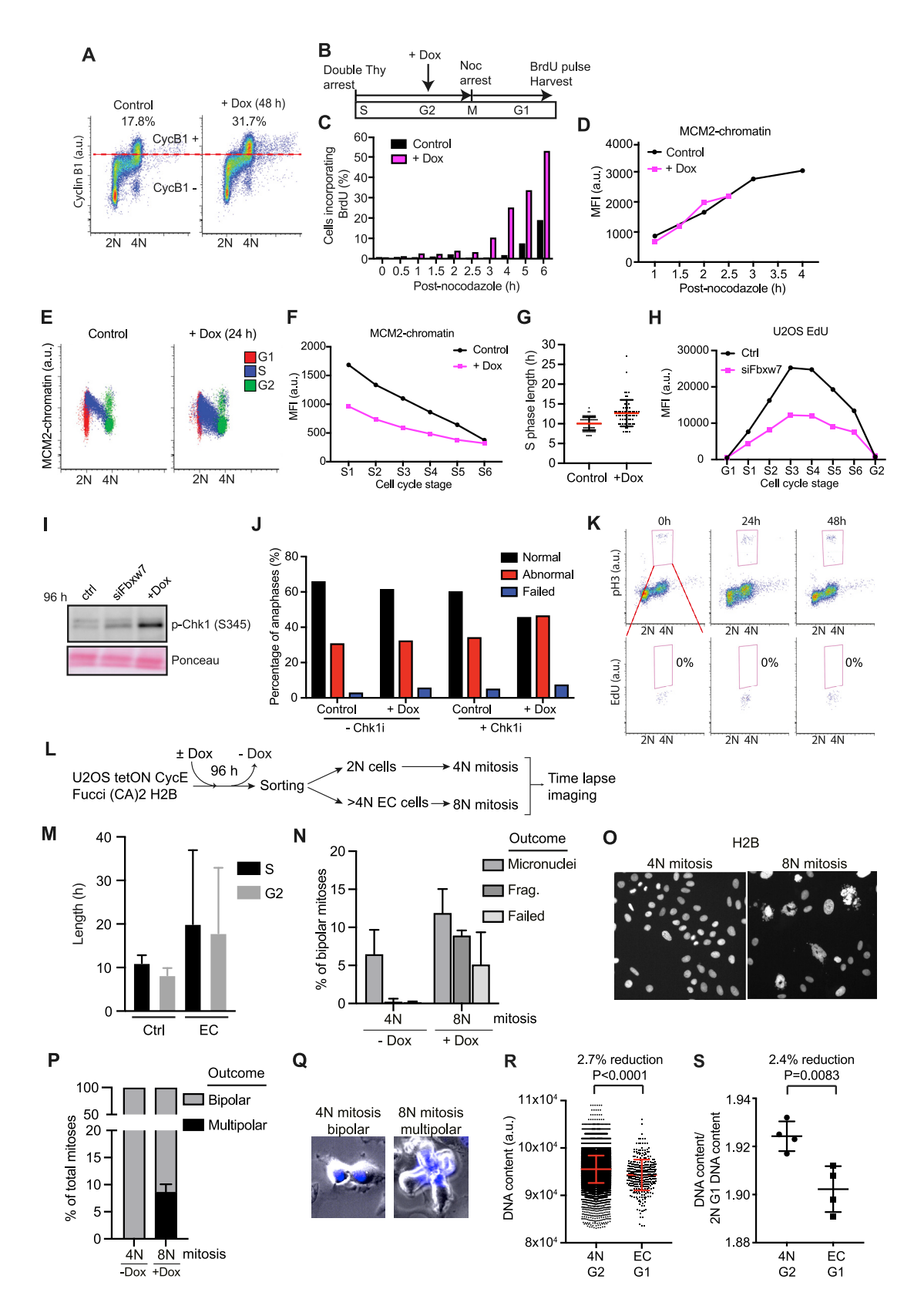






Figure S2. Characterization of replicative stress in cyclin E-expressing cells and endoreduplicated cells, related to Figure 2

(A) FACS analysis of cyclin E-expressing U2OS cells for cyclin B1 level and DNA content.

(B–D) U2OS cells were synchronized using double thymidine and nocodazole, and treated as in (B). Quantification of the percentage of cells incorporating BrdU by FACS at different time points is shown in (C). The level of chromatin-bound MCM2 is shown in (D).

- (E) FACS analysis of chromatin bound MCM2 level on cyclin E-expressing U2OS cells. G1, S, and G2 phases were colored; G1: 2N, EdU-. S: 2N-4N, EdU+. G2: 4N, EdU-.
- (F) S phase was divided as in Figure 2D. Chromatin-bound MCM2 level was analyzed by FACS in cyclin E-expressing U2OS cells.
- (G) S phase lengths of cells measured in FUCCI live-cell imaging. At least 60 cells were analyzed for each condition.
- (H) EdU incorporation analysis by FACS in siFbxw7-treated cells.
- (I) Immunoblot showing phosphorylated Chk1 (S345) expression in siFbxw7-treated cells.
- (J) U2OS H2B-mCherry cells were induced to express cyclin E for 24 h and then treated with 100 nM Chk1 inhibitor and live cell imaged for 12 h. Quantification of abnormal and failed mitosis is shown.
- (K) U2OS cells expressing cyclin E were stained with pH3 and EdU. Mitotic cells were identified as pH3+ cells. The percentage of EdU+ cells is shown.
- (L–Q) Schematic of the experimental approach (L). Mean lengths  $\pm$  SDs of S and G2 phases of sorted 2N and >4N EC cells are shown in (M). The percentage of bipolar mitoses ending with micronucleus generation, nuclear fragmentation (Frag.), or cytokinesis failure (Failed) are shown in (N). Example still images of the H2B-mTurquiose channel are shown in (O). The percentages of bipolar and multipolar mitosis are shown in (P). Example composite images of H2B-mTurquoise (blue) and phase-contrast channels for bipolar and multipolar mitosis are shown in (Q).
- (R and S) Cells in Figure 2H were stained with DAPI for DNA content analysis. DNA content level for individual cells in a representative experiment is shown in (R) and relative DNA content is averaged as shown in (S) (n = 4). Statistical significance was examined by unpaired t test.



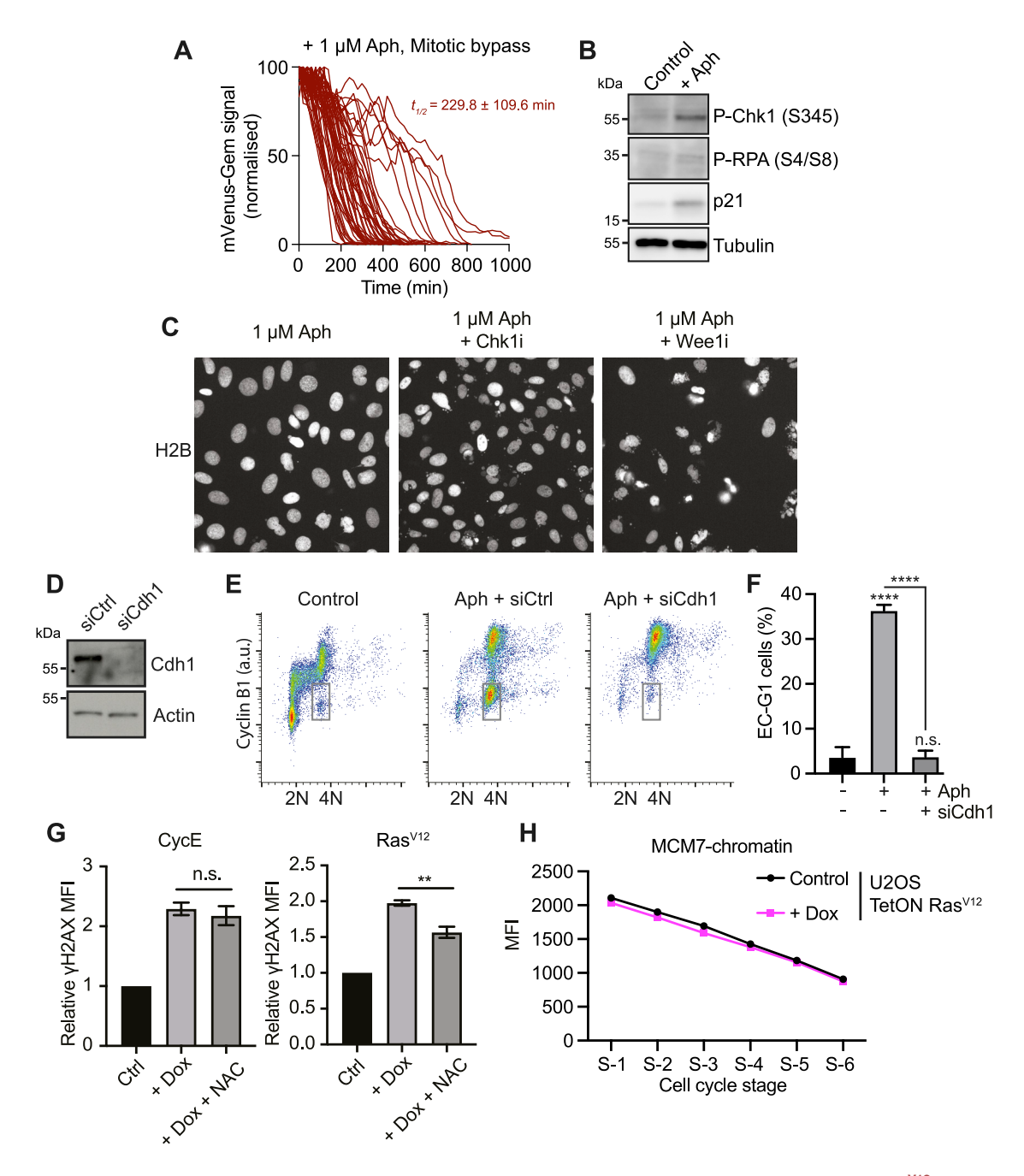


Figure S3. Involvement of the G2 checkpoint and Cdh1 in aphidicolin-induced mitotic bypass; replicative stress in Ras<sup>V12</sup>-expressing cells, related to Figure 3

(A) Normalized data on the time-course degradation of mVenus-Gem. Each line represents a single-cell tracking (n > 50). Mean half-life ( $t_{1/2}$ ) values with SDs of mVenus-Gem degradation are shown in the figure and main text.

- (B) Immunoblots showing DNA damage markers after 72-h 1  $\mu$ M aphidicolin treatment in U2OS cells.
- (C) Example still images of the H2B-mTurquiose channel of cells in Figure 3B.
- (D–F) U2OS cells treated with 1  $\mu$ M Aph were incubated with siRNA to knockdown Cdh1. Immunoblots showing Cdh1 knockdown are in (D). Cells were analyzed by FACS (E). The mean percentage of EC-G1 cells with SDs is shown in (F) (n = 3). Statistical significance: \*\*\*\*p < 0.0001, Tukey's method.
- (G) U2OS cells induced (+ Dox) to express CycE or Ras<sup>V12</sup> were incubated with 5mM N-acetyl cysteine (NAC). Quantification of >4N cells by FACS analysis with SDs is shown (n = 3). Statistical significance: \*\*p < 0.01, paired t test.
- (H) Mean fluorescence intensities (MFI) for chromatin-bound MCM of Ras<sup>V12</sup>-expressing U2OS cells.





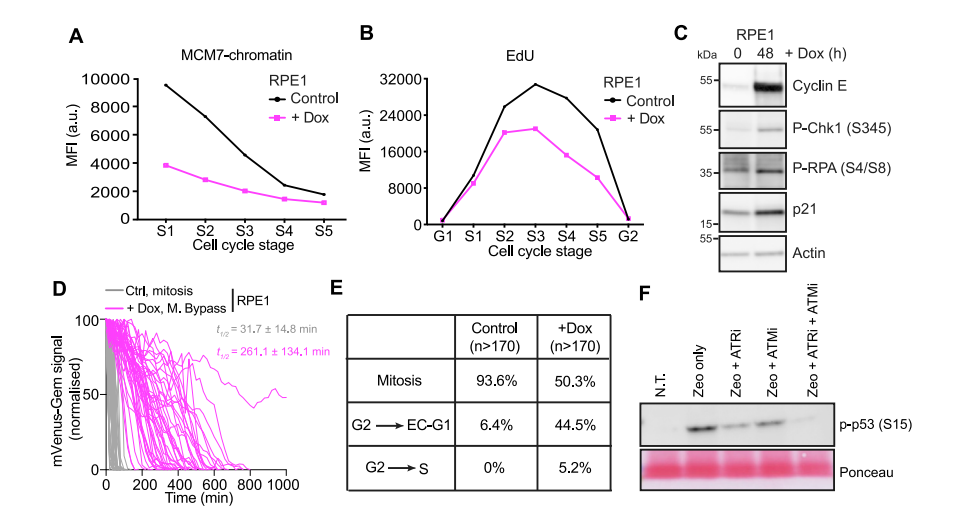
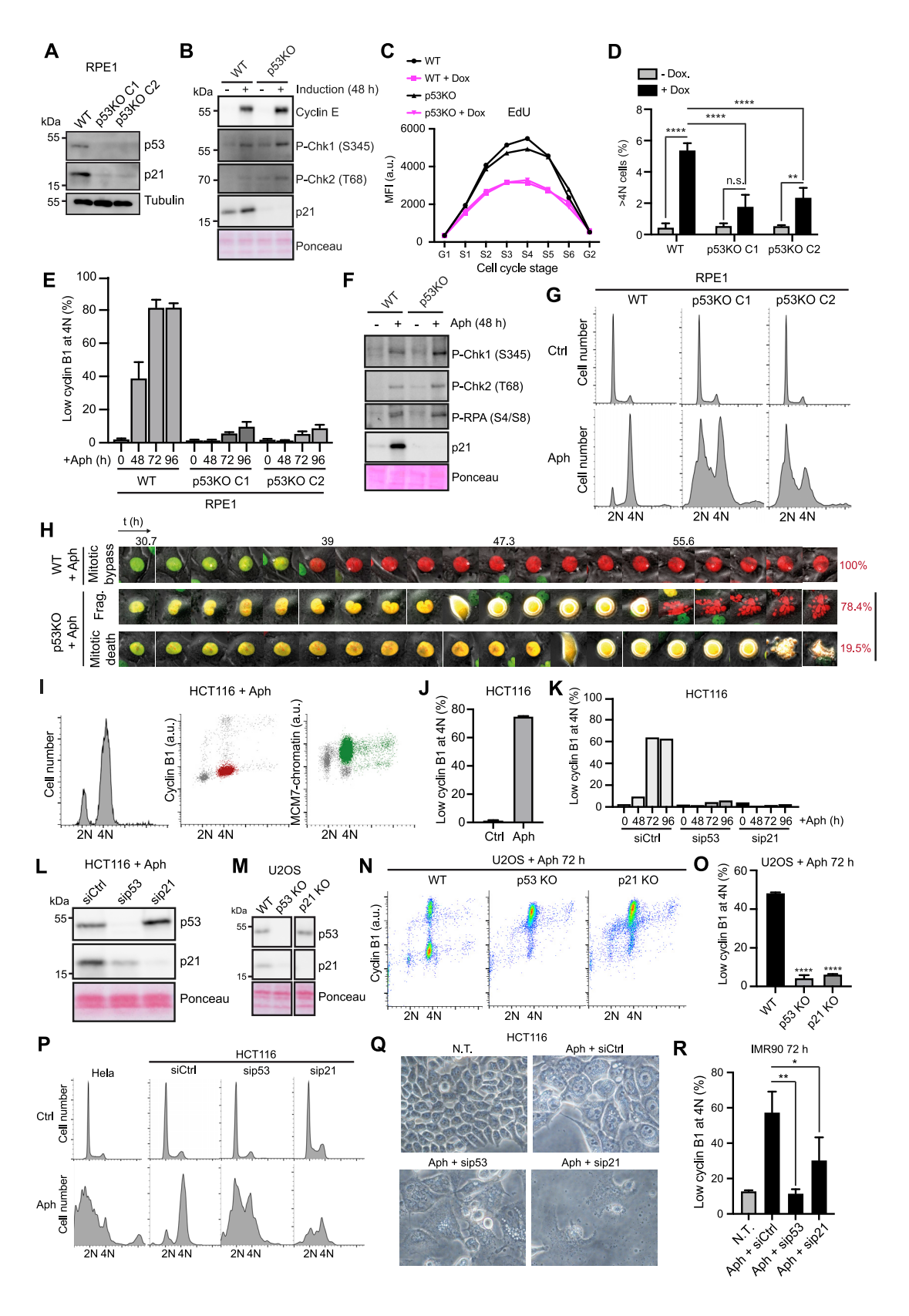


Figure S4. Characterization of replicative stress in cyclin E-expressing RPE1 cells; aberrant G2 transitions, related to Figure 4

(A and B) RPE1 cells were analyzed by FACS as in Figure 2D.

- (C) Immunoblots showing DNA damage markers.
- (D) Normalized time-course degradation of mVenus-Gem in cyclin E-expressing RPE1 cells that bypassed mitosis (n > 40 for each condition). Mean half-life ( $t_{1/2}$ ) values with SDs are shown in the figure and main text.
- (E) The percentages of cell-cycle transitions from G2 in cyclin E-expressing RPE1 cells.
- (F) To show the ATM and ATR inhibitors are functional, we added the inhibitors to zeocin-treated U2OS cells that are supposed to activate both ATM and ATR pathways. Immunoblot showing phosphorylated p53 (S15) expression in zeocin-treated U2OS cells after 6-h supplementation with inhibitors of ATR or ATM.









#### Figure S5. Involvement of p53 and p21 in aphidicolin-induced mitotic bypass, related to Figure 5

- (A) Immunoblots showing knockout of p53 in RPE1 cells (clone #1&2).
- (B) Immunoblots showing DNA damage markers in RPE1 WT and p53 KO cells expressing cyclin E.
- (C) EdU incorporation analysis by FACS of RPE1 WT and p53 KO cells expressing cyclin E.
- (D) Quantification of RPE1 WT and p53 KO cells with >4N DNA content after 96-h expression of cyclin E. Mean percentages with SDs are shown (n = 3). Statistical significance: \*\*p < 0.005; \*\*\*\*p < 0.0001, Tukey's method.
- (E) Cells were treated with 1 μM aphidicolin and analyzed for cyclin B level and DNA content by FACS. The mean percentage of EC-G1 cells with range is shown (n = 2).
- (F) Immunoblots showing DNA damage markers.
- (G) DNA content analysis by FACS on cells treated with 1  $\mu$ M aphidicolin for 72 h.
- (H) Images of example cells in Figure 5D showing mitotic bypass, mitotic death, and nuclear fragmentation are shown. The mean percentage of different outcomes is shown on the right (n = 3).
- (I) HCT116 cells were treated with 1  $\mu$ M aphidicolin for 72 h before being analyzed for cyclin B level, chromatin-bound MCM7 level, and DNA content by FACS. ECG1 cells are identified and labeled in red. Cells with high MCM7 at 4N or >4N DNA content are labeled in green.
- (J) Quantification of the percentage of EC-G1 cells in (I) with range is shown (n = 2).
- (K) HCT116 cells were treated with 1 μM aphidicolin, supplemented with siRNAs, and analyzed as in (E).
- (L) Immunoblots showing knockdown of p53 and p21 in HCT116 cells.
- (M) Immunoblots showing knockout of p53 and p21 in U2OS cells.
- (N and O) Cells were treated with 1  $\mu$ M aphidicolin for 72 h before being analyzed for cyclin B by FACS (N). The percentage of EC-G1 cells with range is shown in (O) (n = 2). Statistical significance: \*\*\*\*p < 0.0001, Tukey's method.
- (P) Hela and HCT116 cells were treated with 1  $\mu$ M Aph and siRNAs were used to knock down p53 and p21 in HCT116 cells for 72 h. DNA content analysis by FACS is shown.
- (Q) Representative wide-field images of HCT116 in (P).
- (R) IMR90 cells were treated as in (P). Quantification of the percentage of EC-G1 cells with SDs is shown (n = 3). Statistical significance: \*p < 0.05 and \*\*p < 0.005, Tukey's method.



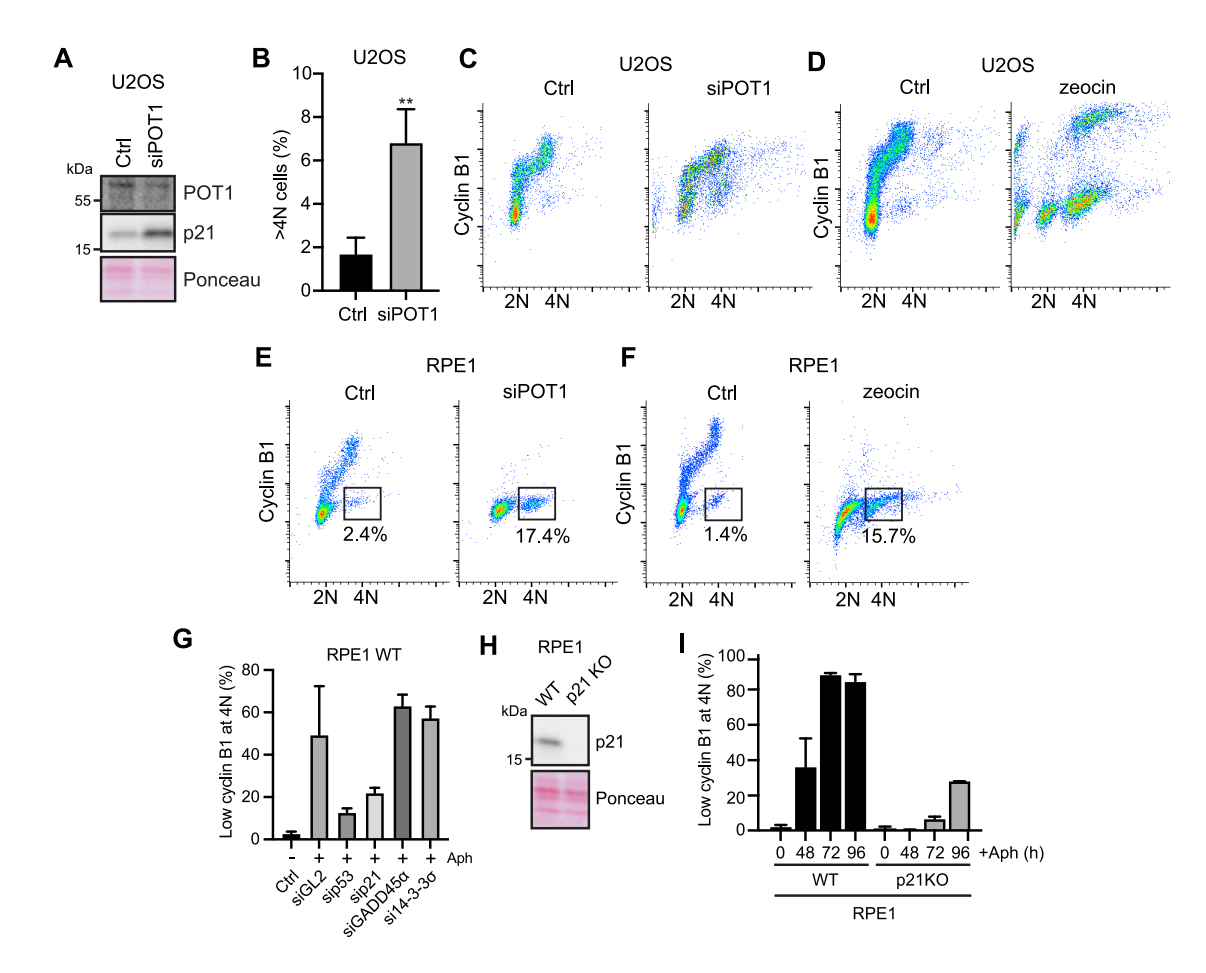


Figure S6. POT1 knockdown-induced mitotic bypass, involvement of p21 in mitotic bypass, related to Figure 5

- (A) Immunoblots showing POT1 and p21 in POT1-depleted U2OS cells.
- (B) POT1-depleted U2OS cells were analyzed by FACS. Quantification of >4N cells with SDs is shown (n = 3). Statistical significance: \*\*p < 0.005, unpaired t test.
- (C) FACS analysis of U2OS cells treated with siPOT1 for 96 h.
- (D) FACS analysis of U2OS cells treated with 100 μg/ml zeocin for 96 h.
- (E) FACS analysis of depleted with POT1 for 96 h. Numbers indicate the percentage of EC-G1 cells.
- (F) FACS analysis of cyclin B level and DNA content on RPE1 cells treated with 100 μg/ml zeocin for 96 h. Numbers indicate the percentage of cells with a low cyclin B level at 4N DNA content (EC-G1 cells).
- (G) Downstream effectors of p53 were depleted in RPE1 WT cells treated with 0.5 μM aphidicolin for 72 h. Quantification of EG-G1 cells with SDs is shown (n = 3). (H) Immunoblot showing knockout of p21 in RPE1 cells.
- (I) RPE1 p21 KO cells were analyzed as in Figure S5E. The percentage of EC-G1 cells with range is shown (n = 2).



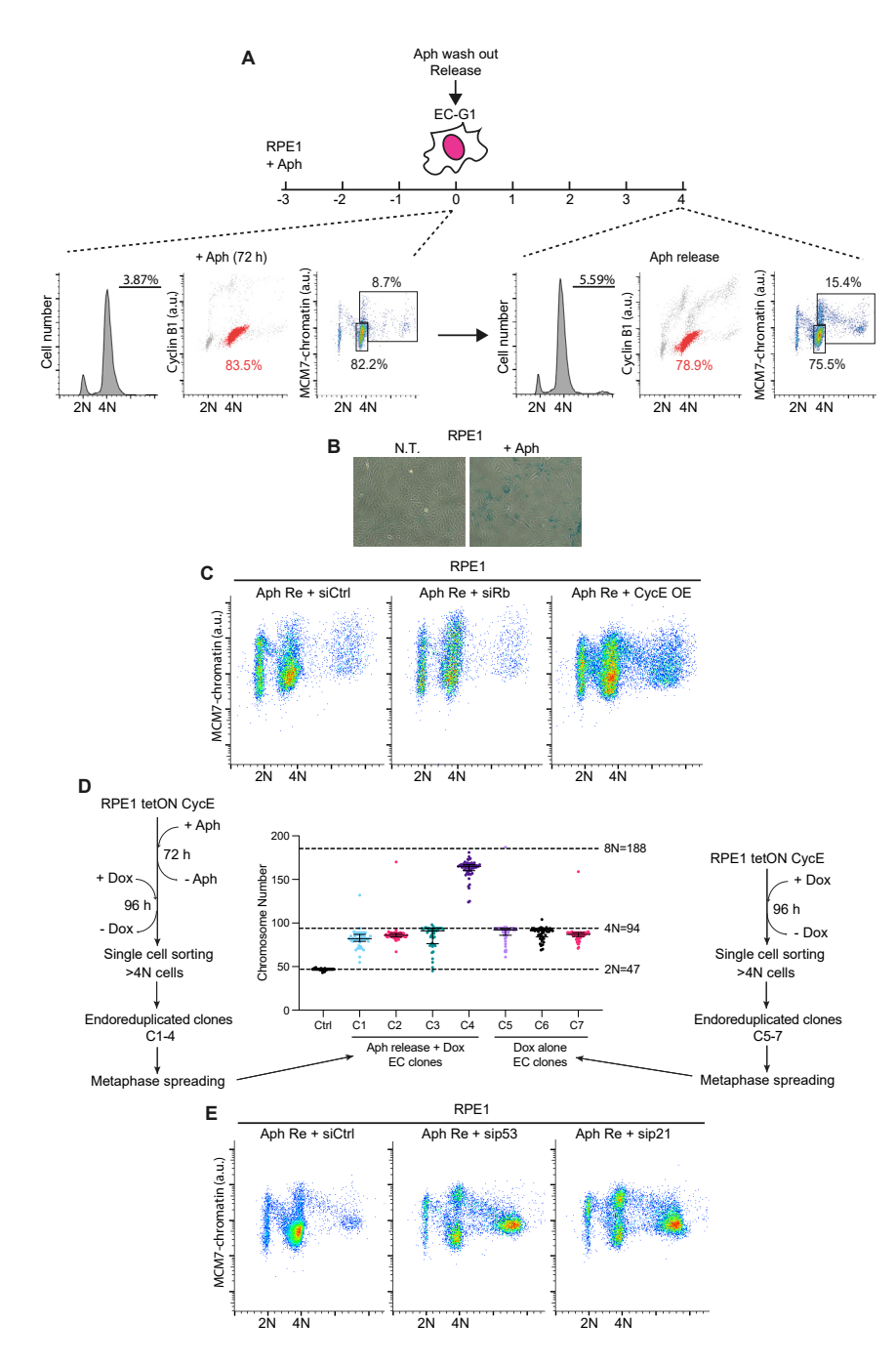


Figure S7. Knockdown of p53, p21, and Rb promotes cell-cycle re-entry of senescent EC-G1 cells, related to Figure 6

(A) Schematic of the experimental approach is shown on top. Cells were analyzed by FACS. EC-G1 cells are identified and labeled in red.

(C) RPE1 cells were treated as in Figure 6B and analyzed by FACS at 96 h post aphidicolin release for DNA content and MCM loading. siRNAs were used to knock down Rb at the point of release.

<sup>(</sup>B) Representative wide-field images of RPE1 cells treated with 1  $\mu M$  aphidicolin for 96 h.

The blue color indicates  $\beta$ -galactosidase activity.

<sup>(</sup>D) Chromosome number analysis of RPE1 endoreduplicated single-cell clones.

<sup>(</sup>E) RPE1 cells were treated as in Figure 6B and analyzed by FACS at 96 h post aphidicolin release for DNA content and MCM loading. siRNAs were used to knock down p53 or p21 at the point of release.